RECONFIGURABLE MIMO ANTENNA SYSTEM WITH DIRECTION FINDING CAPABILITY FOR COGNITIVE RADIO PLATFORMS

BY

RIFAQAT HUSSAIN

A Dissertation Presented to the

FACULTY OF THE COLLEGE OF GRADUATE STUDIES

KING FAHD UNIVERSITY OF PETROLEUM & MINERALS

DHAHRAN, SAUDI ARABIA

In Partial Fulfillment of the
Requirements for the Degree of
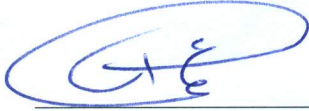
DOCTOR OF PHILOSOPHY

In

ELECTRICAL ENGINEERING

JANUARY 2015

KING FAHD UNIVERSITY OF PETROLEUM & MINERALS

DHAHRAN- 31261, SAUDI ARABIA

DEANSHIP OF GRADUATE STUDIES

This thesis, written by Rifaqat Hussain under the direction his thesis advisor and approved by his thesis committee, has been presented and accepted by the Dean of Graduate Studies, in partial fulfillment of the requirements for the degree of **DOCTOR OF PHILOSOPHY IN ELECTRICAL ENGINEERING.**
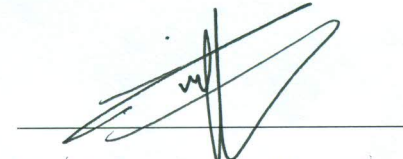
Dr. Mohammad S. Sharawi
(Advisor)

Dr Ali A. Al-Sheikhi
Department Chairman
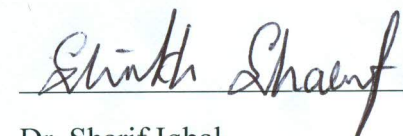
Prof. Husain M. Masoudi
(Member)

Prof. Salam A. Zummo
Dean of Graduate Studies

Prof. Raj Mittra
(Member)

25/2/15
Date

Dr. Ali Muqaibel
(Member)

Dr. Sharif Iqbal
(Member)

To my beloved wife and my lovely kids ILYAS AHMED, SALMAN AHMAD and my little angel HIRA BANO

ACKNOWLEDGMENTS

TABLE OF CONTENTS

CHAPTER 6   DF USING SP INTEGRATED WITH RECONFIG-
URABLE ANTENNA   154

CHAPTER 7   CONCLUSION AND FUTURE WORK   186

REFERENCES   189

LIST OF TABLES

LIST OF FIGURES

THESIS ABSTRACT

NAME: Rifaqat Hussain

TITLE OF STUDY: Reconfigurable MIMO Antenna System with Direction Finding Capability for Cognitive Radio Platforms

MAJOR FIELD: Electrical Engineering

DATE OF DEGREE: January, 2015

In the near future, the revolutionary technique of cognitive radio (CR) will be adapted for efficient spectrum utilization in 4G/5G wireless standards. The front end of a CR consist of a sensing antenna for spectrum scanning and a reconfigurable antenna for communication and band selection purposes. Multiple-input multiple-output (MIMO) reconfigurable antennas are used in CR platforms to enhance the throughput of such systems.

This work is aimed to design a novel reconfigurable MIMO antenna system with direction finding capabilities for cognitive radio platforms. All antennas elements and the microwave structure for direction finding are intended to be planar in structure for easy integration with the IC's and other low profile components to be accommodated within wireless handheld devices. The frequency of interest is the wireless band covering 700 MHz and 3 GHz. The design of sensing and reconfigurable antenna systems to cover 0.7∼3 GHz is a challenging job because of the limited size of wireless handheld devices. Moreover, the design of a compact radio frequency (RF) based direction finding (DF) system and its integration with CR platforms is another challenging task especially that it became a requirement in second generation cognitive radios and such integration is rare to find in liter-

ature.

In this work, several 2-element and 4-element reconfigurable MIMO antenna designs have been investigated in details and their performance metrics are assessed. An ultra-wideband(UWB) sensing antenna is proposed for frequency bands between 0.7∼3 GHz with compact size. A 2-element reconfigurable MIMO antenna system is integrated with an UWB sensing antenna to form a complete integrated solution for CR platforms. Two versions of the integrated designs are presented with a substrate size of 60×120 mm². A microwave direction finding (DF) circuit based on the six-port passive system is presented in this work. Single and dual angle resolution compact six-port structures are designed to cover the wide frequency bands from 1.68∼2.25 GHz to allow for direction finding capabilities both in 2D and 3D. The maximum error obtained was 16º.

This work presents the first compact integrated reconfigurable MIMO antenna system along with an UWB sensing antenna on a single substrate with compact size covering the aforementioned frequency ranges along with direction finding capability. The antenna systems were tested for system level performance with six-port circuit for radio frequency direction finding.

مُلخّص الرسالة

الاسم الكامل:	رفاقت حسين
عنوان الدراسة:	منظومة هوائيات قابلة للتغير ومتعددة المدخلات والمخرجات مع خاصية تحديد مكان المرسل لأنظمة الراديو المعرفي
التخصص:	الهندسةالكهربائية
تاريخ الدرجة العلمية:	يناير 2015

إن ثورة تقنية الراديو المعرفي والذي يقوم فيه طرف الإرسال بالتحقق من الترددات التي يتم استخدامها والتي لايتم استخدامها ويقوم المرسل بتغيير تردد النظام إلى تردد متاح للاستخدام سيتم استخدامها في المستقبل القريب للاستفادة قدر الإمكان من النطاق الترددي المقدم من تقنيات 4G/5G.

إن أول جزء من تقنية الراديو المعرفي يتكون من هوائي استشعار لفحص النطاقات الترددية وأنتنا أخرى قابلة للتشكل والتغير والتي ستقوم بعملية الاتصال بعد تهيئتها للعمل على نطاق معين. إن الهوائيات القابلة للتغير ذات المداخل والمخارج المتعددة سيتم استخدامها في أنظمة الراديو المعرفي للخروج بنظام ذو إمكانات عالية.

هذا العمل موجه لتصميم هوائي قابل للتغير ذو مداخل ومخارج بطريقة جديدة وجعل النظام يتمتع بقدرة على تحديد مكان المرسل لأنظمة الراديو المعرفي. جميع عناصر الهوائي ومجسمات المايكروويف لإيجاد المرسل مصممة لأن تكون مسطحة وذلك يجعل من وضعها في الدوائر والأنظمة المعقدة أمرا سهلا آخذين بالاعتبار ضرورة الحصول على أصغر الأحجام وذلك لإضافتها للأجهزة اللاسلكية الصغيرة. إن التردد المستهدف هو نطاق الشبكة اللاسلكية من 700 ميجاهرتز إلى 3 جيجا هرتز. إن عملية تصميم هوائي الاستشعار عملا صعبا وتحديا كبيرا، خصوصا مع محدودية المساحة المتوفرة بالأجهزة اللاسلكية. زيادة على هذا التحدي، إن تصميم نظام مبني على شبكات الراديو لتحديد مصدر الإرسال ودمجه مع بيئة الراديو المعرفي تحدي آخر خصوصا أن هذا الدمج أصبح مطلبا للجيل الثاني من أنظمة الراديو المعرفي والذي لا يتوفر غالبا في الأنظمة القديمة.

في هذا العمل، سيتم بحث عدة تصاميم ذات عنصرين أو أربعة عناصر للهوائيات القابلة للتغيير، وسيتم تقييم أدائهم أيضا. تم اقتراح هوائي استشعار ذو نطاق عريض للترددات بين 700 ميجا هرتز و3 جيجا هرتز وذات حجم صغير. تم دمج هوائيات ذات عنصرين وقابل لإعادة التشكل على نمط المداخل والمخارج المتعددة مع هوائي استشعار ذو نطاق عريض لتوفير حل متكامل لأنظمة الراديو المعرفي. تم تطوير نسختين من هذا النظام المتكامل على مادة ذات أبعاد 120×60 مم^2. وتم أيضا تقديم دائرة كهربائية بتقنية المايكروويف لتحديد جهة

الارسال مبنية على نظم المداخل الستة لتغطية الترددات من 1.68 – 2.25 جيجا هرتز. أكبر خطأ في تحديد زاوية المرسل كان بمقدار 16°درجة.

هذا العمل يقدم أول نظام متكامل باحتوائه على هوائي الاستشعار إضافة إلى الهوائيات القابلة للتغيير ذات المداخل والمخارج المتعددة مبنية على قطعة واحدة ذات حجم صغير وتغطي الترددات السابق ذكرها مع القدرة على تحديد اتجاه المرسل بموجات الراديو.

CHAPTER 1

INTRODUCTION

The need of wireless handheld devices with additional data demanding features has grown rapidly in the last few years. Compact form factor wireless handheld devices with powerful computing, high performance and compatible with new wireless standards are required for new generation communication systems. Some of the enabling attributes to fulfill such demands in mobile communication devices include direction finding capability, antenna reconfigurability and adaptive beam scanning. These characteristics are required in wireless handheld devices for next generation software defined radio (SDR) and cognitive-radio (CR) platforms. In addition, the higher data rate requirements and reliability of transmitted data within wireless hand-held communication devices are met by embedding multi-input multi-output (MIMO) antenna systems in such platforms. Since the antenna system and its features directly affect the overall wireless communication system performance, it is critical to design novel antenna systems that provide as many of such attractive features as possible. This work targets this goal.

1.1 Wireless evolution and trends

The era of analog-based mobile generation (1G) was started in late 1970s while the first cellular communication system was deployed in 1981 in Norway followed by the United States and the United Kingdom. The system was operating in the 900 MHz band with analog modulation and supported only voice calls and text

Figure 1.1: The evaluation of mobile phones.

data. 1G was followed by second generation (2G). The mostly used and popular technology of 2G was the Global System Mobile (GSM) standard. The operation band of the first GSM standard was 900 MHz with 25MHz frequency spectrum. Today, GSM frequency bands cover 900MHz and 1.8 GHz bands throughout the world while 1.9 GHz band is used in US. 2G technology supported both voice and data but with drastically enhanced data rates compared to 1G [1].

Wireless local area network (WLAN) started its operation in late 1990s and was advancing in parallel with mobile phone technology. In early 2000s, wireless standards such as Bluetooth and Zigbee were widely used in small wireless hand-held devices and mobile terminals. Cellular phone technologies of 3G and 4G were deployed in 2006 and 2011, respectively. With the advent of each new generation, there were several times increase in data rate capability and was in excess of 100 Mbps. This enabled the services like high definition video calls, real time video transfer, video conferencing and high definition live streaming.

Advances in antenna design and fabrication of microelectronics circuitry has made a fabulous change in the sizes of mobile phones. The evaluation of mobile phones size over a period of time is shown in Figure 1.1. The huge and bulky brick-

like mobile phones of 1G has been transformed to sleek and stylish smart phones with compact packaging. The size reduction is accompanied with integration of much more complex and advance functions in these wireless devices.

The primary purpose of 3G was to develop a new protocol to enhance the mobile experience. While, on the other hand, 4G was established to meet the new levels with multi-service capacity in a compact and portable mobile phone device. Thus, it was the integration of all the mobile technologies like GSM, GPRS, Wi-Fi, Bluetooth and many more. It should be capable of supporting various wireless standards and operate across several frequency bands. Thus, multi-band or frequency reconfigurable antennas are a vital part of 4G wireless devices and must be embedded within the device to cover various frequency standards [2].

1.2 Multiple-input-multiple-output (MIMO) technology

Multiple input, multiple output (MIMO) is wireless communication technology that use multiple antennas both at transmitter and receiver ends. MIMO antenna systems are used to increase the capacity and reliability of the data by utilizing multiple antennas at both communication ends. In 4G wireless technology, the three main constituents to enhance the data rate capabilities are

1. Adaptive modulation and coding (AMC)

2. Implementation of orthogonal frequency division multiplexing (OFDM)

3. Use of MIMO technology

The first two elements are related to data encoding and modulation in adaptive way to improve the performance over the time varying wireless channels. MIMO technology is concerned with the implementation of multiple antennas at both ends of the wireless system. MIMO technology is being utilized in 4G wireless standards and beyond to achieve higher data throughput in multipath wireless

channels. In a MIMO system, data sent from the transmitter passes through different paths and thus the data received at the receiver end has a high probability of good representation of transmitted data in the fading and multipath environment. Thus, this increase the data rate when parallel stream of data are sent from transmitter antennas. The block diagram of a MIMO system is shown in Figure 1.2 [2].
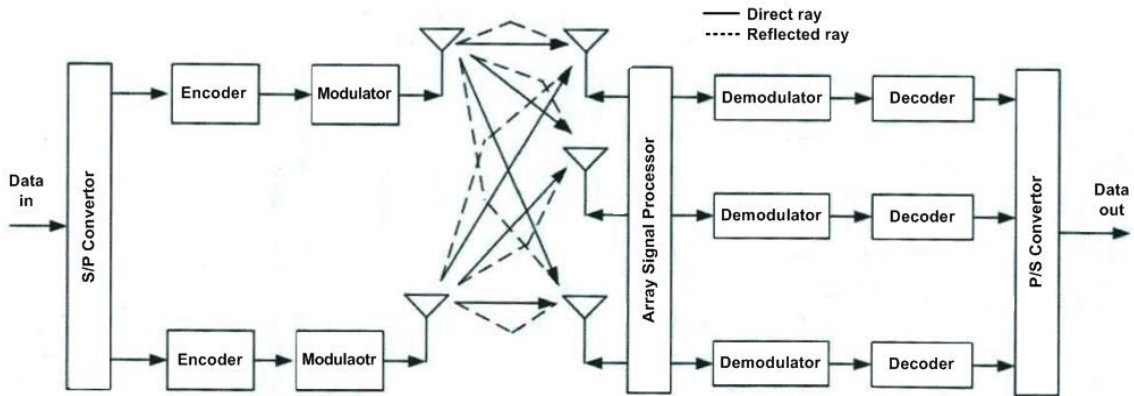
Figure 1.2: MIMO system block diagram [1].

The channel capacity for a MIMO system can be carried out using the modified Shannon equation [2] as,

$$C = MBlog_2\left(1 + \frac{N}{M}SNR\right) \tag{1.1}$$

where C is the channel capacity (in bps), SNR is the signal to noise ratio of the wireless communication channel, B is the bandwidth (in Hz), M is the number of antennas at the transmitter side, and N is the number of antennas at the receiver side. Channel capacity is directly related to number of antenna elements with low correlation radiation pattern. The performance is degraded significantly for high mutual coupling between antennas or high correlation radiation pattern. Thus, the design of MIMO antennas system with anticipated high data rate is greatly dependent on the way MIMO antennas are designed with low correlation and mutual coupling.

4

Printed antennas are widely used in mobile terminals and wireless handheld devices for MIMO operation. Printed MIMO antennas have attractive features of low cost, ease of fabrication and ease of integration. The mutual coupling between closely spaced antenna elements should be reduced to increase the MIMO throughput. Thus the use of multiple antenna elements and characterizing their performance is an inevitable task in modern antenna design. MIMO antenna systems with reconfigurable front ends for efficient bandwidth utilization are becoming popular in recent years [3].

1.3   Cognitive Radios

According to International Telecommunication Union, Radio Communication Sector (ITU-R) ITU-R Report SM.2152 define a cognitive radio (CR) as [4]:

"A radio system employing technology that allows the system to obtain knowledge of its operational and geographical environment, established policies and its internal state; to dynamically and autonomously adjust its operational parameters and protocols according to its obtained knowledge in order to achieve predefined objectives; and to learn from the results obtained."

According to the Federal Communications Commission (FCC) spectrum regularity authority in United States,. a cognitive radio (CR) is defined as *"A (softwaredefined) radio that can change its transmitter parameters based on interaction with the environment in which it operates"* [5].

The concept of the revolutionary technique of a cognitive radio (CR) (an extension of the SDR) first appeared in literature in 1999. It is an intelligent technique in communication system for radio devices and associated networks. The communication between radio devices and the network is likely to be in such a manner to be able to adjust their operating parameters as per their need as well as learning from the experience as well. Since then, significant research work has been done related to CR topic. Standardization bodies have initiated several plans to standardized the CR system in United States, Europe and AsiaPacific regions. One step forward, regulatory bodies like FCC in USA and Office of Communications

(OFCOM) in UK have already authorized to use white TV bands for unlicensed devices. In radio communication conference (WRC) 2012, regulatory plans were discussed in detail and the possible implementation of CR system architecture was suggested [6].

1.3.1 Spectral Congestion

In a wireless system, communication take place at particular common frequencies sharing a common medium. Recent tremendous growth in wireless devices and services resulted in spectral congestion. Thus, it became a cause of substantial concern keeping in mind the available anticipated wireless devices and demands for services in the near future. The spectral congestion occurred because of sub-optimal frequency allocation by strict spectrum licensing processes. For example the 850 MHz and 1.9 GHz allocated for cell phones in the USA. The excessive use of particular applications results in particular frequency congestion. The cell phone user may experience dropped calls or busy lines.

The inefficient frequency usage could be resolved by using the unlicensed spectrum. However, it requires to develop new protocols for multi-users to be efficient and avoid harmful interference. Two approaches are generally deployed for efficient spectrum sharing: (1) spectral underlay approach (ultra-wideband(UWB)) (2) spectral overlay approach (cognitive radio). In UWB or spectral underlay approach, a secondary user transmit signals using low power spectral density (PSD) to avoid any interference with the primary user. In this approach, a significant data rate is achieved by compensating the low PSD with extra large bandwidth. On the other hand, in spectral overlay approach, dynamic spectrum access (DSA) is utilized for spectrum sharing. This approach is a main concern of the implementation of CR for spectrum utilization [7].

1.3.2 Dynamic Spectral Acess (DSA)

In DSA, the allocated spectrum could be utilized by secondary users for temporarily unused frequencies to avoid any possible spectral congestion. The concept of

DSA is elaborated in Figure 1.3 [7]. An energy detector is used in real time scenario to detect the power level for determining the spectral occupancy. In the given diagram, colored cuboid are used to show the spectral occupancy of the entire spectrum with time used by different protocols with different power levels. Any unused or less used frequency results in spectrum holes and are shown in green discs. The idea of DSA is looking for these spectral holes to utilize these unused frequencies. Consequently, congestion could be avoided with efficient spectrum utilization. As a matter of fact, spectrum regularity bodies are continuously exploring new standards and protocols to realize the dream of CR system magic [7].
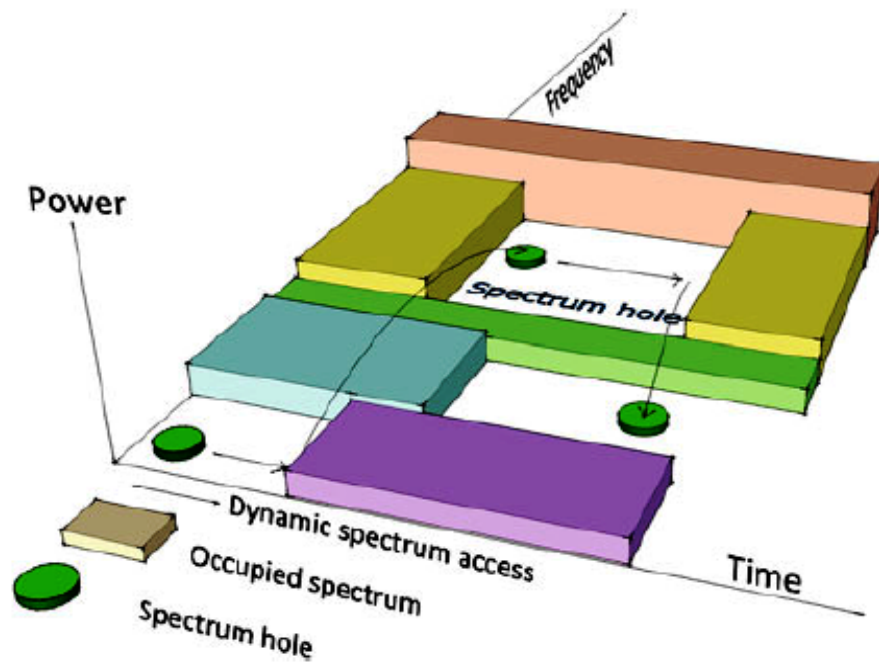
Figure 1.3: Concept of DSA [7].

1.4 Radio Frequency Direction Finding

Radio frequency (RF) direction finding (DF) identifies the source location based on the incoming RF signals. RF based DF schemes are gaining popularity in commercial applications. DF has a wide range of applications in military, avionics, emergency services and in wireless communication devices. The basic principle of

a DF system is its ability to estimate the angle-of-arrival (AoA) of an incoming signal from a distant target object. Classical direction finding techniques consist of an antenna array followed by single or multiple receivers. Multiple-channel DF algorithms such as Multiple Signal Classification (MUSIC) and Estimation of Signal Parameters via Rotational Invariance Technique (ESPRIT) extract the AoA information of the incoming waves from a target object using the phase information from each antenna simultaneously [8, 9].

In various practical scenarios especially in mobile systems, implementations of multiple receiver DF algorithms are not feasible. So, single channel DF techniques are used commonly in such scenarios. Single channel DF techniques rely on complex and computationally intensive digital signal processing (DSP) algorithms that prohibit their use in mobile terminals [10]. Radio frequency (RF) direction finding (DF) identifies the source location based on the incoming RF signals. RF based DF schemes gained popularity in commercial applications over the past few decades [11]. Microwave structure based DF schemes are generally low cost and less complex, thats why they have gained popularity in last few years. The six-port (SP) architecture is a key component in microwave based DF systems and is also becoming popular in microwave measurements due to its accurate and potentially low cost [12]. It has wide range of applications in RF direction finding (DF), precise displacement measurements, direct conversion receivers and in radar sensors.

1.5   Motivation and Problem Statement

The use of wireless handheld devices has increased tremendously in recent years. These wireless devices include laptops, mobile phones, tablets, smart mobile phones and wireless handheld direction finding devices. New features are continuously added to these devices. Intensive processing, online video streaming, online gaming, video and audio conferencing require high speed data. Generally, these wireless handheld devices conform to 4G wireless standards. In [13], it was estimated that by the end of year 2017, the interpolated demand of such devices

is going to be increased to 3 billion covering multiple standards, which is another requirement of next generation devices.

Thus, the design of compact and efficient reconfigurable antennas and MIMO antenna systems integrated with DF capabilities as well as efficient band utilization are becoming a necessity within mobile phones and other wireless handheld devices according to the 4G wireless standards and upcoming 5G ones [14].

The second generation of CR places several challenging requirements to meet the anticipated features of such platforms. Reconfigurable MIMO antennas are required to provide high data rates with efficient spectrum utilization. This combines the challenges of designing reconfigurable antennas to cover multiple wireless standards with that of designing MIMO antenna systems with good performance metrics such as isolation and low correlation characteristics. Covering the lower bands of 4G wireless standards adds to the complexity of the problem. The 700/800 MHz frequency bands poses a real challenge when designing printed MIMO antennas and the designing of the UWB sensing antenna. Being able to perform beam forming and thus requiring a DF capability of the next generation CR rises another challenge when coming up with a compact integrated architecture combining reconfigurability, MIMO and DF capabilities within a single portable devices. This work will try to come up with a complete solution integrating these features for CR systems.

1.6   Work Contributions

The objective of this work is to design a novel reconfigurable MIMO antenna system with direction finding capabilities for cognitive radio platforms for 4G wireless standards. All antennas (reconfigurable MIMO and UWB sensing antenna) and microwave structure for direction finding were aimed to be planar for easy integration with the IC's and other low profile components so that they could be easily accommodated within wireless handheld devices. The frequency of interest is the wireless band between 700 MHz up to 3 GHz.

To achieve the desired characteristics of reconfigurability in a MIMO antenna

system with direction finding capability, put several challenges that needed to be overcome to accomplish the desired tasks. These issues included coming up with novel solutions for the size of the antennas at low frequency bands. In addition to antenna size limitation that requires novel miniaturization, control circuitry is embedded within the given antenna structure to achieve the desired frequency reconfiguration out of it. Additionally, a CR system requires an UWB sensing antenna to scan the wide frequency band.

The design of the sensing antenna with the strict dimensions of a mobile terminal size is itself a challenging job as the sensing antenna is required to cover the lower frequency bands as well (i.e. 700 MHz). Moreover, the performance of the MIMO system degrades significantly for closely spaced antennas due to high mutual coupling. To enhance the performance of the reconfigurable MIMO antenna system, it was necessary to improve the isolation between the different antenna elements. In addition, direction finding capability of a RF source was required within the same architecture. To overcome all these challenges and to have a compact reconfigurable MIMO antenna with good isolation, an UWB sensing antenna and compact microwave structure for direction finding capability all integrated within a single platform is the ultimate target of the proposed work.

The contributions of this work are summarized as follows:

1. A novel compact two element reconfigurable MIMO antenna design based on modified printed inverted F-shaped antenna (PIFA) elements covering several well known frequency bands including LTE, GSM and WLAN, integrated with an UWB sensing antenna for cognitive radio platforms occupying the size of a standard smart phone size of $65 \times 120 \times 5.4$ mm^3. The design was successfully implemented and tested and covered low frequency bands as low as 700 MHz. Two versions of the reconfigurable MIMO antennas were obtained. One using PIN (p-type,intrinsic material,N-type) diodes and another using varactor diodes.

2. A two element reconfigurable MIMO antenna system based on modified meander-line antennas integrated with an UWB sensing antenna on a single

two layer substrate occupying 65×120×1.56 mm^3. The antenna system was designed and tested.

3. Two designs of a 4-element reconfigurable MIMO antenna systems based on modified meander-line antennas and using varactor and PIN diodes for frequency switching. They occupied a board area of 65×120×1.56 mm^3.

4. A novel planar 4-element reconfigurable MIMO antenna using ground (GND) current control for frequency reconfigurability.

5. Compact low frequency single and dual six-port (SP) microwave circuit design and implementation for 1.7 ∼ 2.2 GHz bands for single and dual angle resolution DF systems to be embedded in wireless handheld devices.

6. A two element reconfigurable modified PIFA MIMO and sensing antenna integrated with a SP circuit. This final design was a complete system working in two modes of operation:

   (a) Communication mode using reconfigurable and sensing antennas for CR platforms.

   (b) Beamforming mode using SP structure for RF DF.

1.7 Dissertation Layout

This work focused on the design and implementation of integrated reconfigurable MIMO antenna systems with direction finding and spectrum sensing capabilities for cognitive radio platforms in small wireless handheld devices. This section provides an overview of the layout of this work.

Chapter 2 overviews reconfigurable MIMO antenna, different types of reconfigurable antennas, MIMO performance metrics, UWB sensing antenna and its significance in the CR system, and direction finding using the SP technique. Chapter 3 provides the complete literature survey on cognitive radio antennas and SP for RF DF.

Chapter 4 discusses the results of different types of reconfigurable MIMO antennas. Chapter 5 discusses reconfigurable MIMO antenna embedded with UWB sensing antennas for CR platforms. Two different designs are presented with complete results discussion and MIMO performance parameter evaluation.

Chapter 6 discusses the SP technique for RF DF. Two different SP designs are presented with their complete features and discussion on simulated and measured results. The chapter also discusses the integration of the SP circuit with MIMO reconfigurable antennas and UWB sensing antenna. Chapter 7 concludes the work with recommendation for future work.

CHAPTER 2

THEORETICAL BACKGROUND

The revolutionary technique of a CR (an extension of the SDR) is a system with efficient utilization of frequency spectrum. The front end of a CR consists of two antennas, (1) an ultra wide-band (UWB) sensing antenna and (2) a reconfigurable communication antenna. Dynamically changing the basic radiating characteristic of the antenna system is termed as antenna reconfigurability. Reconfigurable antennas are able to change their operating fundamental characteristics i.e. resonance frequency, radiation pattern, polarization and impedance bandwidth. Radar systems are also utilizing CR techniques for efficient bandwidth utilization [15].

So, a CR system can be defined as a radio having the capability to sense the spectrum and communicate. Thus, a CR platform contains an UWB sensing antenna to sense the spectrum and reconfigurable antennas for communication.

The high data rate requirements has increased exponentially over the last few years in wireless communication systems due to the demand for more multimedia applications. To meet the high rate requirements and efficient utilization of the frequency spectrum, MIMO antennas within CR platforms became a viable solution. The second generation CR should be capable of sensing the frequency spectrum, switch to different bands of operation, can change the transmission

parameters as well as utilize the multiple antennas [14]. The abilities of CR ensures efficient utilization of power and comprehensive use of the spectrum. In addition, beamforming capability is required in such CR platforms. In order to maximize the transmission in a beam forming mode of operation, a DF technique needs to be integrated. The SP microwave DF technique will be utilized in this work and integrated within the reconfigurable MIMO, sensing antenna system in one platform.

In this chapter we will cover some background about the various components of the CR with MIMO capability. We will go over the antennas required and parameters that characterize MIMO antenna systems. We will close this chapter by the features and use of the SP as a DF system.

2.1 Spectrum Sensing

Spectrum sensing is of vital importance in intelligent dynamic spectrum access for CR platforms. To sense the spectrum reliably used by primary users and its allocation to secondary users is the most critical job in dynamic spectral access for CR application. The frequency allocation to secondary users with minimum effects on the primary users spectrum is the key of CR communication.

2.1.1 Significance of UWB Sensing

In CR platform, dynamic spectrum access can be realized by UWB instantaneous scanning. The most challenging job in CR communication systems is the realization of an UWB sensing antenna followed by a wideband digitizer. The problem become more severe for CR system realization for wireless handheld devices with compact form factor. The UWB sensing followed by ultra-wide RF bandwidth digitizer is of particular interest. The RF digitizer digitizes the specified ultra-wide bandwidth in real time. Once the unused or less used spectrum slots are sensed, it can be allocated to secondary users without affecting the licensed users. New architectures have been investigated over years to tackle the problem of wideband

spectrum sensing and new ways are constantly underway to make the spectrum sensing more reliable in CR platforms [7].

2.1.2 UWB Sensing Antenna

The UWB antenna is an important part of a CR. The wide band of the antenna is utilized for spectrum sensing. UWB antennas has been the topic of last few decades and have been used in many commercial applications. In our design solution, the UWB antenna will be utilized only for scanning of the spectrum and thus be called a sensing antenna.

Two types of antennas are widely used for UWB applications in CR. These two antennas are the printed dipole and monopole antennas. Printed planar monopole antennas are a good choice to work with as sensing antennas in wireless communication systems for CR platforms. They have wide impedance bandwidth, low profile, easy fabrication and have an omnidirectional radiation pattern. The major challenge here is to have a compact size UWB antenna that can cover lower frequency bands of LTE 4G standard (i.e. 700 MHz)

2.2 The Reconfigurable MIMO Antenna System

An antenna is a critical and important part in any wireless communication or radar systems. The field of antenna design is vigorous and dynamic. There are numerous types of antennas covering a wide range of applications and features. So, the choice of an antenna and its evaluated performance are critical for successful design. Because of the fixed characteristics of an antenna system, it imposes certain limitations and difficulties in improving the system performance after it is completed. These limitations may include strict constraint on the volume of the wireless handheld device which restrict the operating configurations of bandwidth and frequency.

To address the strict area constraint, it is suitable to consider reconfigurable antennas with the existing volume that can be made reconfigurable using elec-

tronic circuitry in different frequency bands, can exhibit various radiation patterns and can be polarization reconfigurable. Thus, this reconfiguration will enable the antenna to dynamically adapt with system requirements or environmental conditions to enhance the overall system performance.

MIMO technology is an enabling technique used to increase the channel capacity and hence data rate by employing multiple antennas on both sides of the communication link. This can be done without using any extra power in transceivers or having wider bandwidth (according to Shannon capacity limit).

Thus, the design of reconfigurable MIMO antennas that comply with high data rate requirements and provide efficient utilization of the available bandwidth by switching to different operating bands is highly desirable to be implemented in wireless handheld devices and mobile terminals.

2.2.1 Frequency Reconfigurable Antennas

In modern communication systems, frequency reconfigurable antennas are important and have been used widely. In frequency reconfiguration, the same antenna aperture is utilized for many frequency bands resulting in a compact design. Frequency reconfigurable antennas are broadly classified into two categories: continuous and switched frequency reconfiguration antennas. In continuous frequency agile antennas, the transition between different bands take place in a smooth manner. While on the other hand in switched tunable antennas, they use some kind of switching mechanism to operate at distinct and/or separated frequency bands. Both kinds of antennas in general share a common theory of operation and reconfiguration is achieved in the extent of the effective length changes via parasitic loading that enable operation over different frequency bands.

Some examples of such antennas are given in the literature review. In [16], a meander line reconfigurable antenna was presented. The reconfigurability of the antenna was achieved using a PIN diode. A PIN diode was working as a switch to connect the different parts of the antenna. In this way, the antenna was tuned to different wireless bands and was switched between 4G LTE and other wireless
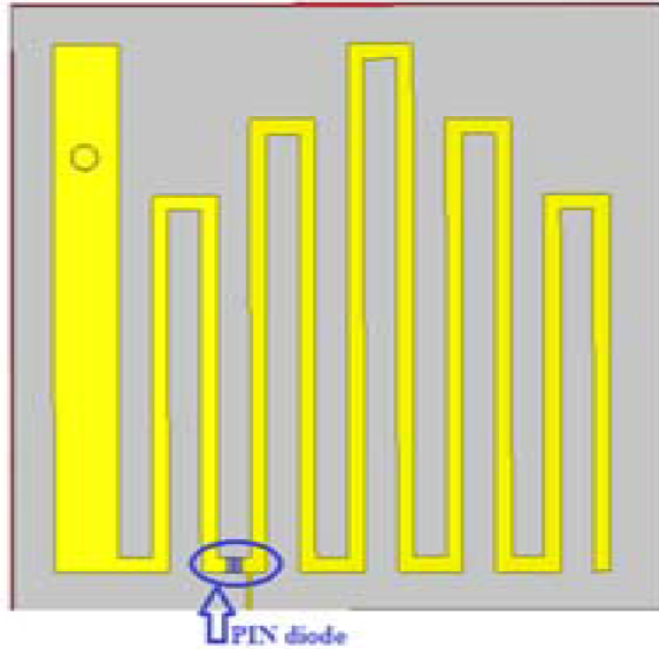
Figure 2.1: The meander line patch [16].

communication standards. The proposed structure had a dimension of 40×40 mm^2 and is shown in Figure 2.1. The design was intended to cover 4G LTE Band 3, GSM and GPS bands when PIN diode was conducting while WLAN and WiMAX bands when diodes were switched off. The reflection coefficient of the proposed structure is shown in Figure 2.2. The reflection coefficient curve shows the good matching within the desired bands.[1]

2.2.2 Polarization Reconfigurable Antenna

Polarization reconfigurable antennas are used in some communication systems. Multipath fading in a communication system may be mitigated by polarization diversity while dual polarized antennas can be used to increase the channel capacity [17]. Polarization reconfigurable antennas can be used in varying environments to provide immunity to interfering signals and are helpful in improving the com-

[1]PIN diodes are used to change the electrical length of the antenna by connecting various sections, thus increasing its length lower its resonance frequency. The opposite is while the use of varactor diodes loads the antenna and change its reactive part by changing the varactor capacitance thus changing its resonance frequency.
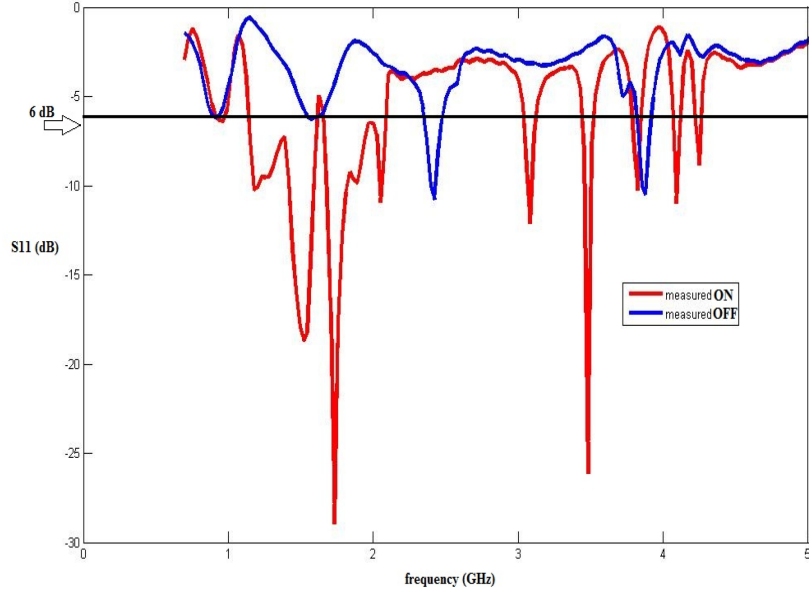
Figure 2.2: The measured antenna reflection coefficient for when the switch is ON and OFF [16].

munication link [18].

The polarization of an antenna can be determined by the direction of the current flow on the antenna. The direction of current flow on the surface of an antenna can be translated directly into the polarization of the electric field in the far field of the antenna. Polarization agility in an antenna structure can be achieved by changing the direction of the flow of current. This can be achieved by changing the antenna structure and feed configuration. For polarization reconfiguration, any modification in the structure can switch the sense of polarization. The polarization may be linear, circular or elliptical. The main challenge in achieving polarization reconfigurability is compensation for the significant changes in impedance or frequency characteristics.

In [19], a tunable microstrip antenna was presented. In this presented design, a dual linearly polarized microstrip antenna was designed. The circular polarization was achieved by tuning the resonance slightly off the intended operating frequency. The presented design was realized on board with $\epsilon_r = 3.55$ and the total board size was equal to 4×4 in^2 and is shown in Figure 2.3. Figure 2.3(a) shows the front view of radiating element while Figure 2.3(b) shows the tuning elements and

18
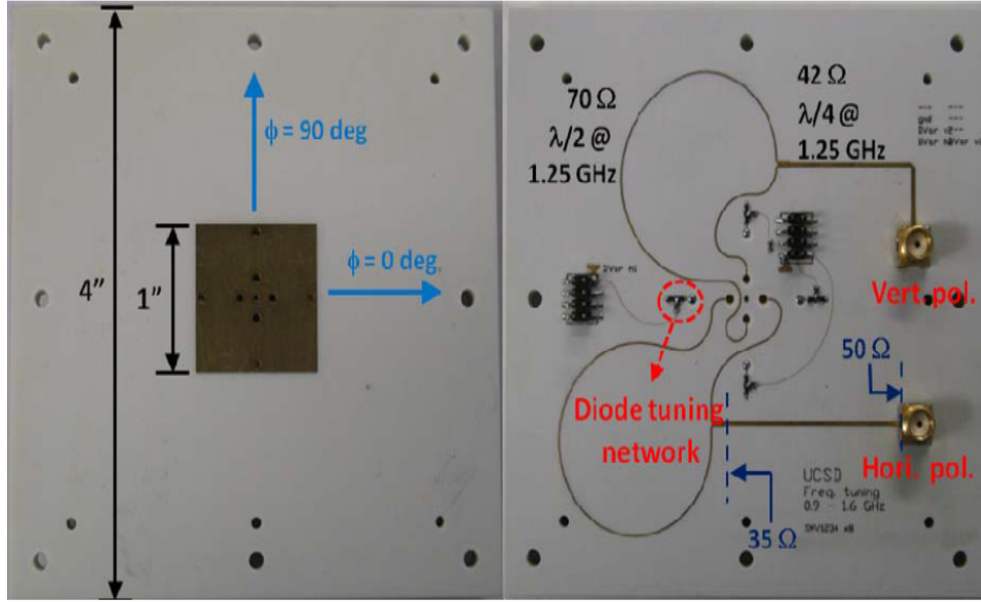
Figure 2.3: Hardware realization of microstrip antenna element; (a) front view of radiating element and (b) back view of feed network and tuning element [19].

feed network.

2.2.3 Radiation Pattern Reconfigurable Antenna

Pattern reconfigurable antennas are gaining wide acceptance in wireless communication technologies due to their potential in improving the system performance. Pattern reconfigurable antennas are helpful in systems to avoid noisy environments, helpful in anti-jamming techniques, improve security by dynamically changing the radiation pattern, can perform scanning for target objects and energy can be saved by directing signals toward intended users [20].

The radiation pattern of an antenna depends on the electric/magnetic currents on the antenna that can be translated to map the radiation pattern from the structure, thus forming a relationship between source current and the resultant radiation pattern. This relationship can be helpful in determining pattern reconfigurability. This pattern reconfigurability may result in changing the operating frequency.

For reconfigurable radiation pattern antenna, a design procedure is started by

19
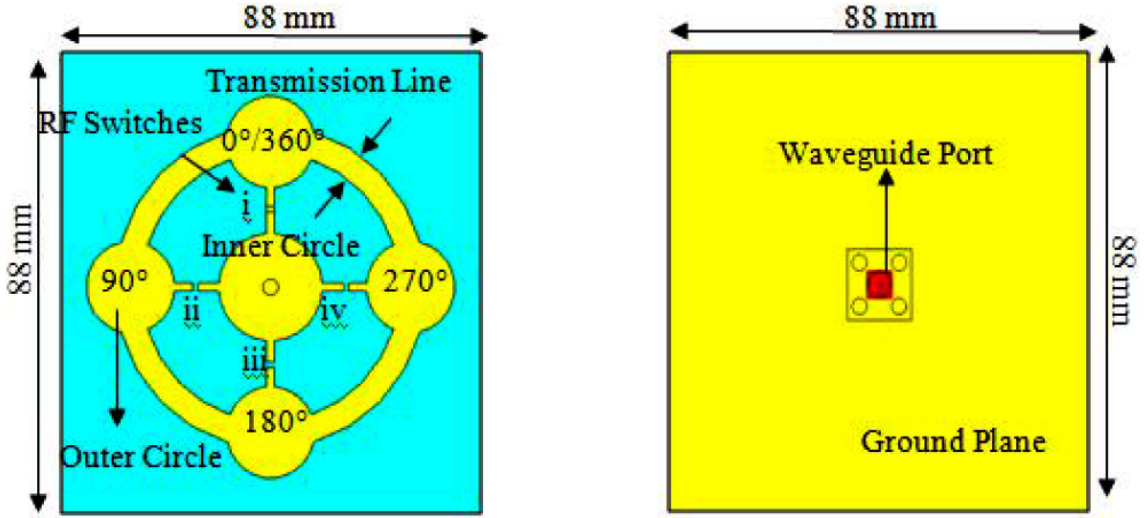
Figure 2.4: Geometry of the proposed antenna in [22].

considering the source current distributions and its magnitude and phase. Some baseline design is selected and then different structure parameters are altered to acquire the desired current distribution. The design should be optimized without changing the frequency response and impedance bandwidth of the antenna significantly. The alternate solution is to compensate for the changes in impedance with tunable matching circuits. To avoid the antenna mismatch issues, the feed network can be isolated from the reconfigurable part thus allowing for nearly fixed frequency response with pattern agility [21].

In [22], a beam-steering textile antenna for wireless body area network (WBAN) applications was presented. The coaxially fed antenna was integrated with four RF switches at optimized positions. Different combinations of RF switches were used to tilt the beam at four distinct position. The beam steered angles were 0°, 90°, 180° and 270° . The presented antenna was realized on Felt substrate with size 52×85 mm^2. The radiating elements of proposed antenna were fabricated using Shieldit Super textile as its conductive element with a thickness of 0.17 mm and conductivity of 6.67×10^5 S/m. The proposed design is shown in Figure 2.4 while in Figure 2.5, the simulated results are shown of the steered beam at four different directions.
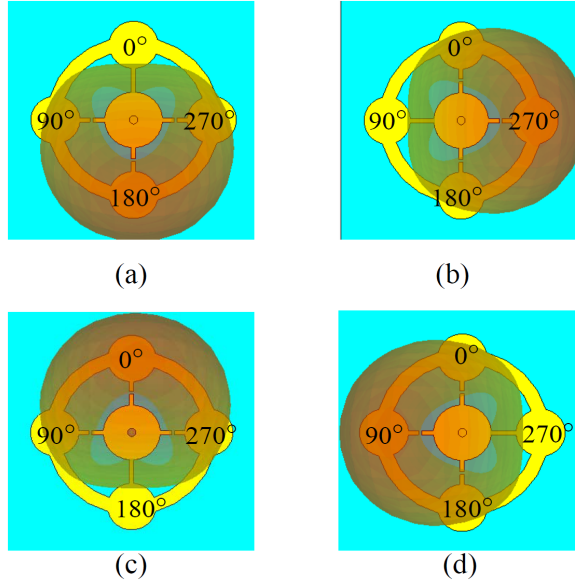
Figure 2.5: Simulated 3D pattern of PIN diode configurations (a) Beam tilted at 180° (b) Beam tilted at 270^o(c) Beam tilted at 0^o(d) Beam tilted at 90° [22].

2.3 Evaluation of the Performance of MIMO Antenna Systems

MIMO systems are an important part of modern communication. The front-end of a MIMO system is the MIMO antenna. Therefore the design and performance characteristics of this antenna is important and directly affect the overall system performance. Thus, an optimum design is required to achieve the minimum acceptable performance metrics within compact size and suitable for wireless hand-held devices. The MIMO system can provide improved performance in multipath and non-line-of-sight (NLOS) environment.

Performance evaluation of MIMO antenna systems is critical and crucial. The conventional parameters of an antenna's performance like s-parameters and far field radiation characteristics are inadequate. The parameters that are important to characterize a MIMO antenna system include the s-parameters, the radiation patterns, the total active reflection coefficient (TARC) [23], the mean effective gain (MEG) [24], the correlation coefficient [25] and the channel capacity [26].

2.3.1 Resonance and Isolation

The scattering parameters or s-parameters is a measure of antenna performance that gives information about its resonance, bandwidth and isolation between various elements in an array. This basic definition applies to MIMO systems as well. In a MIMO system, the same frequency response is expected from all elements with good isolation. The diversity gain of a MIMO system is directly related to the number of uncorrelated channels and efficient paths . Therefore, high isolation (low mutual coupling) is required between antenna elements.

2.3.2 Total Active Reflection Coefficient (TARC)

S-parameters are used to get some preliminary results about antenna resonance but it lacks to completely describe the frequency response especially its effective bandwidth. In order to characterize the MIMO antenna system, a new parameter "Total Active Reflection Coefficient" (TARC) was introduced. It can be defined as the ratio of the square root of the total reflected power to the square root of the total incident power. Mathematically it is expressed as [23];

$$\Gamma = \sqrt{\frac{\Sigma|b_i|^2}{\Sigma|a_i|^2}} \tag{2.1}$$

where b_i and a_i is the reflected and incident signals, respectively. The incident and reflected signals are related to each other by the s-parameter of the MIMO antenna system. They are given as [23];

$$[b] = [S].[a] \tag{2.2}$$

where S is the $N{\times}N$ scattering parameter matrix of the N element MIMO antenna system.

From(2.1), it can be concluded that the TARC values varies between 0 and 1. TARC has a value equal to one when the incident signal is reflected entirely while zero value corresponds to total radiation with no reflection. TARC versus fre-

quency plot gives the effective bandwidth of the MIMO antenna. Usually, TARC is computed in decibels. TARC also gives a measure of the antenna efficiency of a lossless MIMO antenna system. TARC is calculated for different combinations of excitation signals at the input ports. To calculate TARC from the measured s-parameters of an N-element MIMO antenna system, (2.2) is used to calculate the reflected signals. The incident signals are taken with unity amplitude and different phase differences. After calculation of reflected signal, (2.1) is used to calculate the TARC of the MIMO antenna system.

2.3.3 Antenna Efficiency

Antenna efficiency is an important parameter in MIMO antenna systems. It is necessary to know the efficiency of an antenna as it is directly related to diversity and multiplexing gain of a MIMO antenna system. Antenna efficiency can be defined as the sum of its radiation efficiency and reflection efficiency. Reflection efficiency can be computed using the value of s-parameters and TARC while the radiation efficiency cannot be computed from these values. Different methods have been reported in literature to measure radiation efficiency of the antenna [27].

In the gain and directivity method, the ratio of the gain and directivity gives the antenna efficiency. This method involves the measurement of far field radiation patterns of the antenna using anechoic chamber. Wheeler cap method is a simple method of efficiency measurement [27]. This method involves only the measurements of reflection coefficient from the antenna using network analyzer. The procedure of this method is outline here. First the reflection coefficient of the test antenna is measured. Then, the antenna is then placed on a ground plane and covered with a conducting cap and the reflection coefficient of the antenna is measured again. The radiation efficiency is then found using [27];

$$\eta = 1 - \frac{1 - |\Gamma_{cap}|^2}{1 - |\Gamma_{in}|^2} \tag{2.3}$$

The basic principle behind this is that when the antenna is covered by the cap

radiated signal is reflected back to the antenna. So, low loss antennas will have have high reflection at the input while for the lossy antenna, the reflected signal will be small due to losses within the antenna structure.

2.3.4 Correlation Coefficient

The correlation coefficient is a measure of signal correlation received by the MIMO antenna system due to antenna patterns. It is a function of the radiation patterns of the MIMO antenna elements. Mutual coupling between MIMO antenna elements badly affect the diversity performance of a MIMO antenna system. The correlation coefficient (ρ) is the square root of the envelop correlation (ρ_e). The envelop correlation between two antenna elements is computed from their far field radiation characteristics and is given as [25];

$$\rho_e = \frac{|\int \int F_1(\theta, \phi) * F_2(\theta, \phi) d\Omega|^2}{\int \int |F_1(\theta, \phi)|^2 d\Omega \int \int |F_2(\theta, \phi)|^2 d\Omega} \tag{2.4}$$

where F_i is the radiation pattern when element $'i'$ is active.

The value of ρ lies between 0 and 1. The minimum value corresponds to highly uncorrelated antennas while maximum value shows the correlated antenna elements as behaving a single antenna. In the new 4G standards, for a good diversity performance, the value of ρ is required to be less than 0.3 [25]. The calculation of the correlation coefficient is difficult as it involves the radiation patterns of the antenna elements. However, if the MIMO antenna is operating in a uniform multipath environment which is the one where fading envelope is Rayleigh distributed, the incoming field arrives in the horizontal plane only, the incoming fields orthogonal polarizations are uncorrelated, the individual polarizations are spatially uncorrelated, and the time-averaged power density per steradian is constant [28], then the correlation coefficient between two antenna elements can be computed from it s-parameters if the antenna efficiency is also high. It is given as [25];

$$\rho = \frac{|S_{11} * S_{12} + S_{21} * S_{22}|}{\sqrt{(1 - |S_{11}|^2 - |S_{21}|^2)(1 - |S_{12}|^2 - |S_{22}|^2)}} \tag{2.5}$$

2.3.5 Radiation Pattern

The radiation pattern is a measure of the far field strength as a function of space of an antenna. In MIMO antenna systems, the radiation patterns of each element are assumed to be independent with orthogonal directional maximum locations to have high uncorrelated channels. To calculate the radiation pattern of an element of a MIMO antenna, the element is excited by a source and the rest of the antenna elements are terminated with a 50 Ω load. The field patterns are then obtained either by simulation or by measuring them at an antenna testing facility.

2.3.6 Mean Effective Gain

The gain of an antenna is an important parameter of a MIMO system. The mean effective gain (MEG) is a measurement of the coverage area and achievable data rates of the system. The directive gain of an antenna gives misleading results in mobile communication environment. In such scenarios, the MEG of the system is calculated. The MEG of an antenna operating in an urban mobile environment is determined by the mutual relation between the field patterns of the antenna and the statistical distribution of the signal in the environment.

For a mobile wireless environment the MEG of an antenna system can be computed from its two-dimensional field patterns. It is given as [29];

$$MEG = \int_0^{2\pi} \left[\frac{XPD}{1+XPD} E_\theta + \frac{1}{1+XPD} E_\phi \right] d\phi \qquad (2.6)$$

In (2.6) XPD is the cross polarization discriminator. It can be defined as the ratio of the horizontally polarized component to vertically polarized component of the incident signal. The value of MEG is -3 dB for urban environment with 100 % efficient antenna while for practical designs, the value can be as low as -12 dB. The MEG for MIMO antenna system is calculated by finding the field patterns while the other elements are terminated with a load. The MEG of MIMO antenna elements are expected to be the same. For MIMO antenna systems, the difference

of the MEG values should not exceed 3 dB.

2.3.7 Channel Capacity

A MIMO system is used to increase the channel capacity by utilizing the multiplexing gain. The design of a MIMO antenna has profound affect on the multiplexing gain of the MIMO system. Therefore, the antenna is also evaluated for the upper limit of channel capacity it can give in a particular environment. For this, either measurements are carried out in a real environment or theoretical models are used which predict the performance of the antenna based on the radiation characteristics of the antenna elements. Recently, reverberation chambers were designed to evaluate the channel capacity and other performance metrics of the MIMO antenna [30]. The reverberation chamber emulates an isotropic multipath environment of similar type as of urban or indoor environments. Thus it helps in measuring the MIMO system channel capacities without driving around in the urban environment or moving around in with measurement equipment in an indoor one.

In [26], a channel capacity measurement model of a MIMO antenna system is presented. The channel capacity model is based on the 2D radiation patterns of the antenna. For the same MIMO antenna system at both ends, the channel matrix H is given as [26];

$$H = \sqrt{\Psi} G \sqrt{\Psi} \qquad (2.7)$$

where G is a random matrix with independently identically distributed complex Gaussian entries. Ψ is the transmit and receive correlation matrix. The entries of Ψ matrix are calculated using [26];

$$\Psi_{i,j} = \frac{\mu_{ij}}{\sqrt{\mu_{ii}\mu_{jj}}} \qquad (2.8)$$

$\mu_{i,j}$ is calculated based on the field patterns of antenna element i and j. It is given

as;

$$\mu_{ij} = \int_0^{2\pi} [XPDA_{i\theta}A_{j\theta}^* + A_{i\phi}A_{j\phi}^*]d\phi \qquad (2.9)$$

where A_θ and A_ϕ are the 2D radiation patterns of antenna elements (i,j) in the two planes. Thus, the radiation patterns of the elements of MIMO antenna systems are required in estimating the performance of the antenna in terms of channel capacity when they are used in any environment.

2.4   Six-Port Based Direction Finding

Microwave structure based low cost direction finding (DF) systems have gained popularity over last few decades. Six-port (SP) techniques are widely used in microwave metrology and becoming a key component in low cost RF DF systems. It has a wide range of applications such as in RF DF, precise displacement measurement, direct conversion receivers, and in radar sensors.

The SP circuit was initially used as a low cost alternative to network analyzers. Most of the work carried out in area of RF direction finding (DF) using the SP started in late 90's. A number of SP circuits were designed to be used in beam direction finding systems. All these systems are used to find the azimuth angle of a distant target object (i.e. a single angle for the incoming wave) [31].

In modern wireless systems, it is highly desirable to achieve dual or multi-band operation using a single circuit. DF systems using SP cover many frequency bands and have been used in different scenarios. Most of the proposed SP DF systems in literature use a single SP circuit for angle of arrival (AoA) estimation in one plane and also operate at frequencies higher than 2 GHz.

The details of the SP structure and operating conditions for direction finding and deriving the equations for its dual angle results and its application are discussed in details in chapter 6.

2.5 Conclusions

In this chapter, the theoretical background for the front end and antenna system of a end of CR platform were discussed. The two important front-end antenna elements are the UWB sensing antenna and the reconfigurable communicating antenna. Several examples for both antenna types were given. To increase the throughput of the communication system, MIMO reconfigurable antennas are used as communicating antennas. MIMO antennas are characterize using MIMO parameters performance metrics were discussed in details. RF DF using the microwave SP technique was also discussed in the last part of this chapter.

CHAPTER 3

LITERATURE SURVEY

The Cognitive Radio (CR) is an emerging radio architecture technology that appeared in literature in 1999 [32]. The concept of a CR in a communication system is based on dynamic and opportunistic spectrum utilization. It was aimed to efficiently utilize the available bandwidth to save available resources. The two essential antennas for CR applications are the sensing antenna and the communication antenna. The hierarchy of the antennas used in CR platforms is shown in Figure 3.1 and are categorized as follows .

1. Sensing Antenna

    (a) Monopole Antenna

    (b) Dipole Antenna

2. Communication Reconfigurable Antenna (Using PIN diode, Varactor diode, metamaterial (MTM), MEMS switches)

    (a) Reconfigurable Antenna

    (b) Reconfigurable MIMO Antenna

This chapter will cover the literature review for sensing and reconfigurable MIMO antenna systems for CR platforms as well as RF based DF systems using the SP technique.
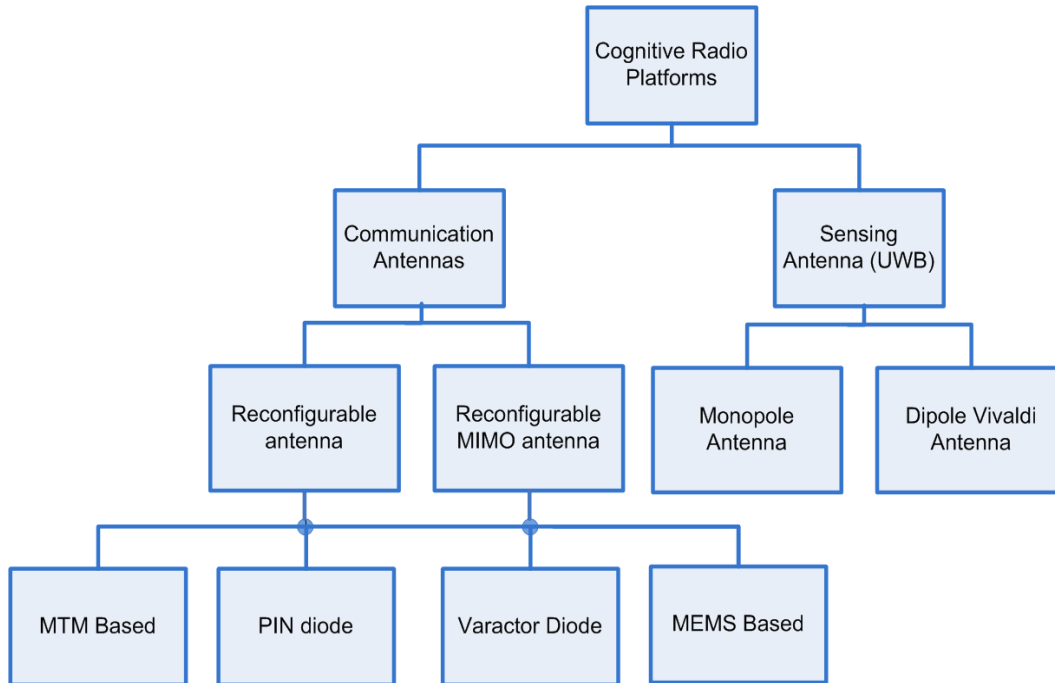
Figure 3.1: Classification of CR Antennas.

3.1 Sensing Antennas for CR

Two types of antennas are generally employed to get the ultra-wide-band (UWB) sensing antenna in CR platform. These two antenna types are the dipole and monopole. A summary of main references of sensing antennas based on their starting frequency (f_s) are given in Figure 3.2.

3.1.1 Dipole Antenna as a Sensing Antenna

Dipole antennas are the most widely used for UWB operation with high efficiency. A Vivaldi antenna is a printed version of a dipole antenna and is popular in CR platforms for its compact printed structure and UWB operation. The main benefits of Vivaldi antennas are their broadband characteristics and easy fabrication in its planar printed structure form. Vivaldi antennas are fed by microstrip lines and can be matched with ease.

A number of Vivaldi antennas appeared in literature [33–43]. In [33], a printed Vivaldi type antenna was presented with UWB characteristics starting from 3.1 GHz to 10.6 GHz and is shown in Figure 3.3. The design was realized on a Roger
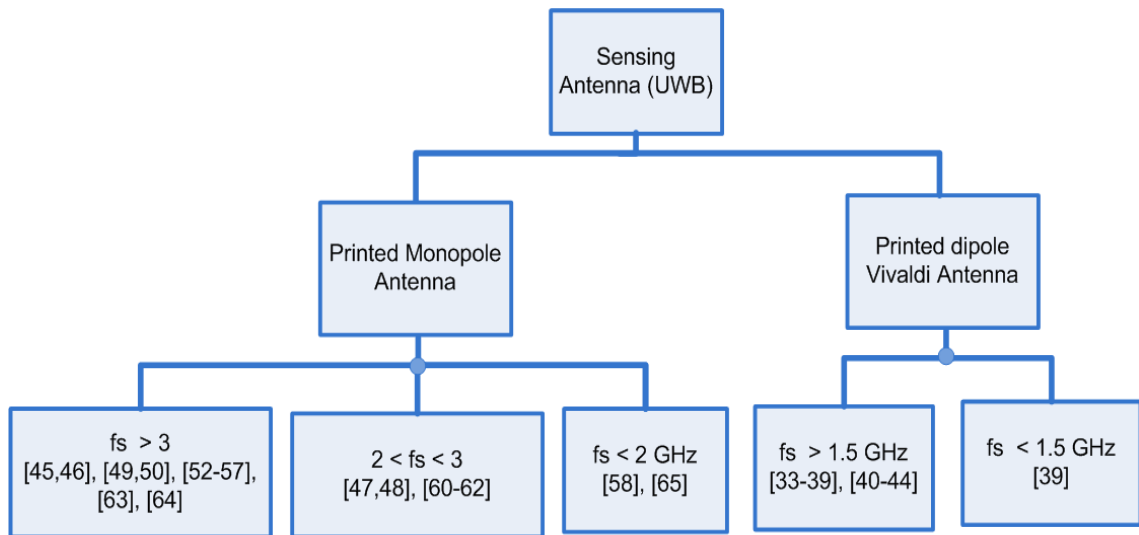
Figure 3.2: Classification of Sensing Antennas.
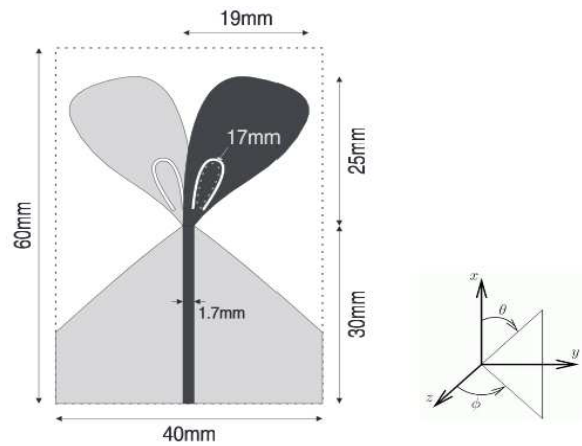
Figure 3.3: Geometry of Vivaldi antenna with U-shaped slot [33]

RO4350B substrate having a thickness of 0.762 mm with a total area equal to 38×60 mm^2 and $\epsilon_r = 3.48$. In addition, a U-shaped slot was introduced in the structure to mitigate the interference between WLAN band and UWB operation.

In [34] a printed antipodal Vivaldi type antenna was presented with UWB characteristics from 3.1 GHz to 10.6 GHz. This design was intended to radiate or receive short pulses in UWB range with little distortion and hence getting minimal error and high data rate. In [35], a circuit method approach was presented to design UWB Vivaldi antenna from 3.1 GHz to 10.6 GHz. The proposed method was a systematic approach to design the parameters and variances to the Vivaldi antenna in the given frequency bands. A small size antipodal Vivaldi antenna with dimensions 43×25 mm^2 was presented in [36]. The proposed antenna covered frequency bands from 3.1 GHz to 10.6 GHz. The small structure of the design made this suitable to be integrated with other planar structure.

In recent years, additional features were being added with UWB Vivaldi antenna. In [37], a compact, novel antipodal Vivaldi antenna was presented. The same design was loaded with split ring resonator (SSR) to reject any interference in the $5 \sim 6$ GHz band of UWB antenna and is shown in Figure 3.4. The size of the proposed antenna was 35×32 mm^2. In [38], a modified anti-podal antenna was presented covering a frequency band from $4 \sim 50$ GHz. The proposed design is shown in Figure 3.5. The size of the proposed antenna was 64×64 mm^2.

In [39], a low frequency band vivaldi type antenna was presented for wideband operation. The proposed design was working from $1 \sim 3.2$ with antenna size equal to 140×144 mm^2. The proposed design in shown in Figure 3.6.
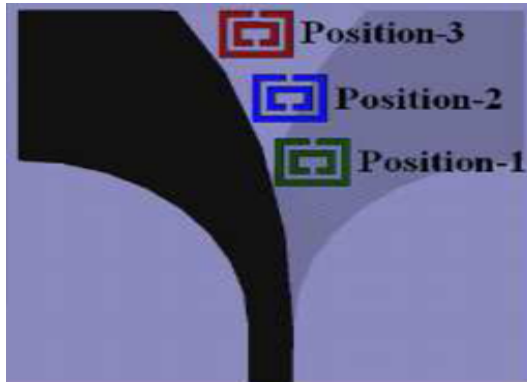
Figure 3.4: SRR loaded antipodal Vivaldi antenna [37].
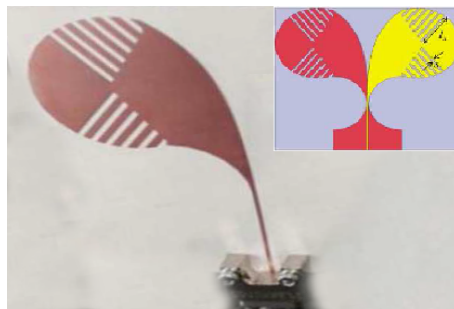
Figure 3.5: Geometry of Modified Vivaldi antenna [38]
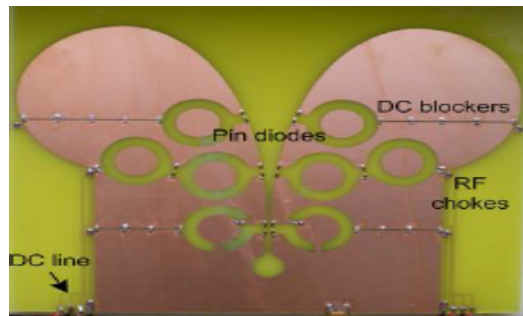
Figure 3.6: SRR loaded antipodal Vivaldi antenna [39].

In [40], a broadband dipole antenna was presented covering a frequency band from 2.4 ∼ 4.02 GHz for CR application. The same antenna was employed in 2 × 2 MIMO antenna system. The geometry of the proposed design is shown in Figure 3.7. The proposed broadband dipole was a high gain antenna with good cross polarization characteristics. The size of the proposed antenna was 85× 15

33
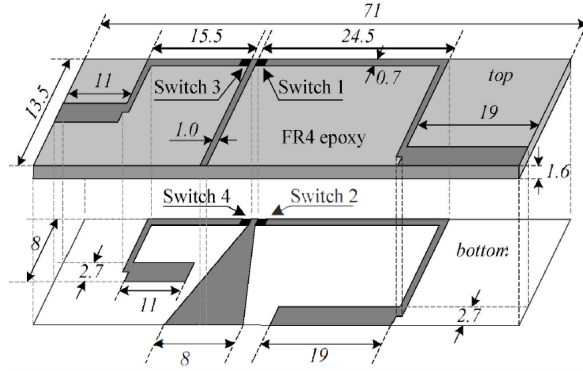
Figure 3.8: Geometry of UWB dipole [44].

mm^2. In [44], a dipole antenna was proposed covering a frequency band from 2.41 ~ 6.88 GHz and is shown in Figure 3.8 . The same antenna was used as a radiation agile antenna by controlling the flow of current in various branches of proposed structure. Two parasitic branches were connected through switches to the dipole. By switching the current by means of RF switches, the flow of current also changed which result in radiation pattern. The size of the proposed antenna was 71× 13.5 mm^2.
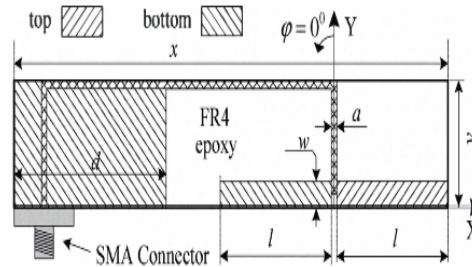
Figure 3.7: Geometry of broadband dipole antenna [40]

Printed dipole antennas are a good choice to achieve UWB operation and can be integrated in CR platform as sensing antenna. The recent trends in CR application is embedding multifunction antennas within the same UWB structure. All of the aforementioned work covered bands higher than 1.5 GHz except [39], that had a size of 140×144 mm^2.

3.1.2 Monopole Antenna as a Sensing Antenna

Monopole antennas are popular and widely used because of their high radiation efficiency and UWB operation. The printed version of a monopole is very popular in CR platforms as the sensing antenna. The key features of printed monopoles are their UWB operation, ease of fabrication, simplicity and ease of integration with other planer structures used in CR platform. The microstrip feed to printed monopoles can be optimized for input impedance matching of the antenna. To meet the various frequency band requirements UWB antennas are designed with different structure shape, and size along with bending or meandering.

A number of monopole antenna designs for CR applications were presented in literature. Most of available designs cover frequency bands above 1.5 GHz. Several UWB monopole designs are available covering frequency bands from 3∼10 GHz [45–57]. This is the most commonly used band found in literature for sensing antennas in CR applications. Different shapes of monopoles have been reported in literature to achieve the UWB operation. The commonly used shapes for monopoles are oval shape [45], wine-glass shape [47], fork shape [48], polygon shape antenna [49], hour-glass shape [53], oval [58] and egg shape [59] covering frequency bands from $3 \sim 10$ GHz. Generally, the oval shape design or some of its varient have been used in these antennas for covering the $3 \sim 10$ GHz band.
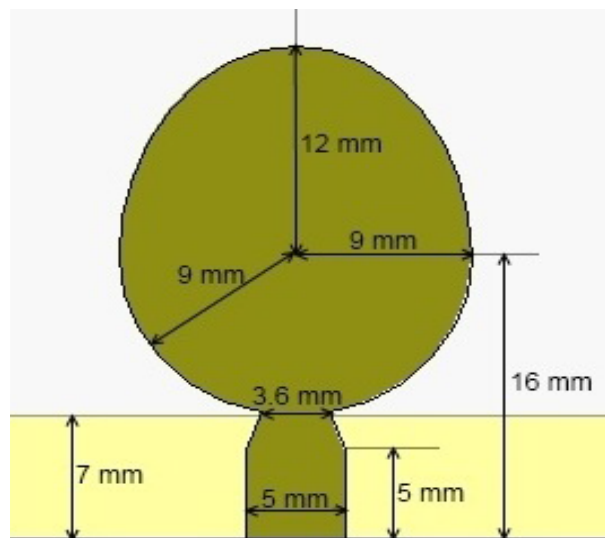
Figure 3.9: Ovel shape UWB monopole antenna [45]

An oval shape antenna was presented in [45] and is shown in Figure 3.9. The proposed antenna covered a frequency band from $3 \sim 11$ GHz with a total size equal to 30×30 mm^2. The microstrip-line fed printed monopole is realized on a Taconic TLY substrate with thickness 1.6mm with ϵ_r equal to 2.2. In [46], an UWB monopole antenna was presented with overall dimensions of 65.5×58 mm^2 and is shown in Figure 3.10. In [47], an UWB monopole antenna was presented with compact size with overall dimensions of $34 \times 31 \times 0.88$ mm^3 and is shown in Figure 3.11. This design was unique in a sense that the same UWB band antenna was made reconfigurable using PIN diodes. The switching from UWB to narrow band operation resulted in radiation pattern reconfigurability. This antenna used the same feed line that was used fo the reconfigurable part of antenna.
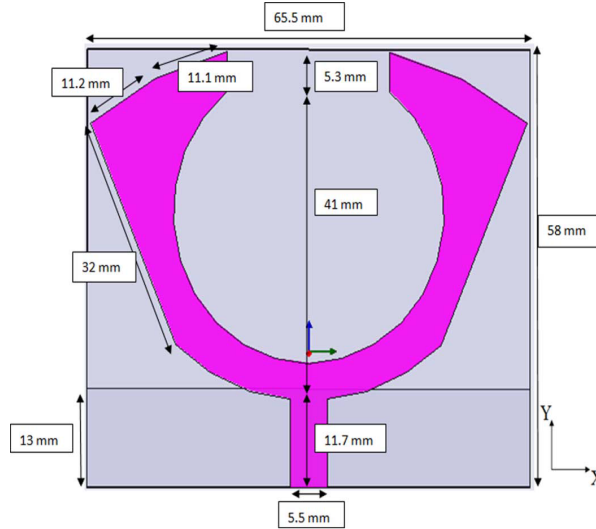
Figure 3.10: Modified ovel shape UWB monopole antenna [46]

In [60], a monopole sensing antenna was presented covering the frequency band $2\sim5.5$ GHz. The sensing antenna and reconfigurable antennas were embedded within the same structure with a total dimension of 100×47 mm^2. A miniature UWB antenna was presented in [61] with total size 55×50 mm^2. The UWB covered $2\sim10$ GHz.

A relatively low frequency design of UWB was presented in [58]. This design covered the frequency band from $1.5\sim12$ GHz and is shown in Figure 3.12. Several UWB monopole design were also reported in literature with different bands from
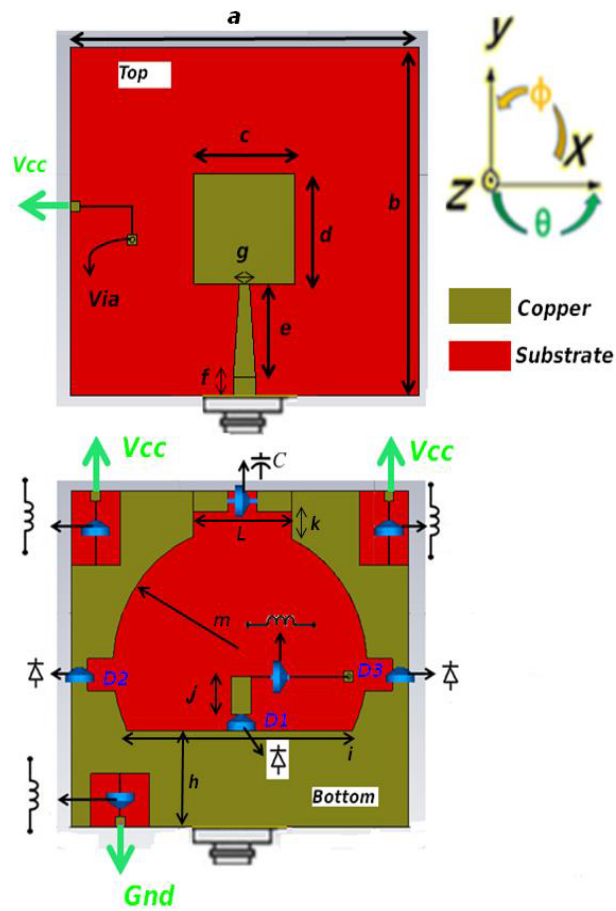
Figure 3.11: Geometry (top and bottom) of the proposed reconfigurable ultrawideband antenna [47].
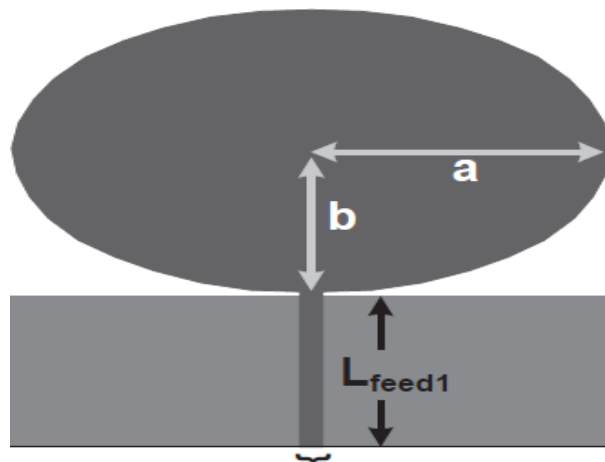
Figure 3.12: Geometer of UWB antenna antenna [58].
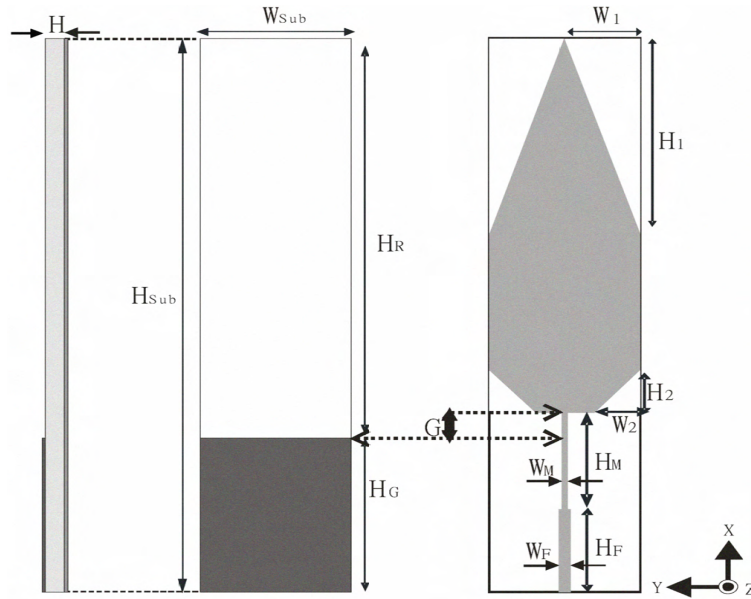
Figure 3.13: Geometer of UWB antenna [65].

2∼14 GHz [62–64]. In literature, most of the the designs covered frequency bands above 1.5 GHz. Only the single design was found in literature to operate below 1.5 GHz [65]. This is mainly because of the size limitation of wireless devices that cannot accommodated large antennas working in lower bands of operation. In [65], a printed monopole was presented covering a frequency bands from 530 ∼ 3000 MHz as shown in Figure 3.13. The over all size of the antenna was 200× 40× 1.6 mm³. The design was realized on FR4 substrate with a relative dielectric constant of 4.4. The frequency bands covered by this antenna were the DVB band (530 ∼ 860 MHz), GSM band, (890∼ 960 MHz), DCS band (1710∼ 1880 MHz), PCS band (1850∼ 1990 MHz), UMTS band (1920∼ 2170 MHz) and WLAN band (2400 ∼ 2484 MHz) [65]. This antenna is prohibitively large that is why it is practically useless.

3.2 Methods of Achieving Reconfigurability

Generally, the basic reconfigurable parameters controlled in printed antenna structures include,

1. Frequency Reconfigurable Antenna

2. Polarization Reconfigurable Antenna

3. Radiation Pattern Reconfigurable Antenna

The methods or components that are employed for achieving reconfigurability are:

1. Varactor Diodes

2. PIN Diodes

3. RF MEMS

4. Metamaterial Based structures

5. Other types

Figure 3.14 shows the classification of reconfigurable antennas available in literature. Each of the major reconfigurable parameters will be discussed in details in the following sections.
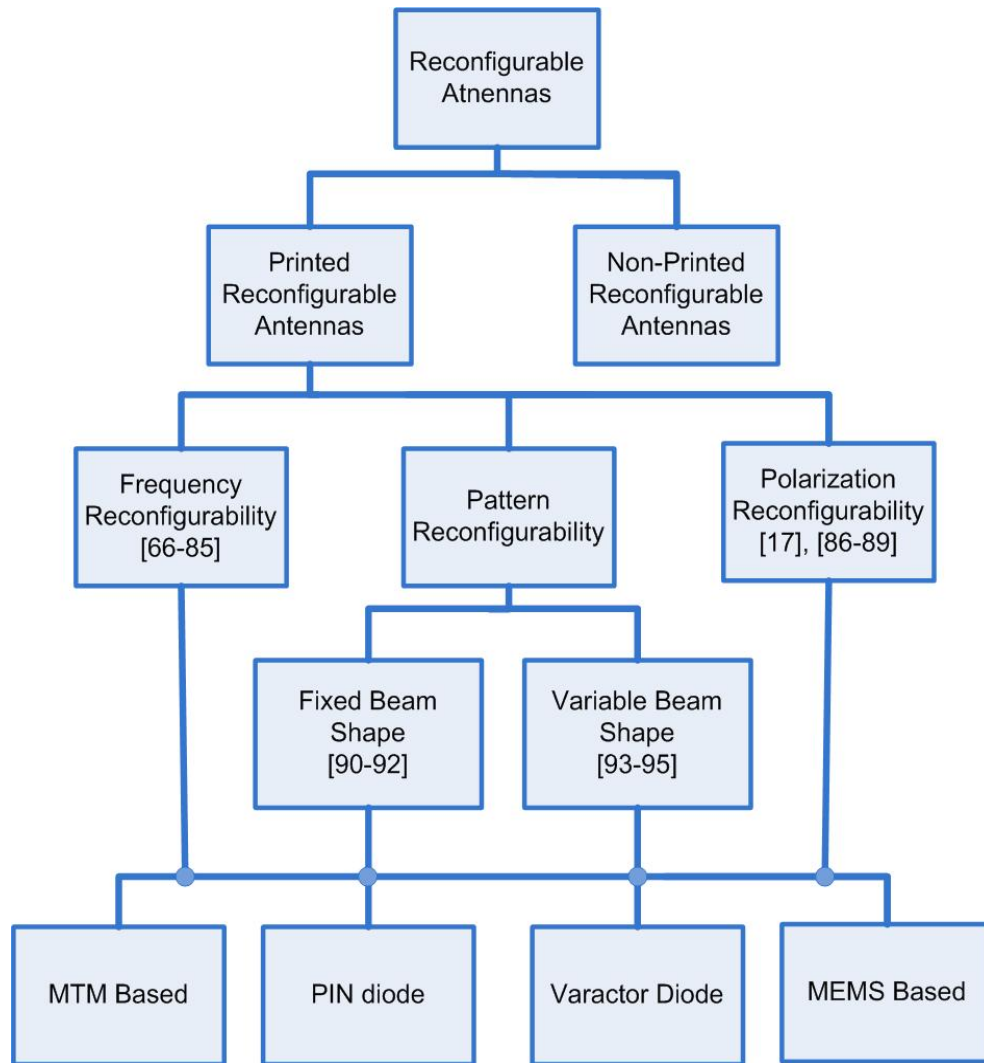
Figure 3.14: Classification of reconfigurable antennas.

3.2.1 Frequency Reconfigurable Antennas

Frequency reconfigurable antennas are those whose operating frequency or bands of frequencies covered can be changed or controlled. This allows such antennas to cover several narrow bands of various standards. A summary of frequency reconfigurable antenna based on the frequency of operation are categorized in Figure 3.15.
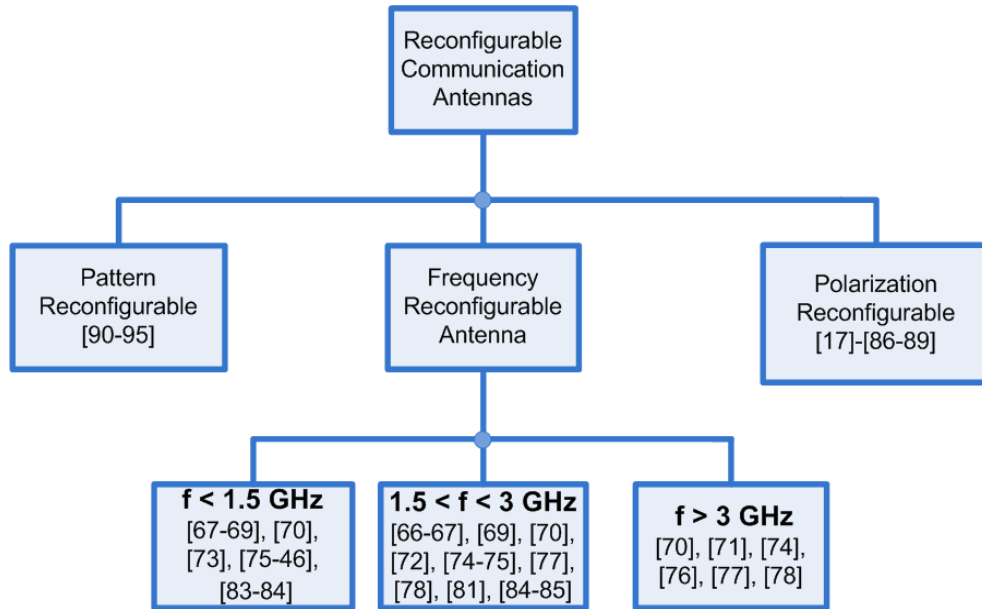
Figure 3.15: Classification of reconfigurable antennas.

In [66–72], varactor diode based frequency reconfigurable communication antennas were presented. Most the proposed designs cover frequency bands from 0.5 ∼ 5 GHz. In [66], a compact monopole design with F-slot was proposed that was loaded with varactor diodes for frequency tuning and is shown in Figure 3.16. The covered frequency bands were DCS, PCS, and UMTS. The frequency tuning can be obtained in 1.70∼2.15 GHz. An F-shaped slot is embedded in a rectangular monopole patch to accommodate the varactor. The size of the proposed design was 50×37.5 mm^2. In [67], dual band frequency reconfigurable slot antenna was presented. Varactor diodes were used to load this antenna. With this setup, a frequency reconfigurable antenna was achieved working in the band of 1.3∼2.67 GHZ. The size of the proposed design was 150×150 mm^2. In [68], a frequency and polarization reconfigurable microstrip patch antenna was presented. A number of small patch antennas were connected by varactor diodes. By controlling the bias voltage of the varactor diodes, frequency and polarization reconfigurability was achieved. The operating range of this antenna was 890∼ 1500 MHz. The size of the proposed design was 70×70 mm^2.

In [69], a compact frequency reconfigruable antenna was presented for mobile devices. The proposed antenna was a varactor loaded PIFA for frequency diver-
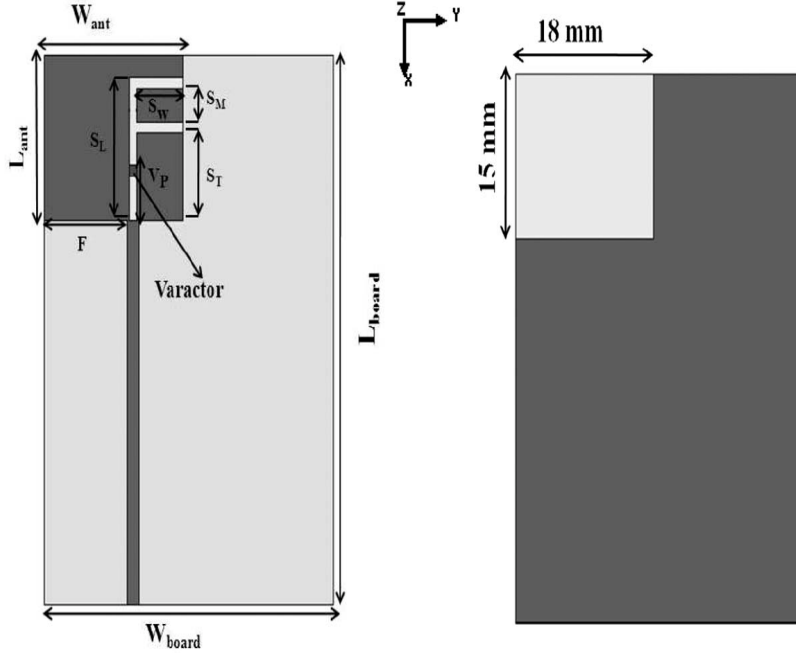
Figure 3.16: Geometry of F-slot monopole antenna [66].

sity. The proposed antenna for single band operation was tunable from 1.6 ∼2.3 GHz while dual band operation was achieved from 780∼1020 MHz and 1700∼2140 MHz. The size of the proposed design was 80×50 mm^2. In [70], a compact frequency reconfigurable PIFA was presented. The proposed antenna was loaded with varactor diodes working in the frequency bands from 0.7 GHz, 2 GHz, 3.5 GHz and 5 GHz The size of the proposed design was 50×40 mm^2. In [71], a semicircular microstrip antenna was proposed as frequency reconfigurable antenna. The proposed design was covering frequency bands from 0.5 ∼ 0.9 GHz and 2.1∼ 2.3 GHz. The size of the proposed design was 50×30 mm^2.

In [73–80], PIN diode based reconfigurable antenna were presented. In [73], a reconfigurable PIFA antenna was proposed to achieve frequency reconfigurable antenna. In the proposed antenna, two PIN diodes were used to get quad-band of GSM900/GSM1800/GSM1900/UMTS). The size of the proposed design was 45×75 mm^2. In [74], a high efficiency frequency reconfigurable antenna based on PIN diode was proposed operating at 2.45 GHz and 5.8 GHz. The size of the proposed design was 70×70 mm^2. In [75], reconfigurability of a compact inverted-F antenna with switchable feeds was presented. The proposed antenna acquired
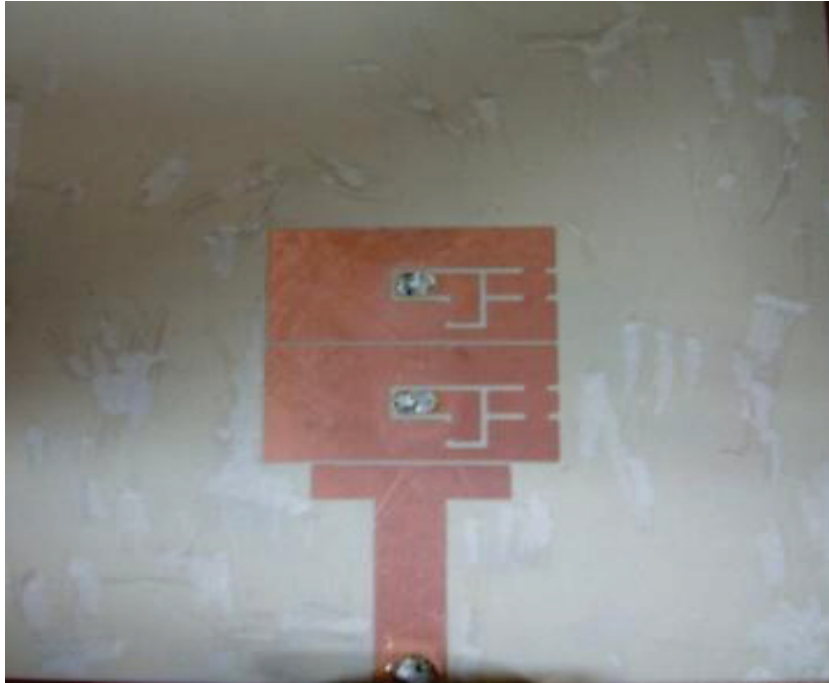
Figure 3.17: Geometry of MTM based frequency reconfigurable antenna [81].

bands of GSM850 (824∼894 MHz), GSM900 (890∼960 MHz), DCS (1710∼1880 MHz), and PCS (1850∼1990 MHz). The size of the proposed design was 50×70 mm^2. In [76], a C-slot patch antenna was proposed. The proposed antenna was working in dual-band mode and a wideband mode from 5 ∼7 GHz. The size of the proposed design was 50×50 mm^2.

Metamaterial based reconfigurable antenna were proposed in [81, 82]. In [81], metamaterial (MTM) based frequency reconfigurable design was proposed. A mushroom structure-based zeroth order resonant (ZOR) antenna was used to realize the proposed design. The frequency of reconfigurability was achieved from 2 GHz ∼ 2.25 GHz. The proposed design is shown in Figure 3.17. In [82], MTM inspired antennas was investigated for reconfigurability. The proposed antenna was frequency reconfigurable covering frequency range form 1.6 ∼ 2.23 GHz. The total dimension of the proposed design was 30×30 mm^2.

MEMS switches based frequency reconfigurable antennas were presented in [83–85]. In [84], frequency-reconfigurable mobile terminal antenna design was presented. with a tuning range of one octave is presented. The design was tuned using MEMS switches. The reconfigurable bands covered by this antenna were
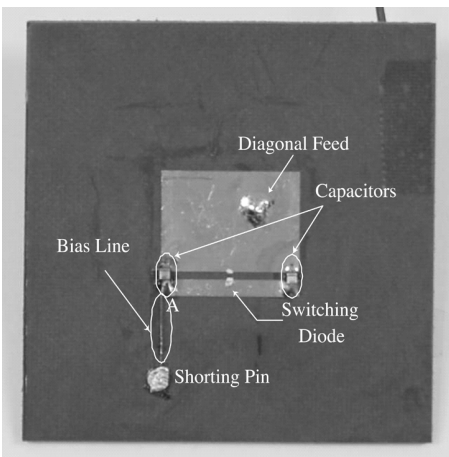
Figure 3.18: Photograph of a fabricated RH and LH circularly polarized antenna prototype [86].

GSM/900 and GSM/1800. The total dimension of the proposed design was 40×98 mm^2.

3.2.2 Polarization Reconfigurable Antennas

In a polarization reconfigurable antenna, the polarization can be controlled to support various polarization modes of operation. Several number of polarization reconfigurable antennas have been reported in literature [17, 86–89]. In [17], dual polarized reconfigurable antenna was proposed. The reconfigurability in antenna structure was achieved by creating L-shape slot in ground structure with PIN diode for switching to connect various parts of the antenna. The proposed antenna was working at 5.8 GHz. The proposed design size was 20×35 mm^2. In [86], polarization reconfigurable microstrip antenna was presented. Reconfigurability was achieved by a coupling slot and the open stub of the feed line by PIN diodes. PIN diodes were used for switching to achieve vertical and horizontal polarizations. The size of proposed design was 100×100 mm^2 and is shown in Figure 3.18.

In [87], single patch antenna was proposed as polarization reconfigurable antenna. The antenna exhibited right-handed circular polarization at 4.2 GHz while left-handed circular polarization was achieved at 4.55 GHz. The size of proposed design was 60×60 mm^2. In [88], right-hand circular polarization (RHCP) and left-hand circular polarization (LHCP) were achieved using novel reconfigurable

coplanar waveguide (CPW)-fed square slot antenna. Switching between antenna Reconfiguration were obtained using PIN diodes. The proposed design was working at frequency band from $2 \sim 3$GHz with size of the substrate used was 50×50 mm^2. In [89], a polarization reconfigurable slot antenna was proposed to achieve vertical and horizontal polarizations. The proposed design was working at frequency band from $610 \sim 680$ MHz with size of the substrate used was 86×70 mm^2.

3.2.3   Radiation Pattern Reconfigurable Antennas

In literature, two types of radiation pattern reconfigurable antenna are reported.

1. Radiation Pattern Reconfigurability with Fixed Beam Shape

2. Radiation Pattern Reconfigurability with Variable Beam Shape

In [90–92], a radiation pattern reconfigurability with fixed beam shape is reported while in [93–95], radiation pattern reconfigurability with variable beam shape were presented. In [90], pattern and frequency reconfigurable microstrip antenna was proposed working at around 3.7 GHz band. The proposed design is shown in Figure 3.19. The proposed design was was working at two frequency bands. At 3.7 GHz, the proposed design was exhibited radiation pattern of normal patch antenna while at 6 GHz, the broadside patterns was observed. The proposed antenna was realized on substrate with size 25×25 mm^2.

In [91], dual reconfigurable antenna was proposed. It was working as frequency reconfigurable antenna and direction of radiation pattern was made controllable using PIN diodes. The proposed antenna maximum radiation direction shifts between $\pm35^o$ with respect to broadside while maintaining a constant VSWR bandwidth and center frequency. The size of the proposed design is 50×50 mm^2. In [92], PIN diodes were used to to make the annular slot antenna as radiation pattern reconfigurable at 5.8 GHz.

In [93,94], printed antennas were presented. These two antennas were radiation pattern reconfigurable. The proposed antennas were working as omnidirectional
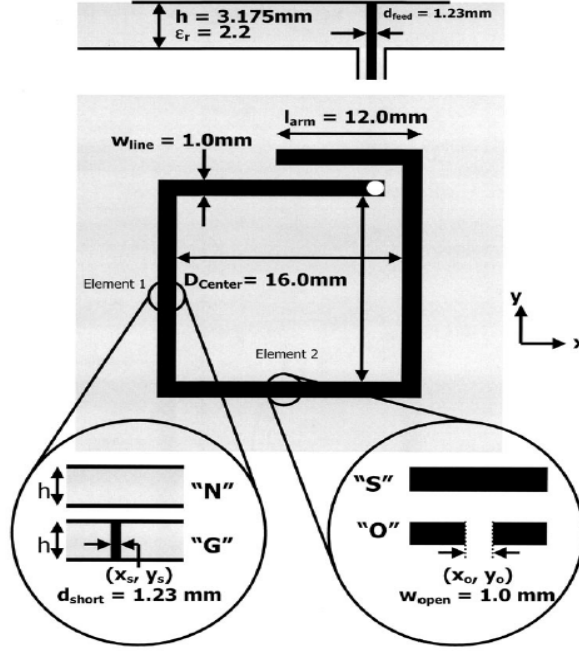
Figure 3.19: Pattern reconfigurable antenna Geometry with fixed beam width [90].

and directional pattern reconfigurable antenna. In [95], a horizontally polarized reconfigurable microstrip antenna was proposed. The RF switches were used to steer the beam in the desired direction or suppress the beam in particular direction. The size of the proposed design is 65×65 mm^2.

3.3 Reconfigurable MIMO Antenna Systems

The requirements of high data rate and dynamic configuration of antenna parameters in wireless handheld devices resulted in investigation of reconfigurable MIMO antenna systems. A number of research papers have been reported in this area. An attempt is made to classify MIMO printed reconfigurable antenna based on their types and frequency ranges they cover. A detailed diagram is shown in Figure 3.20.

In [96], a printed reconfigurable 2×1 MIMO system based on dipole antennas was presented. The length of the dipole antenna was changed to achieve the reconfigurability using PIN diodes. The two operating bands of 2.3 GHz and 3.5 GHz were achieved using this antenna setup with a total size of 66×38 mm^2.
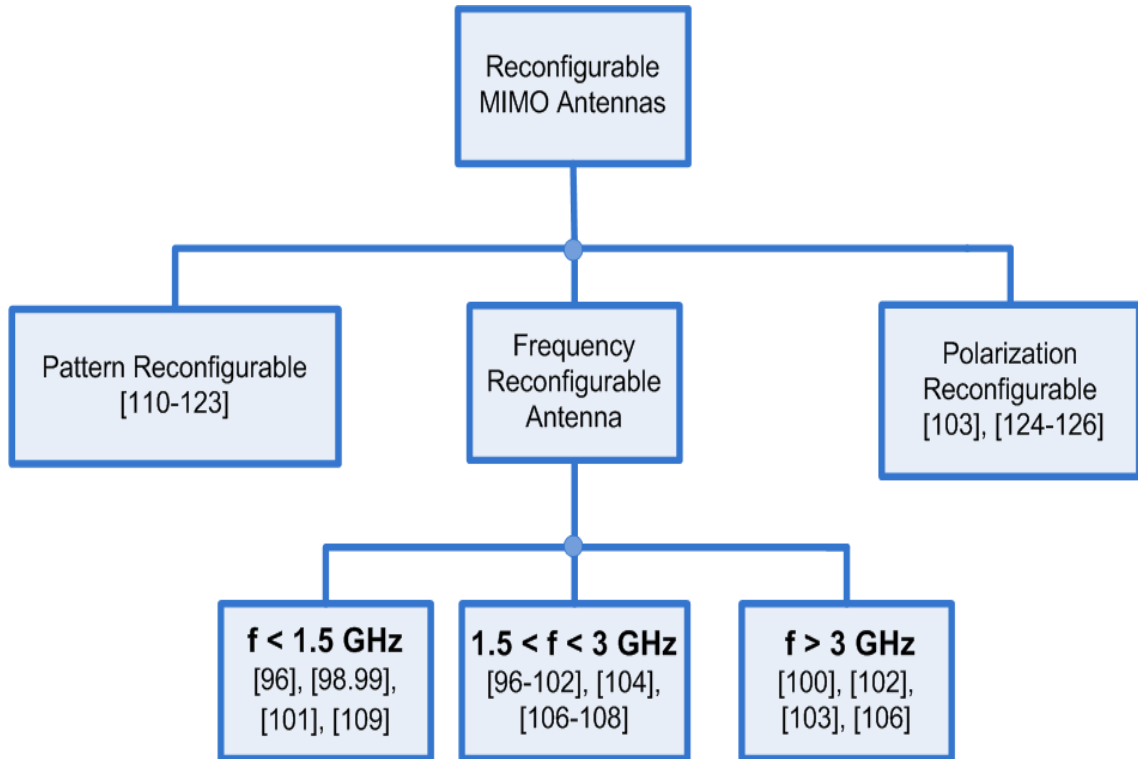
Figure 3.20: Classification of reconfigurable MIMO antenna.

A printed fractal tree antenna was proposed in [97] to improve the data rate in a MIMO system. The proposed design was flexible for its various parasitic lengths to be added to the fractal tree, thus improving the diversity pattern. The proposed antenna was working in the frequency band of $1.7 \sim 2.6$ GHz depending on the switch position. The channel capacity measurement was carried out and showed the data rate improvement in the proposed design. Figure 3.21, shows the channel capacity measurement of such design. This shows that improvement of channel capacity of 2×2 MIMO link using pattern diversity.

In [98], a dipole-chassis antenna was utilized in a 2×1 MIMO system. In this type of antenna structure, the coupling elements are displaced from the handset chassis, thus the mobile handset chassis is also working as a radiating element. Varactor diodes were used to tune the antenna. Two frequency bands of 646 $\sim$ 848 MHz and 1648 $\sim$ 2074 MHz were tuned successfully with a reasonable bandwidth. The size of the proposed antenna was 118×40 mm^2 and is shown in Figure 3.22. In [99], 2×1 MIMO antenna was presented. The design was realized
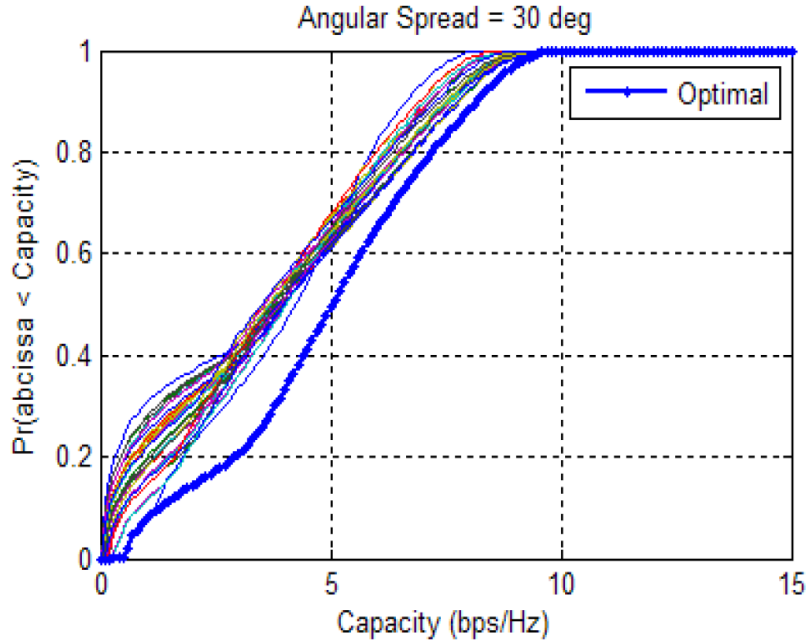
Figure 3.21: Channel capacity measurements [97].

on FR4 substrate with height 1.6 mm. With the frequency reconfigurable MIMO antenna, the achieved frequency bands were 860 MHz, 1900 MHz and 2400 MHz. In [100], printed frequency reconfigurable MIMO was presented. The frequency bands covered by this design is WLAN band (2400 $\sim$ 2483 and 5150 $\sim$ 5350 MHz) and the m-WiMAX band (3400 $\sim$ 3600 MHz). PIN diodes were used to tune the antenna in different bands. The proposed MIMO array was highly isolated with isolation less than-20 dB and correlation coefficient is less than 0.25 in all bands. The diversity performance was evaluated by the correlation coefficient and mean effective gain and showed excellent values. In [101], portable MIMO-LTE antennas with high Q were proposed that can be accommodated in different wireless handheld devices. The frequency reconfigurability was achieved using a varactor diode. The frequency bands are 796 MHz and 2.3 GHz.

In [102], frequency reconfigurable inverted-F antenna (PIFA) was proposed for MIMO application. The PIN diodes were used to achieve the frequency tuning in different bands. The available bands by this design are 2.3$\sim$2.4 GHz, 2.5$\sim$2.7 GHz, and 3.4$\sim$3.6 GHz. The isolation was improved in MIMO system by creating a slot between the different MIMO elements. The isolation was less than -30
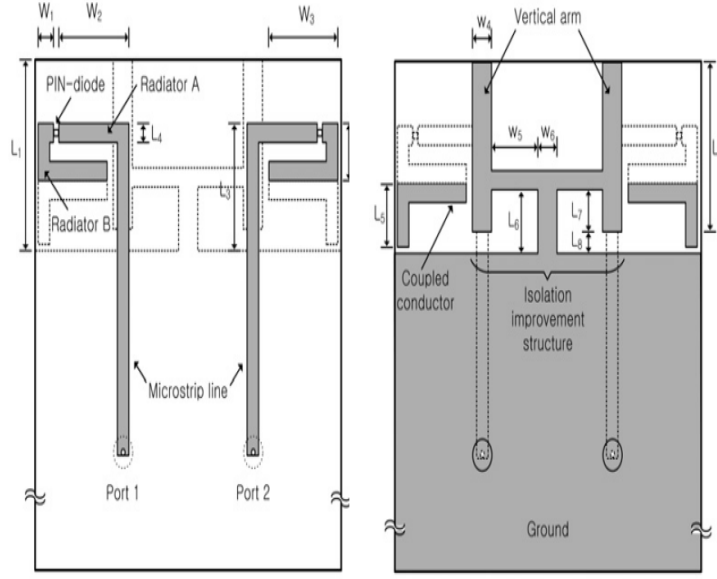
Figure 3.22: Frequency Reconfigurable MIMO antenna system [98].

dB which results in improved performance of MIMO antenna system. The two elements were put on a dielectric substrate of size 90×50 mm^2.

The antenna elements of the MIMO systems in [96–103] were reconfigured for frequency diversity by using the most commonly technique of reconfigurability i-e either by PIN diode or using the varactor diode.

MEMS based technology is another commonly used technique for frequency agile antenna. A number of MEMS based reconfigurable antenna are reported in literature operating a different frequency bands [104–109]. MEMS based reconfigurable antenna was proposed in [104]. The proposed antenna was targeting WiMax applications, used electro-mechanical switches (MEMS). The antenna was both frequency and radiation pattern reconfigurable. The proposed antenna was multi-functional MEMS-reconfigurable pixel antenna (MMRPA). The proposed antenna was a matrix of 13×13 metallic pixels interconnected through MEMS switches. Each element has a dimension 1.2×1.2 mm^2 and inter-element spacing was 2 mm. A very low frequency band was achieved in [109] using a PIFA based MIMO antenna system. The reconfigurability was achieved using MEMS switches, thus achieving low frequency bands of 160 MHz, 450 MHz and 800 MHz. The proposed fabricated model of the antenna is shown in Figure 3.23. The proposed

49
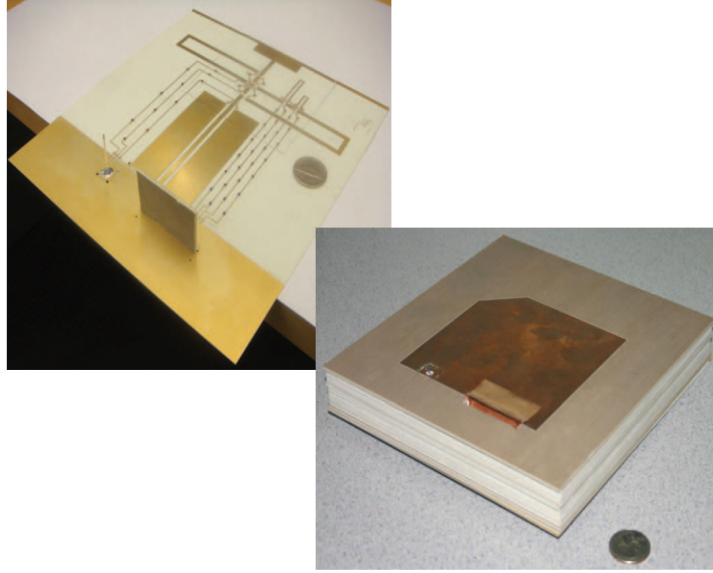
Figure 3.23: Geometry of fabricated MEMS based reconfigurable MIMO antenna [109].

antenna size was 180×195 mm^2.

A large number of pattern reconfigurable MIMO were reported in literature. Pattern diversity of reconfigurable MIMO can be utilized for efficient signal transmission, power saving and in secure communication. In [110], U-slot patch antenna was presented for MIMO application. U-slot antenna was connected to shorting posts using PIN diodes is shown in Figure 3.24. By position of different switches, the antenna exhibit different radiation pattern at same resonating frequency of 5.32 GHz. The size of the proposed antenna was 12×12 mm^2. Similarly, the design proposed in [111, 112] were also used 5.3 GHz band for pattern reconfigurability. In [113], radiation pattern reconfigurable MIMO antenna was presented working at 2.3 GHz. Two different radiation pattern were obtained by controlling the biasing voltage of PIN diodes. In [114], circular patch antenna was presented for pattern diversity in MIMO system. The frequency band of operation was 2.4 ~ 2.6 GHz. The radius of circular patach antenna was 4mm. In [115–123], pattern reconfigurable based MIMO antennas were presented. These antennas could be used in the frequency bands from 1.8 ~ 2.4 GHz.

Polarization reconfigurable MIMO antennas are reported in [103, 124–126]. In [124], a new class of MIMO antenna system was defined coined it as multi-
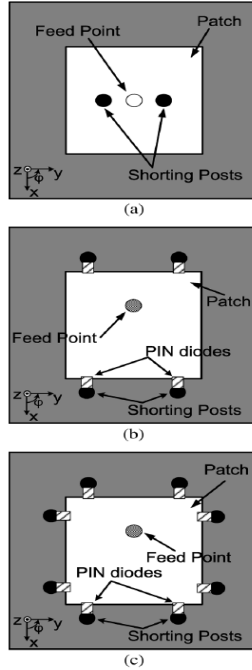
Figure 3.24: Pattern Reconfigurable patch antenna with shorting post and PIN diodes. (a)Reference antenna,(b)antenna with four shorting posts,(c)antenna with eight shorting posts [110].

function reconfigurable antennas (MRAs). This class of antenna were exhibited polarization reconfigurability. The size of the proposed antenna was 30×90 mm^2. In [126], patch antenna was presented to achieve the polarization reconfigurability in MIMO antenna system to improve the capacity. Reconfiguration is achieved by switching in various parts of the antenna into the current path. PIN diodes were used to alter the path of current. The propose antenna exhibited polarization and pattern diversity antenna depending on the switch position in the current path. The size of the proposed design was 51×51 mm^2.

3.4   Antenna Systems for CR Platforms

Over the past few years, reconfigurable antennas for CR applications have been investigated extensively. The focus was either on the design of reconfigurable antennas or reconfigurable communication antennas embedded with the sensing antenna. Most of the designs available in literature for wireless handheld de-

vices are single element non-reconfigurable antennas. However, frequency reconfigurable antennas for communication wireless devices are growing fast over past few years. In [127] frequency-reconfigurable antenna was presented for CR platform in wireless communication devices. The frequency band covered was from 1.64~2.12 GHz. The circular substrate area with radius 94 mm and height 6 mm was used for the said design implementation. In [128] frequency reconfigurable PIFA antenna was presented for m-WiMAX communication systems. The frequency range covered were 2.3~2.4, 2.5~2.7 and 3.4~3.6 GHz. The area of the single element PIFA was 10.5×11 mm^2 on a ground plane area of $90 \times 50 \times 6.4$ mm^3. In [129], a frequency-reconfigurable antenna was proposed for mobile phone application. The proposed PIFA design is embedded with monopole antenna as shown in Figure 3.25. The dimension of PIFA element was $4 \times 36 \times 5$ mm^3 with monopole antenna integrated in the same space. The proposed antenna modeled a folder-type mobile phone with two ground planes with dimensions 40×75 mm^2 and 40×70 mm^2, respectively The frequency bands covered by PIFA were LTE (698~806 MHz) or GSM900 (880~960 MHz) while monopole antenna was used for PCS1900 (1.85~1.99 GHz) and m-WiMAX (3.4~3.8 GHz) or WLAN (5.15~5.35 GHz).

In [130], a single element PIFA was presented for WLAN and LTE bands for wireless handheld devices. The frequency bands covered was 2.1~2.9 GHz. The size of PIFA was $16 \times 33 \times 6.5$ mm^3 with a ground plane dimensions of 45×100 mm^2. In [59], a frequency reconfigurable printed Yagi-Uda dipole antenna with varactor loading for CR applications was proposed covering the lower frequency bands of 400~750 MHz. The total area of this work was 745×360 mm^2. A CR frequency reconfigurable antenna was presented in [131], covering frequency bands between 1.6~2.6 GHz. The total substrate area was 30×41 mm^2. All these designs [59, 127–131] were single element reconfigurable antenna proposed are suitable for CR applications.

Since CR front ends require sensing the frequency spectrum of the environment as well as provide narrow band reconfigurable antenna operation, the wider band sensing antenna along with the narrower band one were proposed in different
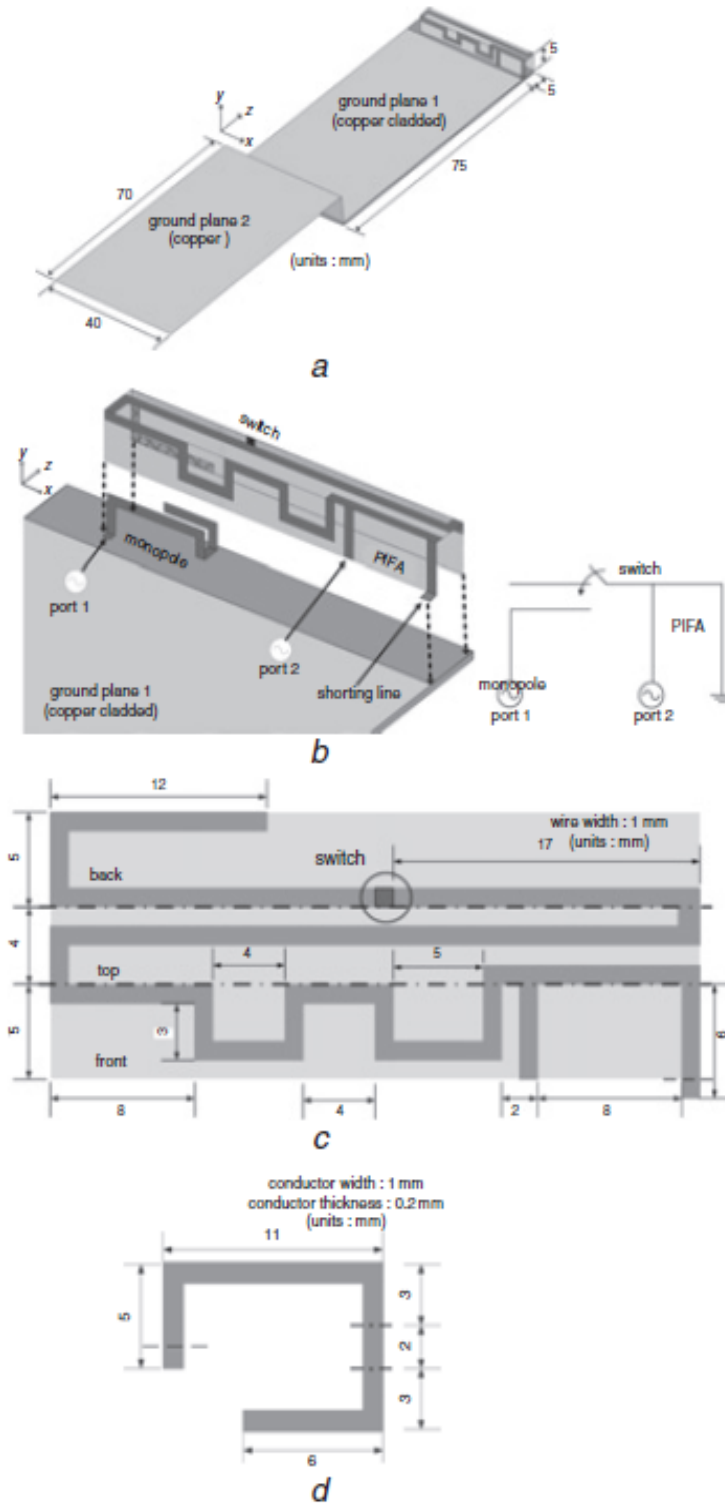
Figure 3.25: Geometry of the proposed antenna [129].

53

ways in literature. In [48], a single optically controlled reconfigurable antenna was proposed for CR platforms. Four bands of operations were achieved, one ultra-wideband mode 2.65∼10.3 GHz and three narrow bands at 3.55∼5.18 GHz, 5.12∼6.59 GHz and 7.10∼8.01 GHz. The total area of the substrate used was 33.54×49 mm^2. In [49], two different structure antennas were presented, one structure was an ultra-wideband (UWB) antenna covering 3.1∼11 GHz and the other was a triangular-shaped frequency reconfigurable antenna. The substrate size of the proposed antenna was 58×65.5 mm^2.

In [132], a dual antenna structure was proposed for CR application with a total substrate size of 50×70 mm^2. The UWB sensing antenna was designed to operate in the frequency range from 2.1∼10 GHz. The reconfigurability was achieved by rotational motion of a stepper motor connecting different radiating parts with input. Five different bands were obtained, 2.1∼3 GHz, 3∼3.4, 3.4∼5.56, 5.4∼6.2 GHz and 6.3∼10 GHz.The design was bulky and not suitable for mobile terminals.

In [52], a combination of a wideband sensing antenna and a narrow band reconfigurable antenna was presented on a single substrate with dimension of 50×50 mm^2. The UWB antenna was covering frequency range from 3∼11 GHz while four cases were observed for the reconfigurable antenna with resonance frequencies, 5.44 GHz, 8.88 GHz, 4.84 GHz, 8 GHz, 4.56 GHz, 7.48 GHz, 3.88 GHz, 6.36 GHz. Several other designs were reported in literature containing both sensing and reconfigurable antennas on the same substrate covering frequency bands above 2 GHz [43, 46, 133].

Two element MIMO antennas with two sensing antennas were presented in [134]. It was operating in the frequency band between 3∼6 GHz with dimensions of 70×80 mm^2. In [135], a reconfigurable MIMO filtenna was presented for CR applications along with sensing antenna for interweave and underlay CR systems as shown in Figure 3.26. The reconfigurable antenna structure was integrated with band-pass filter for interweave system and band-reject filter for underlay system. The antenna reconfigurability was achieved based on the mode of filter. The filter and its integration with antenna is termed as filtenna. The proposed designs were realized on substrate area of 70×80 mm^2 for interweave system and 65×70
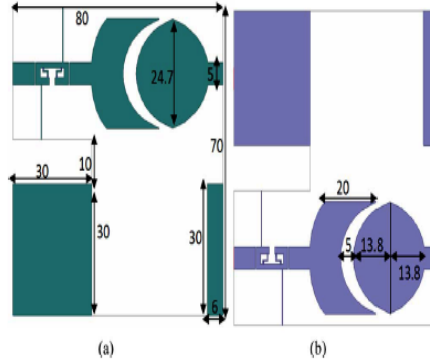
Figure 3.26: (a) The top layer structure of the interweave MIMO based antenna system (b) the bottom layer structure [136]

.

mm^2 for underlay system. Both the sensing and the reconfigurable antennas were designed for frequency range 3~6 GHz.

3.5 SP Based Direction Finding

SP measurement techniques have been available in literature since 1970's while the official birth year of the SP measuring techniques was 1977 when Glenn F. Engen and Cletus A. Hoer published several papers in this area. This was the first time when the comprehensive theoretical background of the six-port reflectometer (SPR) and its operating principle was presented with its optimum design [136–138].

With the advent of SP measurement technique, its calibration was the most important job in microwave metrology. Different approaches were adopted to develop techniques for the calibration of the SP architecture. The calibration becomes simpler if more known standards are used at the expense of accuracy as measurements are prone to uncertainties due to more standard loads. Moreover, using more standards results in limiting the frequency range. The first calibration of a SPR was reported in [139] using seven standard loads. In [140] and [141], calibration techniques have been developed to find the calibration constant using four standard loads while a fifth standard load was used as a fixed or sliding matched termination to improve accuracy [142].

The conventional SPR consists of power dividers and directional couplers. An X-band waveguide based SPR was reported in [143] which is bulky in nature. To decrease the dimension of the SPR, a microstrip clone of the waveguide SPR was developed which was also reported in [143]. It consisted of 3-dB lunge couplers and wilkinson power dividers

The next era of the SP measurement technique was to explore its applications in industry, military and in civil use. There are many publication in high power that were cited in [143], including high power SPR developed for industrial applications at 2.45 GHz, with power handling capacity up to 30 kW. The SPR had a practical application in RF direction finding.

Classical techniques of RF direction finding are based on multiple antenna systems employing single or multiple receivers. Classical techniques such as multiple-receiver DF algorithms; Multiple Signal Classification (MUSIC) and Estimation of Signal Parameters via Rotational Invariance Technique (ESPRIT) use simultaneous phase information from each antenna to estimate the AoA of the signal of interest [8, 9]. These techniques require multiple receivers. In many scenarios where mobile systems are needed, multiple receivers are impractical. Thus, single receiver techniques are of interest. But most of the existing techniques for single receiver direction finding are either old analog techniques or expensive digital techniques [10, 144]. To overcome the intensive processing of RF direction finding digital signal processing (DSP) algorithms, microwave measurement based SP technology is used. This multi-port measuring technique is gaining wide acceptance due to its precise and low processing requirements in microwave systems.

Microwave structure based low cost DF systems have gained popularity over last few decades. The SP architecture is becoming a key component in low cost RF DF systems. It has a wide range of applications such as in RF DF, precise displacement measurement, direct conversion receivers, and in radar sensors. The SP circuit was initially used as a low cost alternative to network analyzers [136]. Additionally, a number of SP circuits were designed to be used in beam direction finding systems. All these systems are used to find the azimuth angle of a distant target object (i.e. a single angle for the incoming wave) [11, 12, 31, 145]. In modern

wireless systems, it is highly desirable to achieve dual or multi-band operation using a single circuit. Most of SP based DF systems cover high frequency bands (i.e above 2 GHz) [11, 12, 145–147].

Most of the work carried out in area of RF direction finding (DF) using the SP started in late 90's. DF systems using SP cover many frequency bands and have been used in different scenarios. Most of the proposed SP DF systems in literature use a single SP circuit for AoA estimation in one plane and also operate at frequencies higher than 2 GHz [11, 12, 31, 145–147]. In addition, the available designs are not optimized and compact to be accommodated within wireless handheld and mobile devices.

In [31], SP based direction finding system is proposed. In this design, the maximum phase error observed was $\pm 2^o$. This design is not compact but the unwieldy part of this design is its calibration which is the cumbersome job.

In [145], a single board SP architecture having an area of 85 $\times$85 mm^2, was proposed covering a frequency range of 2 GHz to 2.45 GHz. The maximum phase error reported was $\pm 5^o$. The size and frequency band used in this design made it unsuitable to be fitted in the wireless handheld devices. The SP circuit is shown in Figure 3.27. A dual-SP design is proposed in [12] for high resolution AoA estimation, aiming to minimize the ambiguity in the phase measurement. The design was compact, fabricated with lumped elements operating at a high frequency band of 24 GHz. Although the design was compact but it covered high frequency bands and thus is inappropriate for use within wireless handheld devices. The dual-SP circuit is shown in Figure 3.28.

In [146], a very low phase error ($\pm 0.2932^o$) design was reported. The error at the output was calibrated using support vector regression (SVR) technique. The higher frequency bands 5-6 GHz was covered in the proposed design. The design is not compact and used at higher frequency bands with additional intensive SVR processing for phase calibration which made the design inappropriate choice for wireless handheld devices. In [147], a Ka band SP design was presented that was fabricated with lumped elements. This given design was not compact as it was not fabricated on a single board and also covered higher frequency bands. So,

this design is not a right choice to meet wireless standard in mobile terminals. The Ka-band based SP circuit is shown in Figure 3.29. In [148], a SP based wave correlator was proposed. This design requires calibration for phase measurement for beam direction finding. Moreover, this design was tested experimentally in the high frequency band of 8~12 GHz. This made the design to be unlikely used in the wireless handheld devices.
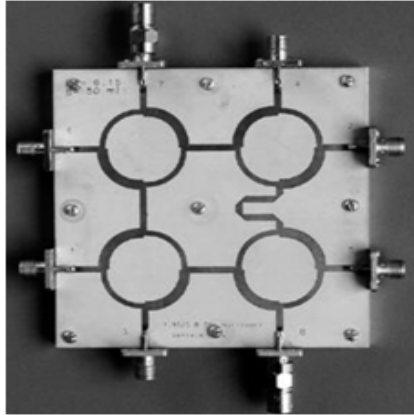
Figure 3.27: Geometry of microwave passive SP circuit [145].
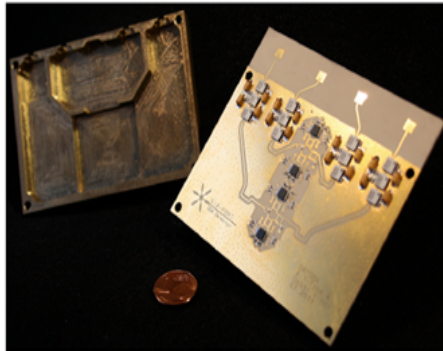
Figure 3.28: Dual-SP circuit for phase error minimization [12].
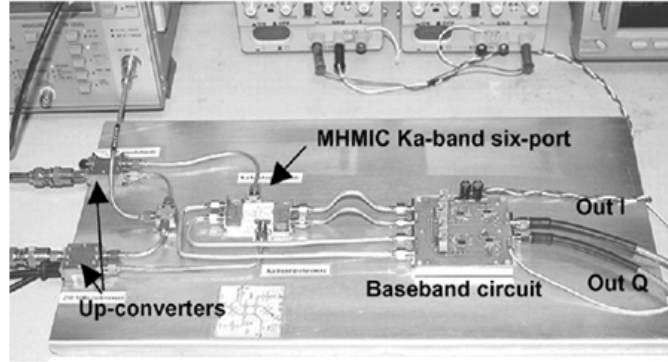
Figure 3.29: Ka-band based six-port circuit [147].

In [149], artificial neural network (ANN) techniques based calibration was proposed for SP design. The application of this design was in direction finding receivers but the lack of self-calibration made this design not feasible to be used in mobile terminals for cognitive radio and SDR platforms. A dual-SP design was proposed in [150] and the same design is elaborated more in [151]. The main purpose of this design was to minimize the error in the phase measurement. This design was compact but operating at a high frequency band of 24 GHz. So, this design is not a right choice for use within wireless handheld devices. In [152], a 77 GHz direction finding system is proposed for radar application.

3.6 Conclusions

In this chapter, a comprehensive literature review was presented for reconfigurable MIMO antenna systems for cognitive radio platforms. The possibility of RF based DF was also investigated that might be a feature for MIMO application in beamforming in 4G wireless application. Most of the work done related to CR platforms covered frequency bands above 2 GHz due to the strict size constraint in implementation. None of the previous works provided complete integration of the MIMO reconfigurable antenna system and UWB sensing antenna on a single substrate board. None of the existing designs cover low frequency bands with mobile device sizes even without MIMO antenna implementation. All the designs provided for DF based on SP were determining the AoA in 2D and none provided

3D DF using dual SP circuits. In future chapters, the contributions of this work will address all these issues.

CHAPTER 4

FREQUENCY RECONFIGURABLE MIMO ANTENNA DESIGNS

Reconfigurable MIMO antennas play a significant role in modern wireless communication devices. Their design has been a hot topic of research over the past decade for 4G wireless standards. In particular, frequency agile MIMO antennas are very popular in CR platforms. In mobile communications, reconfigurable MIMO antennas for CR applications are very useful to efficiently utilize the underutilized spectrum. Thus it can be used to enhance the low spectral efficiency and hence improve the communication. In this chapter, five frequency reconfigurable MIMO antenna designs are presented. These design are analyzed completely with MIMO parameters. Design details, reflection and transmission coefficients curves, gain patterns and antenna efficiencies are provided for each design. All the designs proposed were fabricated using an LPKF-Protomat S103 and scattering parameters were measured at the Antennas and Microwave Structure Design Lab (AMSDL) at the Electrical Engineering Department at KFUPM.

4.1 Modified PIFA Multi-band MIMO Antenna System

In this design, a modified PIFA based reconfigurable MIMO antenna is presented that is compact and suitable for small wireless handheld devices. The proposed design is very versatile as it can be used to cover many frequency bands. The well known frequency bands covered are LTE 900 MHz, GSM 1800, WLAN 2450 MHz with several other bands as well. The switching between different modes is accomplished using PIN diodes that actuate different radiating branches of the antenna.

4.1.1 Antenna Design Detail

The proposed reconfigurable PIFA antennas were mounted on the two corners of a mobile handset size printed circuit board as shown in Figure 4.1 (a). The dimensions of each element were 28×11 mm^2. The proposed design was fabricated on an FR4 substrate with ground plane area of 120×60 mm^2 as shown in Figure 4.1 (b). Figure 4.1 (c) shows the detailed view of the single element PIFA. Figures 4.1 (c) and 4.1 (d) shows the top and bottom views of the elevated modified PIFA while Figure 4.1 (e) and 4.1 (f) shows the side and front view of the whole setup, respectively.

The design procedure of the proposed structure was started with an inverted F-shaped antenna of certain length elevated at certain height without any substrate. The given structure was tuned to resonate above 2 GHz with dimensions 11×28 mm^2. This design was compact but was operating at higher frequency bands with single resonance. The F-shape architecture was added with a meandered line to provide additional paths for the current and hence to achieve more than one resonating mode. For mobile application and other wireless handheld devices, the antenna size should be compact with low frequency bands of operation as well. Hence, the antenna structure was further modified, by folding the structure on the top of the substrate with a planar structure. The total length
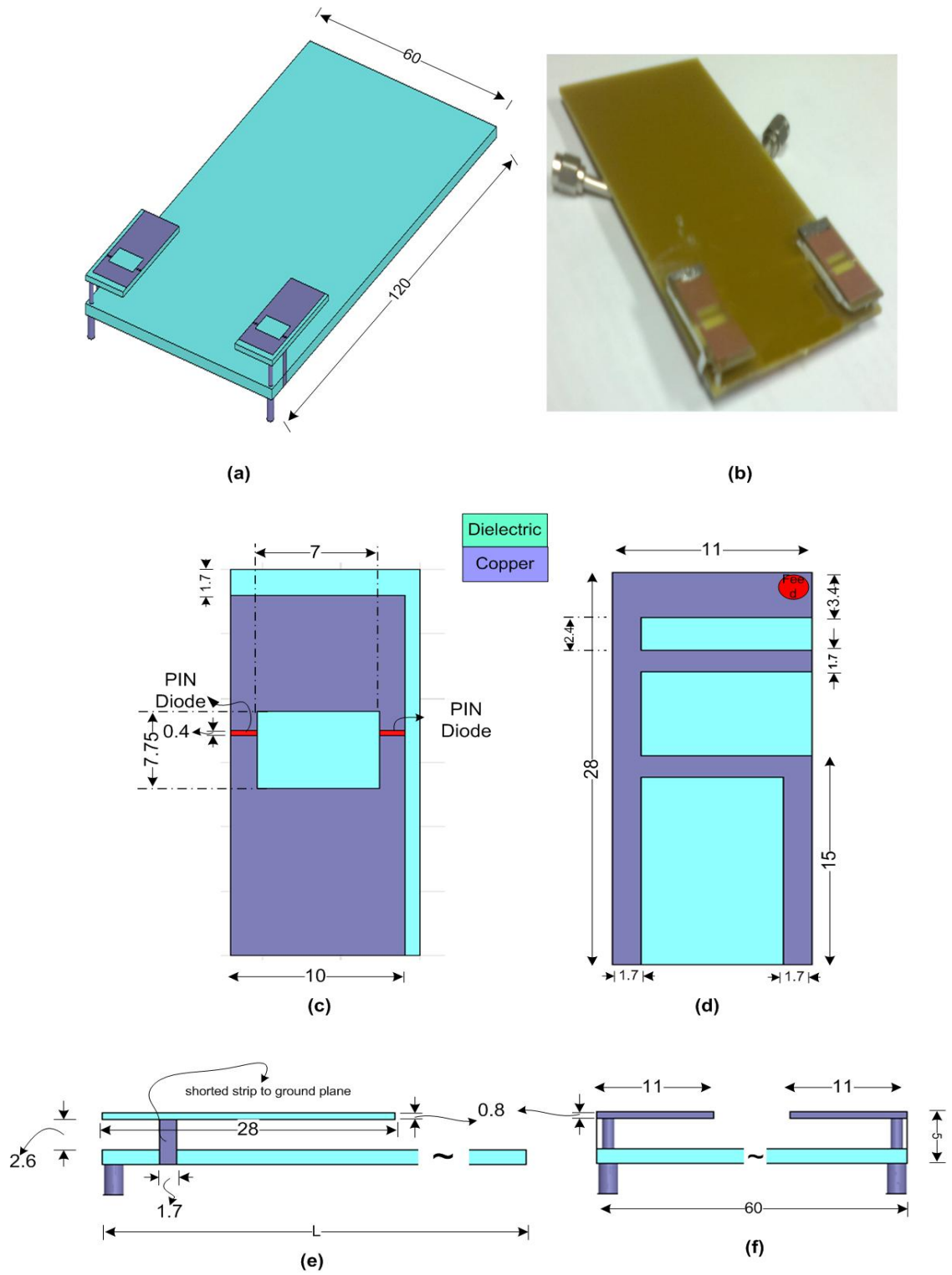
Figure 4.1: Proposed MIMO antenna, (a) HFSS model, (b) Fabricated model, (c) Antenna top side, (d) Antenna bottom side, (e) Side view (f) Front view.

of the antenna was optimized to cover lower frequency bands as well but without reconfigurability. A rectangular slot was created on the top layer to enhance the bandwidth as well as to provide different current paths to achieve reconfigurability by a switching mechanism. Furthermore, two small slots were created in the arms of the rectangular slot to add the PIN diodes for switching. Extensive parametric analysis were performed to optimally place the rectangular slot as well as the position of PIN diodes for maximum bands coverage. Two diodes were used at two slots resulting in four distinct mode of operation. These four modes of operation result in different frequency resonances.

Each element of the modified PIFA consists of radiating lines with a folded patch antenna to lower the resonating frequency towards the lower end of LTE bands. The two PIN diodes act as ON/OFF switches to connect or disconnect the radiating slotted patch element. Four modes of operation were achieved by the switching of the PIN diodes. These modes were 00 (mode 1), 01 (mode 2), 10 (mode 3), 11 (mode 4) where 0 shows the non-conducting state and 1 represent a conducting state of PIN diode. Here, we have used copper tapes to model the PIN diodes.

4.1.2 Simulation and Measurements Results

A-1 Four Modes of MIMO antenna Operation

The antenna was modeled and simulated using HFSS^{TM} and then fabricated and measured. Figures 4.2~4.5 show the simulated and measured reflection coefficients for the MIMO antenna system for its four modes, respectively. The measured results showed close agreement with the simulation ones. A slight shift in the resonant frequency of the fabricated antenna was observed in certain bands because of the substrate properties and the way the modified PIFA was elevated above the ground plane. The antenna had multiple resonant frequencies for all different modes of operation. In mode 1, two operating bands were achieved with center frequencies of 1.35 GHz and 2.45 GHz. Efficiency (η) and envelop correlation coefficient (ρ_e) of these two resonances were 72%, 0.1 and 60%, 0.016,
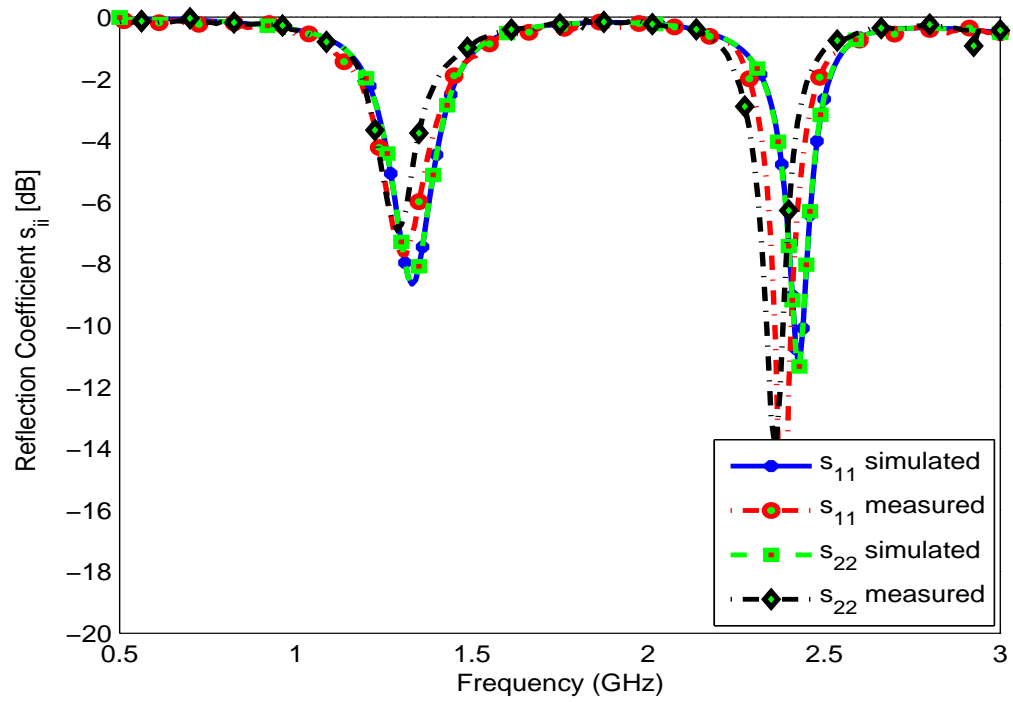
Figure 4.2: Reflection coefficient of reconfigurable antenna in mode 1
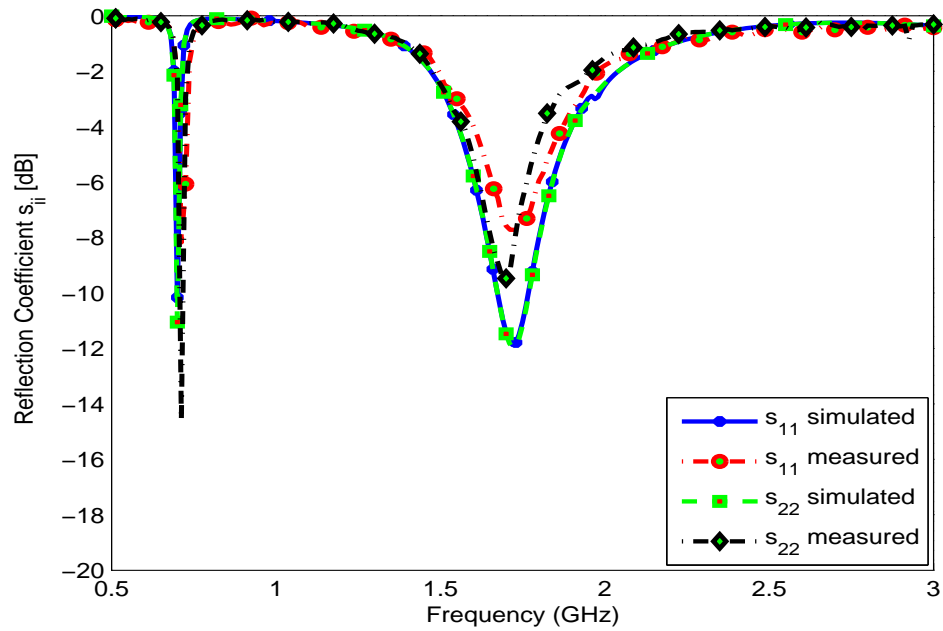
Figure 4.3: Reflection coefficient of reconfigurable antenna in mode 2

respectively. Similarly in mode 2, two operating bands were achieved with center frequencies of 700 MHz and 1.72 GHz with η=17% and ρ_e=0.105 and η=84% and ρ_e=0.0.078, respectively. Mode 3 covered two bands of 930 MHz and 1.55 GHz. The η and ρ_e for these two bands were (42%, 0.09) and (72%, 0.0154), respectively. Mode 4 of the proposed design covered two frequency bands of 940 MHz, and 1.83 GHz. η and ρ_e for these two bands of operation are (45%, 0.098), (63%, 0.0103),respectively.

The proposed reconfigurable antenna is a multi-band design. Generally, in multi-bands structures, more than one mode are excited. The radiation efficiency of the first mode is relatively higher as usually it is the fundamental radiation mode while higher order modes have considerably smaller radiation efficiencies. Generally speaking, for electrically small antennas, the expected gain and efficiency are low compared to standard antennas. The proposed design is also an electrically small antenna (ESA) structure with multi-band operation hence observed lower efficiencies and gain at some modes.

Figure 4.6 and Figure 4.7 shows the simulated and measured isolation curves, respectively, between the two PIFA antenna elements for all modes of operation. The proposed antenna system provides good isolation across all frequency bands of operation with minimum isolation of 10 dB. For good diversity performance of the MIMO antenna system, high isolation between various antenna elements is required.

A-2 Current Density

The proposed reconfigurable MIMO antenna system was analyzed from its surface current densities. The analysis was performed using HFSS simulations. Only the first two modes are presented here for surface current density analysis. Figures 4.8(a) and (b) show the current density by activating antenna-2 at two resonant frequencies of 1350 MHz and 2450 MHz, respectively. The top and bottom layers of reconfigurable antenna-2 with ground plane current density are shown in Figure 4.8. It is clear from Figure 4.8(a), a high current density was observed along the bottom side of inner side and along the edges of the top layer of antenna element.
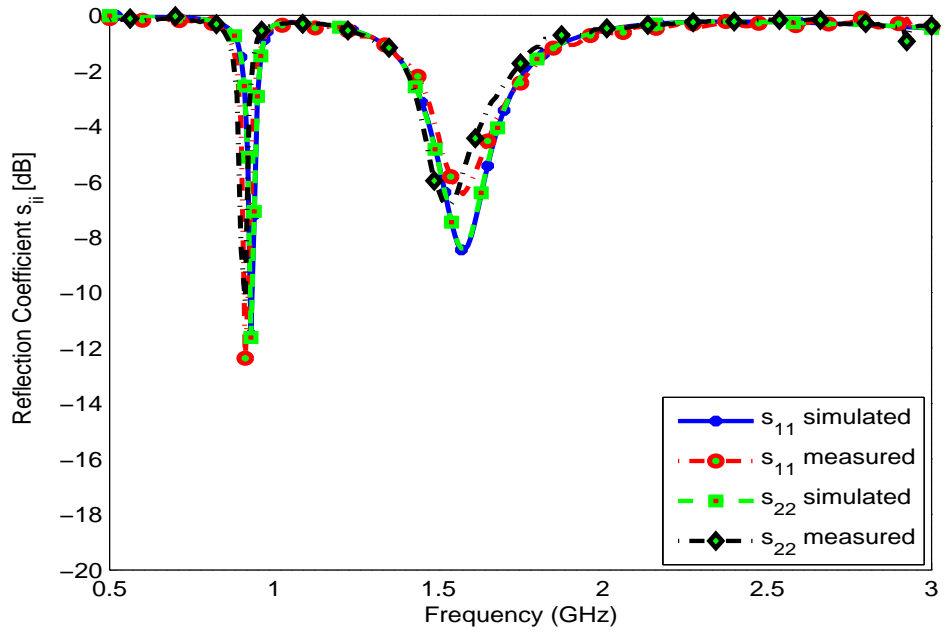
Figure 4.4: Reflection coefficient of reconfigurable antenna in mode 3
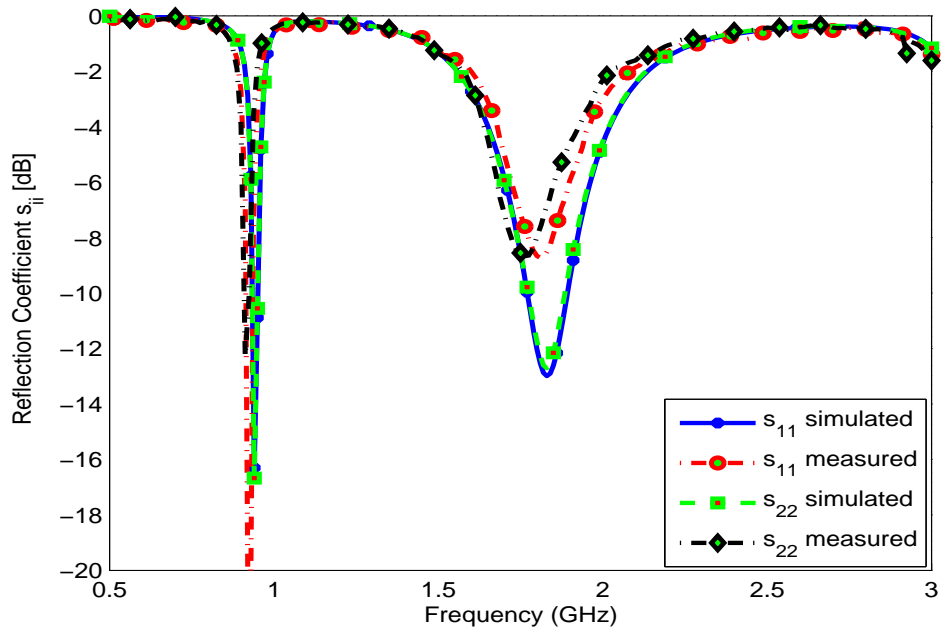
Figure 4.5: Reflection coefficient of reconfigurable antenna in mode 4
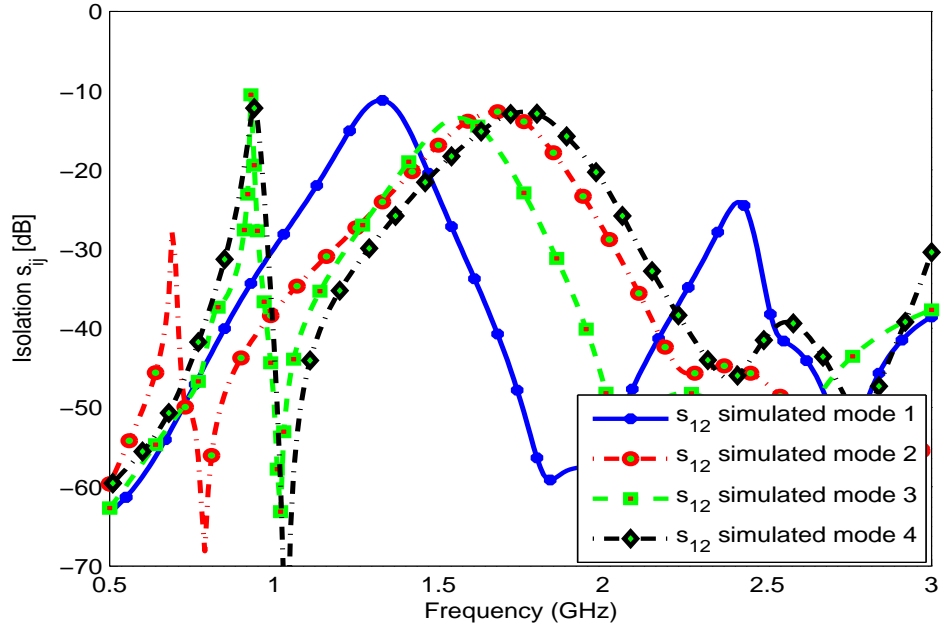
Figure 4.6: Simulated isolation curves between MIMO elements for all modes
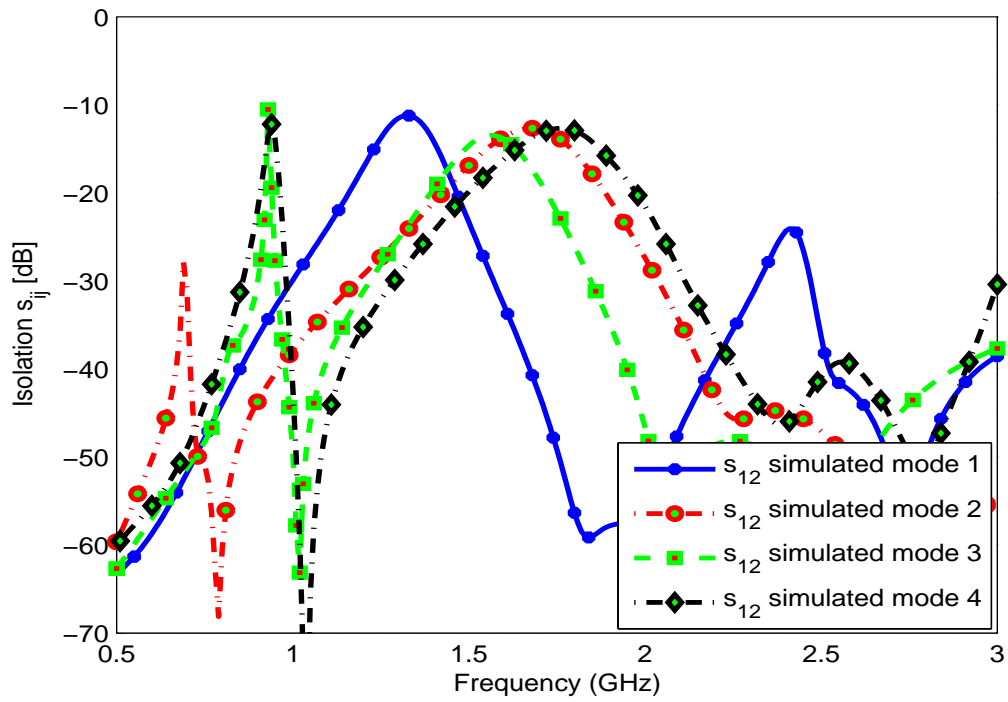
Figure 4.7: Measured isolation curves between MIMO elements for all modes
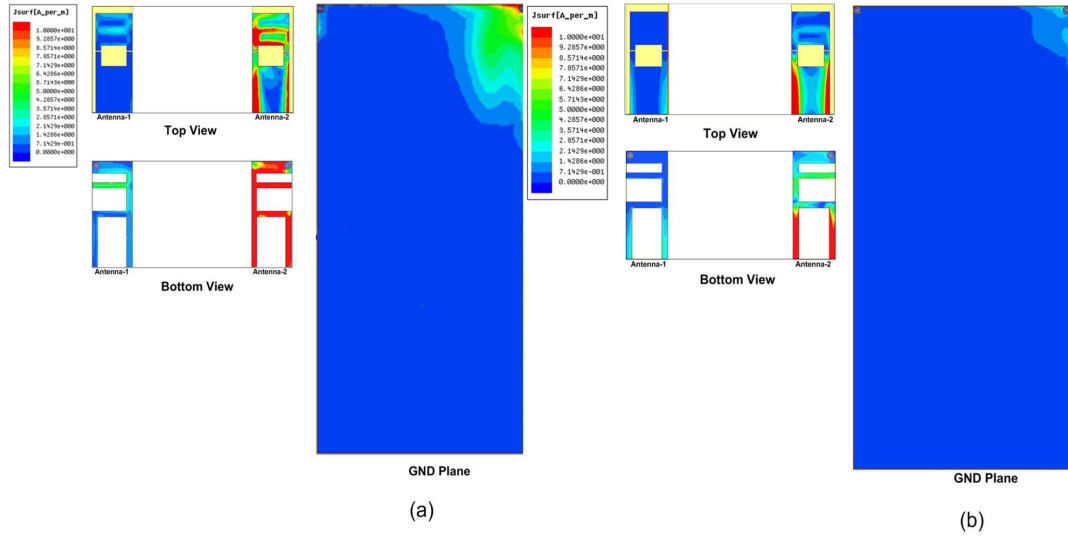
Figure 4.8: Current distribution for the MIMO antenna system at mode-1, Antenna-2 excited: (a) 1350 MHz (b) 2450 MHz.

The ground plane also took part in the radiation as it can be seen from the ground plane. The mutual coupling between two elements are insignificant as it is clear from the current densities.

The same analysis can be extended for the same mode at other band of 2.450 GHz as shown in Figure 4.8(b). Similar behavior was also observed with the excitation of antenna-2 of mode 2 for dual bands at 700 MHz and 1720 MHz as shown in Figure 4.9.

A-3 3-D Gain Patterns

The 3D radiation patterns of the MIMO reconfigurable antenna system were computed using HFSS. The gain patterns were computed for single element at the time while the second elements was terminated with 50 Ω for each mode and each band. The gain patterns of the all modes are given in Figures 4.10 $\sim$ 4.13. In Figure 4.10, the 3D gain pattern is plotted for two bands: 1350 MHz and 2450 MHz while Figure 4.11 shows the 3D gain patterns for 700 MHz and 1720 MHz.

Similarly, Figure 4.12 shows the 3D gain pattern for two bands: 930 MHz and 1550 MHz while Figure 4.13 shows the 3D gain patterns for 942 MHz and 1830 MHz. The maximas of each element is tilted showing lower field correlation that is usually desired. The maximum simulated gain in dBi for all four modes in two
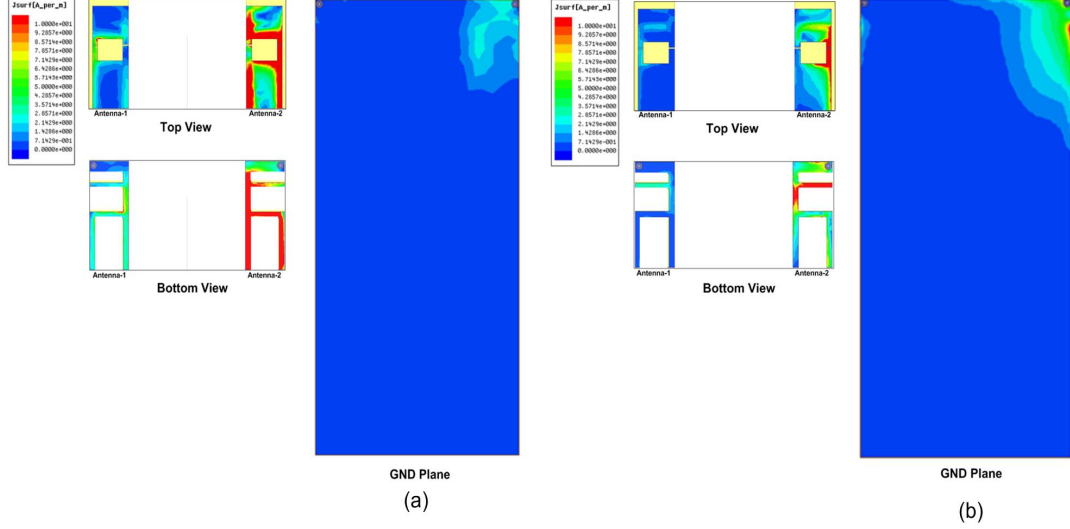
Figure 4.9: Current distribution for the MIMO antenna system at mode-2, Antenna-2 excited: (a) 700 MHz (b) 1720 MHz.

bands are (3.79, 3.83), (-5.3,4.9), (-1.8,3.8), and (-1.32, 5.03), respectively.

4.2 Modified PIFA Dual-Band MIMO Antenna System

In this antenna design, a varactor diode based two element reconfigurable, dual-band, multiple input multiple output (MIMO) antenna is presented. The single antenna element is a modified printed inverted F-shape antenna (PIFA) with radiating lines and a folded patch. (similar basic structure as the one presented in section 4.1). This proposed structure is grounded by a metallic wall for size optimization and compactness. The proposed design is very versatile as it can be used to cover wide frequency bands for dual-band operation. The well known frequency bands covered are GSM-750, GSM-870, LTE-900, LTE-1800, with several other bands as well. The proposed design provides at least -12 dB isolation between its antenna elements.

The distinguishing feature of the proposed design is its dual band and its tunability via voltage control over a wide frequency range including the well known LTE and GSM bands. It exhibits a wide tunable range from 750∼1030 MHz in its
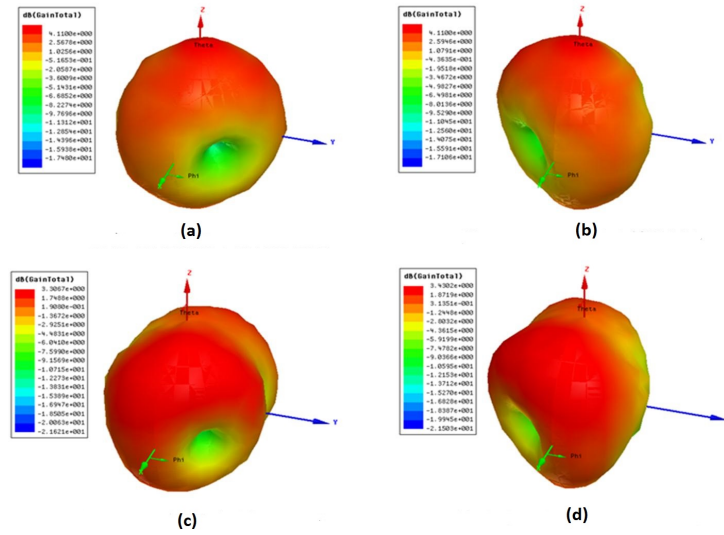
Figure 4.10: Simulated 3D gain pattern Mode-1 (a)Antenna-1 excited at 1350 MHz(b) Antenna-2 excited at 1350 MHz (c) Antenna-1 excited at 2450 MHz (d) Antenna-2 excited at 2450 MHz.
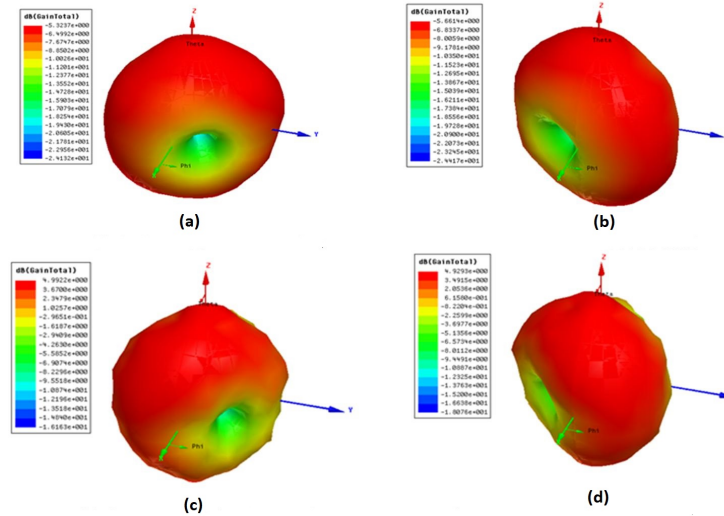
Figure 4.11: Simulated 3D gain pattern Mode-2 (a)Antenna-1 excited at 700 MHz(b) Antenna-2 excited at 700 MHz (c) Antenna-1 excited at 1720 MHz (d) Antenna-2 excited at 1720 MHz.
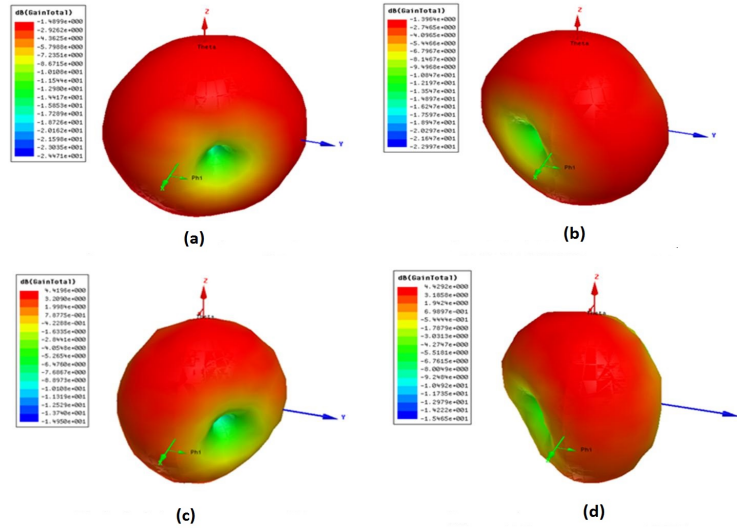
Figure 4.12: Simulated 3D gain pattern Mode-3 (a)Antenna-1 excited at 930 MHz(b) Antenna-2 excited at 930 MHz (c) Antenna-1 excited at 1550 MHz (d) Antenna-2 excited at 1550 MHz.
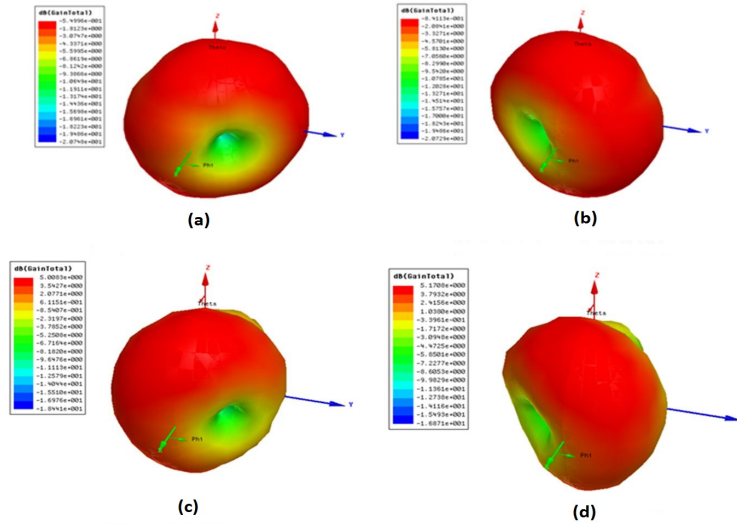
Figure 4.13: Simulated 3D gain pattern Mode-4 (a)Antenna-1 excited at 942 MHz(b) Antenna-2 excited at 942 MHz (c) Antenna-1 excited at 1830 MHz (d) Antenna-2 excited at 1830 MHz.

lower frequency band while the higher band the tunable frequency range it covered 1540 $\sim$ 1940 MHz. This is achieved by applying DC voltage to its varactor diodes.

4.2.1   Antenna Design Details

The proposed varactor based reconfigurable modified PIFA antennas are shown in Fig. 4.14. The HFSS and fabricated models are shown in Figs. 4.14(a) and (b), respectively. The proposed design was fabricated on an FR4 substrate with ground plane area of 120×65 mm^2. The size of the circuit board is assumed to be the size of mobile handset size.

The reconfigurable MIMO elements were mounted on the top corners of the main board with a coaxial feed. The total height of the whole system was 5.8 mm. The two reconfigurable antennas are exactly similar in structure with dimensions of 30×12 mm^2. The detailed schematic of the two MIMO antenna is shown in Fig. 4.15. Fig. 4.15(a) shows the top view of the reconfigurable MIMO elements while Fig. 4.15(b) shows the bottom view of the antenna. The bottom layer of the antenna consists of radiating lines and the coaxial feed. The two antenna elements were fed from the bottom side of elevated board. The design step by step procedure is detailed in section 4.1.1. The only difference in the current design is the use of varactor diodes instead of PIN diodes.

Varactor diodes were embedded on the top side of the antenna to connect the two different radiating parts, thus providing variable capacitance at the junction. The change in capacitance by varying the applied voltage results in different resonating bands and thus providing reconfigurability. The top and bottom layers of the elevated board were shorted through a metallic wall at one side of the board. Figs. 4.15(c) and 4.15(d) show the side and front views of the PIFA setup, respectively.

Each antenna element is embedded with varactor diodes to change the capacitance of the current path and hence resonate at different frequency bands. The biasing circuitry for a single varactor diode is shown in Fig. 4.16. The circuit is a series combination of an RF choke of 1 μH in series with 2.1 kΩ resistor,
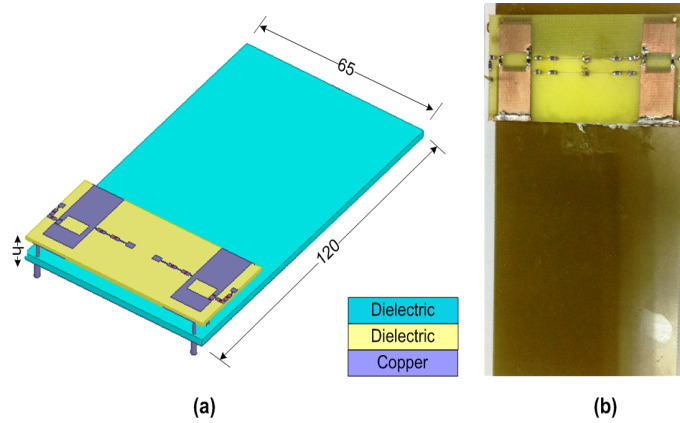
Figure 4.14: Proposed MIMO antenna (a) HFSS model (b) fabricated model.

connecting in series with both terminals of varactor diode. The variable voltage was applied to change the capacitance of varactor diode in reverse bias fashion. The varactor diode used in this design was BB-145. The biasing circuitry was used to bias the varactor and at the meantime, isolate the DC and RF parts of the antenna.

The fabricated model of the proposed design is shown in Fig. 4.17. Fig. 4.17(a) shows the complete 2-element MIMO antenna system while Figs. 4.17(b) and (c) shows the top and bottom layers of the fabricated elevated PIFA structure, respectively.

4.2.2 Simulation and Measurements Results

The antenna was fabricated and its s-parameters were measured at the AMSD Lab at KFUPM. The measured results showed close agreement with the simulation ones. A slight shift in the resonant frequencies of the fabricated antenna was attributed to the difference between the material properties of the substrate defined in the simulation design and the one used for fabrication. In addition, lumped and active elements are modeled in HFSS using the specification given in the date sheet. The real values might have some differences which might be the cause of shift in the frequency.
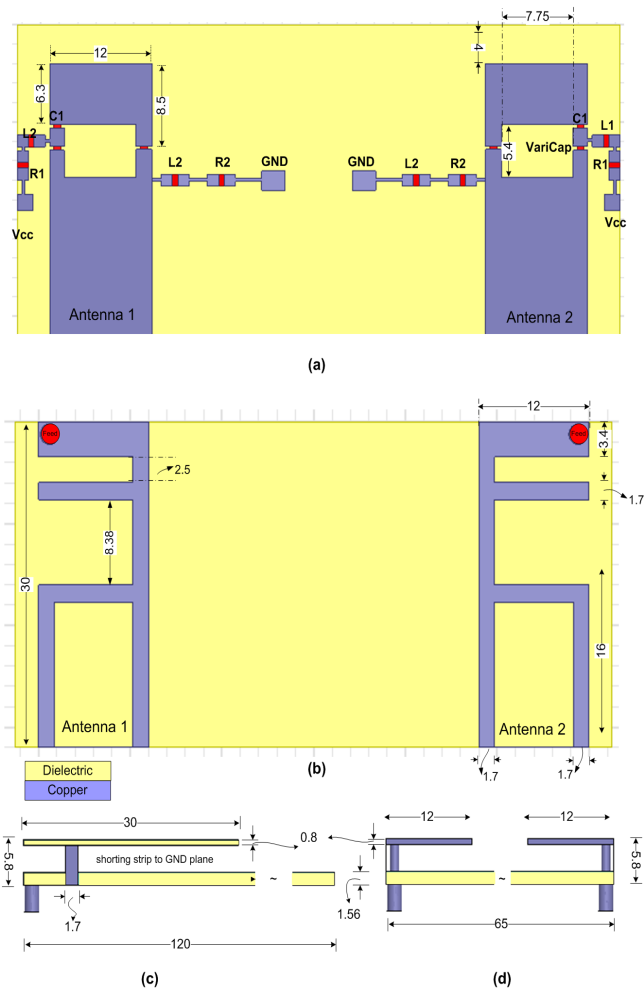
Figure 4.15: Detailed schematic of reconfigurable MIMO antenna (a) Top view (b) Bottom view (c) Side View (d) Front view.
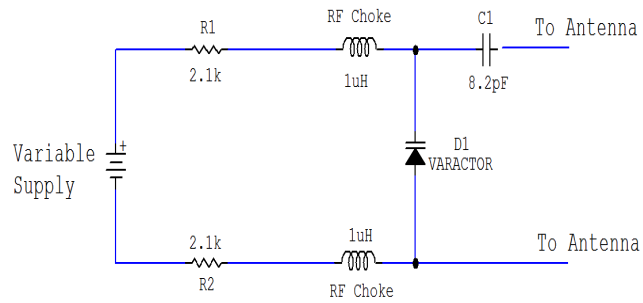
Figure 4.16: Varactor diode biasing circuitry.
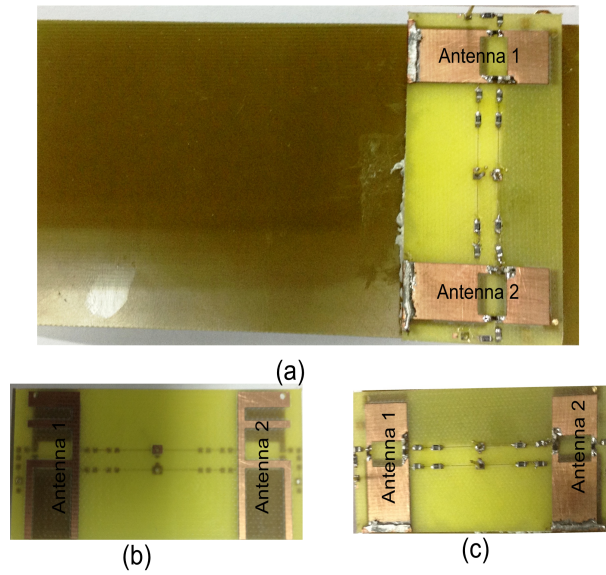
Figure 4.17: (a) Fabricated Modified MIMO PIFA antenna, (b) Fabricated antenna bottom side, (c) Fabricated antenna top view.
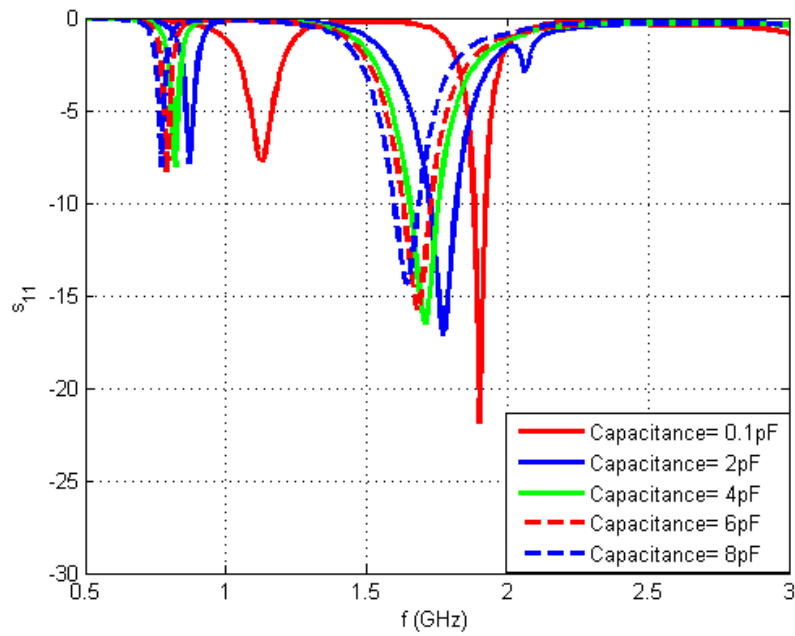
Figure 4.18: Simulated reflection coefficient at antenna 1.
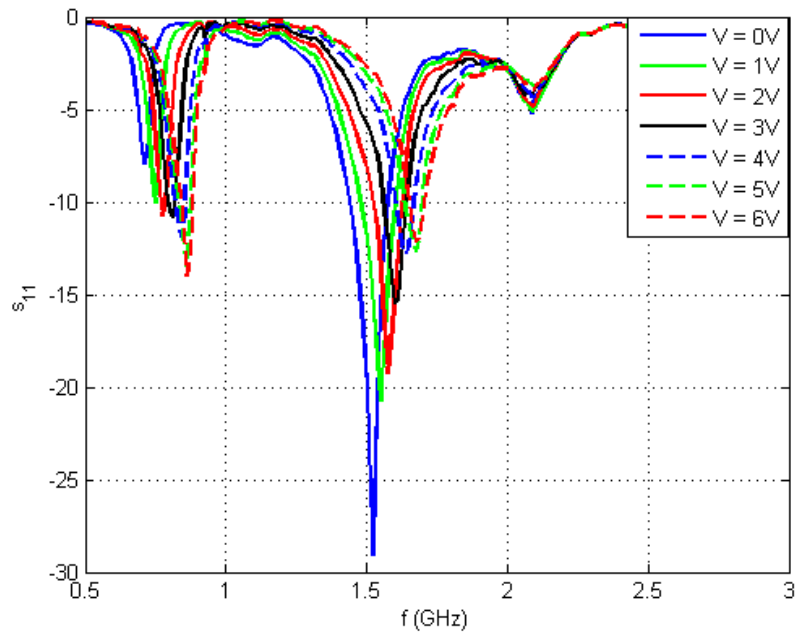
Figure 4.19: Measured reflection coefficient at antenna 1.
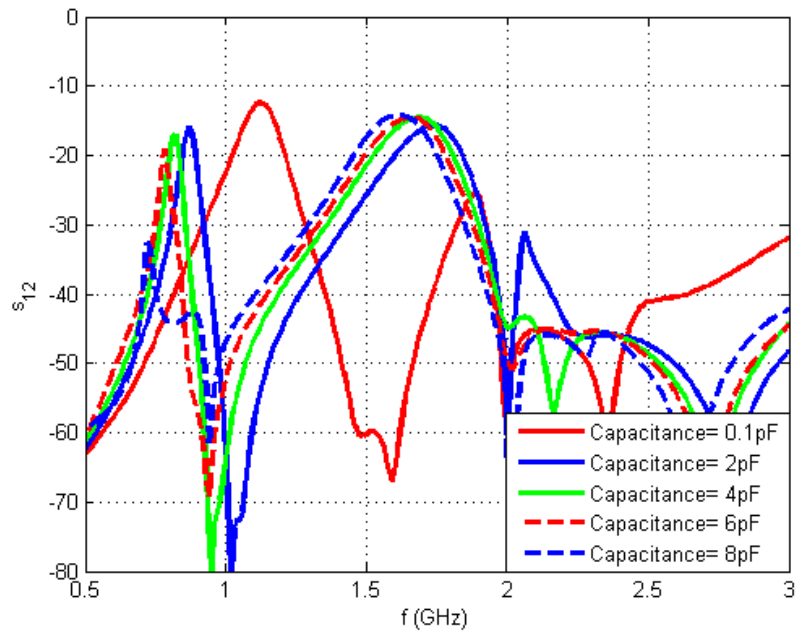
Figure 4.20: Simulated Mutual coupling curves between the two antennas

77
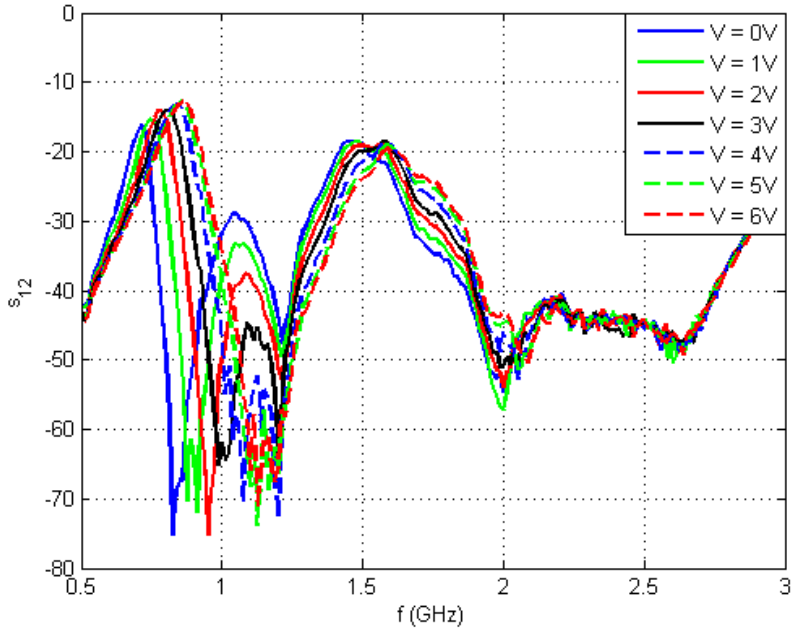
Figure 4.21: Measured Mutual coupling curves between the two antennas.

Table 4.1: Simulated and measured f_c and BW for two bands

		Simulated		Measured	
		f_c(MHz)	BW (MHz)	f_c(MHz)	BW (MHz)
Band-1	Ant-1	820	27	840	60
	Ant-2	820	27	845	58
Band-2	Ant-1	1700	210	1660	160
	Ant-2	1700	210	1665	165

The proposed design is basically dual-band PIFA. Fig. 4.18 shows the simulated reflection coefficient curves of antenna-1 by changing the capacitance of the varactor diode from 0.1 pF to 10 pF. There is a smooth change of resonance from 750 ~1160 MHz in the lower band while the second band smoothly changes from 1540~1900 MHz. Increasing the capacitance tends to decrease the resonating frequency of PIFA. Fig. 4.19 shows the measured reflection coefficient for antenna 1 at port. Fig. 4.20 shows the simulated mutual coupling between the two an-

tenna elements. The isolation is quit good between the MIMO antennas and is less than -12dB. The used varactor (BB-145) had a minimum capacitance of 2.5 pF at 6V. Over this region, the measured results are well matched with simulated ones. The details of simulated and measured center resonances frequencies (f_c) and -6dB bandwidth (BW) for input biasing voltage equal to 4 volts are shown in Table 4.1. Fig. 4.21 shows the measured mutual coupling between two antenna elements at various biasing points. The minimum measured -6 dB bandwidth in the lower band was 27 MHz while in the upper band was 210 MHz for all resonant frequencies. The difference in the bandwidth of simulated and measured values are because of the mismatch of input impedances which might hit the efficiency.

Table 4.2: Simulated Peak gain, Efficiency and Envelop correlation coefficient

		Peak Gain (dBi)	Efficiency (%η)	ρ_e
Band-1	Ant-1	0.436	63	0.053
	Ant-2	0.495	63.12	
Band-2	Ant-1	4.330	86	0.032
	Ant-2	4.334	86.11	

The simulated gain pattern of the two antennas at 825 MHz and 1700 MHz are shown in Figs. 4.22 and 4.23. The simulated peak gains and efficiencies (%η) for both antennas at both bands (with biasing voltage equal to 4 Volts) are given in Table 4.2. The value of envelope correlation coefficient (ρ_e) at both bands (825 MHz, 1700 MHz) are tabulated in Table 4.2 and show acceptable MIMO performance. The proposed design is an ESA structure with dual-band operation and hence observed low (%η) at lower frequency bands.
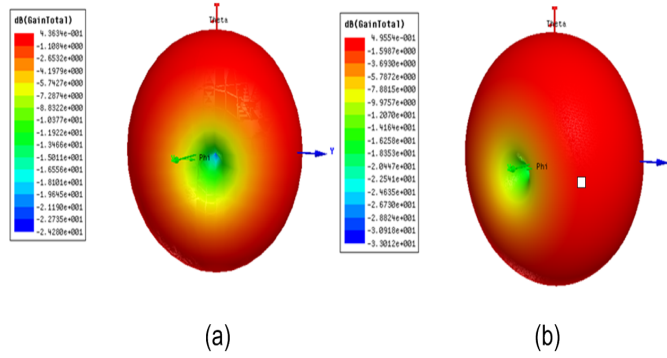
Figure 4.22: Simulated Gain at 825 MHz (a) Antenna 1 (b) Antenna 2.
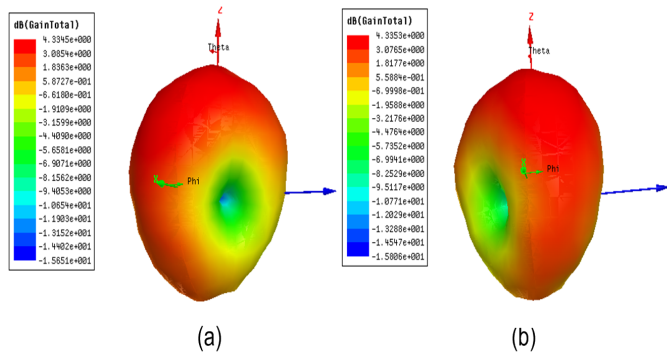
Figure 4.23: Simulated Gain at 1700 MHz (a) Antenna 1 (b) Antenna 2.

4.3 Planar Meander-line Based Compact Two Elements MIMO Reconfigurable Antenna

A novel meandered line, planar inverted F PIFA shape frequency agile multiple-input multiple-output (MIMO) antenna is presented. The proposed dual-element MIMO antenna is compact with frequency tuning capability over a wide-range. The frequency reconfigurability was achieved using a unique combination of PIN and varactor diodes. PIN diodes are used for mode selection while the varactor diode is used to sweep the frequency over a wide band especially below 1 GHz. The proposed single substrate design is compact with small form factor and suitable for small wireless handheld devices for cognitive radio applications. Good MIMO performance metrics were achieved with reasonable isolation.

The distinguishing feature of the proposed design is its operation at low fre-

quency bands starting 573~680 MHz and 834~1120 MHz. Most of the cited planar antenna designs in literature for CR applications were reported to work above 2 GHz that are of comparable sizes.

Moreover, the proposed design is planar and compact making it suitable for mobile CR platforms with additional MIMO capability as well. The size of the single element is 7.9×56.6 mm^2. The complete antenna system fits within a dielectric substrate area of 65×120 ×1.56 mm^3 that is considered a suitable for small portable devices and smart phone.

4.3.1 Design Details

The proposed reconfigurable meandered PIFA MIMO antenna structure is shown in Figure 4.24(a) and (b). Two element MIMO antennas are fabricated on a single substrate board with dimensions 65×120×1.56 mm^3. The board size was selected as a standard size of typical smart phone as the goal was to design planar MIMO antenna for mobile terminals. The design was fabricated on commercially available FR-4 substrate with ϵ_r =4.4. The two antennas are etched out from the top layer of the board while bottom layer is the reference GND plane. The total dimensions of the single element is 7.9×56.6 mm^2.

The detailed view of the two element MIMO antenna is shown in Figure 4.25. Figure 4.25(a) shows the top view of the two similar antenna structures. A unique combination of PIN and varactor diodes were used for frequency reconfigurability. Two modes of operation were achieved using PIN diodes by connecting different radiating parts of the antenna. The fine tuning of the antenna was achieved using varactor diodes and is more effective especially in lower frequency bands. Each antenna element is short circuited with the GND plane via a shorting wall to bring down the resonating frequency. Figure 4.25(b) shows the side of the antenna.

The design procedure was started with the well-known developed model of F-shape antenna with certain length that was resonating at higher frequency bands above 2 GHz. The extra meander lines were added to bring down the resonating frequency below 2 GHz. Parametric analysis were performed to optimally place

the shorting wall to tune the antenna for frequencies below 1 GHz. The design was optimized by parametric sweep for length and position of the shorting wall. Further, two slots were created in the solid structure to add the capacitive effect which might lead to achieve reconfigurability in the proposed architecture by varying the capacitance. The width and position of the slots were simulated extensively to get the optimal point to achieve reconfigurability in the design especially at the lower band of frequency spectrum.

Figure 4.24: Proposed MIMO antennas system for CR platform (a) Top view (b) Bottom view - All dimensions are in millimeter (mm).

The basic PIFA is a grounded patch with length $\lambda/4$ instead of $\lambda/2$ regular patch antenna. The $\lambda/4$ antenna element is optimized for its feed location and position of its shorting post to operate at the desired frequency band. Similarly, a monopole antenna is also a $\lambda/4$ antenna. The proposed antenna is a unique combination of a PIFA and a monopole with expected length of $\lambda/8$ for its res-

onance, with a shorting post width equal to that of the microstrip line. The given antenna is operating at two modes. The length corresponding to mode-1 and mode-2 operations are approximately equal to $\lambda/12$, respectively. The given antenna structure is embedded with a DC blocking capacitor, PIN diode and varactor diode in series with the radiating branch of the antenna. The given design is provided with shorting wall of length 7.9 mm instead of 1.48 mm single shorting strip. The reactive impedances added to the radiating structure further reduce the length of antenna and resonance occurred at approximately $\lambda/12$ length for both modes.

Figure 4.25: Detailed schematic of the two-element reconfigurable MIMO antenna (a) Top view (b) Side view - All dimensions are in millimeter (mm).

The biasing circuitry for a single PIN and varactor diodes is shown in Figure 4.26. The biasing circuit for both diodes is a series circuit of an RF choke and resistor connecting with PIN or varactor diode. RF choke is used to isolate the biasing DC circuit from the radiating antenna. The values used for RF choke and resistor were $1\mu H$ and 2.1 kΩ, respectively. The PIN diode is forward biased using a voltage source equal to 5V while the capacitance of varactor diode is changed

smoothly by using a variable voltage source.

Figure 4.26: PIN and varactor diodes biasing circuitry

(a)   (b)
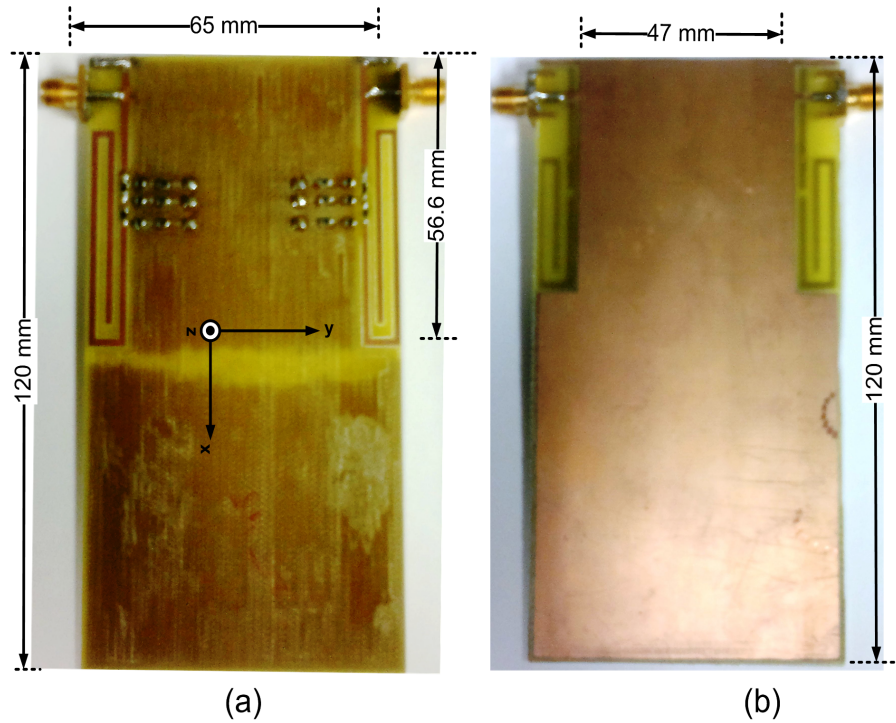
Figure 4.27: Fabricated model (a) Top view (b) Bottom view showing the reference GND plane

The fabricated model is shown in Figure 4.27 that was realized on FR4 substrate. Figure 4.27(a) shows the top view of fabricated model while Figure 4.27(b) shows the reference GND plane of the fabricated design.

4.3.2 Simulation and Measurement Results

The proposed novel frequency agile antenna was modeled and simulated using HFSS^{TM}. The simulated optimized design was fabricated and tested for scattering parameters using an Agilent N9918A vector network analyzer. The gain patterns and efficiencies were measured at King Abdullah University of Science and Technology (KAUST), KSA, using a SATIMO Starlab anechoic chamber.

The proposed MIMO antenna structure having two slots were connected with PIN and varactor diodes. The first slot was embedded with a PIN diode while a varactor diode was connected at the second slot with its associated digital biasing circuitry. The PIN diodes were used to switch the frequency bands by providing different current paths. The PIN diode ON/OFF operation with varactor tuning results in two modes of operations. The details of these modes are:

A-1 Mode-1

In mode-1, the PIN diodes were switched OFF while the varactor diodes were reverse biased. The reverse biased voltage was varied from 0∼6 Volts to vary the capacitance of the current path. However, it has been observed that the capacitance variation has negligible effects on the operating frequency. The resulted simulated and measured reflection coefficients of mode-1 are shown in Figure 4.28. In mode-1, two resonating bands were achieved. The resonating frequencies are 1100 MHz and 2480 MHz with a -6 dB operating bandwidth of at-least 100 MHz in both bands.

A-2 Mode-2

In this mode, the PIN diodes were switched ON to activate the entire radiating structure. The functionality of varactor diodes is critical in mode-2 as the reverse bias voltage significantly changes the resonating frequencies at the lower frequency band below 1 GHz. In mode-2, three resonating bands were achieved with center frequencies 585 MHz, 860 MHz, 2410 MHz for zero biasing voltage. Smooth variation of the operating frequencies were observed for the lower two bands while
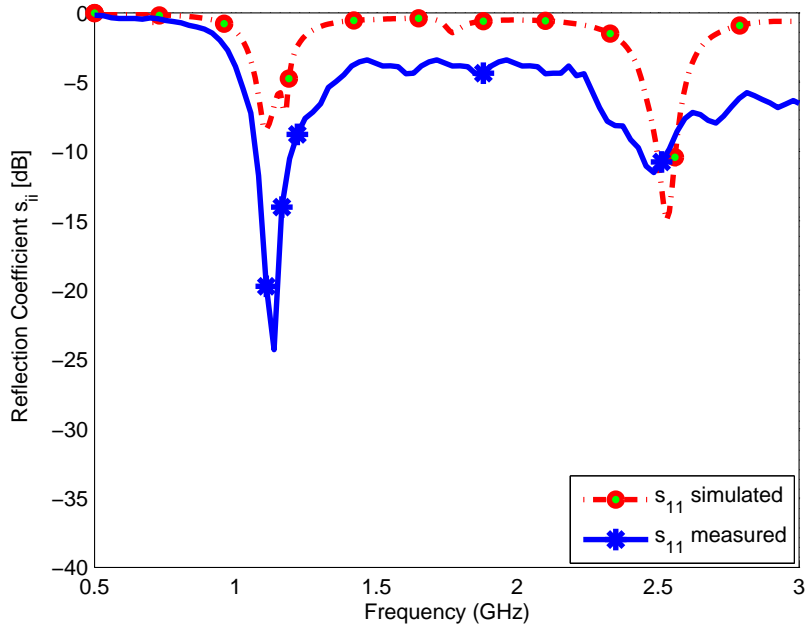
Figure 4.28: Reflection coefficients of the MIMO antenna system - Mode 1.

exhibiting similar behavior as mode-1 at the higher order band. The first resonating frequency was varied between 573~680 MHz while the second band covered 834~1120 MHz. The minimum -6 dB operating bandwidth for all the three bands were 22 MHz, 90 MHz and 120 MHz, respectively. The higher two bands are similar to mode-1.

The simulated reflection coefficients are shown in Figure 4.29 for mode-2 while measured reflection coefficients are shown in Figure 4.30. The simulated and measured isolation curves are shown in Figs. 4.31. The worst case measured isolation was 18 dB between the MIMO antenna elements across the operating band.

The simulated and measured reflection coefficient show close agreement in the results. The slight difference in frequency shift was because of the substrate properties and fabrication tolerances. Moreover, PIN and varactor diodes were modeled according to the data provided by their data sheets. The lack of flexibility of modeling in HFSS might be a cause of frequency drift. The PIN diodes were modeled as resistive and capacitive circuits in forward and reverse bias conditions, respectively, while the varactor diode was modeled as a variable capacitor.

Figure 4.29: Simulated reflection coefficients of the MIMO antenna system - Mode 2.

Figure 4.30: Measured reflection coefficients of the MIMO antenna system - Mode 2.
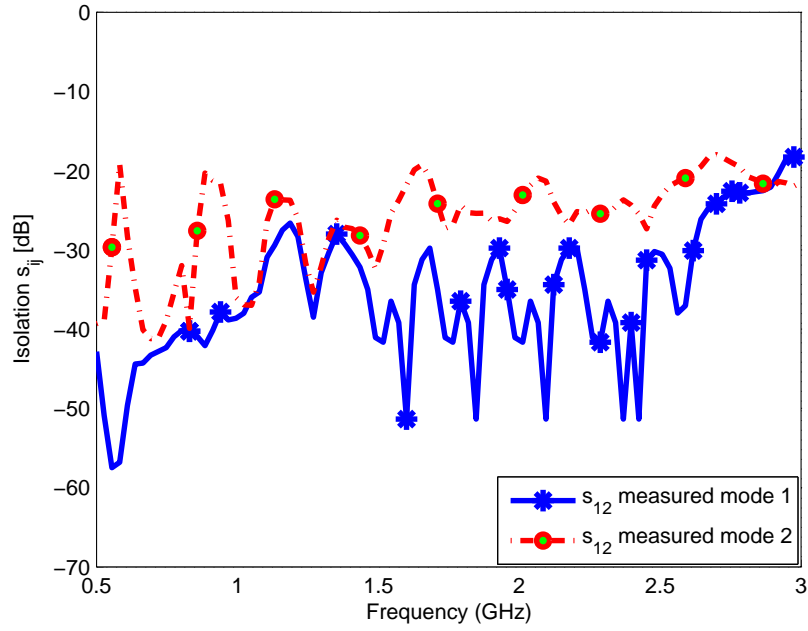
Figure 4.31: Measured isolation between MIMO antenna elements.
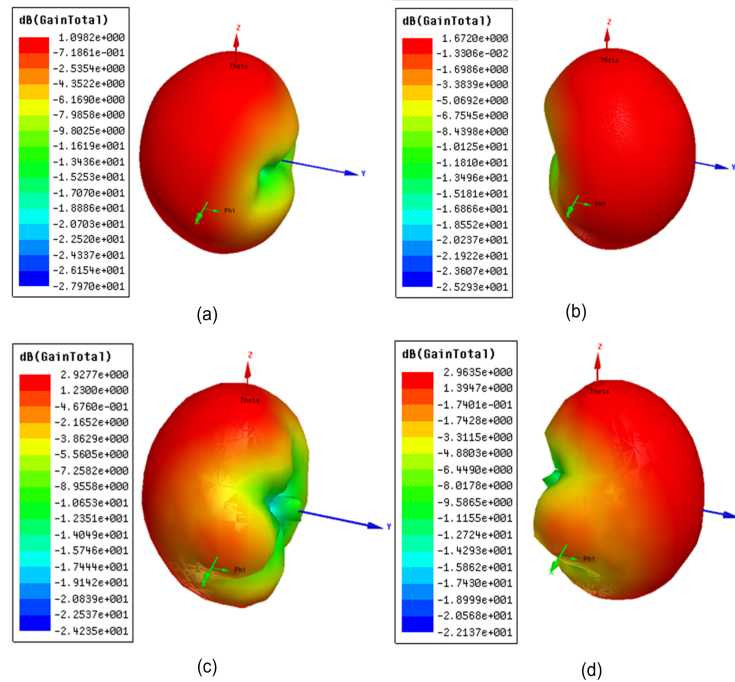
Figure 4.32: Simulated 3D gain pattern Mode-1 (a)Antenna-1 excited at 1100 MHz(b) Antenna-2 excited at 1100 MHz (c) Antenna-1 excited at 2480 MHz (d) Antenna-2 excited at 2480 MHz.

A-3 3-D Gain Patterns

The simulated 3D gain patterns were computed using HFSS for the proposed reconfigurable MIMO antenna. The gain patterns for mode-1 at two different frequencies are shown in Figure 4.32. The simulated 3D gain pattern are plotted for two bands at frequencies: 1100 MHz, 2480 MHz. The maximas of gain pattern for each element are tilted, thus results in lower field correlation.

The minimum frequency for gain measurements was 800 MHz and all values below 800 MHz are represented by (-). The simulated and measured peak gains were (1.02dBi, 2.98dBi) and (0.05dBi, 2.92dBi), respectively, for mode-1 while for mode-2, the values were (-3.01dBi, 2.01dBi, 3.15dBi) and (-, 0.89dBi, 2.85dBi), respectively. The simulated and measured efficiencies (η %) for mode-1 were (40, 72) and (32, 66), respectively, while for mode-2, the values were (21, 56, 76), (-, 44, 67), respectively.

The proposed reconfigurable antenna is considered an ESA structure, with multi-band operation, thus it has low (η %) at certain bands. For electrically small multi-band antennas, the radiation efficiency of the first mode is relatively higher as usually it is the fundamental radiation mode while higher order modes have considerably smaller radiation efficiencies. Generally speaking, ESA have low gain and efficiency because of their miniaturized structure with small aperture area.

A-4 Envelop Correlation Coefficient

Envelope correlation coefficient (ρ_e) were calculated based on radiation patterns. The values for both simulated and measured patterns were (0.025, 0.02) and (0.078, 0.045) respectively, for mode-1 while for mode-2, ρ_e values were (0.078, 0.065, 0.015) and (-, 0.066, 0.02), respectively.

4.4 Planar Meander-line F-Shaped MIMO Reconfigurable Antenna System with Isolation Enhancement

Planar four elements meandered line F shape frequency reconfigurable MIMO antenna with enhanced isolation is presented in this section. The proposed four-element MIMO antenna is compact with frequency tuning capability. The frequency agility was achieved with unique PIN and varactor diodes combinations. PIN diodes are used for mode selection while the varactor diode is used to sweep the frequency over a wide band especially below 1 GHz. The proposed planar four elements MIMO antenna structure is suitable for CR applications. Moreover, the proposed design is planar and compact making it suitable for mobile CR platforms with additional MIMO capability as well. The four element design was adjusted in typical smart phone size which might enhances the data throughput capability of small wireless handheld devices in next generation 4G standards.

4.4.1 Design Details

The four element reconfigurable meandered PIFA MIMO antenna is presented in Figure 4.33(a) and (b). Four element MIMO antennas are fabricated on single substrate board with dimensions $65 \times 120 \times 1.56$ mm^3. The proposed design is suitable to be used in small wireless handheld devices. Planar MIMO antenna structure and its compact size of typical typical smart phone size make it very attractive to be used in 4G standards in mobile terminals. The design was fabricated on Rogers 4003 substrate with ϵ_r =3.55. The four antennas were etched out from the top layer of the board while bottom layer is the reference GND plane. The antenna is not of regular shape. The total dimensions of the single element is summation of 7.9×37 mm^2 and 17.7×19.6 mm^2.
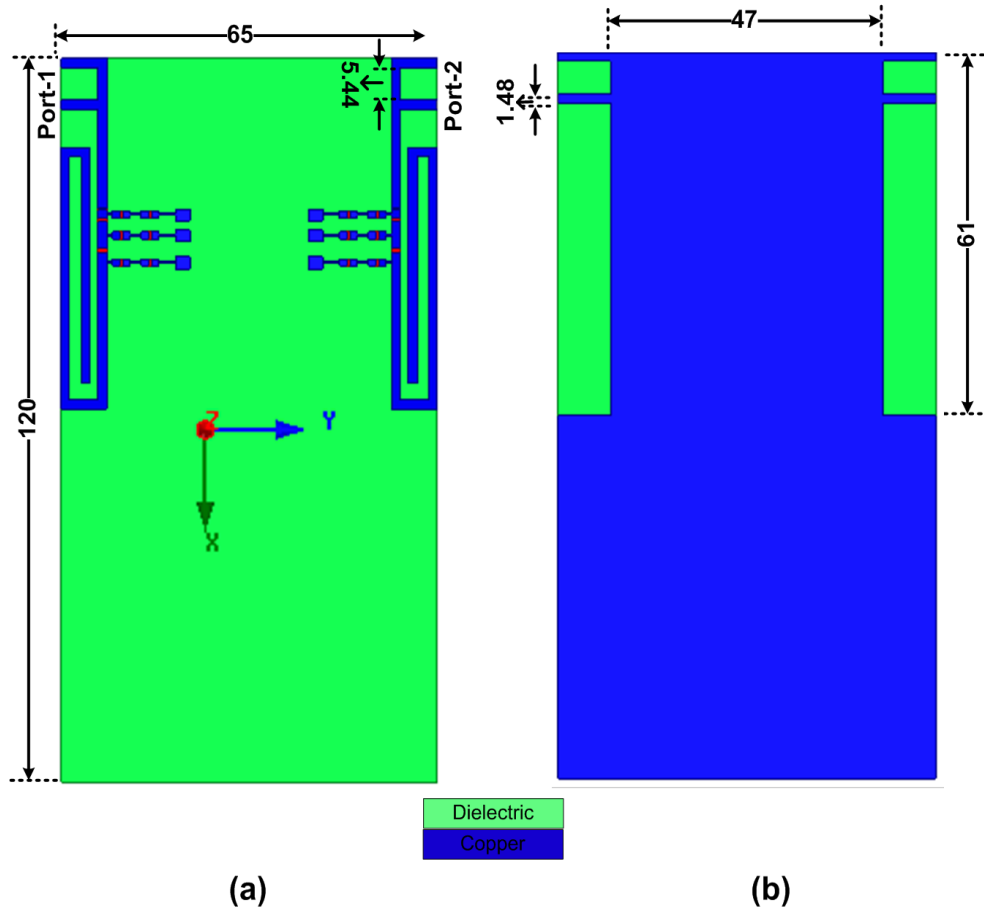
Figure 4.33: Proposed Four elements MIMO antennas system for CR platform (a) Top view (b) Bottom view - All dimensions are in millimeter (mm).

The detailed view of the four element MIMO antenna system is shown in Figure 4.34. Figure 4.34(a) shows the top view of the two out of four similar antenna structures. A unique combination of PIN and varactor diodes were used for frequency reconfigurability. Two modes of operation were achieved using PIN diodes by connecting different radiating parts of the antenna. The fine tuning of the antenna was achieved using varactor diodes and is more effective especially in lower frequency bands. Each antenna element is short circuited with the GND plane via a shorting wall to bring down the resonating frequency. The design procedure was started with the well-known developed model of F-shape antenna with certain length that was resonating at higher frequency bands above 2 GHz. The design procedure of single antenna element is completely described in section
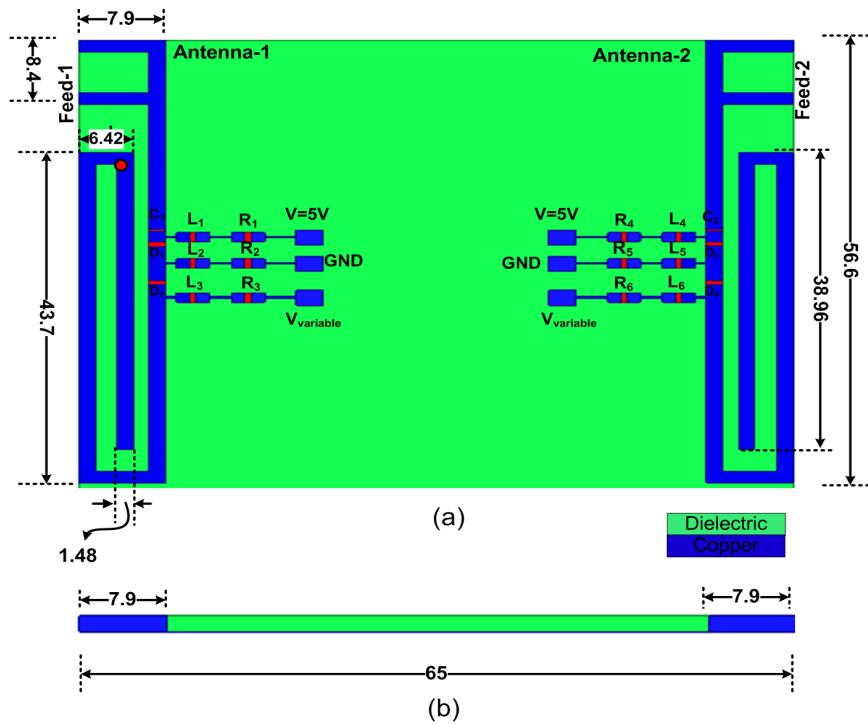
Figure 4.34: Detailed schematic of the two-element reconfigurable MIMO antenna (a) Top view (b) Side view - All dimensions are in millimeter (mm).

4.3.

The biasing circuitry for a single PIN and varactor diodes is similar one shown in Figure 4.26. The biasing circuit for both diodes is a series circuit of an RF choke and resistor connecting with PIN or varactor diode. RF choke is used to isolate the biasing DC circuit from the radiating antenna. The values used for RF choke and resistor were $1\mu H$ and 2.1 kΩ, respectively. The PIN diode is forward biased using a voltage source equal to 5V while the capacitance of varactor diode is changed smoothly by using a variable voltage source.
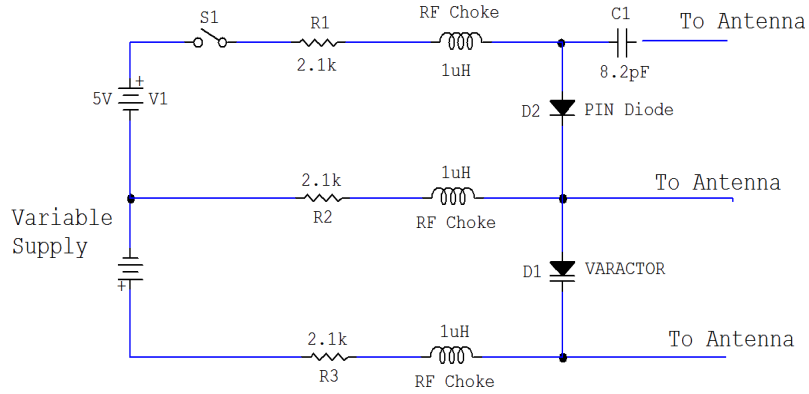
The fabricated model is shown in Figure 4.35 that was realized on Rogers 4003 substrate. Figure 4.35(a) shows the top view of fabricated model while Figure 4.35(b) shows the reference GND plane of the fabricated design.
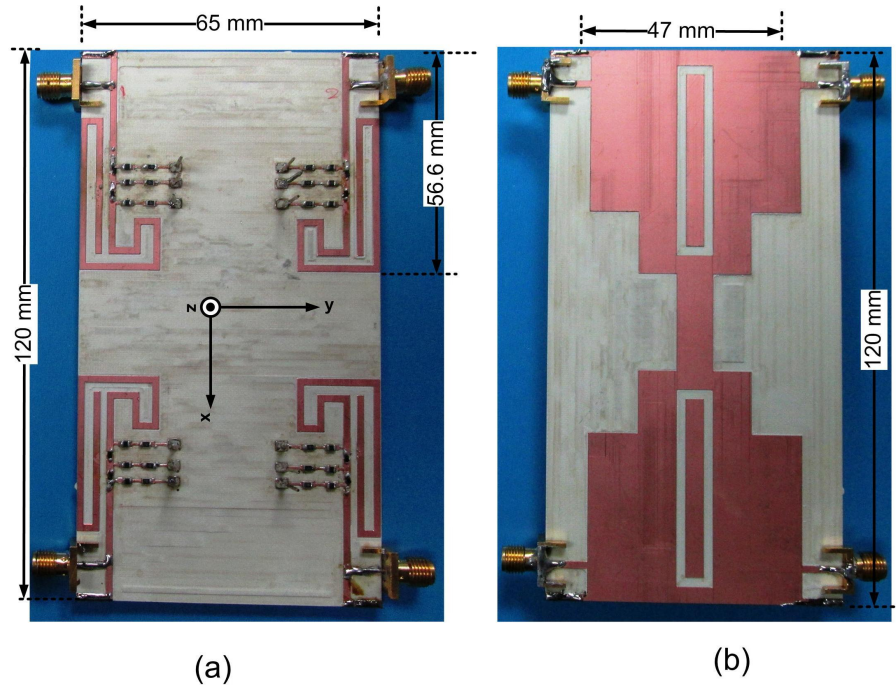
Figure 4.35: Fabricated model (a) Top view (b) Bottom view showing the reference GND plane

4.4.2 Simulation and Measurement Results

Four elements meandered line MIMO antenna was modeled and simulated using HFSS^{TM}. The optimized design was fabricated and scattering parameters were measured using an Agilent N9918A vector network analyzer. The proposed single element MIMO antenna structure was embedded with PIN and varactor diodes. The PIN diodes were used to switch the frequency bands while varactor diodes were used to sweep the tuning range over band of frequencies. The details of these modes are:

A-1 Mode-1

In mode-1, the PIN diodes are switched OFF PIN while the capacitance of varactor diodes is varied by applying reverse bias voltage. The voltage across varactor is varied between 0~6 Volts. In this mode, however the capacitance variation has negligible effects on the distribution of surface current density and hence on the operating frequency. The resulted simulated and measured reflection coefficients
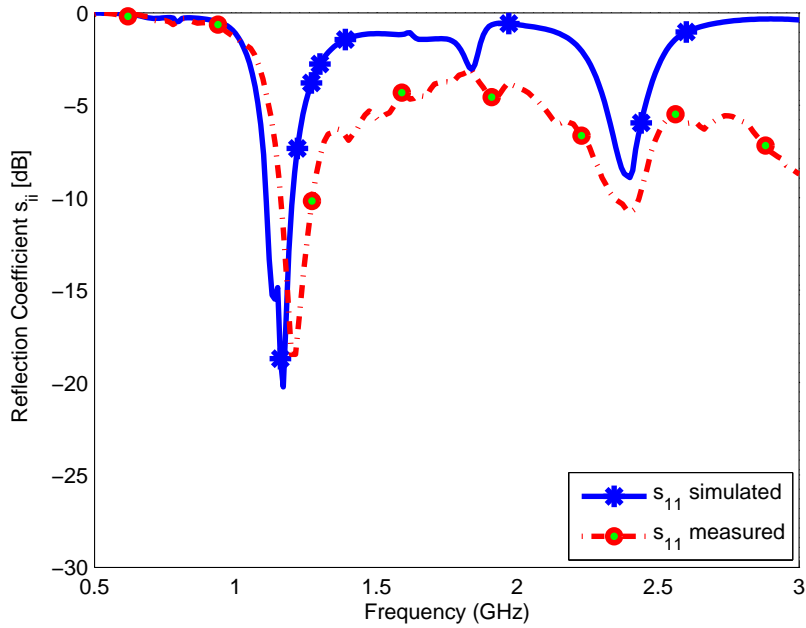
Figure 4.36: Reflection coefficients of the MIMO antenna system - Mode 1.

of mode-1 are shown in Figure 4.36. In mode-1,the operating bands are 1170 MHz and 2420 MHz with a -6 dB operating bandwidth of at-least 100 MHz in both bands.

A-2 Mode-2

In this mode, the PIN diodes are switched ON while the reverse bias voltage is applied across varactor diodes. Varactor diodes play a significant role in this mode. The resonating frequency was smoothly changed at the lower frequency band below 1 GHz. In mode-2, two resonating bands were achieved. Smooth variation of the operating frequencies were observed for the lower two bands while the addition of reactive impedance has insignificant effects on higher frequency bands. The first resonating frequency was varied between 743∼1240 MHz while the second band covered was relatively constant at 2400 MHz. The minimum -6 dB operating bandwidth for the two bands were 60 MHz, and 120 MHz, respectively.

The simulated reflection coefficients are shown in Figure 4.37 for mode-2 while

Figure 4.37: Simulated reflection coefficients of the MIMO antenna system - Mode 2.
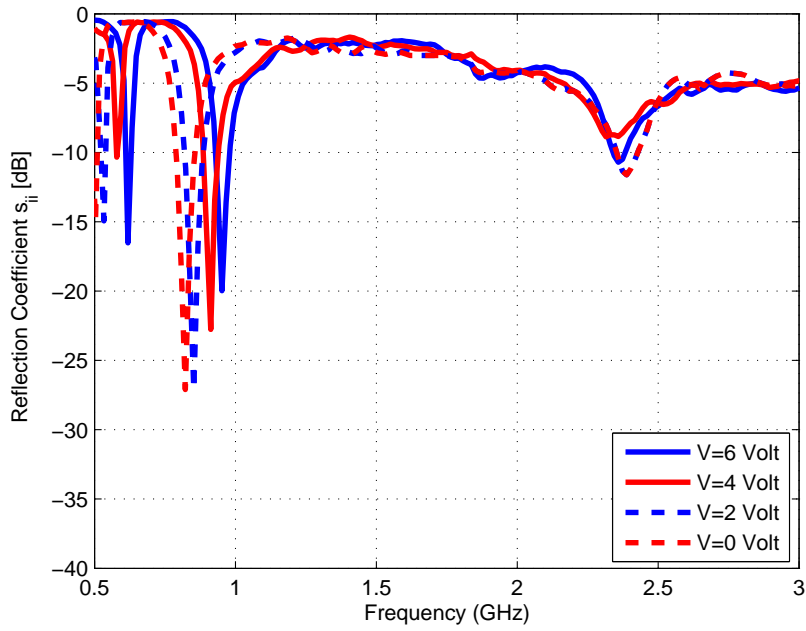
Figure 4.38: Measured reflection coefficients of the MIMO antenna system - Mode 2.
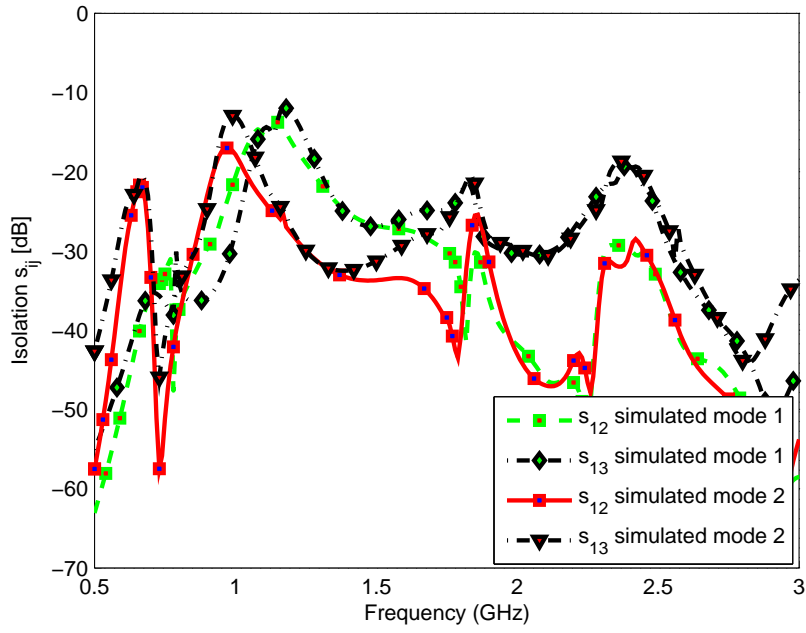
Figure 4.39: Simulated isolation between MIMO antenna elements.
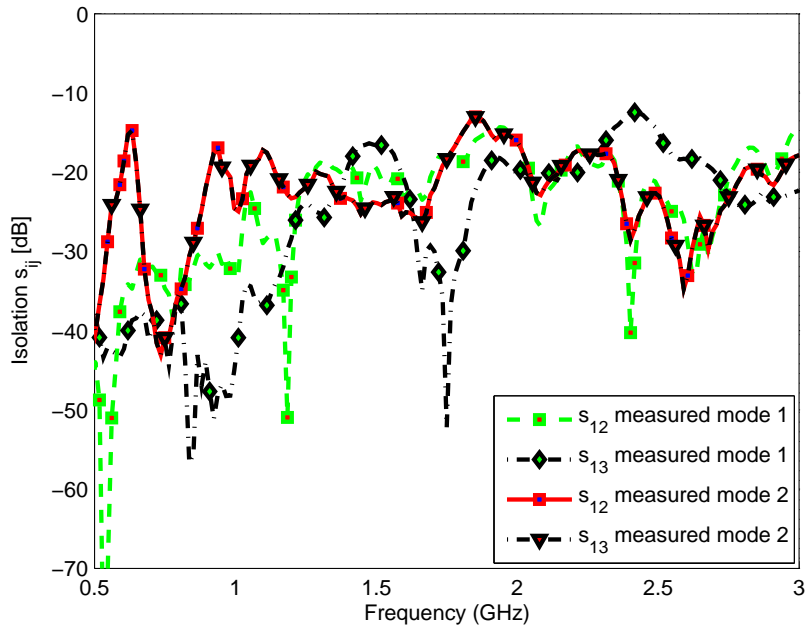
Figure 4.40: Measured isolation between MIMO antenna elements.
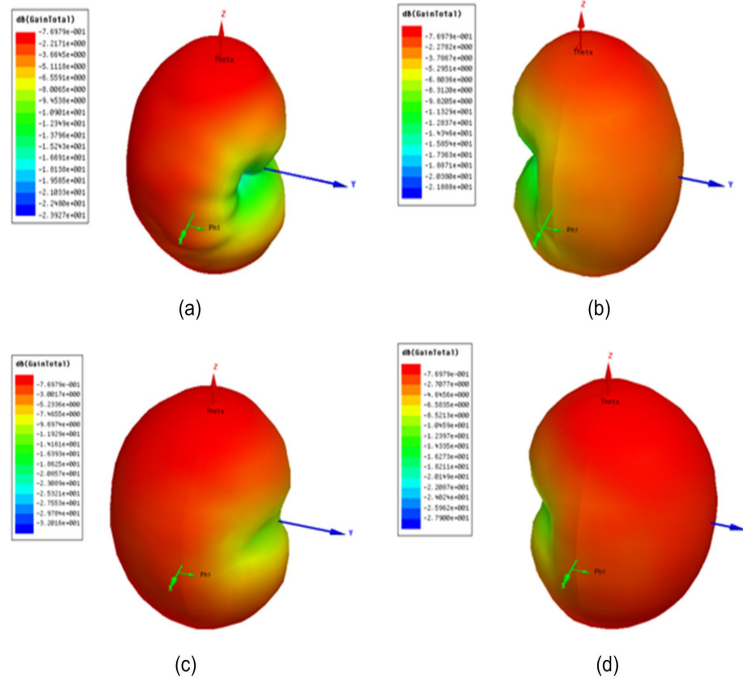
Figure 4.41: Simulated 3D gain pattern Mode-1 (a)Antenna-1 excited at 1160 MHz(b) Antenna-2 excited at 1160 MHz (c) Antenna-3 excited at 1160 MHz (d) Antenna-4 excited at 1160 MHz.

measured reflection coefficients are shown in Figure 4.38. The simulated and measured isolation curves are shown in Figures 4.39 and 4.39, respectively. The worst case measured isolation was 12 dB between the MIMO antenna elements across the operating band. The simulated and measured reflection coefficient show close agreement in the results. The slight difference in frequency shift was because of the substrate properties and fabrication tolerances. Moreover, PIN and varactor diodes were modeled according to the data provided by their data sheets. The lack of flexibility of modeling in HFSS might be the cause of the frequency drift. The PIN diodes were modeled as resistive and capacitive circuits in forward and reverse bias conditions, respectively, while the varactor diode was modeled as a variable capacitor.
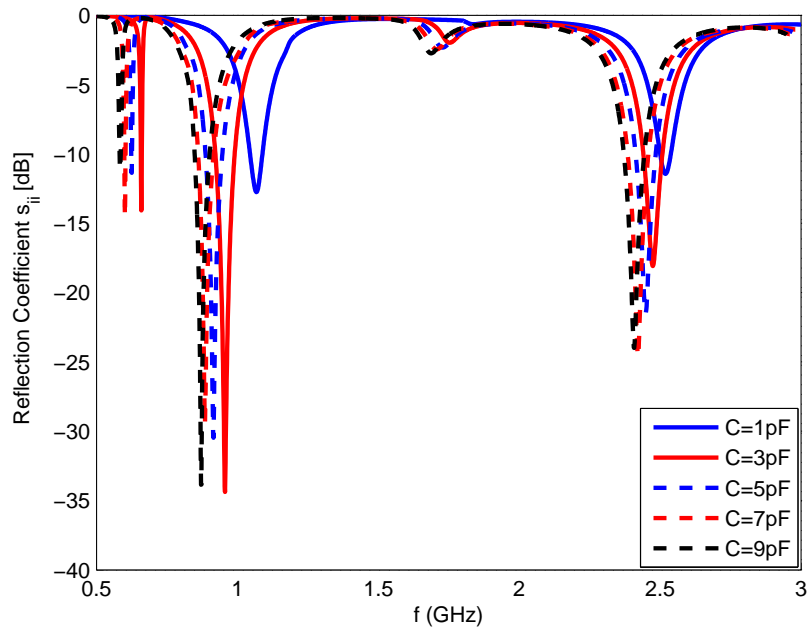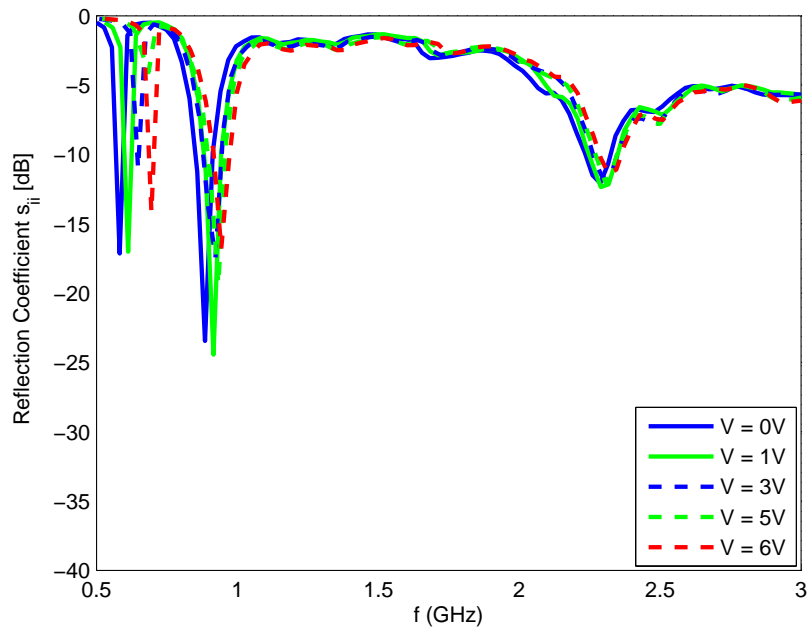
A-3 Gain Patterns and Envelop Correlation Coefficient

The simulated 3D gain patterns were computed using HFSS for the proposed reconfigurable MIMO antenna. The gain patterns for mode-1 at 1160 MHz is

shown in Figure 4.41. The simulated 3D gain pattern for all four antennas are plotted at given frequency band of mode-1. The maximas of gain pattern for each element are tilted, thus results in lower field correlation. The simulated peak gains were (-0.77dBi, 3.521dBi), respectively, for mode-1 while for mode-2, the values were (-1.798dBi, 3.521dBi), respectively. The simulated efficiencies (η %) for mode-1 at two bands were (52, 78), respectively while for mode-2, the values for two bands were (34, 78), respectively. The low efficiency of mode-2 at lower band is because of ESA structure of the proposed design.

Envelope correlation coefficient (ρ_e) were calculated based on radiation patterns. The values for simulated patterns for two modes at resonating bands were (0.014, 0.018) and (0.027, 0.021) respectively.

4.5   Planar MIMO Reconfigurable Antenna System with Ground Plane Reconfigurability Mode

In this design, planar F shape frequency reconfigurable MIMO antenna is presented. The proposed four-element MIMO antenna design is compact with low profile architecture. The proposed design is unique as its ground reference plane is also a part of reconfigurable design. Frequency agility on top layer was achieved with combination of PIN and varactor diodes while the ground plane is embedded with PIN diodes for switching. In this design, PIN diodes are used for mode selection while the varactor diode is used to sweep the frequency over a wide band especially below 1 GHz. The proposed planar four elements MIMO antenna structure is suitable for CR applications in smart phone and small wireless handheld devices in next generation 4G wireless standards.

4.5.1   Design Details

Four element reconfigurable meandered PIFA MIMO antenna is presented in this work and is shown in Figure 4.42(a) and (b). Four element MIMO antennas are

fabricated on single substrate board with dimensions $65\times120\times1.56$ mm^3. The proposed design is suitable to be used in small wireless handheld devices. Planar MIMO antenna structure and its compact size of typical smart phone size make it very attractive to be used in 4G standards in mobile terminals. The design was fabricated on Rogers 4003 substrate with ϵ_r =3.55. The four MIMO elements on top side of the board while reference ground plane is bottom with PIN diode for frequency reconfigurability to cover more frequency bands of interest. The antenna is not of regular shape. The total dimensions of the single element is summation of 7.9×37.02 mm^2 and 11.5×17.7 mm^2.

The detailed view of the four element MIMO antenna system is shown in Figure 4.43. Figure 4.43(a) shows the top view of the two out of four similar antenna structures. Three modes of operation were achieved using PIN diodes by connecting different radiating parts on top layer as well as on the reference radiating planes. The frequency sweep was achieved using varactor diodes over certain bands. Each antenna element is short circuited with the GND plane via a shorting wall to bring down the resonating frequency near the feed point at the short edge. There is one more shorting strip connecting the meandered structure with GND reference plane through PIN diode. This provide extra flexibility to tune the frequency over other frequency bands. The location of this shorting strip in encircled as shown in Figure 4.42(a).

The design procedure was started with the well-known developed model of F-shape antenna with certain length that was resonating at higher frequency bands above 2 GHz. The design procedure of single antenna element is completely described in section 4.3. The design was made more flexible to cover several other bands by providing the control of current path through its GND plane.
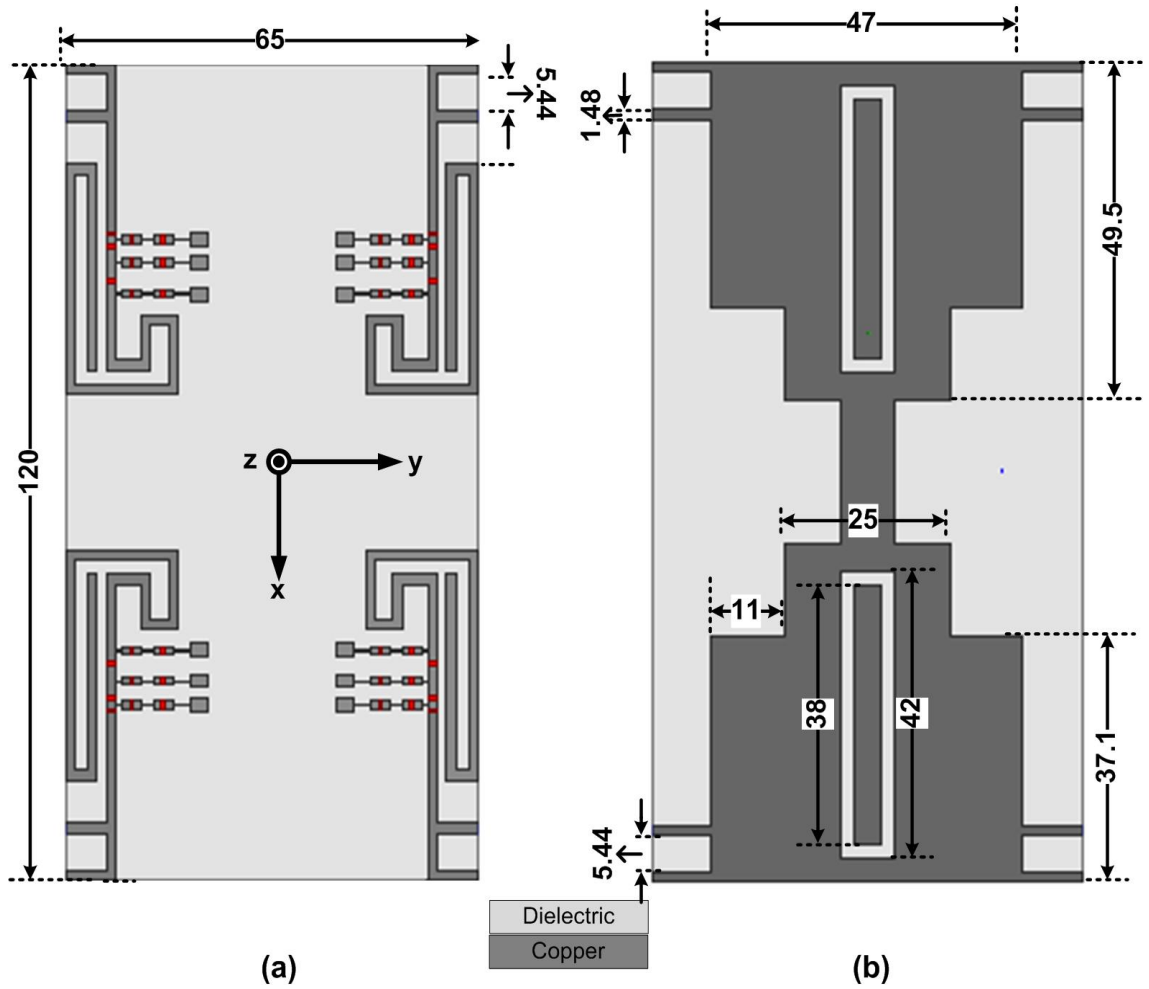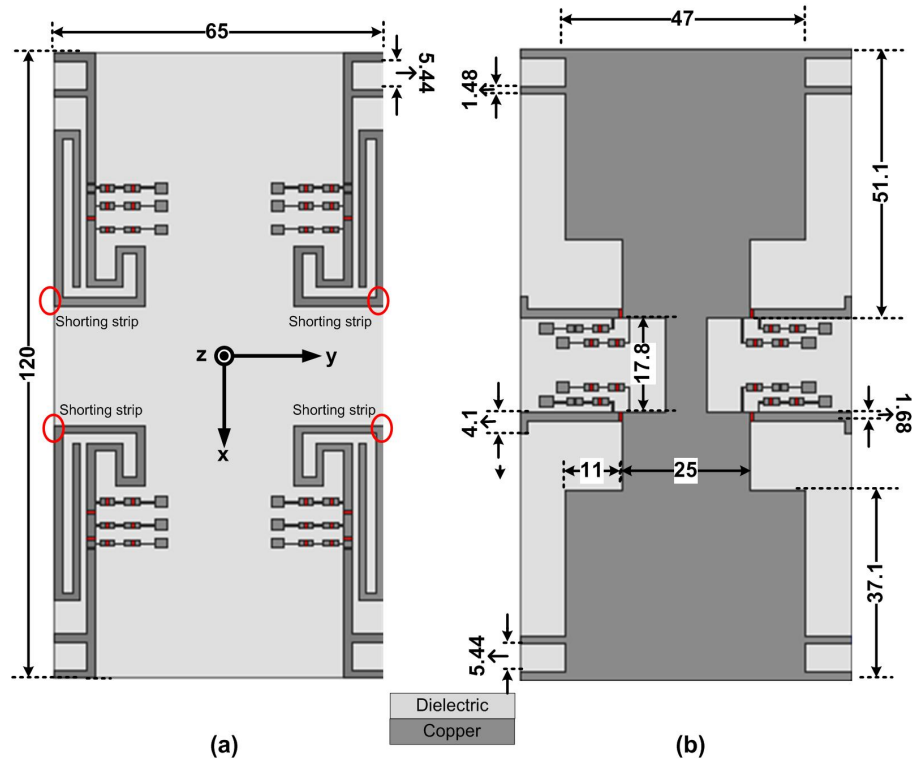
Figure 4.42: Proposed Four elements MIMO antennas system for CR platform (a) Top view (b) Bottom view - All dimensions are in millimeter (mm).
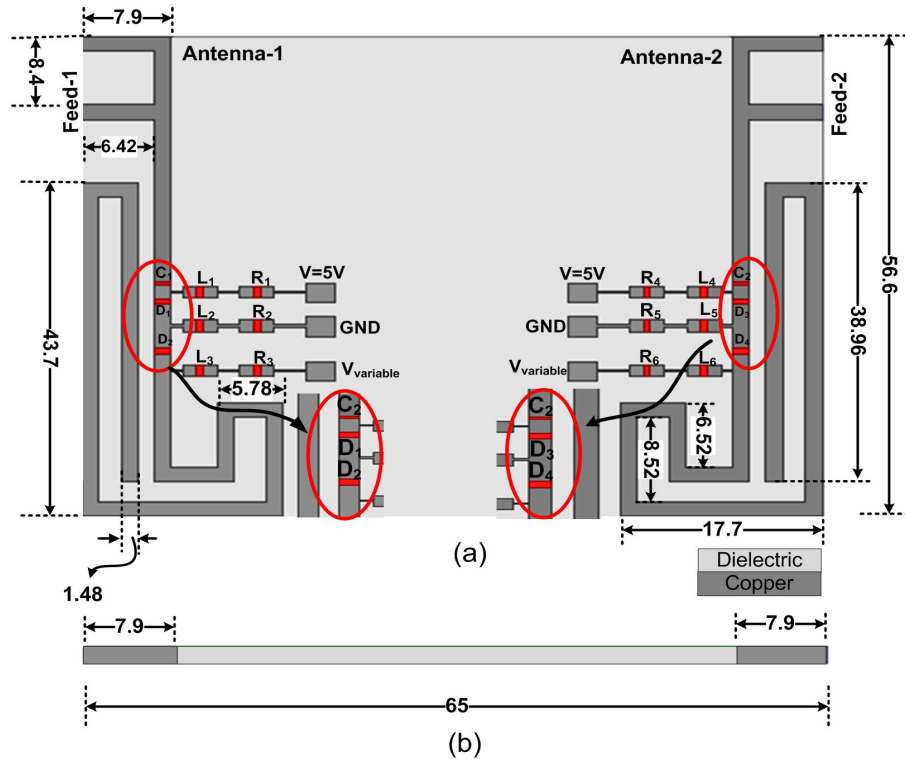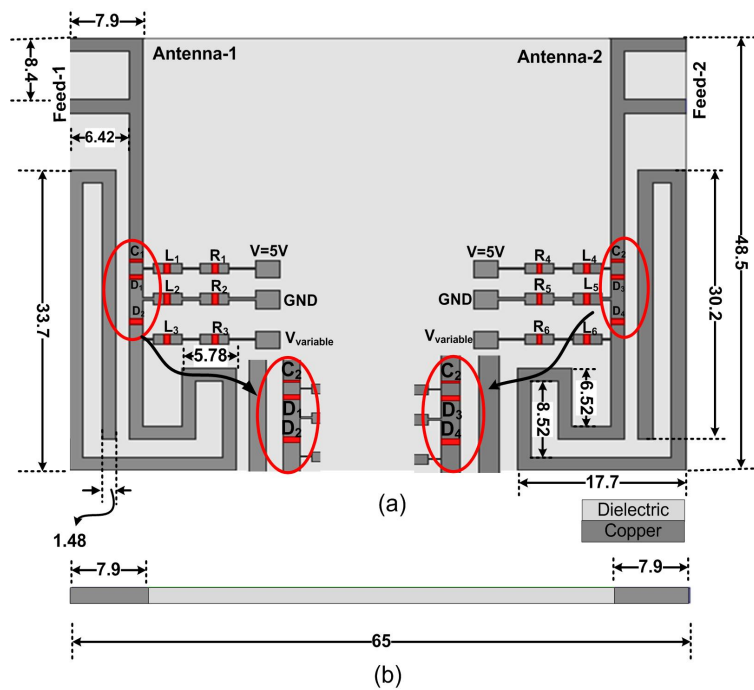

Figure 4.43: Detailed schematic of the two-element reconfigurable MIMO antenna (a) Top view (b) Side view - All dimensions are in millimeter (mm).

The biasing circuitry for a single PIN and varactor diodes is similar one shown in Figure 4.26. The biasing circuit for both diodes is a series circuit of an RF choke and resistor connecting with PIN or varactor diode. RF choke is used to isolate the biasing DC circuit from the radiating antenna. The values used for RF choke and resistor were $1\mu H$ and 2.1 kΩ, respectively. The PIN diode is forward biased using a voltage source equal to 5V while the capacitance of varactor diode is changed smoothly by using a variable voltage source.

The fabricated model is shown in Figure 4.35 that was realized on Rogers 4003 substrate. Figure 4.44(a) shows the top view of fabricated model while Figure 4.44(b) shows the reference GND plane of the fabricated design.

4.5.2 Simulation and Measurement Results

Four elements meandered line MIMO antenna was modeled and simulated using HFSS^{TM}.

(a)   (b)
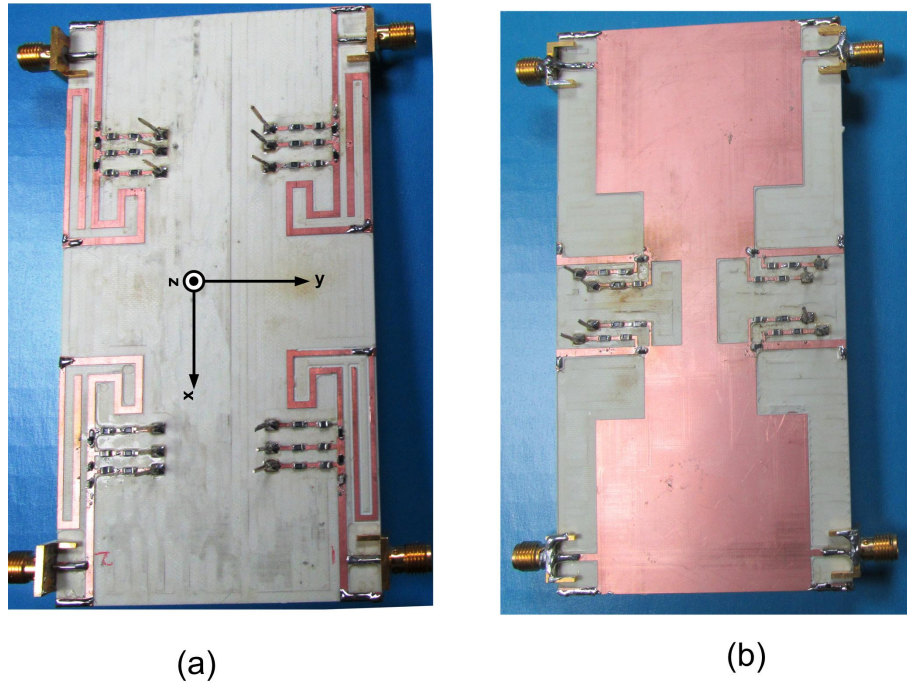
Figure 4.44: Fabricated model (a) Top view (b) Bottom view showing the reference GND plane

The optimized design was fabricated and scattering parameters were determined using an Agilent N9918A vector network analyzer. The proposed single
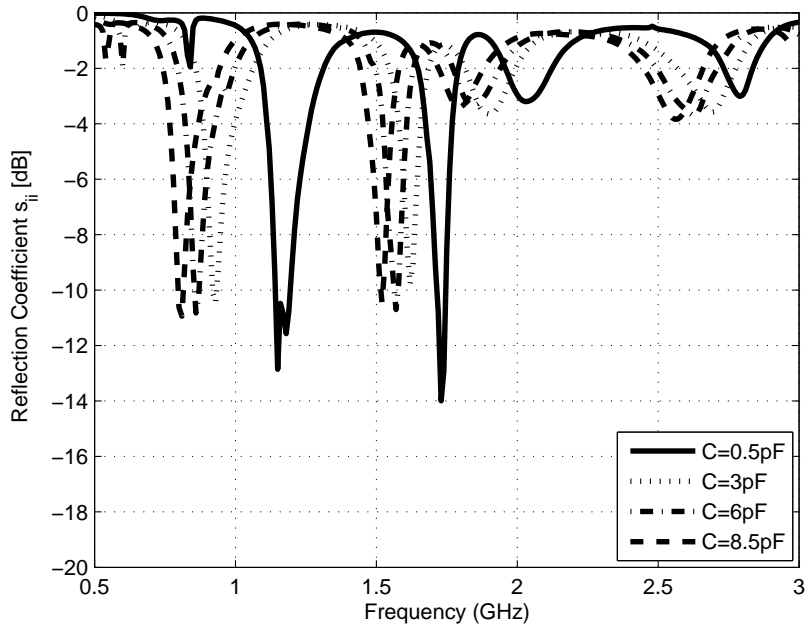
Figure 4.45: Simulated reflection coefficients of the MIMO antenna system-Mode 1.

element MIMO antenna structure was embedded with PIN and varactor diodes on top layer while top layer is connected through PIN diodes by shorting strip to GND planes. The details of these modes are given below:

A-1 Mode-1

In mode-1, all PIN diodes on top and bottom layers are switched OFF while the capacitance of varactor diodes is varied by applying reverse bias voltage. The voltage across varactor is varied between 0~6 Volts. The simulated and measured reflection coefficients of mode-1 are shown in Figures 4.45 and 4.45. In mode-1, basically, two modes of frequency bands are achieved with sweep of frequency bands using varactor diodes. the operating bands are 780~1230 MHz and 1490~1760 MHz. The -6 dB operating bandwidth in both bands are at-least 60 MHz and 50 MHz, respectively.
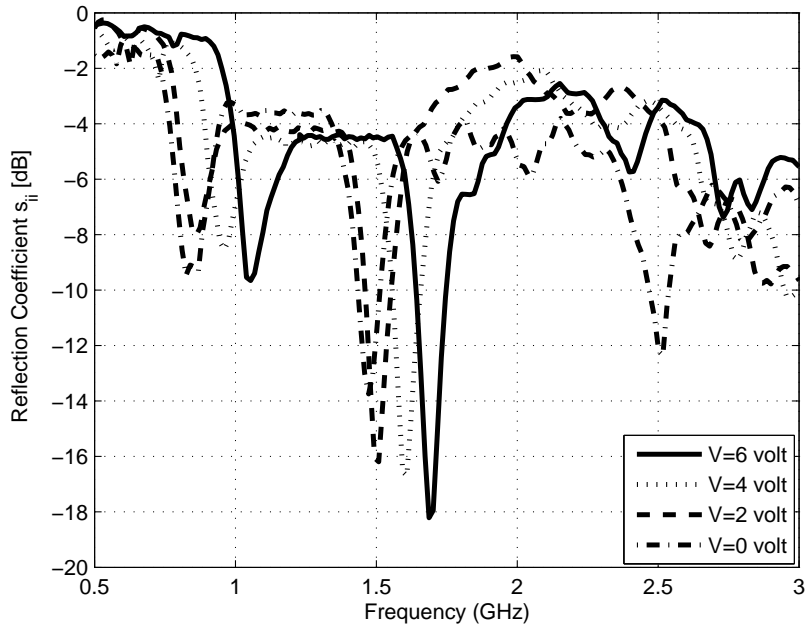
Figure 4.46: Measured reflection coefficients of the MIMO antenna system-Mode 1.

A-2 Mode-2

In this mode, the PIN diodes on top side of the antenna are actuated while the PIN diodes embedded on reference plane were switched OFF. The reverse bias voltage across varactor diodes was varied between 0∼6 volts. In this mode, there are four resonance frequencies bands. This is quite productive mode as it can be used to cover several frequency bands. Smooth variation of the operating frequencies were observed for the lower two bands while the addition of reactive impedance has insignificant effects on higher frequency band at 2.4 GHz. The first two resonating frequency were actually superimposing each other by varying capacitance of varactor. The frequency sweep observed for first two bands were from 610 ∼920 MHz with minimum -6dB bandwidth of 30 MHz. The third resonating bands is varied from varied between 1210∼1430 MHz with -6 dB operating bandwidth of 90 MHz. The fourth frequency band is relatively independent of varactor capacitance and is constant at 2.4 GHz with -6dB operating bandwidth of 100 MHz. The simulated and measured reflection coefficient curves for mode-2 are shown in Figures 4.47 and 4.48, respectively.
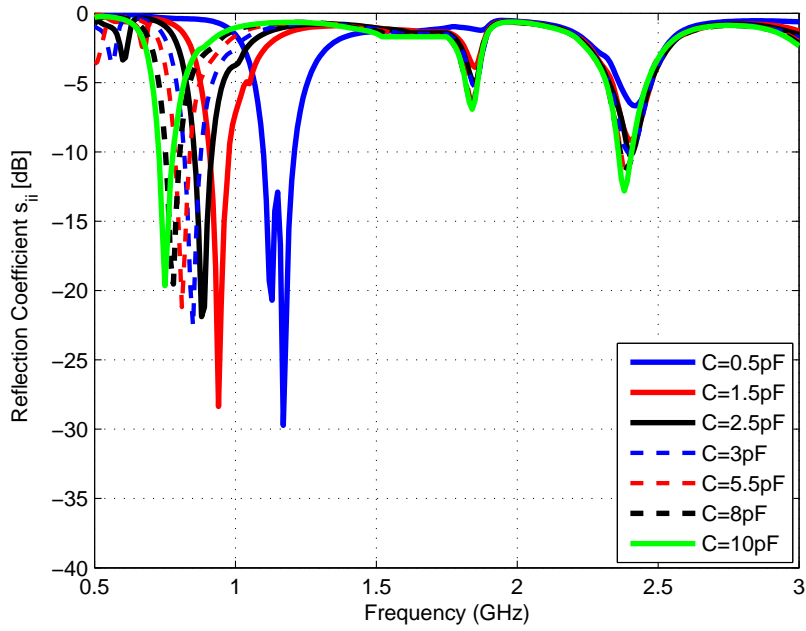
103
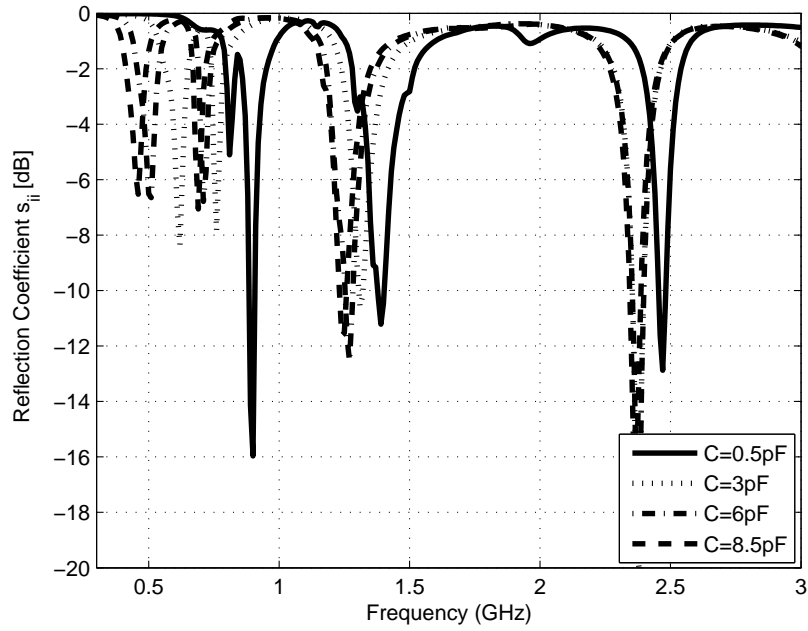
Figure 4.47: Simulated reflection coefficients of the MIMO antenna system-Mode 2.
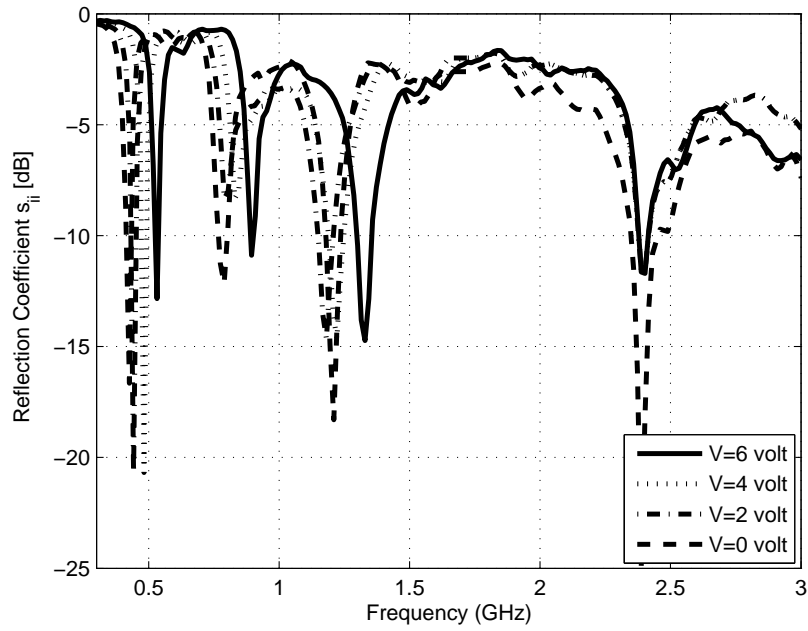
Figure 4.48: Measured reflection coefficients of the MIMO antenna system-Mode 2.
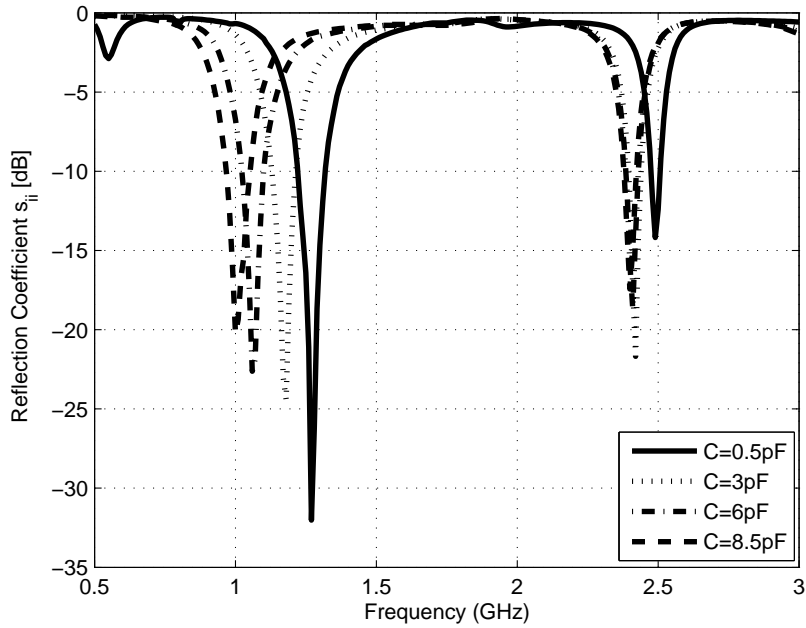
Figure 4.49: Simulated reflection coefficients of the MIMO antenna system-Mode 3.

A-3 Mode-3

In this mode, all the PIN diodes were switched ON on top and bottom side of the board with additional reverse bias voltage across varactor diodes. In mode-3, two resonating bands were achieved. Smooth variation of the operating frequencies were observed for the lower band while the addition of reactive impedance has insignificant effects on higher frequency bands. The first resonating frequency was varied between 940~1350 MHz while the second band covered was relatively constant at 2400 MHz. The minimum -6 dB operating bandwidth for the two bands were 140 MHz, and 90 MHz, respectively. The simulated reflection coefficient curves are shown in Figure 4.49 while the measured reflection coefficient curves for mode-4 are shown in Figure 4.50.

The simulated and measured isolation curves are shown in Figures 4.39 and 4.39, respectively. The worst case simulated and measured isolation were 12.17 dB and 12.46, respectively between the MIMO antenna elements across the operating band. The simulated and measured reflection coefficient show close agreement in the results. The slight difference in frequency shift was because of the substrate
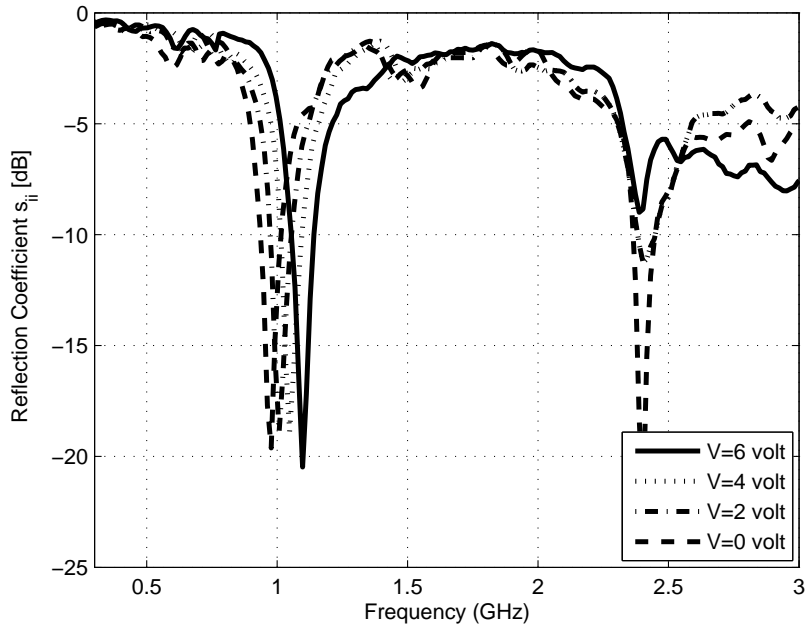
Figure 4.50: Measured reflection coefficients of the MIMO antenna system-Mode 3.

properties and fabrication tolerances. Moreover, PIN and varactor diodes were modeled according to the data provided by their data sheets. The lack of flexibility of modeling in HFSS might be a cause of frequency drift. The PIN diodes were modeled as resistive and capacitive circuits in forward and reverse bias conditions, respectively, while the varactor diode was modeled as a variable capacitor.

A-3 Gain Patterns and Envelop Correlation Coefficient

The simulated 3D gain patterns were computed using HFSS for the proposed reconfigurable MIMO antenna. The gain patterns for mode-1 at 1040 MHz is shown in Figure 4.53. The simulated 3D gain pattern for all four antennas are plotted at given frequency band of mode-1. The maximas of gain pattern for each element are tilted, thus results in lower field correlation. The simulated peak gains were (1.77dBi, -2.99dBi), respectively, for mode-1 while for mode-2, the values were (-6.23dBi, -2.1dBi, -1.43dBi, -0.8 dBi), respectively.Similarly, for mode-3, the simulated peak gain values were (-1.125dBi, -0.8 dBi) The simulated efficiencies (η %) for mode-1 at two bands were (61, 15), respectively, for mode-2,
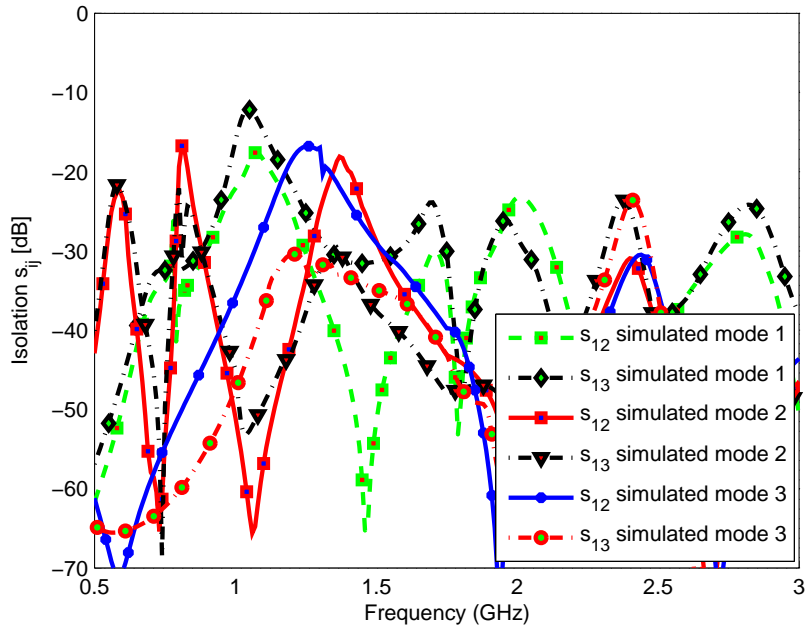
Figure 4.51: Simulated isolation between MIMO antenna elements.
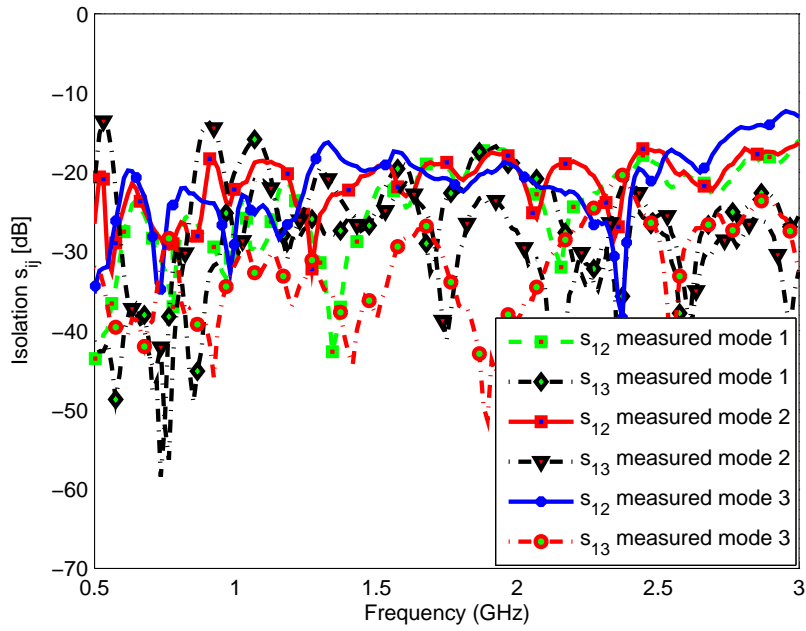
Figure 4.52: Measured isolation between MIMO antenna elements.
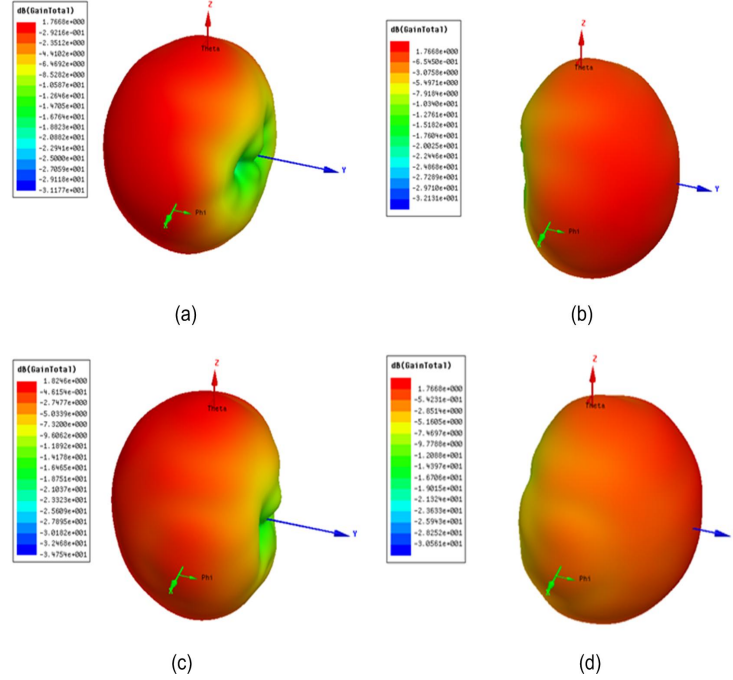
Figure 4.53: Simulated 3D gain pattern Mode-1 (a)Antenna-1 excited at 1040 MHz(b) Antenna-2 excited at 1040 MHz (c) Antenna-3 excited at 1040 MHz (d) Antenna-4 excited at 1040 MHz.

the values for four bands were (15, 23, 35, 38), respectively while for mode-3 the values for two bands were (35, 38), respectively

Table 4.3: Features summary of all designs

S.No	Elements	Size (mm^2)	Bands	Sweep	Compact Design
D-1	2	11×28	8	No	Yes
D-2	2	12×30	2	Yes	Yes
D-3	2	7.9×56.6	5	Yes	Yes
D-4	4	7.9×37+17.7×19.6	4	Yes	Yes
D-5	4	7.9×37.2+11.5×17.7	8	Yes	Yes

The proposed reconfigurable antenna is a multi-band design and hence excites more than one mode. The radiation efficiency of the fundamental radiation mode is relatively high while higher order modes have considerably smaller radiation efficiencies. The proposed design is an ESA structure with multi-band operation

hence the observed lower efficiencies and gain values at some bands are expected.

Envelope correlation coefficient (ρ_e) were calculated based on radiation patterns. The values for simulated patterns for three modes at resonating bands were (0.02, 0.035), (0.017, 0.041, 0.028, 0.035) and (0.085, 0.0412) respectively.

A summary of all designs discussed in this chapter are provided in Table 4.3. The designs given are according to section order (i.e. sections 1.1∼1.5 as D-1∼D-5). The comparison table is provided to compare features such as, size of single element, total number of bands, possibility of frequency sweep across various frequency bands and for its compact structure. The given designs, D-2∼D-5, provide smooth frequency change over a wide bands especially in lower frequency bands. All the designs provided are suitable and recommended to be used in smart phone and small wireless handheld devices.

4.6 Conclusion

In this chapter, five novel compact reconfigurable MIMO antenna design are presented. The antenna designs are based on two modified geometries of meander-line and PIFA based structure. All the designs were analyzed for reconfigurability by PIN diode switching and change in the reactive impedance by varactor diodes capacitance variation. The proposed antenna designs are suitable for CR applications in small wireless handheld devices. The proposed designs can be used at different frequency bands especially below 1 GHz operation. The antennas were also evaluated for MIMO parameters where it showed good performance. All the presented designs conform to MIMO standards and could be utilized in 4G wireless standards. The total space occupied by all design was 65×120 mm^2 which is very compact given the covered frequencies.

CHAPTER 5

INTEGRATION OF SENSING AND RECONFIGURABLE MIMO ANTENNAS FOR CR PLATFORMS

In this chapter, CR antennas are presented that were integrated on a single substrate area with MIMO operation. Very few MIMO antenna designs have appeared in literature that employ reconfigurable MIMO communication antennas along with sensing antenna on same substrate. In this chapter, two MIMO antenna systems along with sensing antenna are presented and analyzed. The proposed designs were intended to cover as many bands as possible between $0.7 \sim 3$ GHz. The proposed sensing antenna is aimed to cover the desired UWB range from $0.7 \sim 3$ GHz. The designs cover several frequency bands including GSM, LTE and WLAN along with other frequency bands. The proposed designs are the first to appear in literature covering low frequency bands (i.e. 700 MHz) within a compact size along with reconfigurability. All the designs proposed were fabricated using an LPKF-Protomat S103 and scattering parameters were measured at the AMSDL at the Electrical Engineering Department at KFUPM.

5.1 Modified PIFA MIMO Antenna with an UWB Sensing Antenna

In CR platforms, the unoccupied or under used spectrum bands are allocated to secondary users. This could be accomplished by deploying sensing of the entire spectrum and switching across the available frequency bands. Most of the work related to CR applications with reconfigurable antenna systems cited in literature were single element with a sensing antenna working above 2 GHz and very few designs with MIMO antenna operation were proposed above 3 GHz.

In the proposed design, a novel modified reconfigurable PIFA-like MIMO antenna is proposed for CR applications. This two element MIMO system is integrated with PIN diodes to tune the antenna over various frequency bands. The distinguishing feature of the proposed design is its operation at low frequency bands from starting 755 MHz and up to 3450 MHz, based on the selection of the reconfiguration mode. Most of the cited designs in literature for CR applications were reported to work above 2 GHz. This work also reports the first UWB sensing antenna that covers sub-GHz bands with compact size.

Moreover, another interesting feature of the proposed design is the integration of the UWB sensing antenna with the reconfigurable MIMO antenna system without any significant addition to the planar structure. The ground plane of the MIMO PIFA is optimized and tuned to work as a sensing antenna during the scanning phase of the frequency spectrum and operates as a ground reference plane during the communication stage. All of the designs known so far use separate sensing and reconfigurable MIMO antennas in CR applications.

Furthermore, the proposed MIMO antenna system is compact and suitable for handheld (smart phones, tablets and PDAs) CR platforms with MIMO capability. The single MIMO element has a total dimension of 12×30 mm^2. The complete integrated antenna was created within a dielectric substrate area of $65 \times 120 \times 5.8$ mm^3. The antenna system cover the bands from $755 \sim 3450$ MHz.

5.1.1   Design Details

The proposed novel frequency reconfigurable modified PIFA MIMO antenna system along with its UWB sensing antenna is shown in Figure 5.1. The complete model consists of two printed circuit boards. The main board with dimensions $65 \times 120 \times 1.56$ mm^3 containing the UWB sensing antenna on the bottom layer and GND plane of the UWB monopole antenna on the top side of the main board. The elevated board containing the modified PIFA MIMO reconfigurable antennas each with dimensions $30 \times 12 \times 0.8$ mm^3. Both designs were fabricated on a commercial FR-4 substrate with ϵ_r=4.4.

The reconfigurable MIMO elements were mounted on the top corners of the main board with a coaxial feed. The total height of the whole system was 5.8 mm. The bottom layer of the main board contained the UWB monopole antenna which was also acting as a reference GND plane for the reconfigurable antennas.

Figure 5.2(a) shows the TOP view of the two reconfigurable modified PIFA MIMO elements with their associated digital biasing circuitry. PIN diodes were used to connect the two different radiating parts at two different points on the top side of the elements thus providing reconfigurability. The switching mechanism of the PIN diodes leads to four distinct modes of operation for each element.

Figure 5.2(b) shows the bottom layer of the reconfigurable MIMO antenna elements. The bottom side consists of radiating lines and the coaxial feed. The two elements were fed from the bottom side. Figure 5.2(c) shows the side view while Figure 5.2(d) shows the front view of the reconfigurable antenna. Both elements were connected to the ground plane through a shorting wall of width 1.7 mm. Figure 5.2(c) shows a zoomed in view to show the shorting wall from the bottom of the elevated antenna to the GND plane. The shorting walls connecting the elevated antenna with the ground plane was used to lower the resonating frequencies of the elements.

The biasing circuitry for a single diode is shown in Figure 5.3. Two diodes were used for each antenna. The circuit is a series combination of an RF choke of 1 μH in series with 2.1 kΩ resistor connecting the PIN diode with the radiating part of
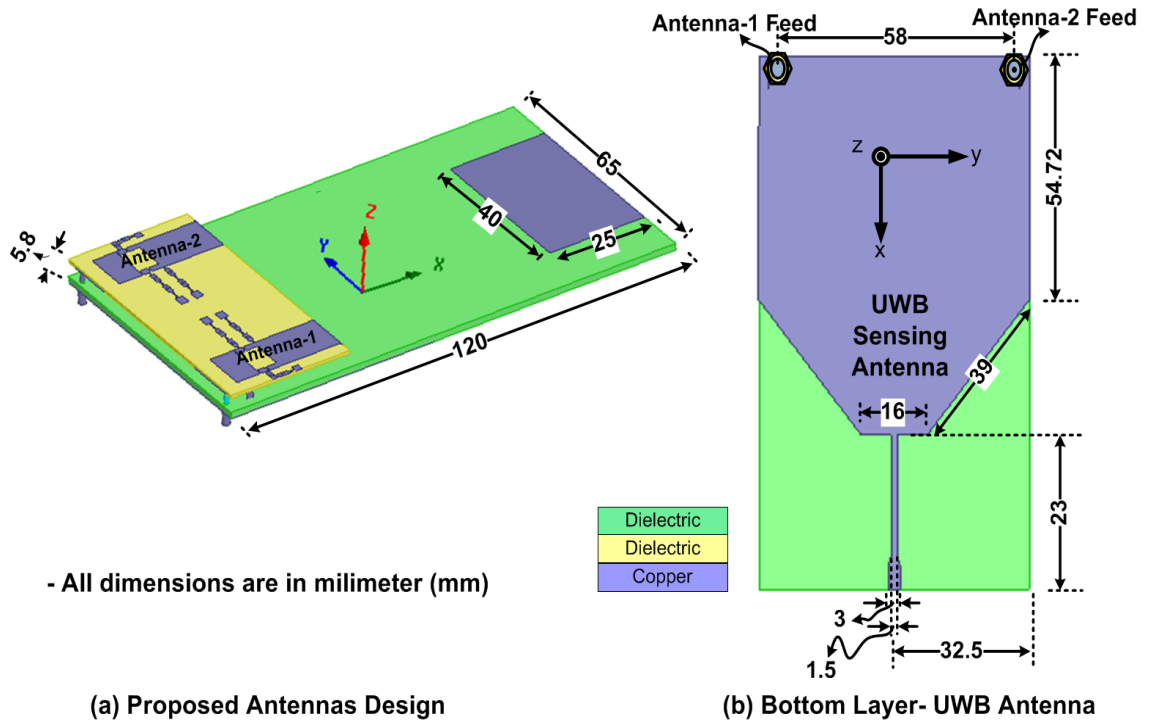
Figure 5.1: Proposed MIMO antennas system for CR platform (a) Top view (b) Bottom view.

antenna. Both terminals of the PIN diode were connected with the RL circuit to isolate the DC and RF parts of the antenna. The value of the resistor is selected to pass sufficient current and within the rating current in the forward biased condition of the PIN diode. The two reconfigurable antennas are exactly similar in structure to form the MIMO system. All the resistor, capacitor and inductor values used in the biasing circuitry were same for all four branches containing the PIN diodes for switching purposes. The fabricated model of the proposed design is shown in Figure 5.4. Figure 5.4(a) shows the top view of the complete 2-element MIMO antenna system integrated with the UWB sensing antenna. Figure 5.4(b) shows the bottom layer of the fabriacted sensing antenna which was also acting as a reference GND plane for the reconfigurable antenna. Figs. 5.4(c) and Figure 5.4(d) show the top and bottom views of the fabricated modified PIFA reconfigurable MIMO antennas, respectively.
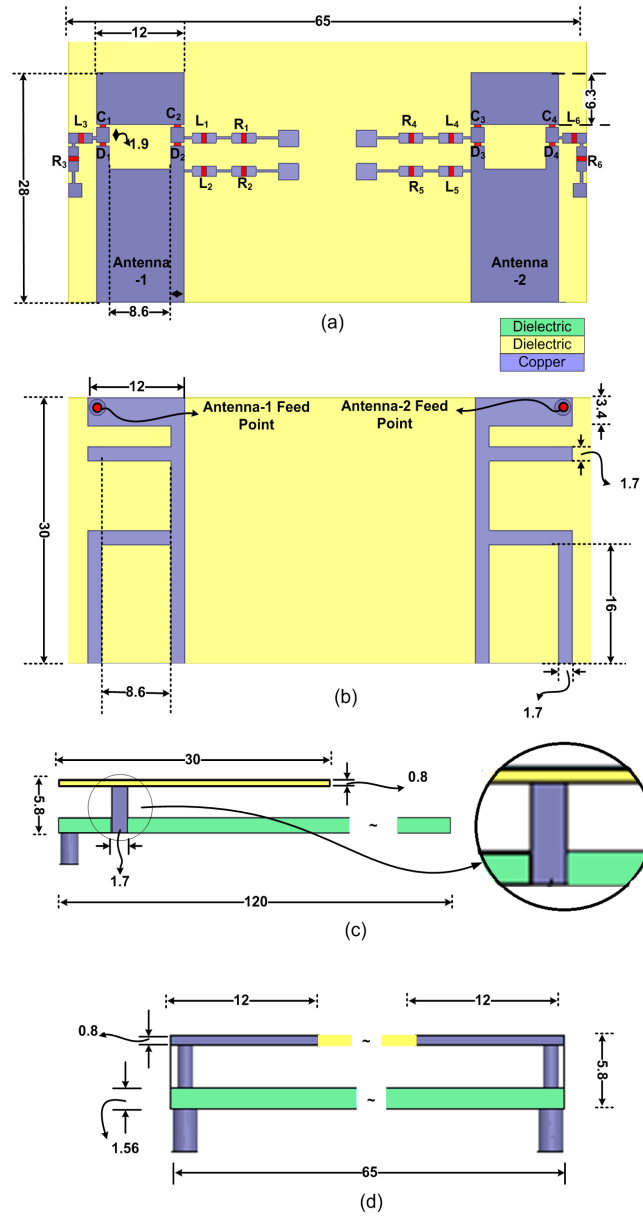
Figure 5.2: Detailed schematic of the two-element reconfigurable MIMO antenna (a) Top view (b) Bottom view (c) Side view (d) Front view - All dimensions are in millimeter (mm).
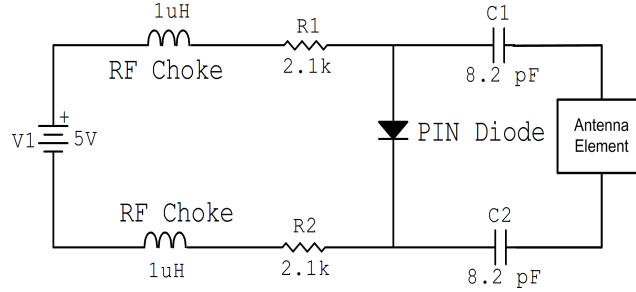
Figure 5.3: PIN diode biasing circuitry

5.1.2 Simulation and Measurement Results

The complete two element reconfigurable MIMO antenna system along with its sensing antenna was modeled and simulated using HFSS^{TM}. The scattering parameters of the fabricated design were measured using an Agilent N9918A vector network analyzer (VNA). The gain patterns and efficiencies were measured at King Abdullah University of Science and Technology (KAUST), Jeddah, Saudi Arabia, using a SATIMO Starlab anechoic chamber. The starting frequency for the chamber was 800 MHz. All measured and simulated results of MIMO antennas and sensing antennas are summarized in the following subsections.

A-1 UWB Sensing Antenna

An UWB sensing antenna is an essential and integral part of CR platforms for channel sensing. The proposed UWB sensing antenna is based on a monopole structure as shown in Figure 5.1. The objective of this antenna was to achieve UWB sensing operation bands of 700$\sim$ 3500 MHz with typical smart mobile handset backplane size of 65$\times$120 mm^2. The design presented cover frequency bands frequency bands from 710$\sim$ 3600 MHz. According to the literature survey conducted, most of the UWB designs for CR platform were operating above 3 GHz and very few were found to be working in the 2 GHz and above keeping in mind the area constraint.

The simulated and measured reflection coefficients are shown in Figure 5.5. The measured results for the fabricated antenna are in close agreement with the simulated results. To check the effect of having a hand on the UWB antenna,
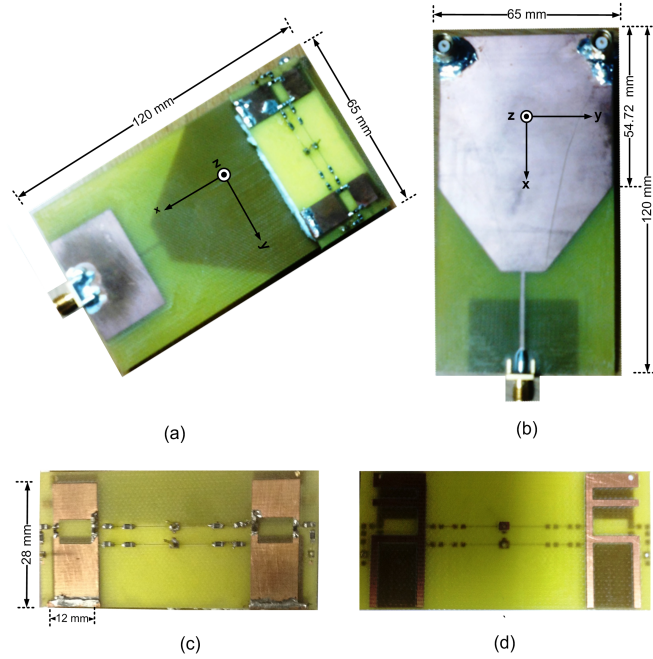
Figure 5.4: Fabricated model (a) Top view (b) Bottom view showing the sensing antenna (c) Top view of reconfigurable MIMO antenna(d) Bottom view of reconfigurable MIMO antenna.

a curve showing the resonance behavior in its presence has little effect on the antenna $|S_{11}|$ curves.

The reconfigurable communication antenna is integrated with sensing antenna by sharing the same substrate and is critical to consider the mutual coupling or isolation between the communication and sensing antennas. Figure 5.6 shows the isolation between sensing antenna and the two element MIMO antennas. It has been observed that the minimum isolation is better than 14 dB in all frequency bands. The sensing antenna for CR applications must possess an omnidirectional radiation pattern. Figure 5.7 (a), (b) and (c) show the simulated 3-D gain patterns of the UWB antenna at three different frequency bands: 800 MHz, 1500 MHz and 3000 MHz, respectively. The simulated and measured 2-D gain patterns in the yz-plane at three different frequencies (800 MHz, 1500 MHz and 3000 MHz) are shown in Figure 5.8. The peak gain and efficiencies for sensing antenna are computed. The simulated and measured results are given in Table 5.1. Good agreement is observed.

116
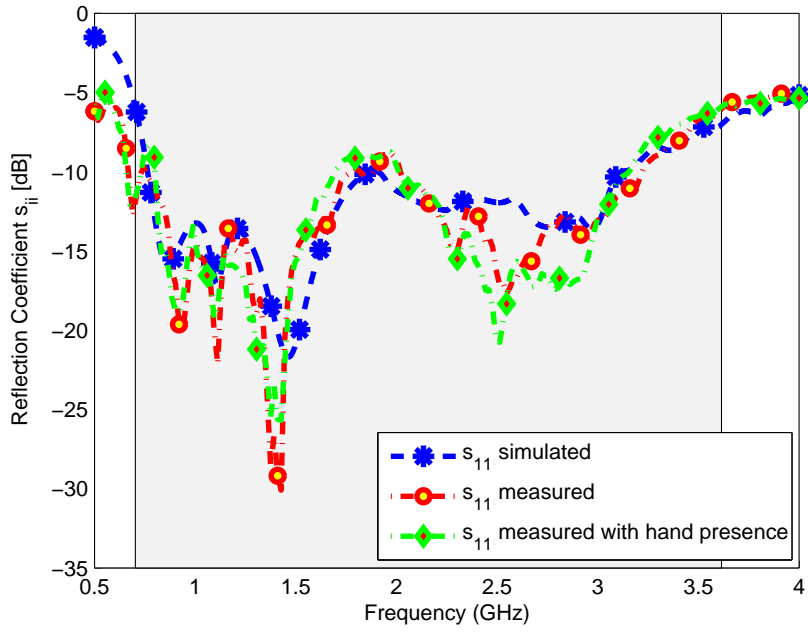
Figure 5.5: Simulated and measured reflection coefficient of UWB sensing antenna.
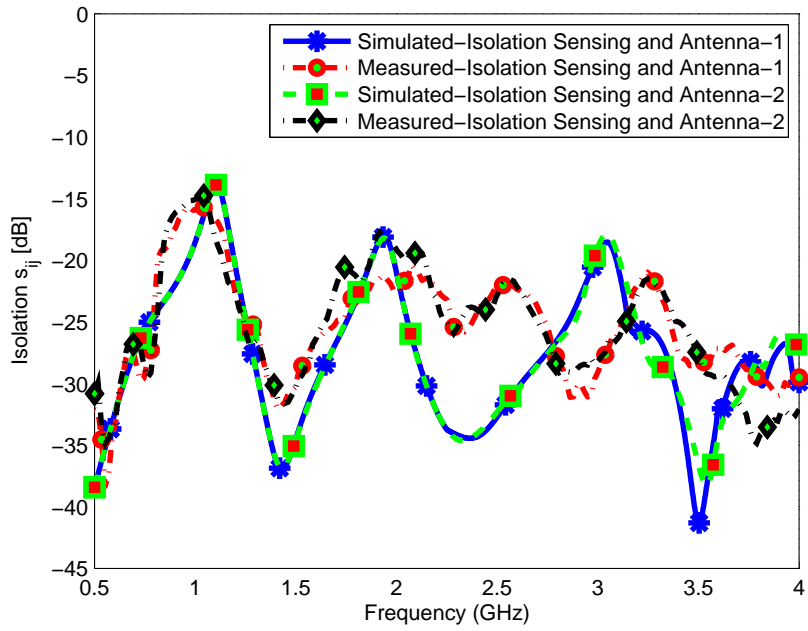
Figure 5.6: Mutual coupling between sensing and MIMO antennas.

117
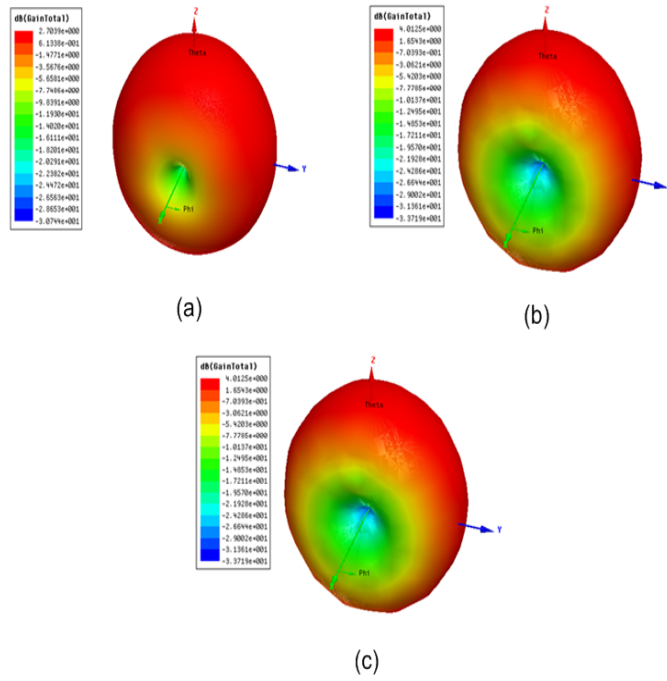
Figure 5.7: Simulated 3-D gain pattern at (a) 800 MHz (b) 1500 MHz (c) 3000 MHz.
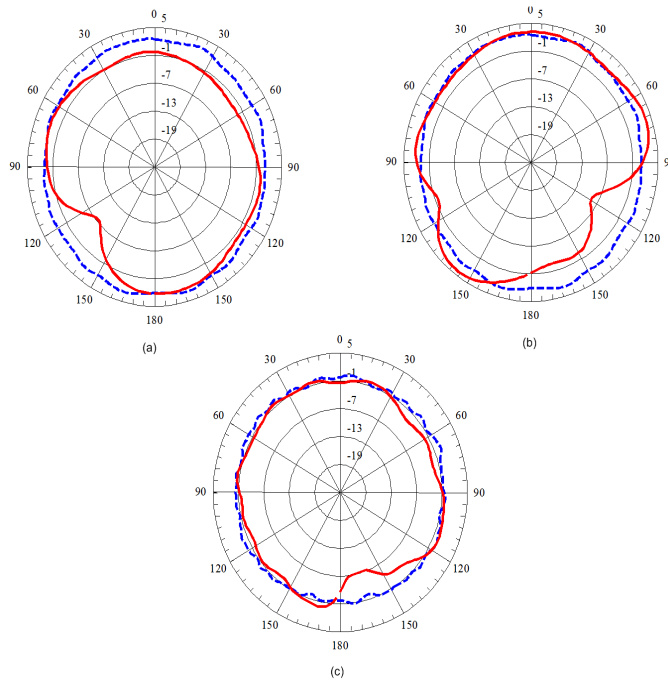
Figure 5.8: Simulated and measured 2D gain pattern in yz-plane. Dashed lines - simulated, solid lines - measured (a) 800MHz (b) 1500MHz (c) 3000MHz.

Table 5.1: Antenna Efficiency and Peak Gain of the Sensing Antenna

	Peak Gain (dBi)		Efficiency (%)	
	Simulated	Measured	Simulated	Measured
800 MHz	2.72	3.19	75	67
1500 MHz	4.01	5.49	91	84
3000 MHz	4.69	3.79	96	87

Table 5.2: Reconfigurable Antenna Operation Modes

S.No	PIN Diode 2	PIN Diode 1
Mode-1 (M1)	OFF	OFF
Mode-2 (M2)	OFF	ON
Mode-3 (M3)	ON	OFF
Mode-4 (M4)	ON	ON

A-2 Reconfigurable MIMO Antenna

Each reconfigurable MIMO element is based on modified PIFA consisting of folded patch with a meander line structure. The bottom side meander structure provide two different current paths resulting in multi-resonances. The top side of the modified PIFA is a discontinuous slotted patch antenna structure. The discontinuity of the antenna is integrated with PIN diodes for connecting or disconnecting the two top parts of the antenna structure. Thus diodes are used to provide more flexibility by its ON/OFF operation. The non-symmetrical structure of the PIFA with PIN diodes results in different radiating lengths which results in multiple bands for various modes of operation. The two PIN diodes in each antenna element results in four distinct operating modes for each MIMO antenna element. The details of modes for PIN positions are given in Table 5.2. These four modes of operation result in different frequency resonances. These modes are:

A-2.1 Mode-1

In this mode, both PIN diodes at the top side of the reconfigurable MIMO antenna are switched OFF. The resulted simulated and measured reflection coefficients of mode-1 are shown in Figure 5.9. In mode-1, the MIMO reconfigurable antenna is resonating at three different bands. The first resonance occurs at 1095 MHz while the second and third resonances occur at 1945 MHz and 3050 MHz with a -6 dB operating bandwidth of at-least 44 MHz in all three bands. A slight shift in observed in the measurement of the third resonance due to the fabrication tolerances that became more significant at higher frequencies.

A-2.2 Mode-2

In this mode, PIN diode 1 is switched ON while PIN diode 2 is switched OFF. The resulted simulated and measured reflection coefficients are shown in Figure 5.10. In mode 2, the antenna resonates at two different bands. The first resonance occurs at 770 MHz while the second resonance occur at 1660 MHz with a -6 dB operating bandwidth of at-least 30 MHz in both bands.
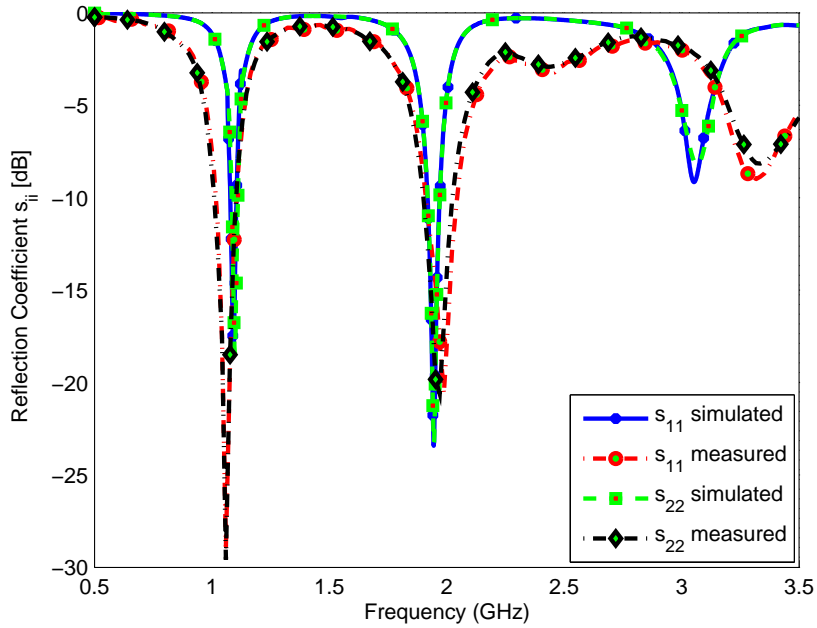
Figure 5.9: Reflection coefficients of the MIMO antenna system - Mode 1.

A-2.3 Mode-3

In this mode, PIN diode 1 is switched OFF while PIN diode 2 is switched ON. The resulted simulated and measured reflection coefficients are shown in Figure 5.11. In mode-3, the antenna is resonating at four different bands. The first resonance occurs at 1000 MHz while the second, third and fourth resonances occur at 1508 MHz, 2450 MHz and 3350 MHz with a -6 dB operating bandwidth of at-least 44 MHz in all four bands. BAP50-02

A-2.4 Mode-4

In this final mode, both PIN diodes at the top side of MIMO antenna are switched ON. The resulted simulated and measured reflection coefficients are shown in Figure 5.12. In mode-4, the MIMO antenna resonate at 1060 MHz and 1760 MHz with a -6 dB operating bandwidth of 50 MHz and 180 MHz respectively.

The details of the measured center resonance frequencies (f_c in MHz) and -6 dB operating bandwidth (BW in MHz) of the reconfigurable MIMO antenna system are shown in Table 5.3 for all modes.
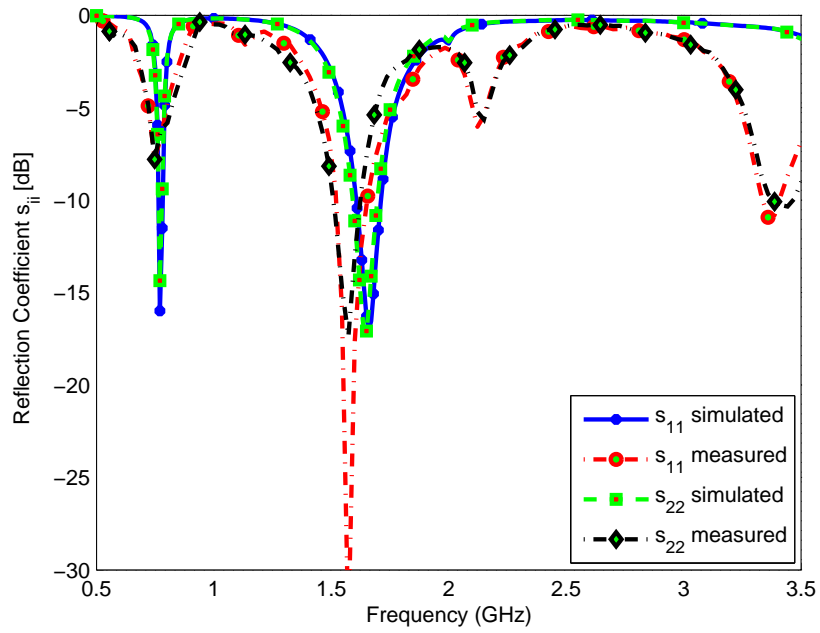
Figure 5.10: Reflection coefficients of the MIMO antenna system - Mode 2.
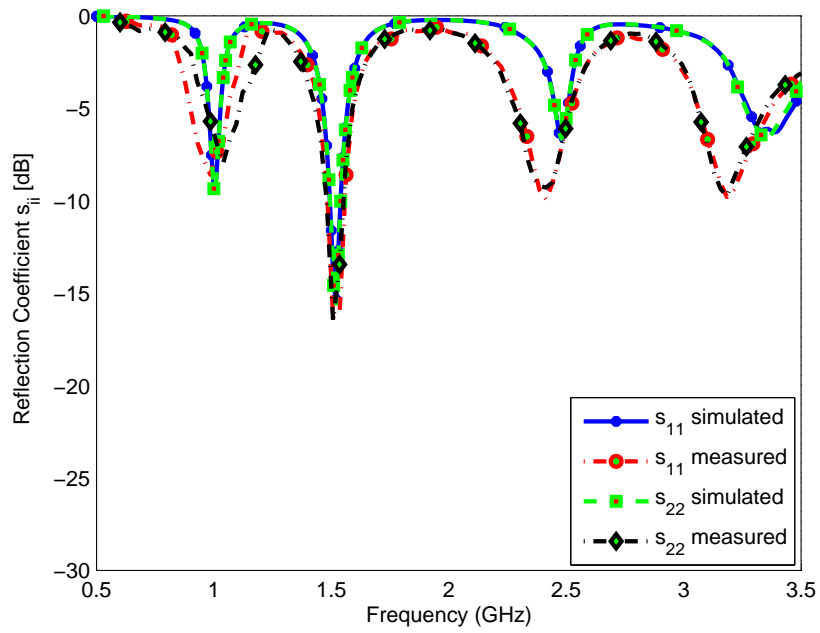
Figure 5.11: Reflection coefficients of the MIMO antenna system - Mode 3.
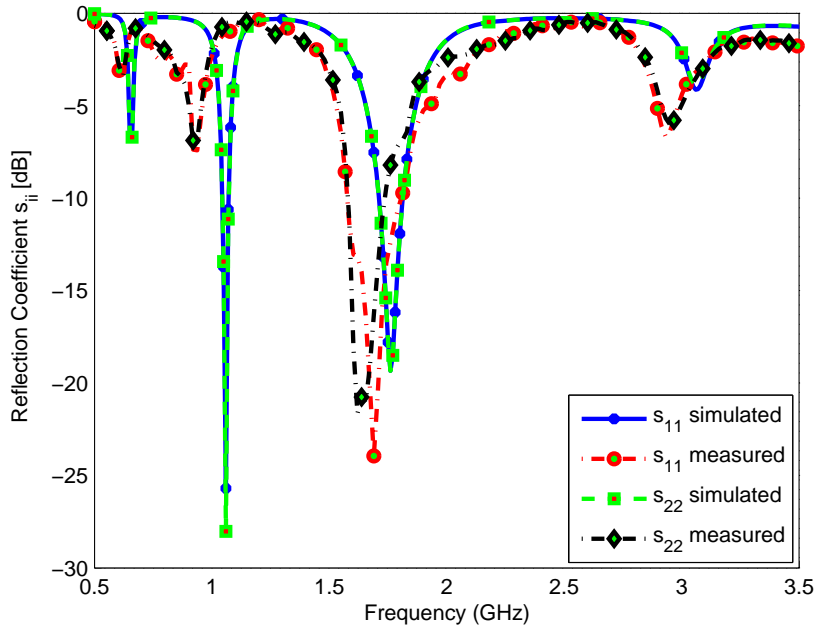
Figure 5.12: Reflection coefficients of the MIMO antenna system - Mode 4.
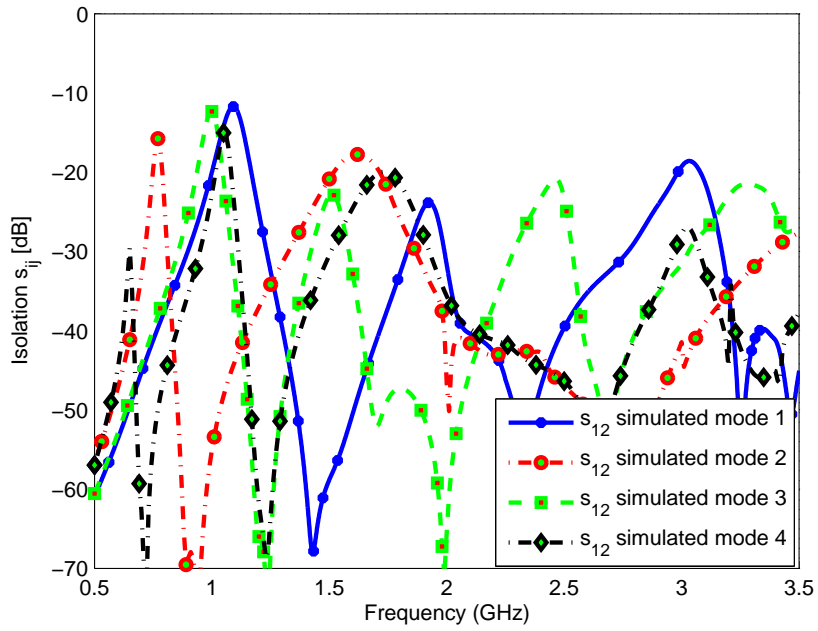
Figure 5.13: Simulated isolation between MIMO antenna elements.

123
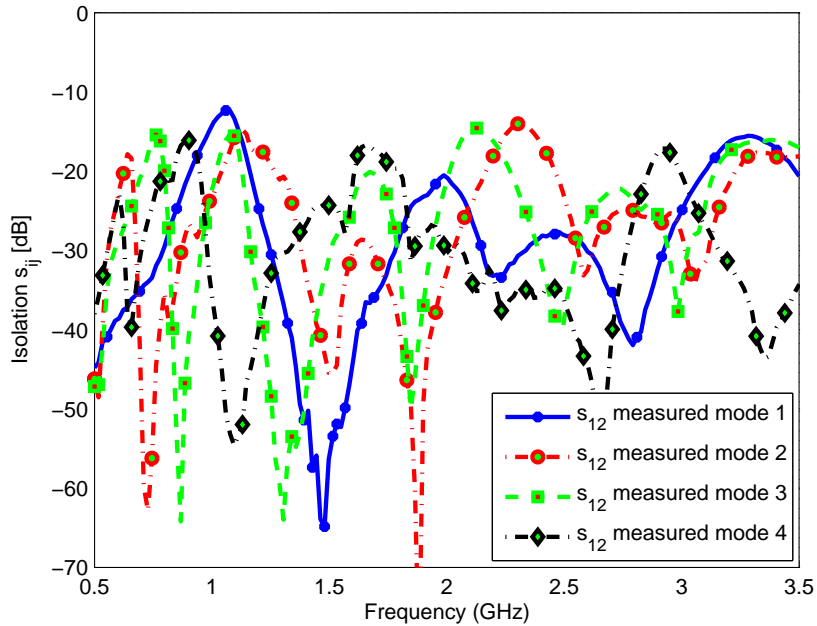
Figure 5.14: Measured isolation between MIMO antenna elements.

From the measured and simulated results, it is evident that close agreement is found between the various modes. The difference in the simulated and measured results were mainly due to the difference in substrate properties of the fabricated antenna and fabrication tolerances. In higher frequency bands, the shift in the frequency was because of the PIN diodes used in the circuit. The fabricated model used PIN diodes, BAP50-02, that can work up to 3 GHz, but we used them up to 3.6 GHz. The insertion loss $|S_{12}|$ of the diode rises significantly above 3 GHz and hence had an adverse effect on its performance above this maximum frequency. In addition, the shift may be because of the lack of modeling flexibility of PIN diodes in HFSS. The diodes were modeled as resistive circuits in forward bias while becoming a capacitive circuits in reverse bias conditions according to their data sheets.

For the MIMO antenna system, mutual coupling between MIMO antenna elements is important to consider. The simulated and measured isolation between MIMO elements are shown in Figs. 5.13, and 5.14 for all four modes. The worst case isolation was 12 dB between the MIMO antenna elements for both simulated and measured values. The obtained isolation values are acceptable for good

MIMO operation.

Table 5.3: Measured Reconfigurable Antenna Bands, Center Frequency (f_c in MHz) and Bandwidth (BW in MHz) For (Antenna-1 (A1), Antenna-2 (A2), All modes (M1, M2, M3, M4))

		Band-1		Band-2		Band-3		Band-4	
		f_c	BW	f_c	BW	f_c	BW	f_c	BW
M1	A1	1060	80	2018	130	3195	160	-	-
	A2	1065	80	2020	130	3195	160	-	-
M2	A1	747	60	1583	210	-	-	-	-
	A2	751	65	1580	220	-	-	-	-
M3	A1	995	110	1510	130	2410	155	3250	160
	A2	1020	110	1515	130	2420	150	3250	160
M4	A1	975	75	1690	210	-	-	-	-
	A2	980	75	1675	215	-	-	-	-

5.1.3 Current Distribution

The proposed reconfigurable MIMO antenna system was also analyzed from its surface current densities obtained from HFSS simulations. The analysis presented here is only for mode-1 and can be extended to other modes of operation as well. Figure 5.15(a) shows the current density on the top surface of antenna-2 at its first resonance of 1095 MHz while antenna-1 and the sensing antennas were terminated with 50Ω. Figs. 5.15(b) and (c) shows the bottom side of the reconfigurable antenna and reference GND plane, respectively. As evident from the figures, a high current density was along the inner side of the meander line and the inner edge of the folded patch at the top side. The ground plane also act as part of the radiator as the bottom side of PIFA is connected directly to the ground plane.
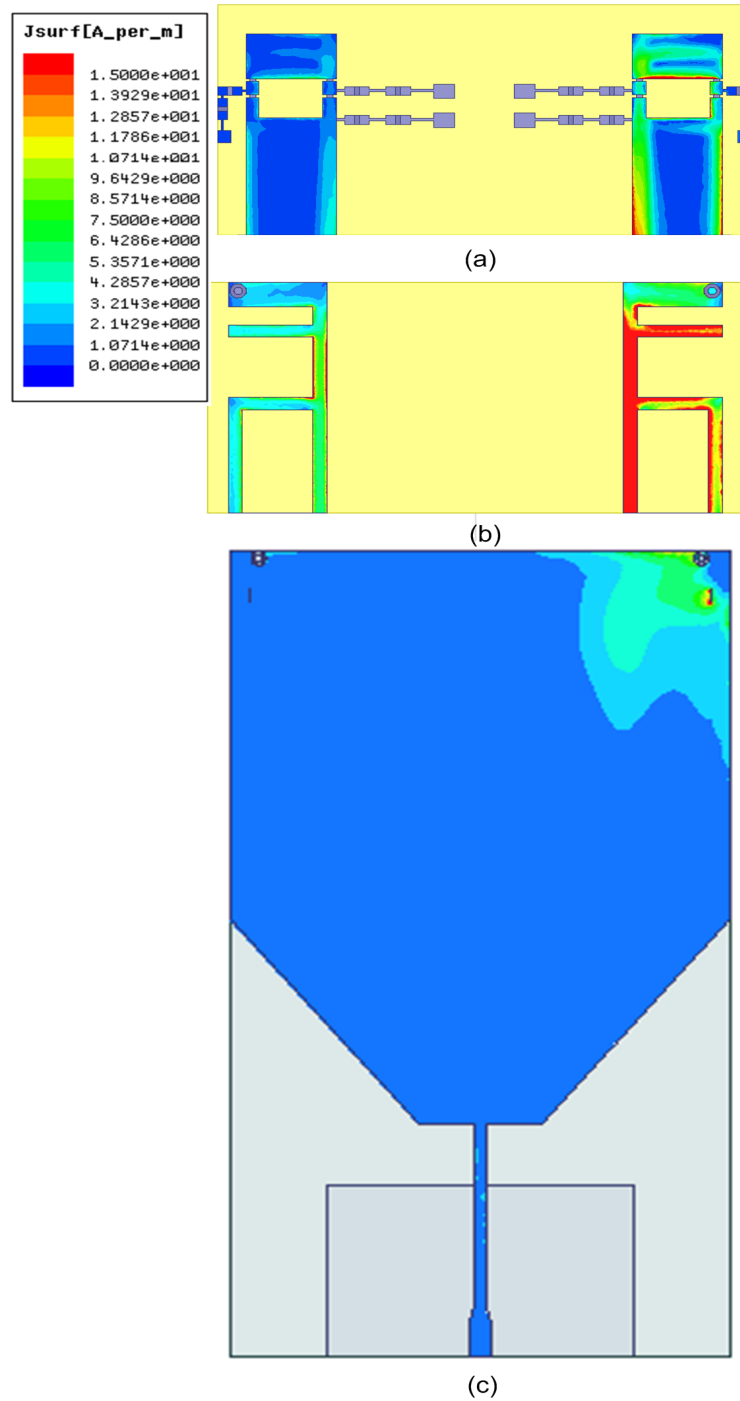
Figure 5.15: Current distribution for the MIMO antenna system at 1095 MHz- Antenna-2 excited: (a) Top layer (b) Bottom layer (c) Ground plane.
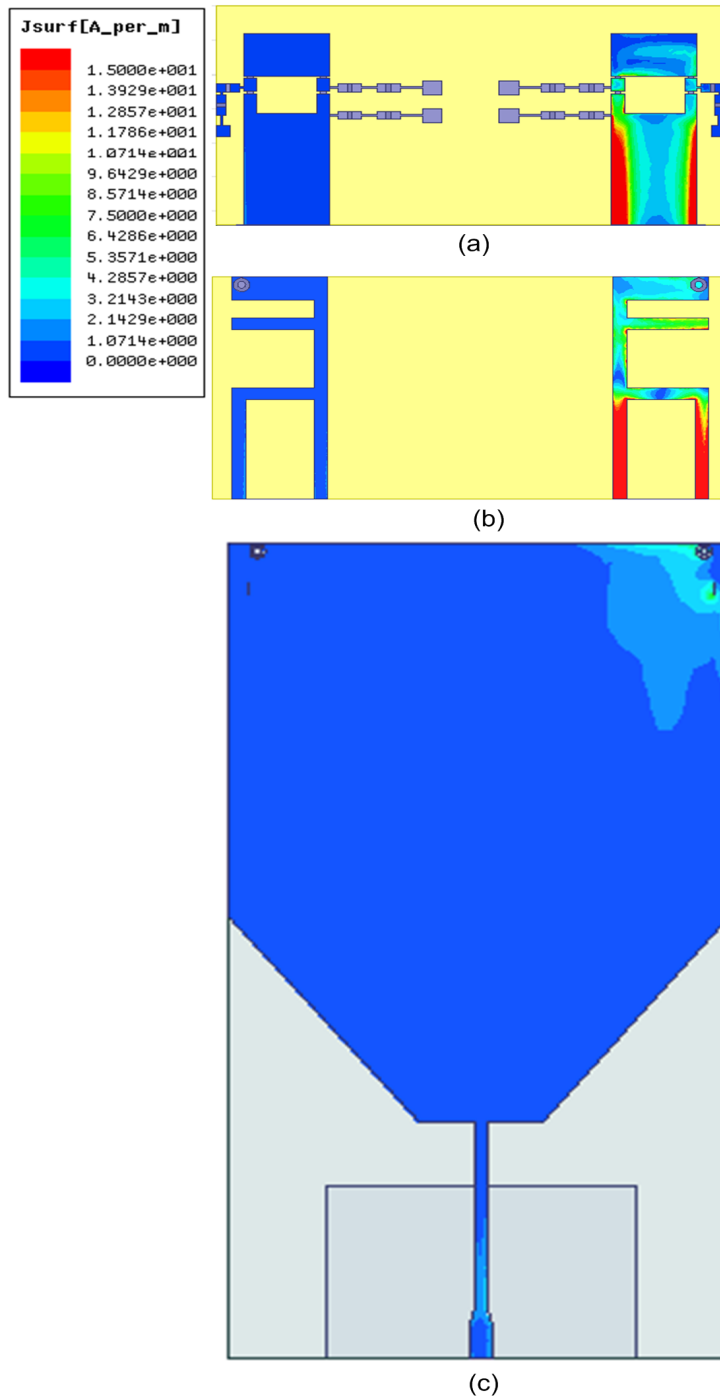
Figure 5.16: Current distribution for the MIMO antenna system at 1945 MHz- Antenna-2 excited: (a) Top layer (b) Bottom layer (c) Ground plane.
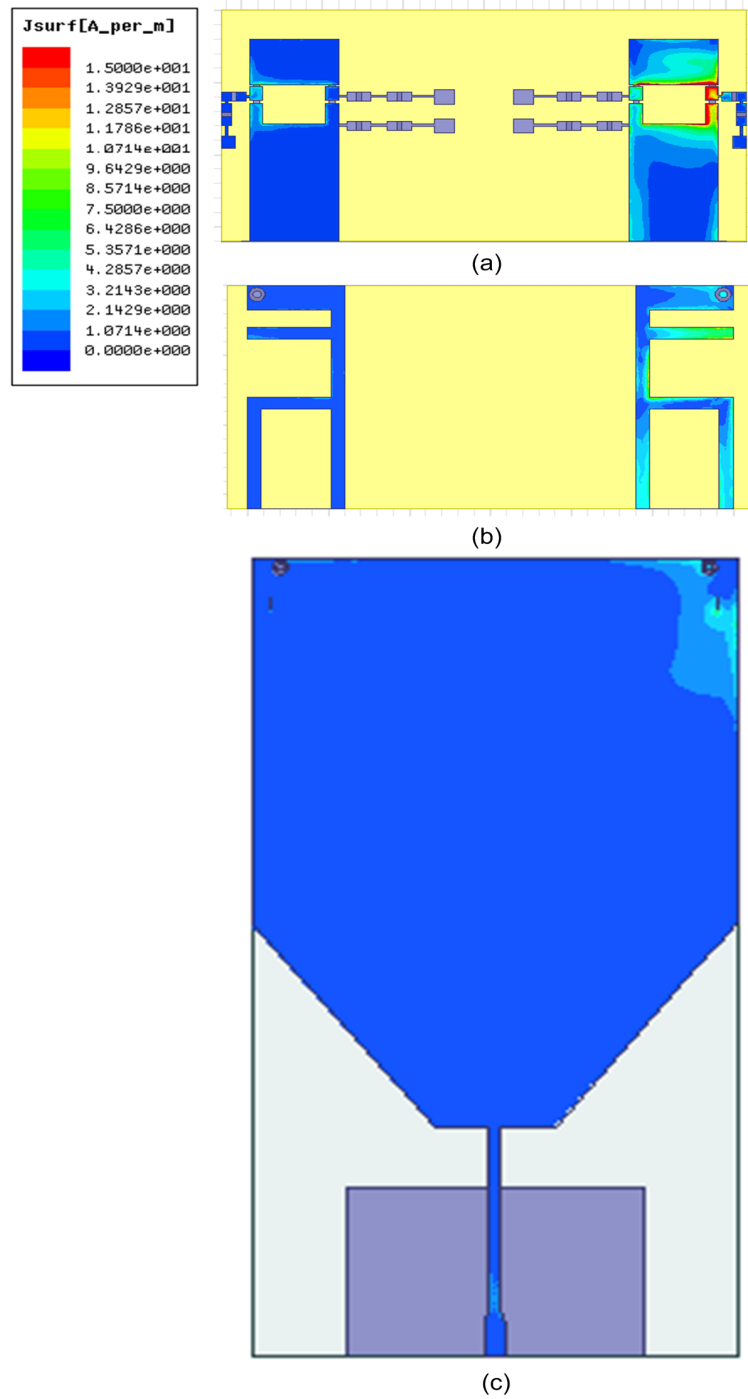
Figure 5.17: Current distribution for the MIMO antenna system at 3050 MHz- Antenna-2 excited: (a) Top layer (b) Bottom layer (c) Ground plane.

Table 5.4: Simulated and Measured Peak Gain (P.G in dBi) and Radiation Efficiencies (η %)

		Band-1				Band-2				Band-3				Band-4			
		Simulated		Measured		Simulated		Measured		Simulated		Measured		Simulated		Measured	
		P.G	η %	P.G	η %	P.G	η %	P.G	η %	P.G	η %	P.G	η %	P.G	η %	P.G	η %
M-1	A-1	0.54	40	-1.2	26	2.99	55	1.56	41	5.2	62	3.2	45	-	-	-	-
	A-2	0.55	40	-1.5	27	3.15	56	1.42	41	5.2	62	3.05	47	-	-	-	-
M-2	A-1	-5.01	22	-	-	3.1	75	2.03	60	-	-	-	-	-	-	-	-
	A-2	-5.03	22	-	-	3.12	74	2.03	61	-	-	-	-	-	-	-	-
M-3	A-1	-3.13	26	-5.23	20	2.25	58	0.27	34	2.53	25	1.25	20	1.53	40	0.12	25
	A-2	-3.13	26	-5.23	20	2.25	58	0.26	35	2.53	25	1.23	19	1.53	41	0.132	254
M-4	A-1	-1.56	37	-2.56	23	3.53	60	2.01	46	-	-			-	-	-	-
	A-2	-1.62	35	-2.7	24	3.54	61	1.97	46	-	-	-	-	-	-	-	-

There is slight coupling on the bottom and top sides of the antenna-1 while the coupling through the ground plane is insignificant. Similar behavior was observed with the excitation of antenna-1 at 1095 MHz.

Similarly, in mode-1 at the second resonance frequency of 1945 MHz, the current densities at the top, bottom and ground planes of the reconfigurable MIMO antenna-2 are shown in Figs. 5.16(a), (b) and (c), respectively. A high current density was around the edges of top side of the antenna and divided lines of bottom side of antenna-2. The coupling was insignificant on the top and bottom of element-1 and even on the ground side.

The current distribution for mode-1 at frequency of 3050 MHz is shown in Figure 5.17. All currents are shown for the 3050 MHz operating frequency of PIFA element-2. It can be seen that the high current levels are around the slot at the top side of the radiating element. The mutual coupling between the two MIMO elements is insignificant.

5.1.4 Far Field Radiation Characteristics of the Reconfigurable MIMO Antenna

The 3D radiation patterns of the proposed reconfigurable MIMO antenna system were computed using HFSS. The gain patterns for each mode and each band

were obtained for one element while the second was terminated with 50Ω. The gain patterns of the first two modes are shown in Figure 5.18 and Figure 5.19, respectively. In Figure 5.18, the 3D gain pattern is plotted for three bands: 1095 MHz, 1945 MHz and 3050 MHz while Figure 5.19 shows the 3D gain patterns for 770 MHz and 1660 MHz. The maximas of each element is tilted showing lower field correlation that is usually desired.

The two-dimensional measured gain patterns of the MIMO antenna systems are presented here for one frequency of each mode. Figure 5.20 shows the normalized measured gain patterns of the proposed MIMO antenna system at 3195 MHz of mode-1. The maximum measured gain at this frequency was 3.2 dBi. All co-pol and cross-pol patterns for the two elements of the MIMO antenna are given in Figure 5.20 (a) and Figure 5.20 (b), respectively. Figure 5.21 shows the measured gain pattern at 1580 MHz of mode-2. All co-pol and cross-pol patterns are given in Figure 5.21 (a) and Figure 5.21 (b), respectively. Similarly, the 2-D gain patterns for mode-3 and mode-4 at operating bands of 1510 MHz and 1690 MHz are shown in Figure 5.22 and Figure 5.23, respectively.

The simulated and measured peak gains in dBi and %η are given in Table 5.4 for all modes of operation. It should be noted that the low efficiency at some bands is due to the fact that this multi-resonance antenna depends on higher order modes for these bands in addition to the fact that the design is fabricated on a lossy substrate (FR-4).

5.1.5 TARC and the Correlation Coefficient of the Reconfigurable MIMO Antenna System

In MIMO antenna systems, efficiency and bandwidth information are insufficient for its comprehensive characterization [153]. Total active reflection coefficient (TARC) and correlation coefficient (ρ) are used for better characterization of MIMO antenna systems. TARC is defined as the ratio of the square root of total reflected power divided by the square root of the total incident power in a
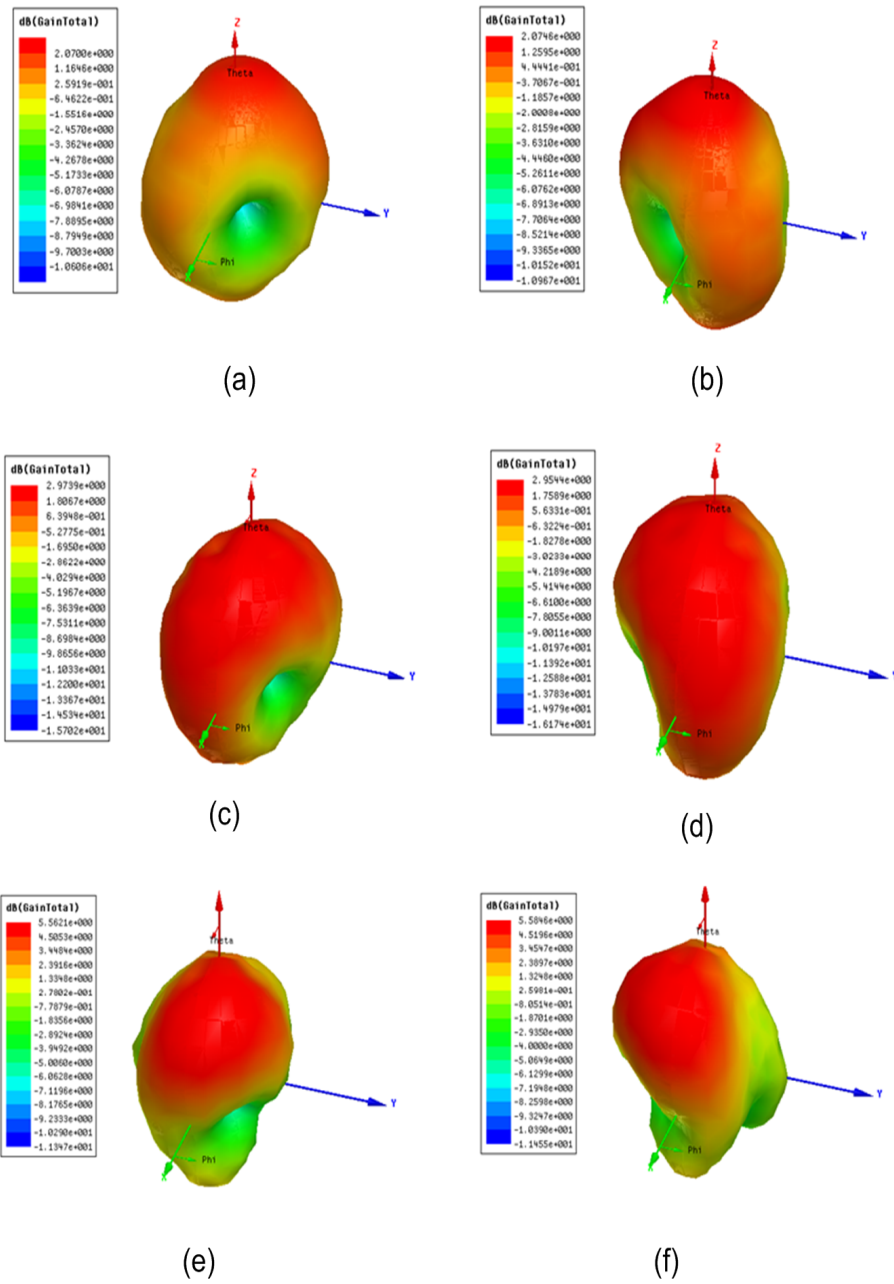
Figure 5.18: Simulated 3D gain pattern Mode-1 (a)Antenna-1 excited at 1095 MHz(b) Antenna-2 excited at 1095 MHz (c) Antenna-1 excited at 1945 MHz (d) Antenna-2 excited at 1945 MHz (f) Antenna-1 excited at 3050 MHz(e) Antenna-2 excited at 3050 MHz.
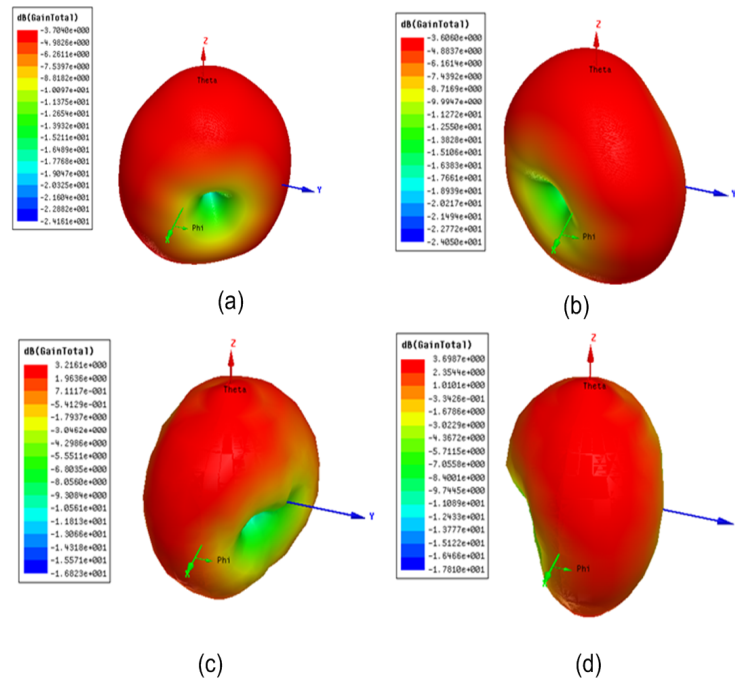
Figure 5.19: Simulated 3D gain pattern Mode-2 (a)Antenna-1 excited at 770 MHz(b) Antenna-2 excited at 770 MHz (c) Antenna-1 excited at 1660 MHz (d) Antenna-2 excited at 1660 MHz.
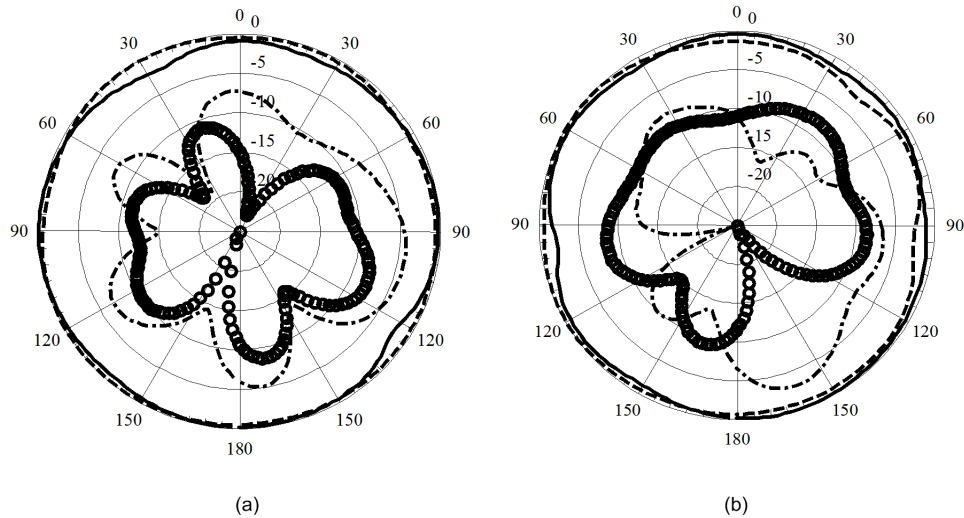
Figure 5.20: Measured normalized gain patterns for the proposed MIMO antenna Mode-1: (a) xz plane at 3195 MHz and (b) yz plane at 3195 MHz. solid: co-pol element 1; dashes: co-pol element 2; circle: cross-pol element 1; and dashes-dot: cross-pol element 2.
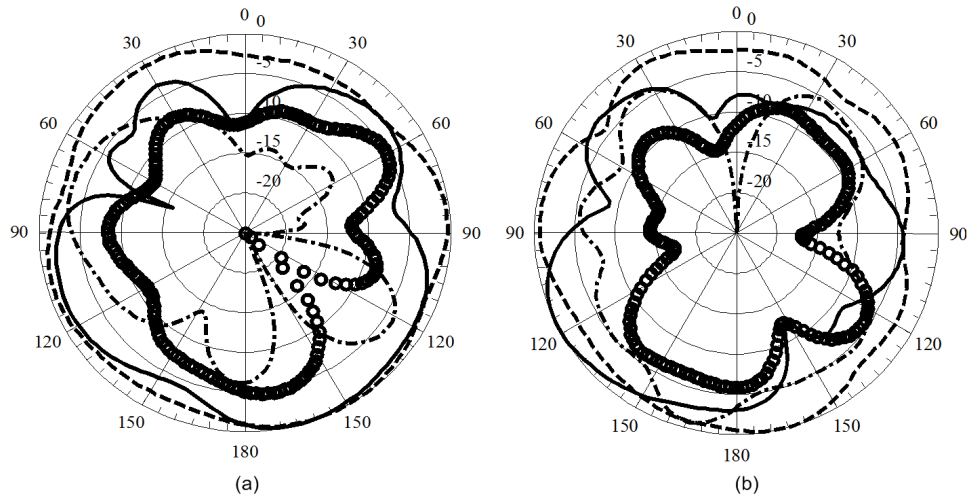
Figure 5.21: Measured normalized gain patterns for the proposed MIMO antenna Mode-2: (a) xz plane at 1580 MHz and (b) yz plane at 1580 MHz. solid: co-pol element 1; dashes: co-pol element 2; circle: cross-pol element 1; and dashes-dot: cross-pol element 2.
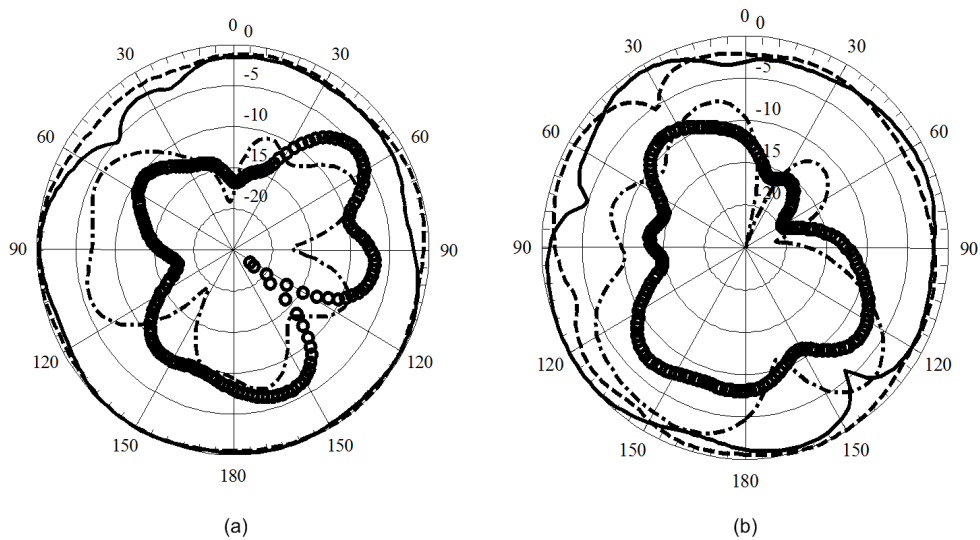
Figure 5.22: Measured normalized gain patterns for the proposed MIMO antenna Mode-4: (a) xz plane at 1510 MHz and (b) yz plane at 1510 MHz. solid Mode=2: co-pol element 1; dashes: co-pol element 2; circle: cross-pol element 1; and dashes-dot: cross-pol element 2.
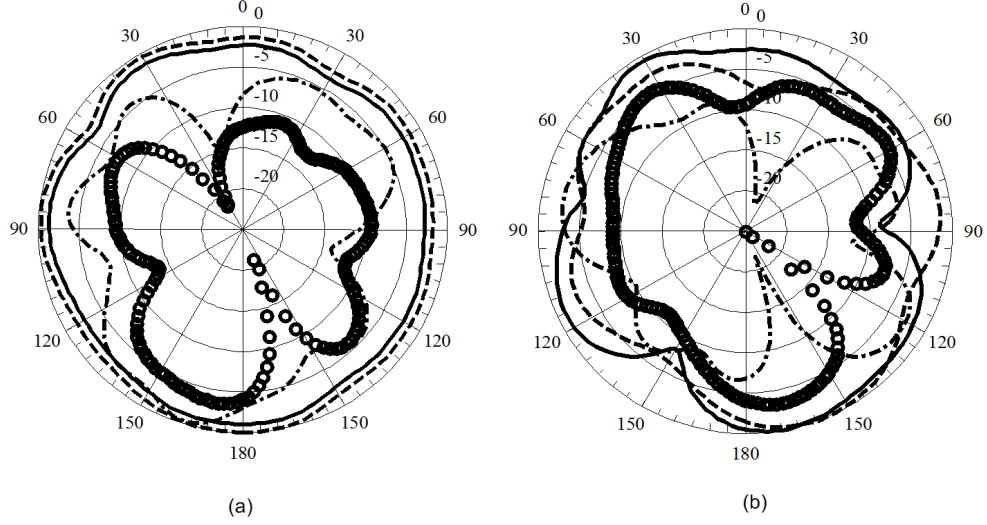
Figure 5.23: Measured normalized gain patterns for the proposed MIMO antenna Mode-4: (a) xz plane at 1690 MHz and (b) yz plane at 1690 MHz. solid: co-pol element 1; dashes: co-pol element 2; circle: cross-pol element 1; and dashes-dot: cross-pol element 2.

multi-port antenna system [2]. TARC is given by:

$$\Gamma_a^t = \frac{\sqrt{\sum_{i=1}^{N}|b_i|^2}}{\sqrt{\sum_{i=1}^{N}|a_i|^2}} \tag{5.1}$$

where a_i and b_i are the incident signals and reflected signals, respectively. They are related to each other as;

$$[b] = [S][a] \tag{5.2}$$

where S is the scattering matrix of the multi-port network.

TARC curves for the proposed MIMO antenna system for all four modes are given in Figs. 5.24 ∼ 5.27. The analysis was carried out by keeping the excitation of one port at $1e^{j0}$ while the phase of the second port is changed with different phase excitations. The TARC curves in all figures shown are for excitation phases 0°, 30°, 60°, 90°, 120° and 150°. TARC curves shows the effective operating bandwidth of the MIMO antenna system. It is clear that the operating bandwidth of the MIMO antenna system will not be affected much by the change in phase excitation of the other ports.

The correlation coefficient (ρ) is a measure of isolation or correlation of the MIMO channels. This metric considers the radiation patterns of the antenna system and their effect on one another when operated simultaneously (which is the case in a MIMO antenna system). The envelop correlation coefficient (ρ_e) can be calculated using the following formula [25]:

$$\rho_e = \frac{|\int \int_{4\pi} [\vec{F}_1(\theta, \varphi) * \vec{F}_2(\theta, \varphi) d\Omega]|^2}{|\int \int_{4\pi} [\vec{F}_1(\theta, \varphi)|^2 d\Omega| \int \int_{4\pi} [\vec{F}_2(\theta, \varphi)|^2 d\Omega} \qquad (5.3)$$

where $\vec{F}_i(\theta, \varphi)$ is the field radiation pattern of the antenna when port i is excited, and $*$ denotes the Hermitian product.
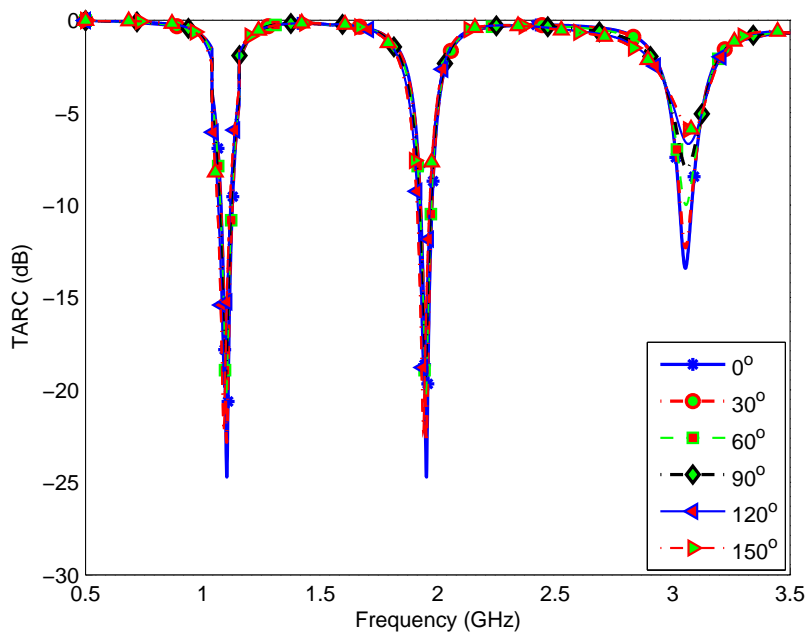
Figure 5.24: Mode-1: TARC curves for the proposed MIMO antenna system
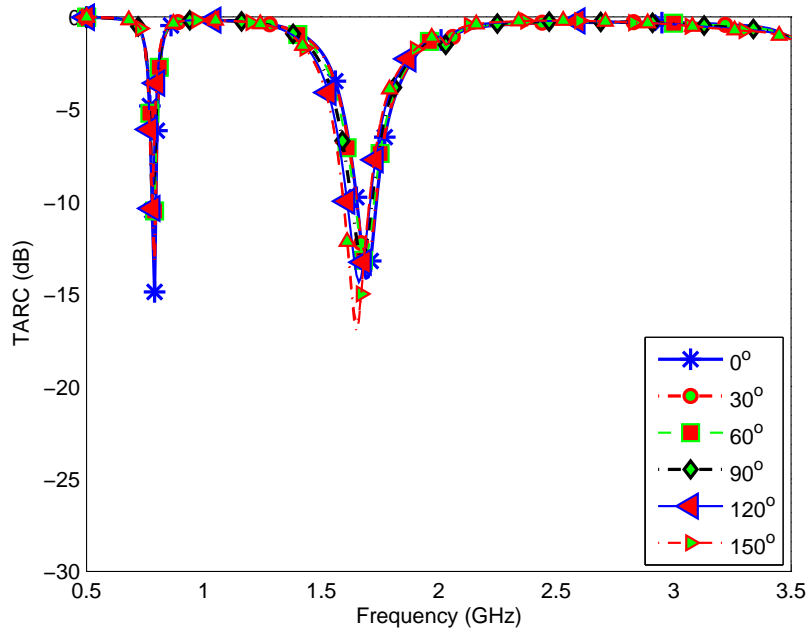
Figure 5.25: Mode-2: TARC curves for the proposed MIMO antenna system.
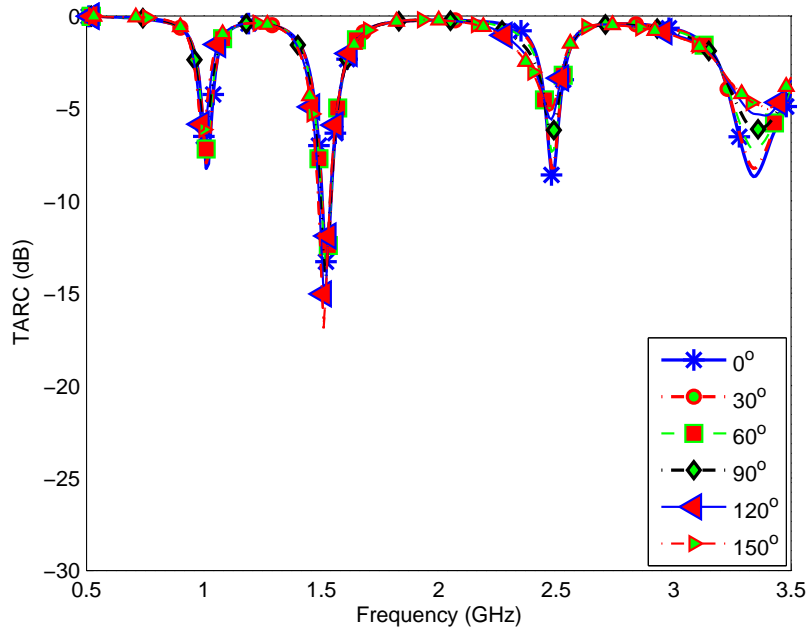
Figure 5.26: Mode-3: TARC curves for the proposed MIMO antenna system.
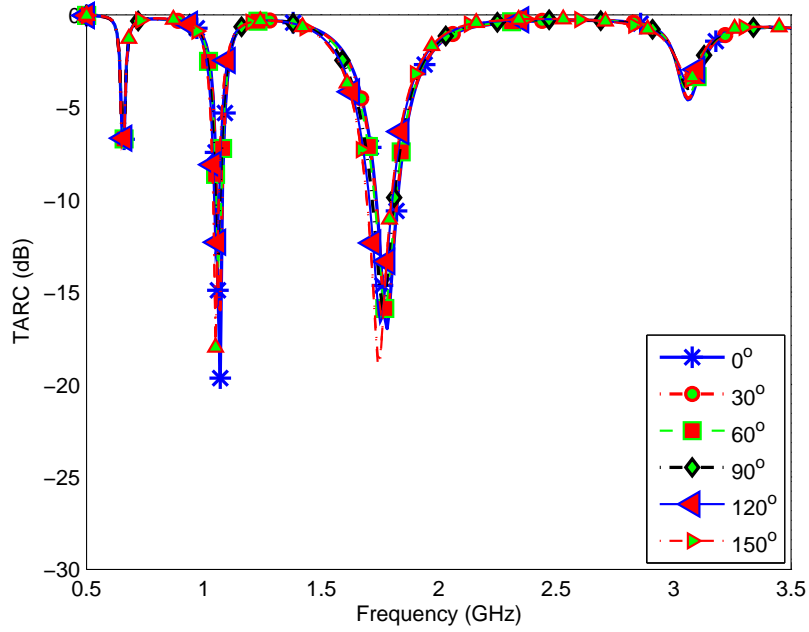
Figure 5.27: Mode-4: TARC curves for the proposed MIMO antenna system.

Envelope correlation coefficient values for both measured and simulated data are summarized in Table 5.5. It is clear that the proposed reconfigurable MIMO antenna system with an integrated UWB antenna for CR applications will satisfy the ρ_e values required for good MIMO operation. Some measured values of ρ_e are missing because of the lower end frequency limitation in the Satimo chamber. The minimum frequency for measurement was 800 MHz.

Table 5.5: Simulated and Measured Envelope Correlation Coefficient (ρ_e) For all Bands (B-1, B-2, B-3, B-4)

	Simulated Results				Measured Results			
	B-1	B-2	B-3	B-4	B-1	B-2	B-3	B-4
M-1	0.17	0.10	0.02	-	0.07	0.25	0.03	-
M-2	0.12	0.006	-	-	-	0.12	-	-
M-3	0.17	0.04	0.01	0.05	0.03	0.17	0.09	0.02
M-4	0.03	0.01	-	-	0.125	0.025	-	

137

5.2 A Planar Reconfigurable MIMO and Sensing Antenna System

In this section, another CR antenna system is presented for wireless handheld devices. The planar MIMO antenna elements are embedded with an UWB sensing antenna to form a complete front end for CR platform. Most of the work related to CR antenna systems cited in literature were single element with a sensing antenna working above 2GHz and very few MIMO antenna systems were proposed above 3 GHz.

In this work, a novel compact meandered line planar reconfigurable MIMO antenna is proposed for CR applications. This two element MIMO system is made tunable in different bands using PIN and varctor diodes. The most distinguishing feature of the proposed design is its planar structure with operation at lower frequency bands starting from 580∼680 MHz and 834∼1120 MHz by using varactor diode tuning. Most of the cited designs in literature cover high frequency designs operating above 2 GHz for CR applications.

Another novel feature of the proposed design is the unique architecture of its UWB sensing antenna and reconfigurable MIMO antenna sharing the same substrate. The reference GND plane of the reconfigurable antenna is optimized to work as a sensing antenna to scan the frequency spectrum while operating as a GND reference plane for the reconfigurable antenna during the communication stage. Moreover, the proposed MIMO antenna system is compact and suitable for CR platforms in wireless handheld devices.

5.2.1 Design Details

The proposed novel frequency reconfigurable meander line planar MIMO antenna system along with its UWB sensing antenna is shown in Figure 5.28(a), (b). The complete system is integrated on single board of dimensions $65 \times 120 \times 1.56$ mm^3. The proposed design was fabricated on FR-4 substrate with ϵ_r =4.4. The top layer of the board contains two meander line MIMO reconfigurable antennas each with

dimensions 7.9×56.6 mm^2. The bottom layer contains the UWB sensing antenna with its GND plane on the top layer of the board. The UWB sensing antenna acts as a GND reference plane for the two element reconfigurable antenna.

Figure 5.29 shows the detailed view of the two meander line reconfigurable MIMO elements along with its biasing circuitry. Both elements are exactly similar in structure. A combination of PIN and varactor diodes were used for frequency reconfigurability. The PIN diodes were used to connect the two radiating parts to switch the operating bands while varactor diodes are used for fine tuning over the lower frequency bands. The single PIN diode connecting the two parts of the antenna results in two modes of operation with smooth frequency variation by varactor diode. Figure 5.29(b) shows the side view of the antenna showing its shorting wall connecting the meander line structure with its reference plane.

The biasing circuitry for a single PIN or varactor diode is shown in Figure 5.29(c). Both diodes have the same biasing circuity. The circuit is a series combination of an RF choke of 1 μH in series with 2.1 kΩ resistor connecting the PIN or varactor diode with the radiating part of the antenna. Both the diodes were connected in series with RF choke to isolate the biasing circuitry from the radiating antenna. The fabricated model of the proposed design was realized on commercially available substrate, FR4, and is shown in Figure 5.30. Figure 5.30(a) shows the top view of the proposed design while Figure 5.30(b) shows the bottom layer of fabricated design. The top and bottom layers are integrated as a single complete system for CR application.

5.2.2 Simulation and Measurement Results

The proposed meander line based reconfigurable MIMO antenna along with the UWB sensing antenna were modeled and simulated using HFSS^{TM}. The fabricated design was tested for scattering parameters using an Agilent N9918A vector network analyzer at AMSD Lab at KFUPM, KSA. The gain patterns and efficiencies were measured at KAUST, KSA, using a SATIMO Starlab anechoic chamber.

The proposed UWB sensing antenna is basically a monopole antenna as shown
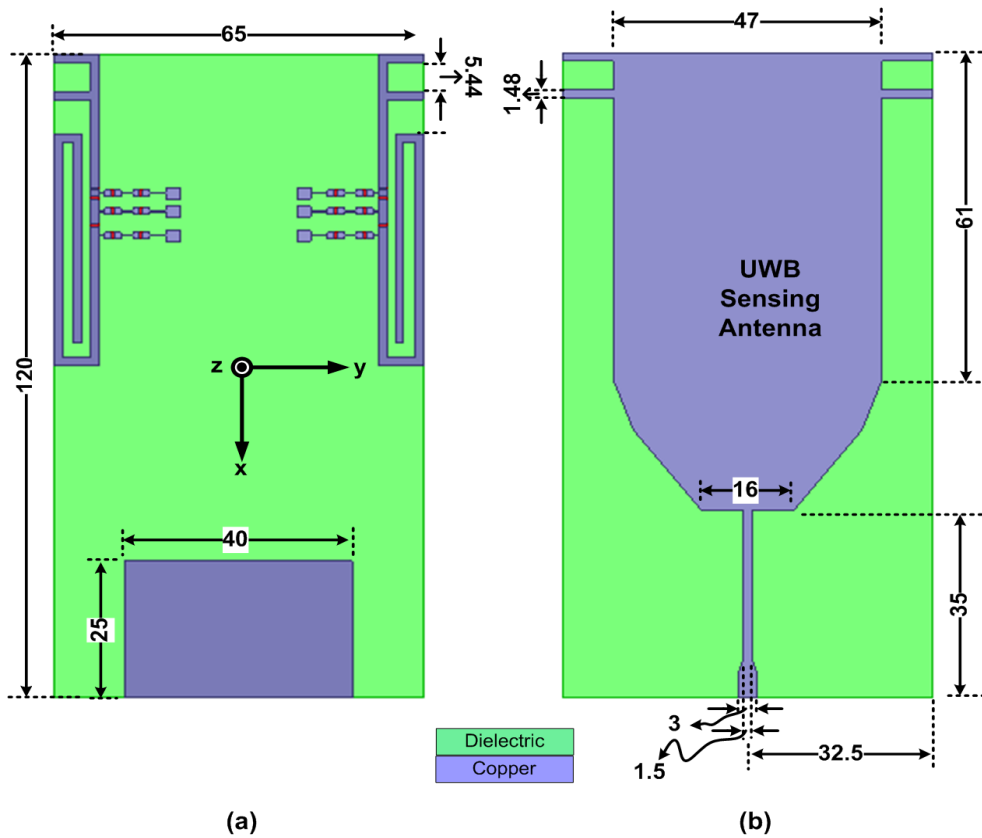
Figure 5.28: Proposed MIMO antennas system for CR platform (a) Top view (b) Bottom view - All dimensions are in millimeter (mm).
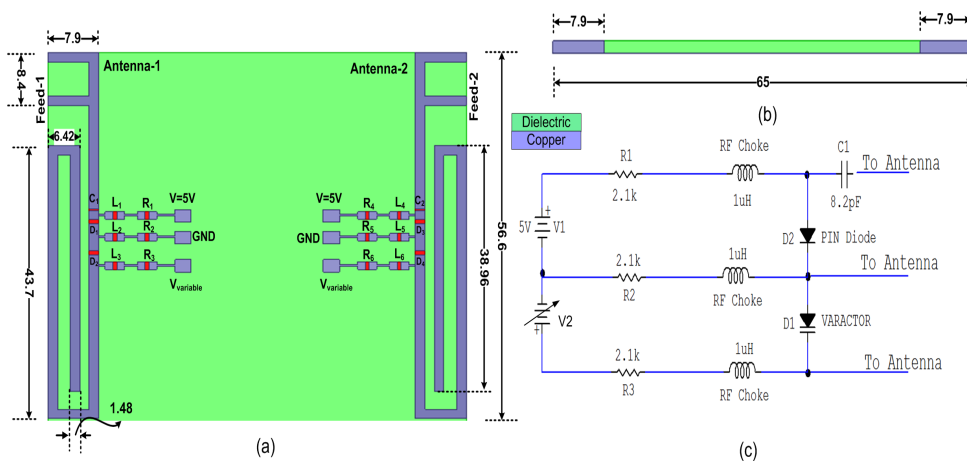
Figure 5.29: Detailed schematic of the two-element reconfigurable MIMO antenna (a) Top view (b) Side view (c) PIN and varactor diodes biasing circuitry - All dimensions are in millimeter (mm).
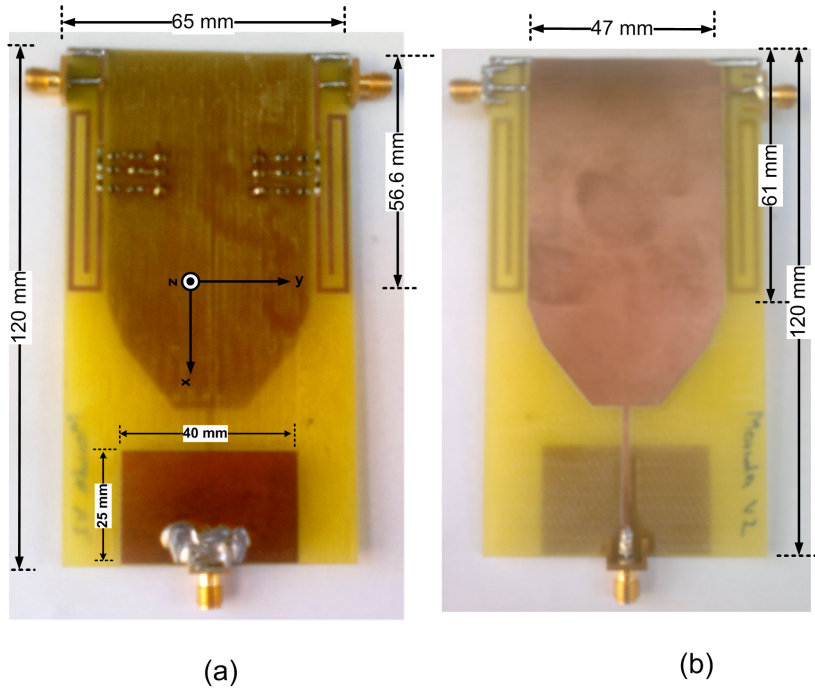
Figure 5.30: Fabricated model (a) Top view (b) Bottom view showing the sensing antenna

in Figure 5.28. The sensing antenna design presented cover frequency bands from 720∼ 3440 MHz. The simulated and measured reflection coefficients for the sensing antenna are shown in Figure 5.31. The measured results for the fabricated antenna are in close agreement with the simulated ones. The basic requirement of the sensing antenna is its omnidirectional radiation pattern for CR applications. The 2-D gain patterns of the sensing antenna in the yz-plane at two different frequencies (800 MHz and 1500 MHz) are shown in Figure 5.32 (a) and (b), respectively. The peak gain and efficiencies are measured at 800 MHz, 1500 MHz and 3000 MHz. The simulated and measured (simulated, measured) peak gain values were (2.26, 2.82),(4.33, 3.83) and (4.26, 4.48) in dBi while percent efficiencies (%η) were (80, 70), (85, 75) and (92, 79).

The proposed reconfigurable MIMO antenna is a meander line structure with two slots to connect the PIN and varactor diodes. The given structure is short circuited on one end with the reference GND plane by shorting walls. The first discontinuity in the antenna structure is loaded with PIN diodes to connect the radiating parts. The second slot is integrated with a varactor diode to vary the

141
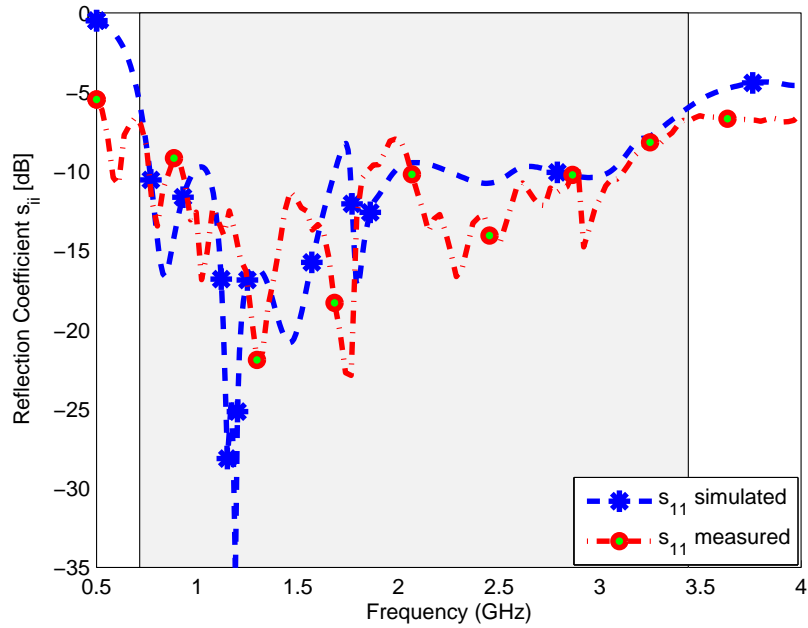
Figure 5.31: Simulated and measured reflection coefficient of UWB sensing antenna.

operating frequency smoothly, especially in the lower frequency bands. The PIN diodes were used to switch the frequency bands. The ON/OFF operation of the PIN diodes results in two modes of operations for the given antenna element. These modes are:

A-1 Mode-1

In this mode, the PIN diode of the reconfigurable MIMO antenna is switched OFF. The capacitance of the varactor diode was varied but it had negligible effect on the operating frequency. The resulted simulated and measured reflection coefficients of mode-1 are shown in Figure 5.33. In mode-1, two resonating bands were achieved. The first frequency band was 1100 MHz while the second resonating frequency was 2480 MHz with a -6 dB operating bandwidth of at-least 100 MHz in both bands.

A-2 Mode-2

In this mode, the PIN diodes were switched ON while the varactor diodes were biased with voltage from 0∼6 volts. The change in capacitance of the varactor
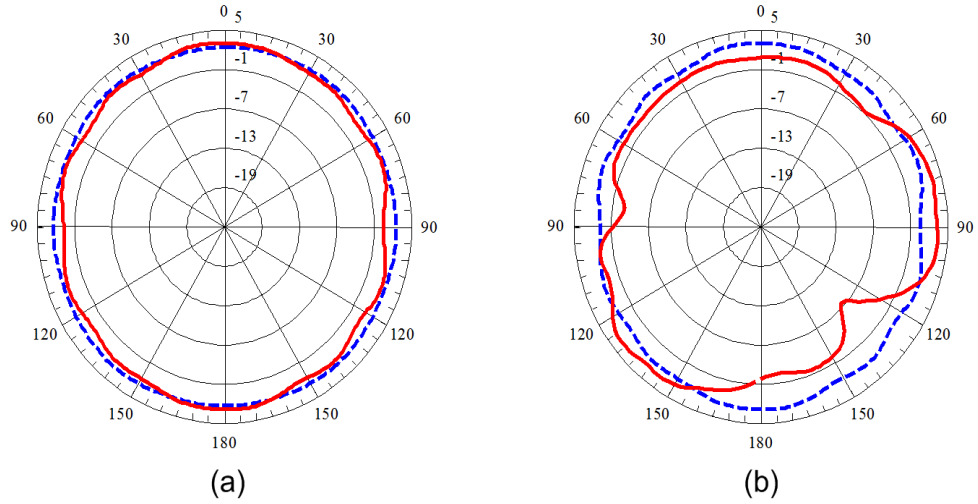
Figure 5.32: Simulated and measured 2D gain pattern in yz-plane. Dashed lines - simulated, solid lines - measured (a) 800MHz (b) 1500MHz.

resulted in a smooth transition of the operating frequencies. In mode-2, three resonating bands were achieved with center frequencies 585 MHz, 860 MHz and 2410 MHz for zero biasing voltage across the varactor diode. Increasing the biasing voltage results in smooth variation of the operating frequency for the lower two bands while the biasing voltage had less effect on the upper frequency band. The first resonating frequency was varied between 573~680 MHz while the second band covered 834~1120 MHz. The minimum -6 dB operating bandwidth for all the three bands were 22 MHz, 90 MHz and 120 MHz, respectively.

The simulated reflection coefficients are shown in Figure 5.34 for mode-2 while measured reflection coefficients are shown in Figure 5.35. The worst case isolation was 11.5 dB between the MIMO antenna elements for both simulated and measured values.

The simulated and measured results are in close agreement as evident from the reflection coefficients curves. The slight frequency shift was because of the substrate properties and fabrication tolerances. Moreover, the shift in frequency may be because of the lack of proper modeling of PIN and varactor diodes in HFSS. The PIN diodes were modeled as resistive and capacitive circuits in forward and reverse bias conditions, respectively, while the varactor diode was modeled as a variable capacitor.

143
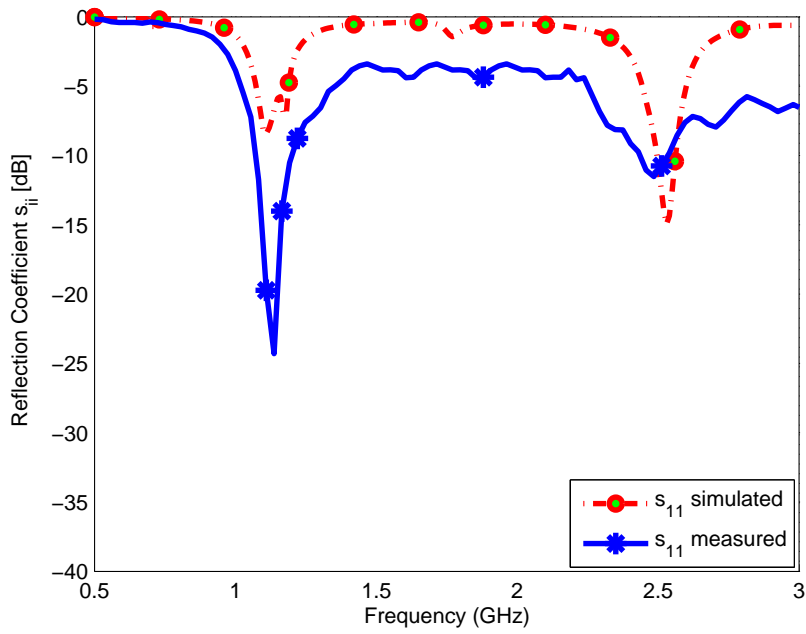
Figure 5.33: Reflection coefficients of the MIMO antenna system - Mode 1.
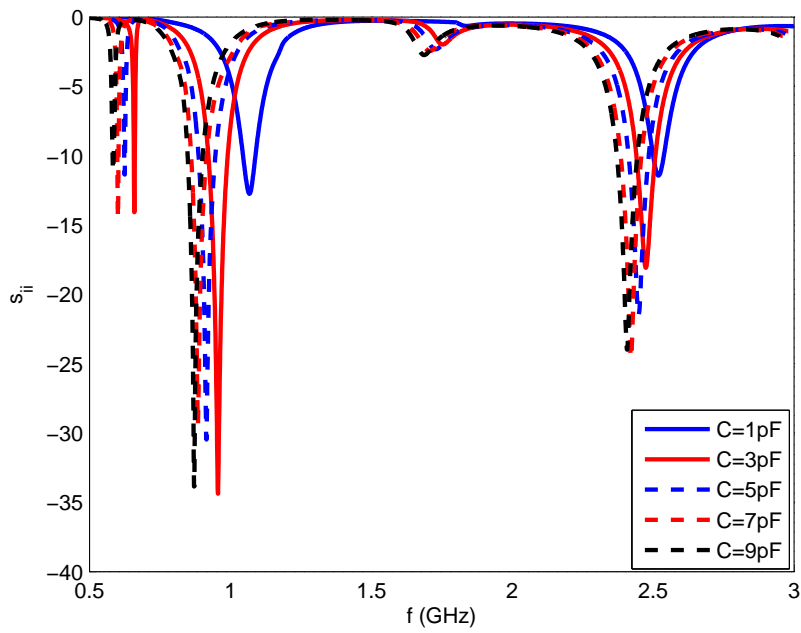
Figure 5.34: Simulated reflection coefficients of the MIMO antenna system - Mode 2.
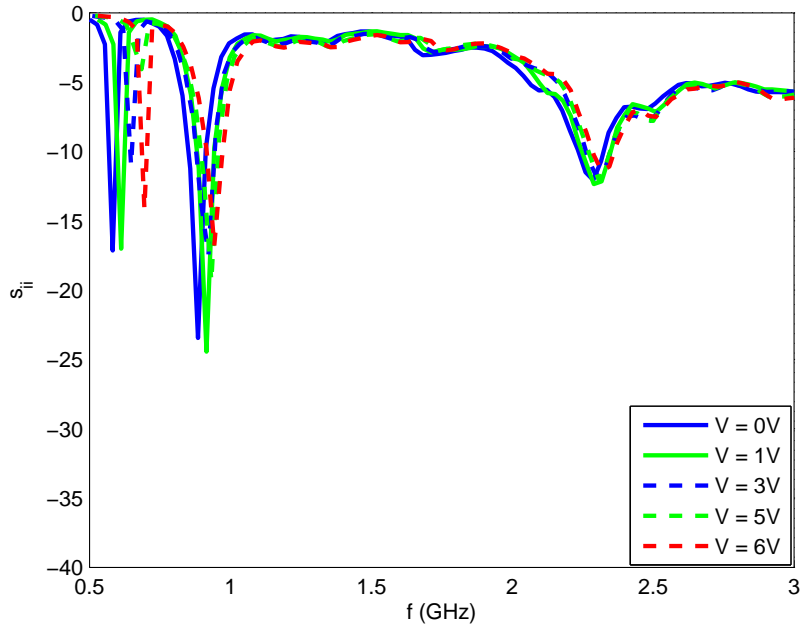
Figure 5.35: Measured reflection coefficients of the MIMO antenna system - Mode 2.

A-3 Gain Pattern and Envelop Correlation Coefficient

The 3D gain patterns of the proposed reconfigurable MIMO antenna system were computed using HFSS. The gain patterns for mode-1 at two bands for both antennas are shown in Figure 5.36. The 3D gain pattern are plotted for two bands: 1100 MHz and 2480 MHz. The maximas of gain pattern for each element are tilted, thus results in lower field correlation. The minimum frequency for measurement was 800 MHz and all values below 800 MHz are represented by (-). The simulated and measured peak gains were (1.02dBi, 2.98dBi) and (0.05dBi, 2.92dBi), respectively, for mode-1 while for mode-2, the values were (-3.01dBi, 2.01dBi, 3.15dBi) and (-, 0.89dBi, 2.85dBi), respectively. The simulated and measured efficiencies (η %) for mode-1 were (40, 72) and (32, 66), respectively, while for mode-2, the values were (21, 56, 76), (-, 44, 67), respectively.

The two-dimensional normalized measured gain patterns of the MIMO antenna systems are presented for mode-1 in Figure 5.37 at frequencies 1100 MHz and 2480 MHz, respectively. All co-pol and cross-pol patterns for the two elements of the MIMO antenna are shown for xz and yz cuts.

145
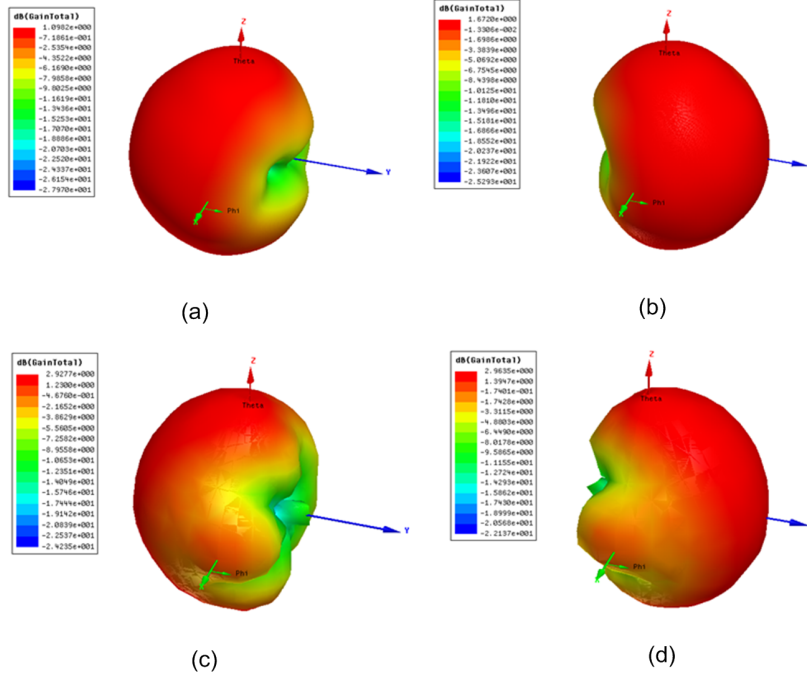
Figure 5.36: Simulated 3D gain pattern Mode-1 (a)Antenna-1 excited at 1100 MHz(b) Antenna-2 excited at 1100 MHz (c) Antenna-1 excited at 2480 MHz (d) Antenna-2 excited at 2480 MHz.
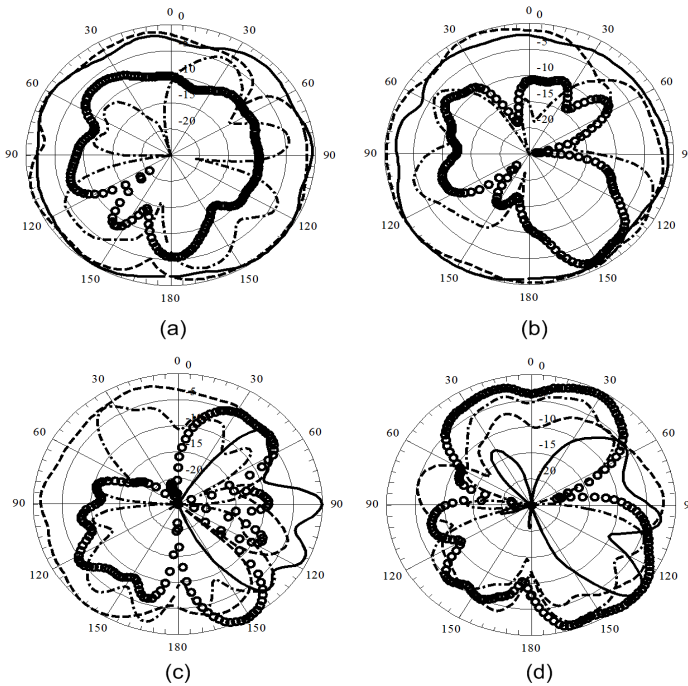
Figure 5.37: Measured normalized gain patterns for the proposed MIMO antenna Mode-1: (a) xz plane at 1100 MHz and (b) yz plane at 1100 MHz (c) xz plane at 2480 MHz and (d) yz plane at 2480 MHz. solid: co-pol element 1; dashes: co-pol element 2; circle: cross-pol element 1; and dashes-dot: cross-pol element 2.

146

Envelope correlation coefficient (ρ_e) values for both simulated and measured patterns were (0.025, 0.02) and (0.078, 0.045) respectively, for mode-1 while for mode-2, ρ_e values were (0.078, 0.065, 0.015) and (-, 0.066, 0.02), respectively.

5.3 Channel Capacity Calculations

The basic purpose of MIMO antenna systems in 4G wireless standards is to increase the throughput in multi-path and fading environments. MIMO antenna systems could be utilized to increase the data rate without additional power consumption or bandwidth increase. Theoretically, channel capacity increases linearly by increasing the number of channels by considering uncorrelated channel. However, for practical MIMO systems, correlation exists between antenna elements. The channel capacity calculation/measurement depends greatly on the correlation among various antennas patterns and types of propagation channels. For better channel capacity, high isolation and low correlation is desirable among the antennas elements. The capacity of a N×N MIMO antenna system is given as [154]:

$$C = log_2 \left(det \left[I + \frac{SNR}{N} HH^* \right] \right) \tag{5.4}$$

where C is the channel capacity, I is the N×N identity matrix, H is the channel coefficient matrix and H* is the conjugate transpose of H. The matrix H contains the information about the phase and gain of the prorogation channel between transmitting and receiving antennas.

In this section, channel capacity is calculated using the 2-D radiation patterns for the MIMO antennas systems described in sections 5.1 and 5.2 and a theoretical channel coefficient matrix (H). This channel model is described in details in section 2.3.7. The cross-polarization discrimination (XPD) is assumed to be 0 dB which is a typical value in mobile scenario in for an urban multi-path environment.[1]

[1]The theoretical model was used due to lack of availability of an SDR platform to conduct the channel capacity measurements at the frequency bands of the designed reconfigurable antennas. The wideband SDR platform that the AMSD Lab has acquired recently is not operational until this moment.

5.3.1 Channel Capacity of Modified PIFA MIMO Antenna Systems

In this section, the channel capacity is calculated for the modified PIFA based MIMO antenna systems described in section 5.1. The average channel capacity in mode-1 at given two bands of 1095 MHz and 1945 MHz are given in Figures 5.38 and 5.39, respectively. The given figures show the channel capacity curves for the two element MIMO antennas, ideal MIMO systems with totally uncorrelated channel and single-input single-output (SISO) system in the LOS environment. It can be seen from curves that the channel capacity curves of the modified PIFA based MIMO antenna system is less than the ideal MIMO antennas system but better than SISO system. The lower channel capacity curve of printed MIMO system is mainly because of channels and antenna systems correlation. The correlation between the channels and antennas deteriorates the the performance of MIMO systems.

Cumulative distribution function (CDF) curves of the channel capacity of given MIMO antennas are shows in Figures 5.40 and 5.41 in LOS environment. It is evident form the given curves that the performance of given MIMO system is less than the ideal capacity but much better than the SISO systems.
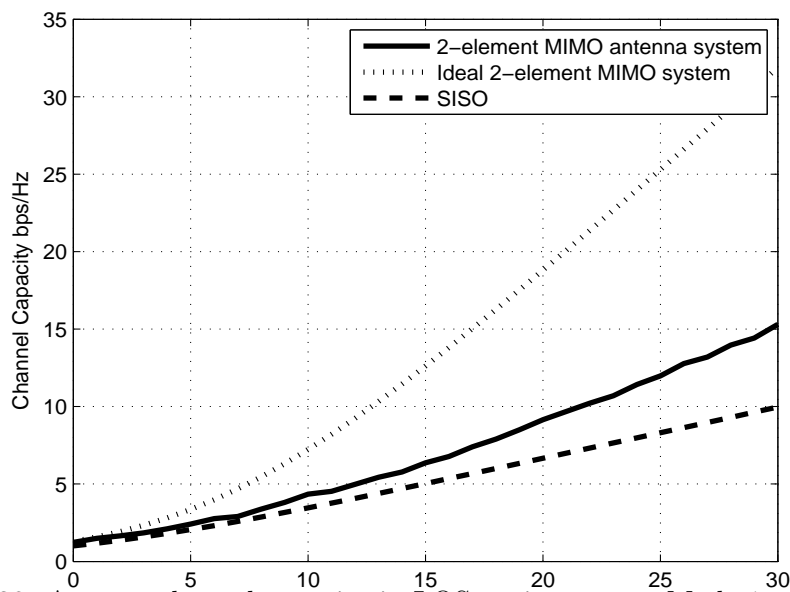
Figure 5.38: Average channel capacity in LOS environment - Mode-1 at 1095 MHz.
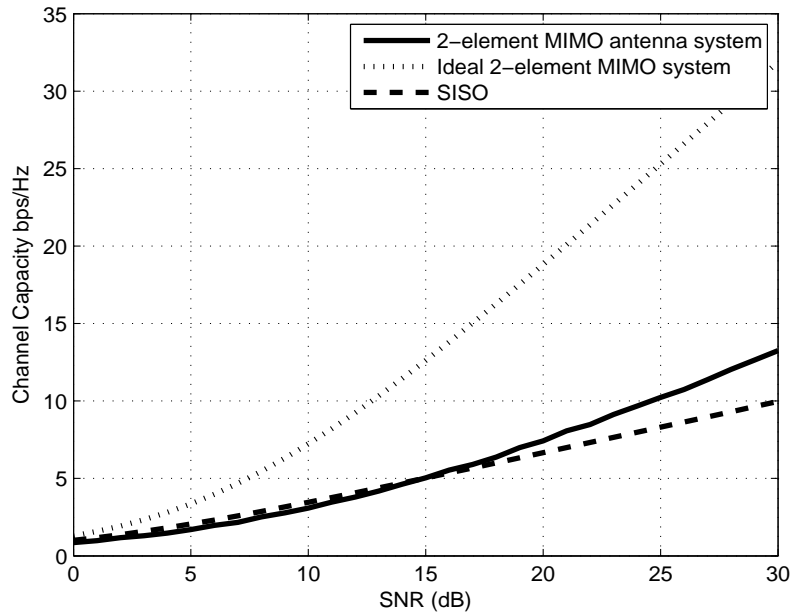
Figure 5.39: Average channel capacity in LOS environment - Mode-1 at 1945 MHz.
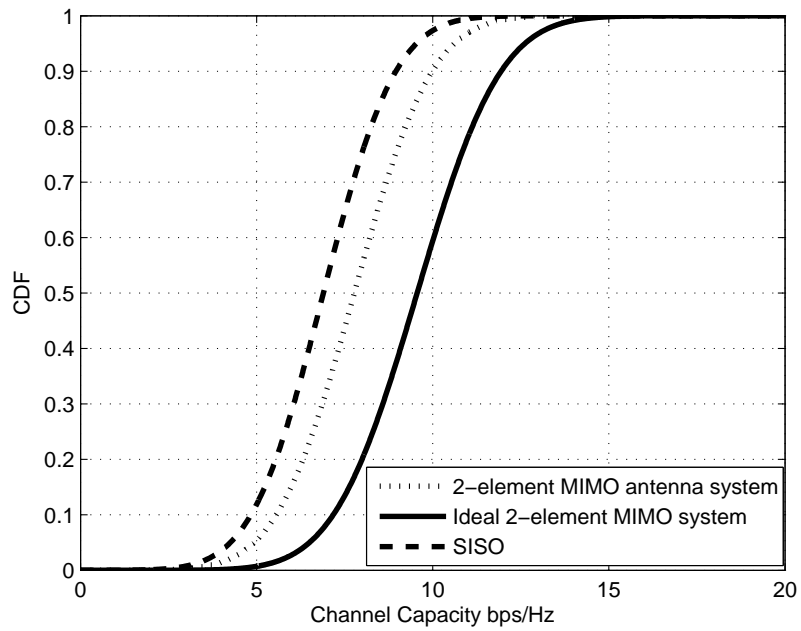
Figure 5.40: CDF of channel capacity - Mode-1 at 1095 MHz.

149
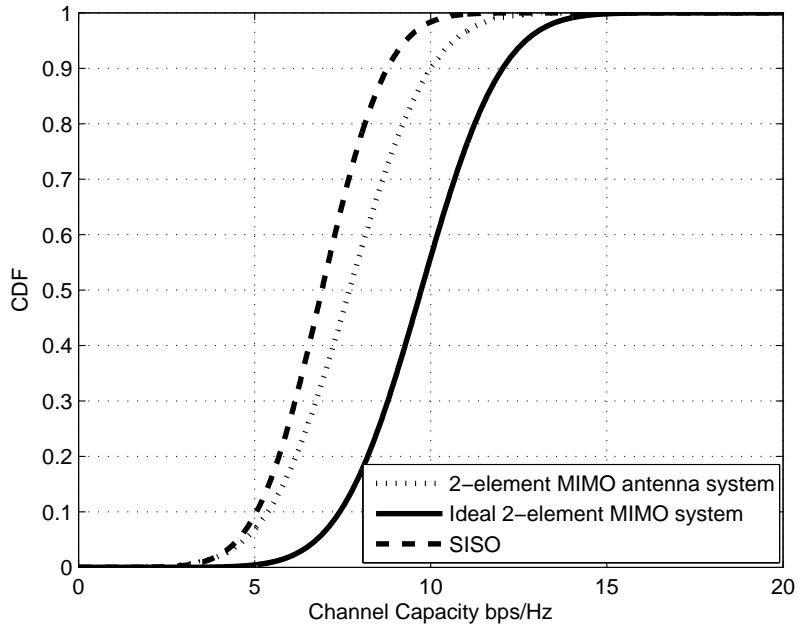
Figure 5.41: CDF of channel capacity - Mode-1 at 1945 MHz.

5.3.2 Channel Capacity of Planar MIMO Antenna Systems

Channel capacity calculations based on the radiation patterns for the planar MIMO antenna system described in section 5.2 is discussed in this section. The average channel capacity in mode-1 at given two bands of 1100 MHz and 2480 MHz are given in Figures 5.42 and 5.43, respectively. The given figures show the channel capacity curves of the two element MIMO antennas, ideal MIMO systems with totally uncorrelated channel and SISO system in the LOS environment. It is evident from the channel capacity curves that planar MIMO antenna system performs well compared to its SISO counter part and its performance is degraded compared to an ideal MIMO system. This is mainly because of the high correlation between MIMO channels and MIMO antennas (note the close proximity of the two MIMO antennas on available device).

The CDF curves of the channel capacity of given planar MIMO antennas at two bands (mode-1: 1100 MHz,2480 MHz) are shows in Figures 5.44 and 5.45 in LOS environment. It is evident form the given curves that the performance

of given MIMO system is less than the ideal capacity but much better than the SISO systems.

Figure 5.42: Average channel capacity in LOS environment - Mode-1 at 1100 MHz.
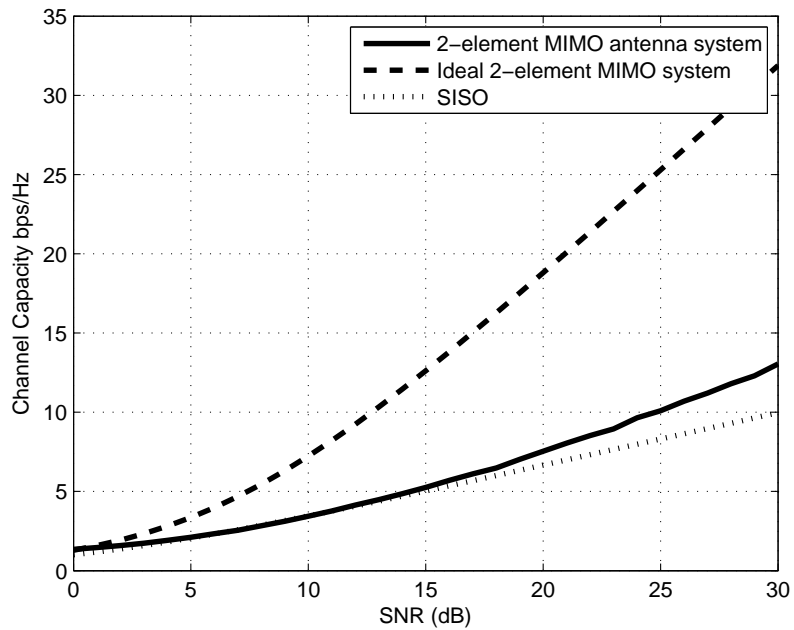
Figure 5.43: Average channel capacity in LOS environment - Mode-1 at 2480 MHz.
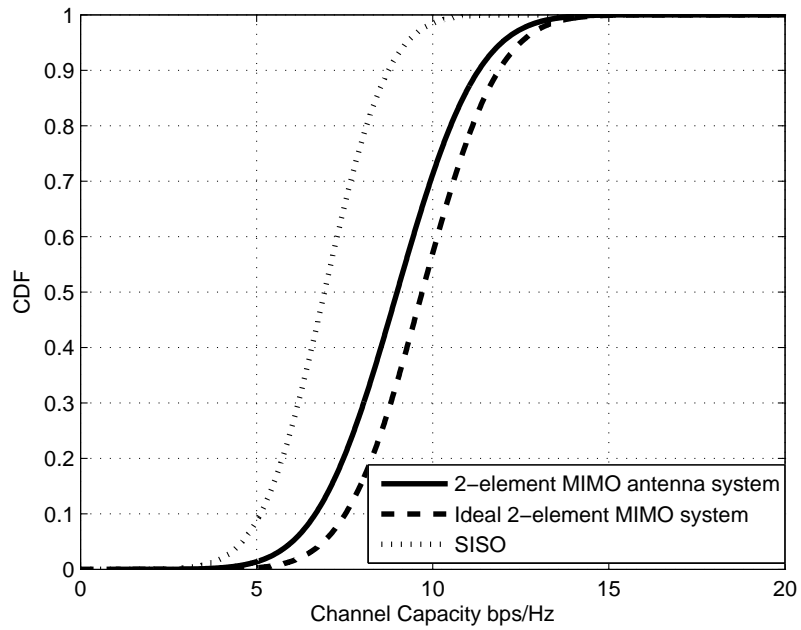
Figure 5.44: CDF of channel capacity - Mode-1 at 1100 MHz.
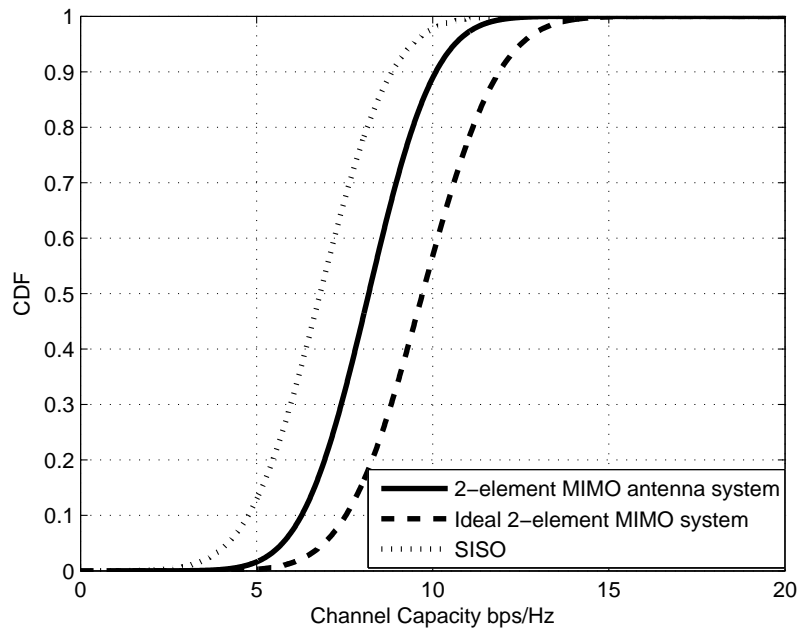
Figure 5.45: CDF of channel capacity - Mode-1 at 2480 MHz.

5.4   Conclusions

In this chapter, two novel compact reconfigurable MIMO antenna systems integrated with an UWB sensing antenna are presented. The proposed antenna designs are the first to appear in literature for integrated CR antennas on a single substrate covering lower frequency bands (i.e. 700 MHz) complying with existing and next generation 4G wireless standards. The concept of using the GND plane as the UWB antenna is unique to both these designs and is the distinguishing feature for compact size antennas. The proposed designs are suitable for CR applications in small wireless handheld devices. The antenna was also evaluated for MIMO parameters where it showed good performance metrics.

CHAPTER 6

DF USING SP INTEGRATED WITH RECONFIGURABLE ANTENNA

6.1   Introduction

The six-port measurement technique was introduced in 1977 by Glen F. Engen at the National Institute of Standards and Technology [136]. The six-port (SP) measuring technique was developed as a method of network analysis in the field of microwave metrology. Network analysis is the measurement of the scattering parameters for a given microwave device, for example the reflection and transmission coefficients. The six-port reflectometer (SPR) is a device used to find the reflection coefficient while the six-port network analyzer (SPNA) is used for the measurements of both reflection and transmission coefficients [136]. So, SPR is a device using SP techniques to measure the reflection coefficients. The SPR, SP structure or SP architecture are synonymously used in literature for this device.

In this chapter, six-port (SP) measuring techniques are introduced followed by the application of SP in RF DF systems. Two compact SP circuits are presented for angle of arrival (AoA) measurements. The first design is a single SP architecture for determining the AoA in a single plane while the second is a dual SP structure for dual angles resolution, ϕ and θ, determination. The single SP

circuit was integrated with a reconfigurable MIMO antenna system as discussed in Chapter 5. The complete system setup is used to assess the accuracy using two SP in compact integrated DF system.

6.2 Six-port Reflectometer

The basic theory of an SPR can be described using a linear SP network, as shown in Figure 6.1. The incoming and outgoing RF signals are described by wave variables, associated with the physical waves traveling along transmission lines. Incident waves are the signals traveling toward a device and are denoted by variable a while the transmitted and reflected waves are designated with variable b.
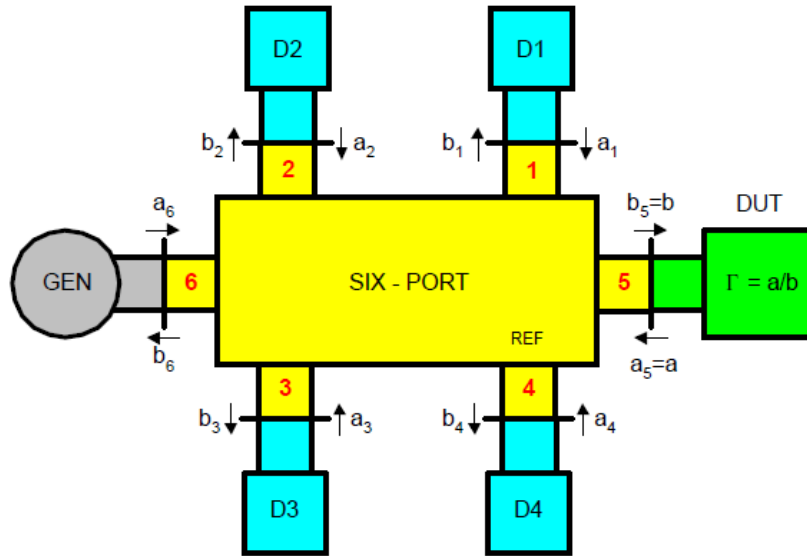
Figure 6.1: Six-port Reflectometer.

SP reflectometer is shown in Figure 6.1. All six ports of an SPR are connected, of which, one port is connected to the incoming signal source (GEN), one is terminated in a device under test (DUT) while the subsequent four ports are connected to power detectors (D1- D4). The DUT is characterized by the reflection coefficient (Γ). All the states of the SP are characterized by twelve variables a_i and b_i, where i = 1,...,6. Reflected and transmitted state variables of the SP are

mutually coupled scattering parameters and can be determined from the scattering matrix of a given SP architecture. Relationship between the inputs and outputs of an SPR with scattering matrix S is given by the equation:

$$
\begin{bmatrix} b_1 \\ b_2 \\ . \\ . \\ b_6 \end{bmatrix} = \begin{bmatrix} S_{11} & S_{12} & . & . & S_{16} \\ S_{21} & S_{22} & . & . & S_{26} \\ . & . & . & . & . \\ . & . & . & . & . \\ S_{61} & S_{62} & . & . & S_{66} \end{bmatrix} \begin{bmatrix} a_1 \\ a_2 \\ . \\ . \\ a_6 \end{bmatrix}
\tag{6.1}
$$

where the scattering matrix S is given by

$$
S = \begin{bmatrix} S_{11} & S_{12} & . & . & S_{16} \\ S_{21} & S_{22} & . & . & S_{26} \\ . & . & . & . & . \\ . & . & . & . & . \\ S_{61} & S_{62} & . & . & S_{66} \end{bmatrix}
$$

The SP four ports (1 to 4) are the detector ports with known loads, for which the reflection coefficient can be found as

$$
a_i = \Gamma_{Di} b_i \qquad i = 1, ..., 4
\tag{6.2}
$$

where Γ_{Di} is reflection coefficient of ith detector. Equation (6.1) shows the relationship between incident, reflected and transmitted signals through the scattering

matrix S, thus forming six linear equations, while the reflection coefficient of each of the four power detectors is given by equation (6.2). This forms a set of ten linear equations that are mutually coupled, with ten constraints (solution of this system should satisfy all condition imposed by these ten equations) and twelve complex variables (a_i, b_i $i = 1, 2...6$). So, it has two degrees of freedom. In this system only two variables can be chosen arbitrarily while the rest can be expressed as linear combinations of the two. In the SP architecture, the signal at port-5 (a_5) is the incident wave on the DUT, while (b_5) is the reflected signal from the DUT. These two signals are considered as the independent variables. By substituting equation (6.2) into equation (6.1) and after algebraic manipulations, we can obtain:

$$
\begin{bmatrix} 0 \\ 0 \\ 0 \\ 0 \\ b \\ b_6 \end{bmatrix} = \begin{bmatrix} (S_{11}\Gamma_1 - 1) & S_{12}\Gamma_2 & S_{13}\Gamma_3 & S_{14}\Gamma_4 & S_{15} & S_{16} \\ S_{21}\Gamma_1 & (S_{22}\Gamma_2 - 1) & S_{23}\Gamma_3 & S_{24}\Gamma_4 & S_{25} & S_{26} \\ S_{31}\Gamma_1 & S_{32}\Gamma_2 & (S_{33}\Gamma_3 - 1) & S_{34}\Gamma_4 & S_{35} & S_{36} \\ S_{41}\Gamma_1 & S_{42}\Gamma_2 & S_{43}\Gamma_3 & S_{44}(\Gamma_4 - 1) & S_{45} & S_{46} \\ S_{51}\Gamma_1 & S_{52}\Gamma_2 & S_{53}\Gamma_3 & S_{54}\Gamma_4 & S_{55} & S_{56} \\ S_{11}\Gamma_1 & S_{12}\Gamma_2 & S_{13}\Gamma_3 & S_{14}\Gamma_4 & S_{65} & S_{66} \end{bmatrix} \begin{bmatrix} b_1 \\ b_2 \\ b_3 \\ b_4 \\ a \\ a_6 \end{bmatrix}
$$

$$(6.3)$$

The signals incident at the power detector of the SP at port-1 to port-4 can be expressed from equation (6.3) as.

$$b_i = A_i a + B_i b = b A_i \left[\frac{a}{b} + \frac{B_i}{A_i} \right] = b A_i \left(\Gamma - q_i \right) \qquad i = 1, ..., 4 \qquad (6.4)$$

In equation (6.4), A_i and B_i are complex quantities which depend on the S-parameter of the SP and the reflection coefficient Γ of the power detectors of the

SPR. In equation (6.4) we have,

$$\Gamma = \frac{a}{b} \qquad and \qquad q_i = -\frac{A_i}{B_i}$$

The output of each power detector can be represented as

$$P_i = |A_i a + B_i b|^2 = P_0 |A_i|^2 |\Gamma - q_i|^2 \qquad (6.5)$$

In equation (6.5), $P_0 = |b|^2$ is the incident power. It is clear that the detector output is proportional to the incoming RF signal. One of the detectors is taken as a reference port, assuming it to respond to signal b of the DUT. The power detected at the reference detector port can be written as

$$P_4 = P_0 |B_4|^2 |d\Gamma + 1|^2 \qquad (6.6)$$

where $d = A_4/B_4 = -1/q_4$. For an ideal reference port, d=0. The normalized power at each of the detector ports can be written as

$$p_i = \frac{P_i}{P_4} = C_i \left| \frac{\Gamma - q_i}{d\Gamma + 1} \right|^2 \qquad i = 1, ..., 3 \qquad (6.7)$$

where $C_i = |A_i/B_4|^2$. Equation 6.7 is the basic equation of a SPR. The relationship between the reflection coefficient Γ of the DUT and the power detectors can be completely characterized by 11 constants from equation (6.7). These constants are called calibration constants.

6.3 Calibration

The calibration of an SPR consists of obtaining the unknowns given in equations (6.4) and (6.7). Calibration is a necessary part of the SPR technique for accurate microwave measurements which is assumed to be the most challenging and formidable job. A considerable efforts had been put by researchers to develop different calibration techniques for the determination of the calibration constants.

In calibration, termination loads are connected to the DUT port and powers are measured at the power detector ports. Termination loads used in calibration are of the following types:

1. Fully known loads (Calibration or impedance standards)

2. Unknown loads or auxiliary loads

3. Partially known loads

4. Sliding loads

The detector powers and reflection coefficients are substituted to the SPR equation (6.7). The resultant set of equations are solved for the unknown calibration constantsn [141, 142].

6.4   AoA Determination using the SP

To find the AoA in elevation (θ -plane) and in azimuth (ϕ -plane) directions, a schematic view of a geometrical model is shown in Figure 6.2. The receiving antennas are separated by distance x and distance y in the plane of the array. Owing to the angle of arrival θ and ϕ; there will be path difference between the two propagation paths. So the propagated RF signals will be shifted with respect to each other by angle $\Delta\theta$ and $\Delta\phi$. The phase difference between the input RF signals incident on the θ-plane and the ϕ-plane can be measured by calculating the path difference between the two antennas within each SP setup. The four elements in the antenna array are assumed to be separated by a distance of $\lambda/2$ in both vertical and horizontal directions, where λ is the wavelength of the operating frequency of interest, Δx and Δy are the path differences between the four antenna elements seen by the incoming RF wave in the x and y directions, respectively. The relationship between path differences and phase differences is given in (6.8). The AoA for θ and ϕ can be calculated using (6.8) and (6.9), respectively.

$$\Delta y = \lambda\frac{\Delta\theta}{2\pi}, \qquad \Delta x = \lambda\frac{\Delta\phi}{2\pi} \tag{6.8}$$
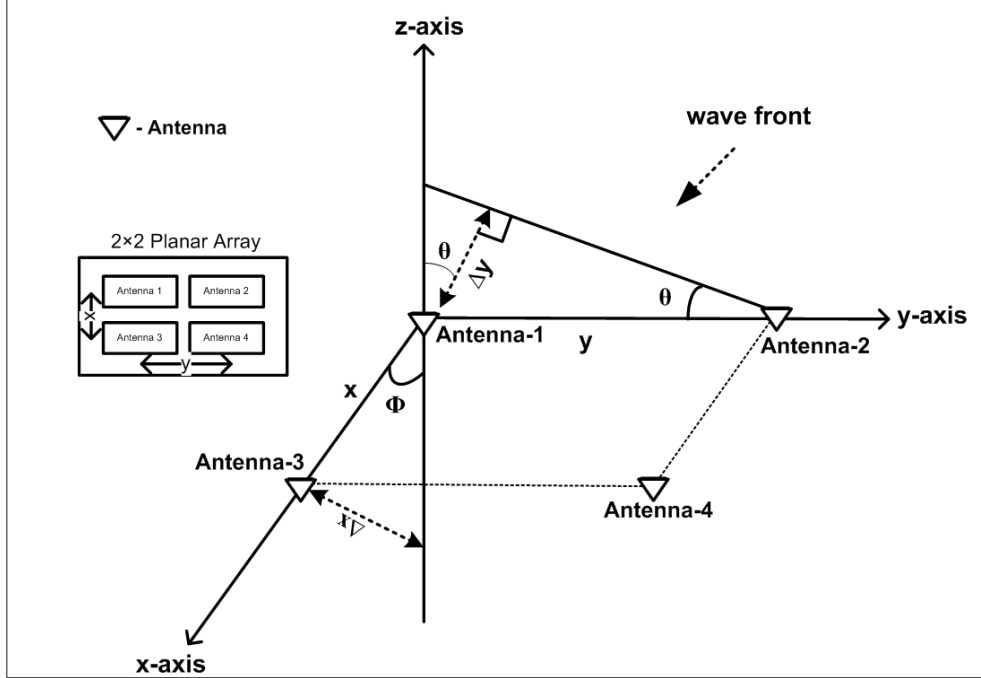
Figure 6.2: Angles of incoming waves with respect to planar array elements.

$$\sin\theta = \frac{\lambda}{y}\frac{\Delta\theta}{2\pi}, \qquad \sin\phi = \frac{\lambda}{x}\frac{\Delta\phi}{2\pi} \qquad (6.9)$$

A possible complete dual-angle resolution, multi-band direction finding system is shown in Figure 6.3. The system would be used to find the 3D AoA of a distant target by finding both θ and ϕ angles of the incoming wave. The proposed dual-SP is designed to operate at much lower frequency bands than what appeared in literature to cover a wide range of wireless standards, especially for the fourth generation cellular phone system and the next generation in wireless data networks. The proposed system covers a wide frequency range starting from 1.68 GHz to 2.25 GHz (higher frequency bands are also supported from 5.2 GHz to 5.4 GHz) and has a compact size that allow it to fit within a standard smart phone size.

Let us consider two input RF signals a_5 and a_6 are incident at SP-1 ports 5 and 6 while a_{13} and a_{14} are incident at SP-2 ports 13 and 14 with different phases. The phase difference between the outputs of these two SP can be written

as $\Delta\theta = \theta_6 - \theta_5$ and $\Delta\phi = \phi_{13} - \phi_{14}$ for SP-1 and SP-2, respectively.

The two SP structures are functionally the same, thus only the reflection coefficient relations for SP-1 architecture will be derived. Let us assume that there are two normalized wave inputs, a_5 and a_6 with different amplitudes and phases incident on port-5 and port-6 given by,

$$a_5 = ae^{j\theta_5} \tag{6.10}$$

$$a_6 = \alpha ae^{j\theta_6} \tag{6.11}$$

where α is the amplitude ratio of the two signals, a_5 and a_6. The RF output signals of SP-1 can be written as a linear combination of the input signals as [147],

$$b_i = a_5 S_{5i} + a_6 S_{6i}, \qquad i = 1, .., 4 \tag{6.12}$$

The resultant signal at output port-1 can be written as

$$b_1 = a_5 S_{51} + a_6 S_{61}$$

$$b_1 = \frac{-j}{2} ae^{j\theta_5} + \frac{j}{2}\alpha a_5 e^{j\Delta\theta}$$

$$b_1 = \frac{a}{2} e^{j(\theta_5 - \frac{\pi}{2})} + \frac{j}{2}\alpha ae^{j(\theta_5 + \Delta\theta)}$$

$$b_1 = \frac{a}{2} e^{j(\theta_5 - \frac{\pi}{2})} + \frac{1}{2}\alpha ae^{j(\theta_5 + \Delta\theta)} e^{-j3\pi/2}$$

$$b_1 = \frac{a}{2} e^{j(\theta_5 - \frac{\pi}{2})} \left[1 + \alpha e^{j(\Delta\theta + \pi)}\right] \tag{6.13}$$

For port-2, the resultant signal is given by

$$b_2 = a_5 S_{52} + a_6 S_{62}$$

$$b_2 = \frac{-a}{2} e^{j\theta_5} + \alpha a_5 \frac{-j}{2} e^{j\Delta\theta}$$

$$b_2 = \frac{-a}{2} e^{j\theta_5} + \alpha a \frac{-j}{2} e^{j(\theta_5 + \Delta\theta)}$$

$$b_2 = \frac{-a}{2}e^{j\theta_5}\left[1 + \alpha e^{j(\Delta\theta + \frac{\pi}{2})}\right] \tag{6.14}$$

Similarly for port-3, the resultant signal is

$$b_3 = a_5 S_{53} + a_6 S_{63}$$

$$b_3 = \frac{-a}{2}e^{j\theta_5} + \frac{-1}{2}\alpha a_5 e^{j\Delta\theta}$$

$$b_3 = \frac{-a}{2}e^{j\theta_5} + \frac{-1}{2}\alpha a e^{j(\theta_5 + \Delta\theta)}$$

$$b_3 = \frac{-a}{2}e^{j\theta_5}\left[1 + \alpha e^{j\Delta\theta}\right] \tag{6.15}$$

and at port-4

$$b_4 = a_5 S_{54} + a_6 S_{64}$$

$$b_4 = \frac{-j}{2}ae^{j\theta_5} + \frac{-1}{2}\alpha a e^{j(\theta_5 + \Delta\theta)}$$

$$b_4 = \frac{-a}{2}e^{j[\theta_5 + \frac{\pi}{2}]} + \frac{1}{2}\alpha a e^{j(\theta_5 + j\Delta\theta)} - j. - j$$

$$b_4 = \frac{-a}{2}e^{j(\theta_5 + \frac{\pi}{2})} - \frac{1}{2}\alpha a e^{j(\theta_5 + \frac{\pi}{2} + \Delta\theta - \pi/2)}$$

$$b_4 = \frac{-a}{2}e^{j[\theta_5 + \frac{\pi}{2}]}\left[1 + \alpha e^{j(\Delta\theta - \frac{\pi}{2})}\right] \tag{6.16}$$

The RF output signals of SP-2 can be written as the linear combination of the input signals as.

$$b_k = a_{13} S_{13k} + a_{14} S_{14k}, \qquad k = 9, .., 12 \tag{6.17}$$

The output of each SP is passed through a power detector to get the DC signal. In this scheme, diodes can be used as power detectors. The output of the power detector can be written as a square magnitude of the RF input signal as given in [145].

$$V_i = K_i |b_i|^2, \qquad i = 1, ..., 4 \tag{6.18}$$

$$V_k = K_k |b_k|^2, \qquad k = 9, ..., 12 \tag{6.19}$$

where K_i and K_k are constants measured in W/V. These constants are specified

162
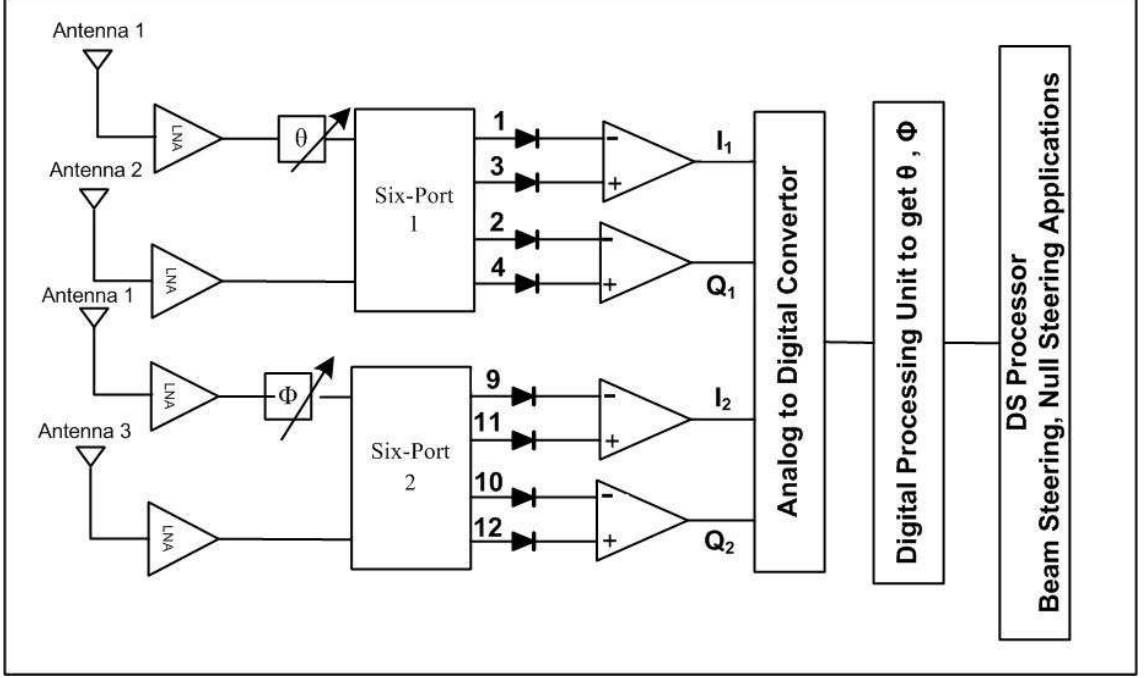
Figure 6.3: Dual Angle Resolution Dual Six-Port Design.

for each power detector showing the relationship between input power to output voltage . Each output of the power detector circuit is passed through a differential amplifier circuit to get the two components in-phase and quadrature (I and Q) [147]. For SP-1 these are I_1 and Q_1 while for SP-2 they are I_2 and Q_2.

$$I_1 = (V_3 - V_1) = K_i a^2 cos(j\Delta\theta) \tag{6.20}$$

$$Q_1 = (V_4 - V_2) = K_i a^2 sin(j\Delta\theta) \tag{6.21}$$

$$I_2 = (V_{11} - V_9) = K_k a^2 cos(j\Delta\phi) \tag{6.22}$$

$$Q_2 = (V_{12} - V_{10}) = K_k a^2 sin(j\Delta\phi) \tag{6.23}$$

Vectors Γ_1 and Γ_2 are defined for the dual SP in terms of the in-phase and quadrature components as

$$\Gamma_1 = (V_3 - V_1) - j(V_4 - V_2) = K_i a^2 e^{j\Delta\theta} \tag{6.24}$$

$$\Gamma_2 = (V_{11} - V_9) - j(V_{12} - V_{10}) = K_k a^2 e^{j\Delta\phi} \tag{6.25}$$

163

Equation (6.24) shows the phase relationship between the input RF incident waves at SP-1 while (6.25) is used to show the phase relationship of the incoming wave at SP-2. The phase difference of the incoming RF wave in the θ-plane can be found using SP-1 while for the ϕ-plane is found using SP-2 by performing the measurements on the baseband signal. A detailed literature survey of SP measurement techniques for RF DF is presented in section 3.5.

6.5   Characterization of the Six-Port Outputs

The direction of the incoming RF waves in azimuth and elevation planes can be easily determined using equation (6.9) based on the determination of the phase differences measured by using the SP given in equation (6.8). But this calculation overlooks the phase error caused by the slight asymmetry of the various SP paths, asymmetry of the power detectors and as well as frequency measurement errors. These errors in the phases were characterized via simulations and by laboratory measurements. In this section, a mathematical analysis is carried out to develop an analytical model to compensate for these errors in order to get high accuracy in phase measurement at the output of each port.

Let

θ'_{5i} is the phase error at output port-i of SP in a_5 + phase error caused by power detectors and differential amplifier

θ'_{6i} is the phase error at output port-i of SP in a_6 + phase error caused by power detectors and differential amplifier

So, the output signal can be written as a linear combination of input signals a_5 and a_6 with phase error at the output of each port. Thus

$$b_i = a_5 S_{5i} + a_6 S_{6i}$$

then,

$$b_1 = a_5 S_{51} + a_6 S_{61}$$

$$b_1 = \frac{-j}{2} a e^{j\theta_5} e^{j\theta'_{51}} + \frac{j}{2} \alpha a_5 e^{j\Delta\theta} e^{j\theta'_{61}}$$

164

$$b_1 = \frac{a}{2} e^{j(\theta_5 - \frac{\pi}{2})} e^{j\theta'_{51}} + \frac{j}{2} \alpha a e^{j(\theta_5 + j\Delta\theta)} e^{j\theta'_{61}}$$

$$b_1 = \frac{a}{2} e^{j[\theta_5 - \frac{\pi}{2}]} \left[1 + \alpha a e^{j(\Delta\theta + \pi)} \frac{e^{j\theta'_{61}}}{e^{j\theta'_{51}}} \right]$$

$$b_1 = \frac{a}{2} e^{j(\theta_5 - \frac{\pi}{2})} e^{\theta'_{51}} [1 + C_1] \tag{6.26}$$

Similarly, for port-2

$$b_2 = a_5 S_{52} + a_6 S_{62}$$

$$b_2 = \frac{-a}{2} e^{j\theta_5} e^{j\theta'_{52}} + \frac{-j}{2} \alpha a_5 e^{j\Delta\theta} e^{j\theta'_{62}}$$

$$b_2 = \frac{-a}{2} e^{j\theta_5} e^{j\theta'_{52}} \left[1 + \alpha e^{j(\Delta\theta + \frac{\pi}{2})} \right] e^{\Delta\theta'_2}$$

$$b_2 = -\frac{a}{2} e^{(j(\theta_5 + \theta'_{52})} [1 + C_2] \tag{6.27}$$

$$b_3 = a_5 S_{53} + a_6 S_{63}$$

$$b_3 = \frac{-a}{2} e^{j\theta_5} e^{j\theta'_{53}} + \frac{-1}{2} \alpha a_5 e^{j\Delta\theta} e^{j\theta'_{63}}$$

$$b_3 = -\frac{a}{2} e^{(j(\theta_5 + \theta'_{53})} [1 + C_3] \tag{6.28}$$

$$b_4 = a_5 S_{54} + a_6 S_{64}$$

$$b_4 = \frac{-j}{2} a e^{j\theta_5} e^{j\theta'_{54}} + \frac{-1}{2} \alpha a e^{j(\theta_5 + \Delta\theta)} e^{j\theta'_{64}}$$

$$b_4 = \frac{-a}{2} e^{j(\theta_5 + \frac{\pi}{2})} e^{j\theta'_{54}} + \frac{1}{2} \alpha a e^{j(\theta_5 + j\Delta\theta)} e^{j\theta'_{64}}$$

$$b_4 = -\frac{a}{2} e^{j(\theta_5 + \frac{\pi}{2})} e^{j\theta'_{54}} [1 + C_4] \tag{6.29}$$

$$\Delta\theta'_i = \theta'_{6i} - \theta'_{5i}, \qquad i = 1, ..., 4 \tag{6.30}$$

where

$C_1 = \alpha e^{j(\Delta\theta + \pi)} e^{j\Delta\theta'_1}$

$C_2 = \alpha e^{j\Delta\theta + \frac{\pi}{2}} e^{j\Delta\theta'_2}$

$C_3 = \alpha e^{j(\Delta\theta + \pi)} e^{j\Delta\theta'_3}$

$C_4 = \alpha e^{j(\Delta\theta - \frac{\pi}{2})} e^{j\Delta\theta'_4}$

θ_5 is the phase of incoming signal at port-5

θ_6 is the phase of incoming signal at port-6

Supposing that four identical detectors $(K_i = K)$ are used, the DC output voltages have an error term, respectively,

$$V_1 = K_1|b_1|^2 = K\frac{a^2}{4}[1 + \alpha^2 - 2\alpha cos(\Delta\theta + \Delta\theta_1')] \tag{6.31}$$

$$V_2 = K_2|b_2|^2 = K\frac{a^2}{4}[1 + \alpha^2 - 2\alpha sin(\Delta\theta + \Delta\theta_2')] \tag{6.32}$$

$$V_3 = K_3|b_3|^2 = K\frac{a^2}{4}[1 + \alpha^2 + 2\alpha cos(\Delta\theta + \Delta\theta_3')] \tag{6.33}$$

$$V_4 = K_4|b_4|^2 = K\frac{a^2}{4}[1 + \alpha^2 + 2\alpha sin(\Delta\theta + \Delta\theta_4')] \tag{6.34}$$

Once the error in each phase of the SP is characterized, the error in the incoming RF wave can be analyzed based on (6.31) –(6.34). This phase error in each path can be compensated for using an additional phase compensation block to have more accurate DF results. This block could be implemented in hardware using field programmable gate array (FPGA) or software based phase compensation can produce the satisfactory results.

6.6   Contribution

RF based DF devices in a wireless hand-held devices are required in modern wireless communication systems especially in the second generation of cognitive radio systems. The primary requirement for such DF systems is to be compact so that it can be accommodated within the small size of wireless handheld terminals. Another key requirement of these DF systems is its operation in the low frequency bands. Most of the designs available in literature are either not realizable on single board [12] or have an issue with dimensions (i.e. one of large sizes) that cannot be accommodated within a mobile phone size [11].

In this work, a compact wide-band direction finding system is proposed that is suitable for wireless handheld and mobile communication devices. The proposed SP design covers a low frequency wide band ranging from 1.68 GHz to 2.25 GHz

with a minimum bandwidth of 570 MHz. The frequency bands covered are mostly commercially available ones for cellular phone operation (3G and 4G). The dimensions of the proposed SP architecture is optimized to be accommodated within a software defined radio and cognitive radio platforms.

Moreover, the proposed design optimizes that in [11] resulting in 40% reduction in total area of the single SP size and yet operates at a lower frequency range. This compact structure having a dimension of $65 \times 65 \times 1.28 \text{mm}^3$ can be easily fitted in a cognitive radio or SDR platforms.

The distinguishing feature and the novelty of the proposed compact dual-SP structure is its ability to find the azimuth (ϕ) as well as the elevation (θ) angles of the incoming wave. All designs available in literature are based on single angle resolution DF systems while the proposed design can be used to find the two angles of the incoming RF wave (i.e. elevation and azimuth).

The proposed compact single SP and dual-angle resolution based dual-SP design can be used in variety of applications in wireless hand-held terminals and other low cost microwave measurement devices as well.

6.7 Six-Port Design Details

The objective of this part of work is to design a SP structure that should be compact and also can operate in lower frequency bands as compared to the other available designs. This section is divided in three sub-sections.

1. Operating Principle of the printed SP

2. A compact single SP design

3. A dual-angle resolution based dual SP design

6.7.1 Operating Principle of a Printed SPR

Several variants of the SPR are reported in literature. The printed SPR is used widely due to its ease of fabrication and development in low power measurements.

In this work, a printed SPR is presented and that is based on [11] and is shown in Figure 6.4 (a) . The printed SPR essentially consists of four 90° hybrid couplers. A single 90° hybrid coupler is shown in Figure 6.4(b) with its scattering matrix S given in equation (6.35).

$$S = \frac{-1}{\sqrt{2}} \begin{bmatrix} 0 & j & 1 & 0 \\ j & 0 & 0 & 1 \\ 1 & 0 & 0 & j \\ 0 & 1 & j & 0 \end{bmatrix} \tag{6.35}$$

A typical SP is a passive circuit having two input ports and four output ports. Each RF output signal is a different linear combination of the two RF input signals. Each input signal is passed through two hybrid couplers each with a loss of 3dB. The magnitude of the typical S-parameters has a theoretical value of -6dB because of the two hybrid couplers. In the SP circuit shown in Figure 6.4 (a), the input ports are port 5 and 6 while the output ports are 1, 2, 3 and 4. Ports 7 and 8 are terminated with 50Ω impedance.The scattering matrix of the proposed SP phase discriminator can be easily obtained using the SP diagram 6.4 (a), and it
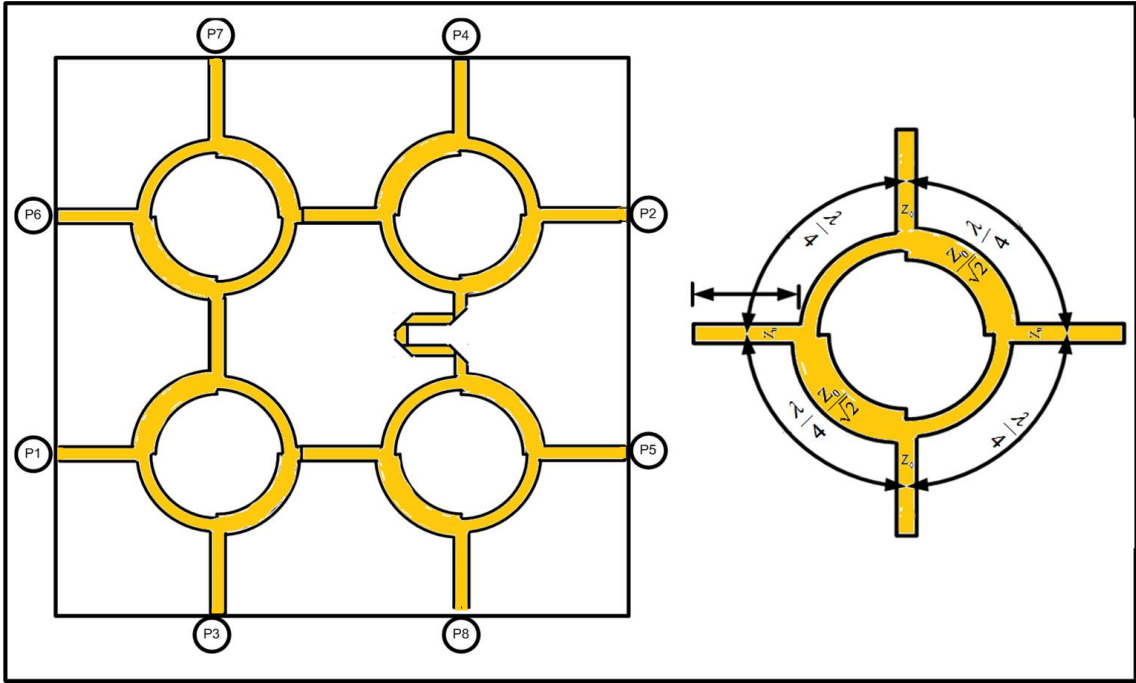
Figure 6.4: (a)Printed SPR (b) Single Hybrid Coupler.

is given in equation (6.36).

$$
S = \frac{1}{2}
\begin{bmatrix}
0 & 0 & 0 & 0 & -j & j \\
0 & 0 & 0 & 0 & -1 & -j \\
0 & 0 & 0 & 0 & -1 & -1 \\
0 & 0 & 0 & 0 & -j & -1 \\
-j & -1 & -1 & -j & 0 & 0 \\
j & -j & -1 & -1 & 0 & 0
\end{bmatrix}
\tag{6.36}
$$
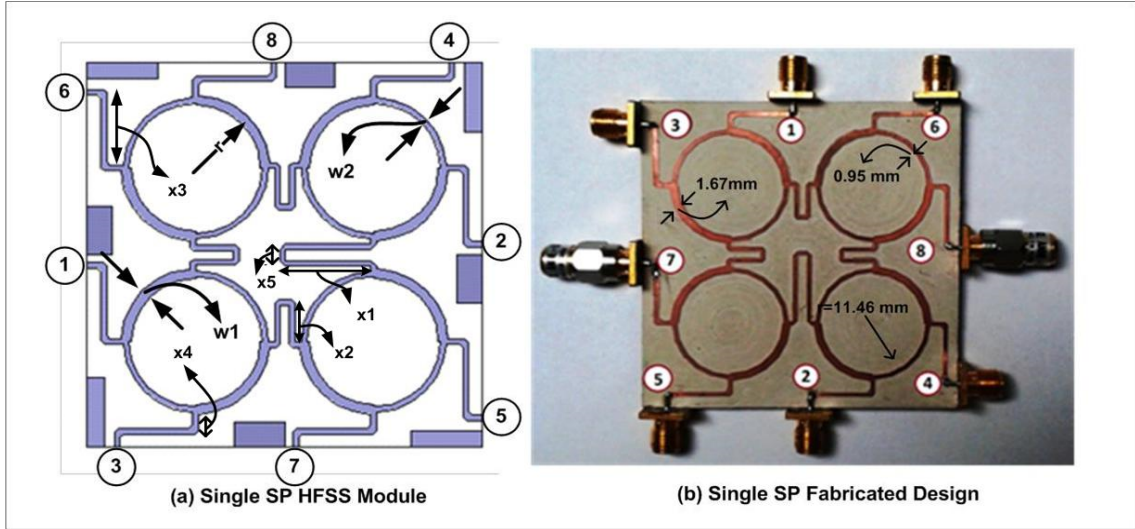
Figure 6.5: Microstrip Six-Port Circuit Layout.

6.7.2 Compact Single Six-Port Design

In this section, the design of a compact single SP is presented. This SP essentially consists of two input ports and four output ports. The input ports are connected to the RF incoming wave (i-e. antennas) while the output is a linear combination of the two inputs. Figure 6.5(a) shows the HFSS optimized design model used in the simulations of the single SP while 6.5(b) shows the fabricated microstrip circuit layout of the wide-band SP microwave printed structure. The design was realized on a Rogers 3006 double layer board with relative permittivity of 6.15 and substrate thickness of 0.64 mm. The total dimensions of the SP board were $65 \times 65 \times 0.64$ mm^3. Port-5 and port-6 are the input ports while output ports are numbered from 1 to 4. Ports 7 and 8 are terminated with 50 Ω impedance. The microstrip line width used for 50 Ω is 0.95 mm. All other dimensions of the SP are shown on in Figure 6.5. In this SP circuit, L=65mm, W=65mm, w1=01.67mm w2=0.95mm, r=11.46mm, h=1.28mm, x1=15mm, x2=7.4mm, x3=13.2, x4=3.6mm and x5=2.4mm.

6.7.3 Dual Six-Port Design

In this section, design details of the dual-angle resolution based dual-SP is provided. By using two SP designs as the one shown in Figure 6.6, we can find the

170
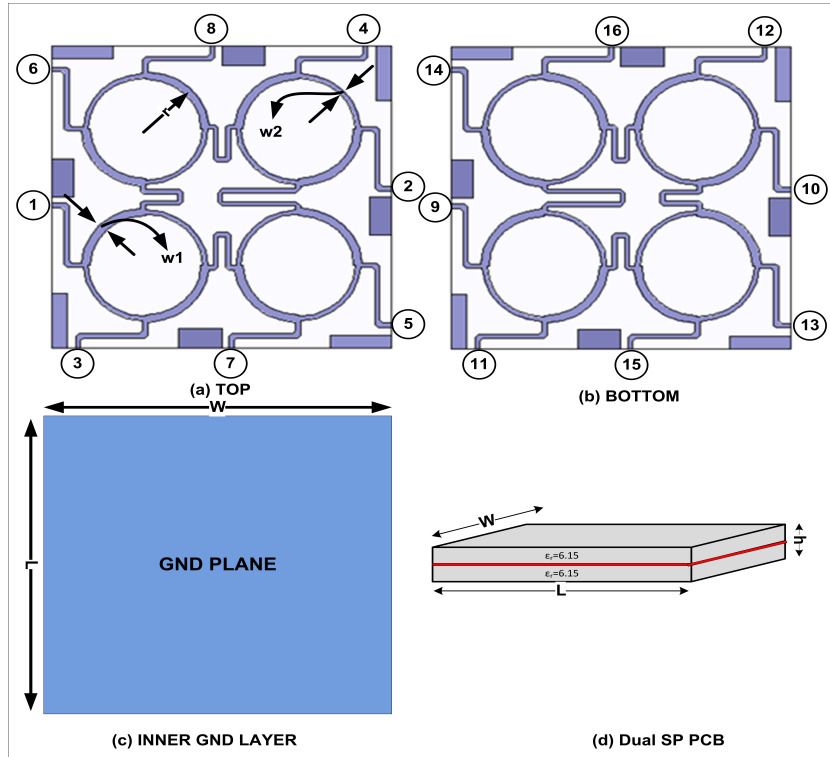
Figure 6.6: The circuit layout of dual-angle SP design.

3D location of an incoming wave in spherical coordinates since we need to resolve for two angles, θ and ϕ. Figure 6.7 shows the circuit layout of a multi-band, dual-angle dual SP microwave printed structure that is a modified version with more compact size than that in [11]. The dual-SPs are printed on a multilayer PCB for 3D angle of arrival (AoA) systems. The design was modeled and optimized using HFSS and then realized on a Rogers 3006 board with relative permitivity of 6.15 and substrate thickness of 0.64mm. The total dimension of the complete dual SP board is $65 \times 65 \times 1.28mm^3$. The two sides of the dual-SP are exactly the same except for the feed positions to allow mounting the SMA connectors. Ports 5, 6 and ports 13, 14 are input ports for SP-1 and SP-2, respectively, while the output ports are numbered from 1 to 4 for SP-1 and 9 to 12 for SP-2. Ports 7, 8 of SP-1 and 15, 16 of SP-2 are terminated with 50Ω impedance. The fabricated dual SP design is shown in Figure 6.7.
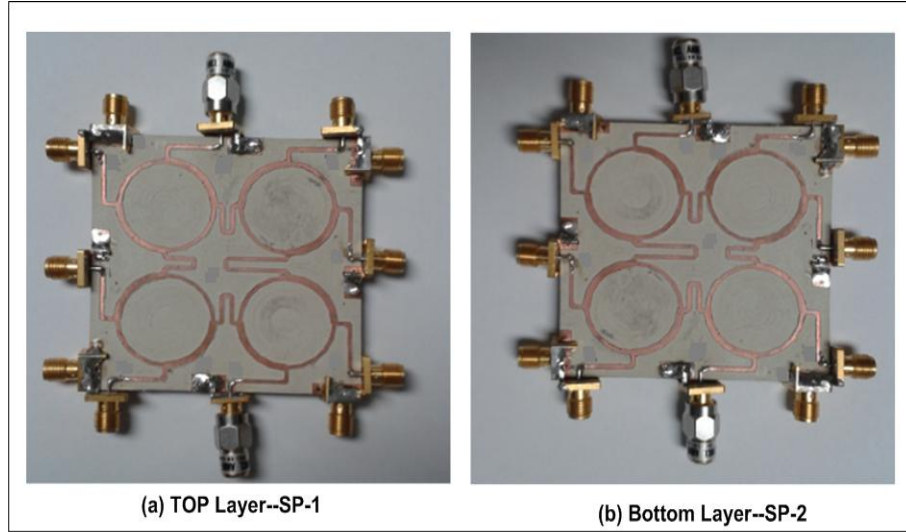
Figure 6.7: Top and Bottom layers of fabricated dual SP design.

6.8 SP Designs Results

The proposed dual SP was optimized using HFSS^{TM} for wide-band dual angle resolution and compact size. The wide-band covers frequencies from 1.68 GHz to 2.25 GHz with a bandwidth of 570 MHz. This frequency covers most of the existing standards for mobile devices. The measurements were performed using an Agilent N9918A VNA. Figure 6.8. shows the simulation and measurement results of the reflection coefficient characteristics of input port-5 and port-6 of SP-1. Similar results were obtained for SP-2. Both SPs are exactly similar in structure and same simulation and measured results were obtained for both design. Figure 6.9 and Figure 6.10. show the simulated and measured transmission loss characteristics of the proposed SP-1. The transmitted S-parameter curves S_{5i} (Figure 6.9.) and S_{6i} (Figure 6.10.) show the good transmission of power at the output ports.

Figure 6.11. and Figure 6.12. show the simulated and measured phases of the transmission loss parameter S_{5i}. The phase measurement results are in good agreement with the theoretical values and simulated ones as the relative phase are of interest and not the instantaneous phases. The simulated phases for S_{6i} are shown in Figure 6.13. while Figure 6.14. shows the measured phases of the transmission loss parameter S_{6i}. The maximum phase error relative to reference port S_{64} was ± 5 for both simulated and measured values.

172
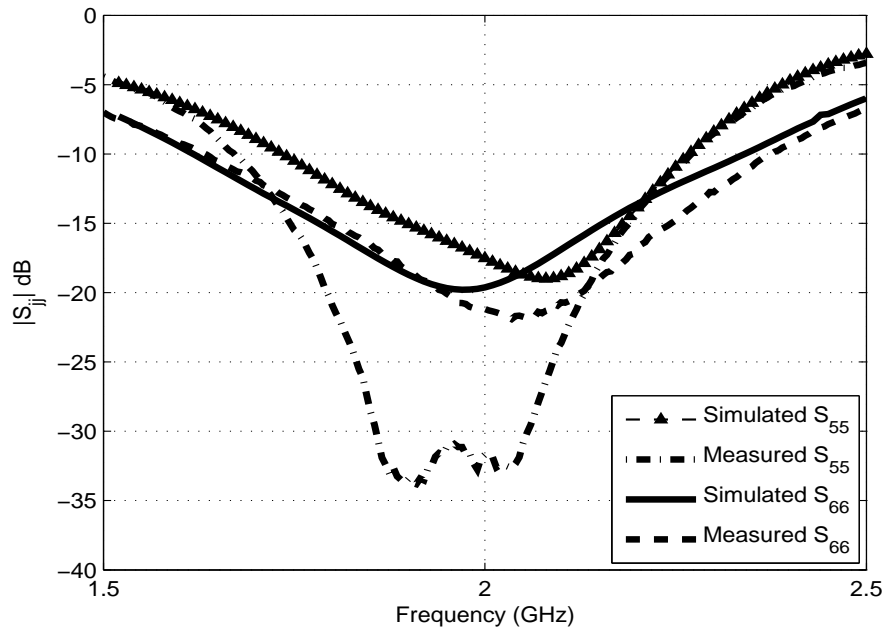
Figure 6.8: Simulation and measurements return loss at Port 6.
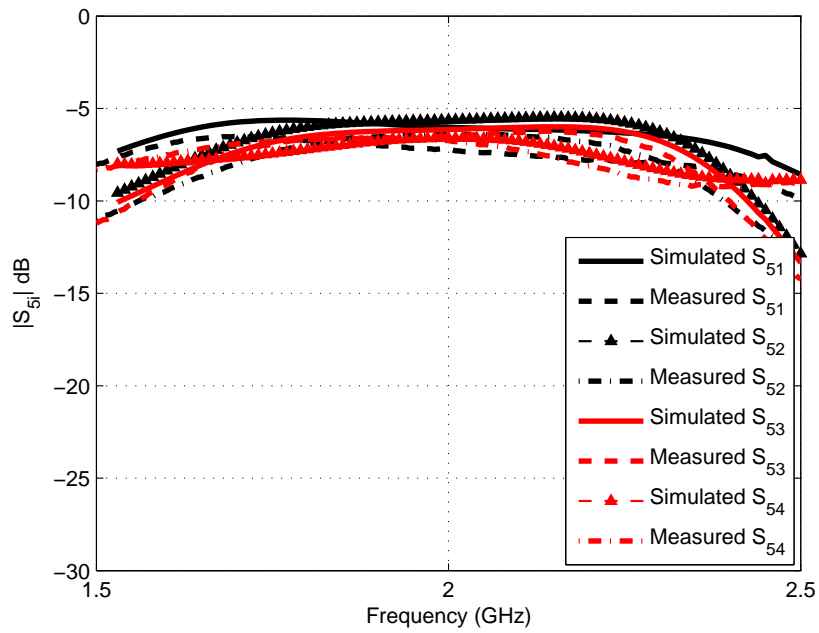
Figure 6.9: Simulated and measured transmission loss S_{5i}

.

173
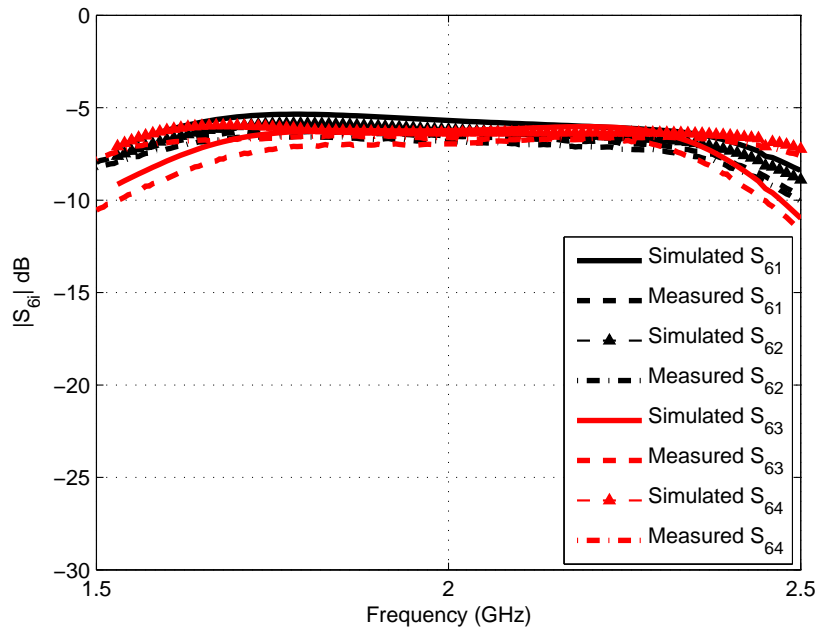
Figure 6.10: Simulated and measured transmission loss S_{6i}
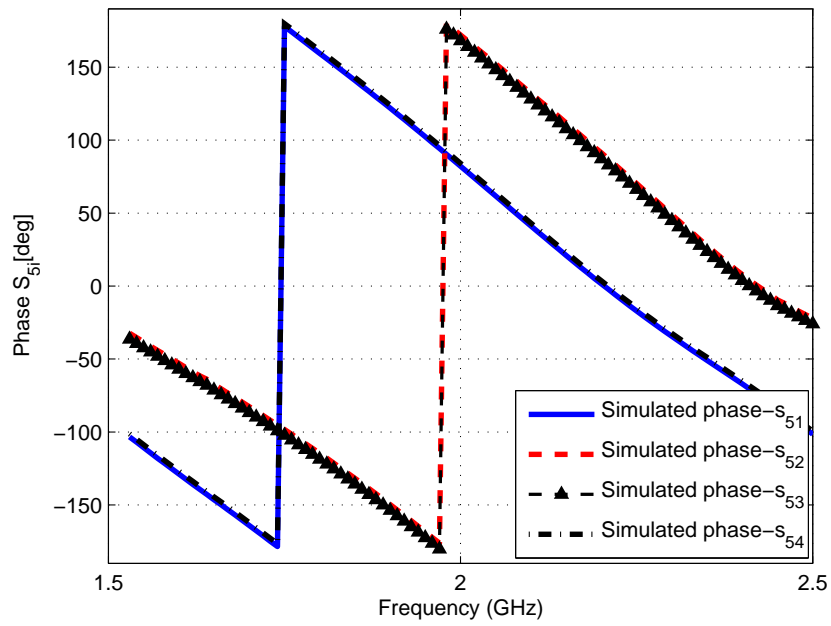
Figure 6.11: Simulated phase S_{6i}

174
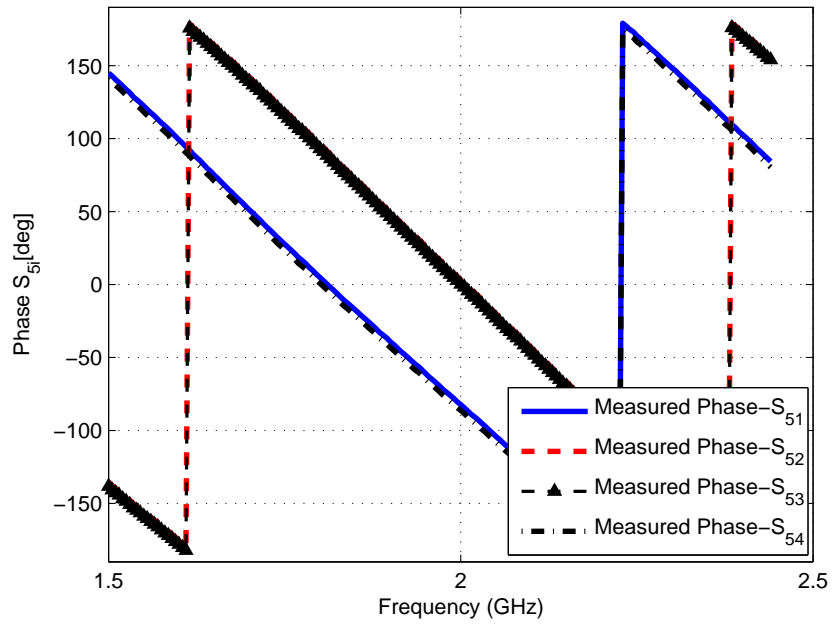
Figure 6.12: Measured phase S_{6i}
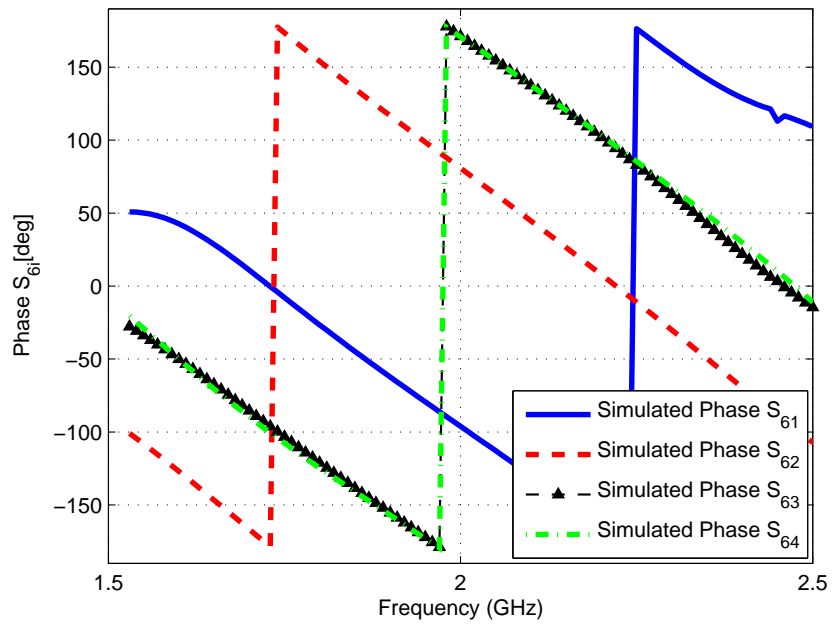
Figure 6.13: Simulated phase S_{6i}

175
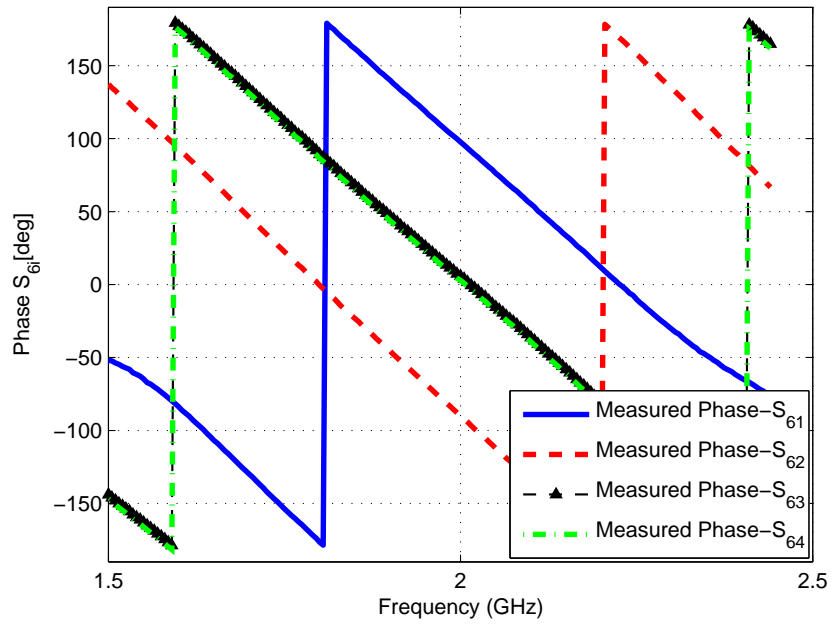
Figure 6.14: Measured phase S_{6i}
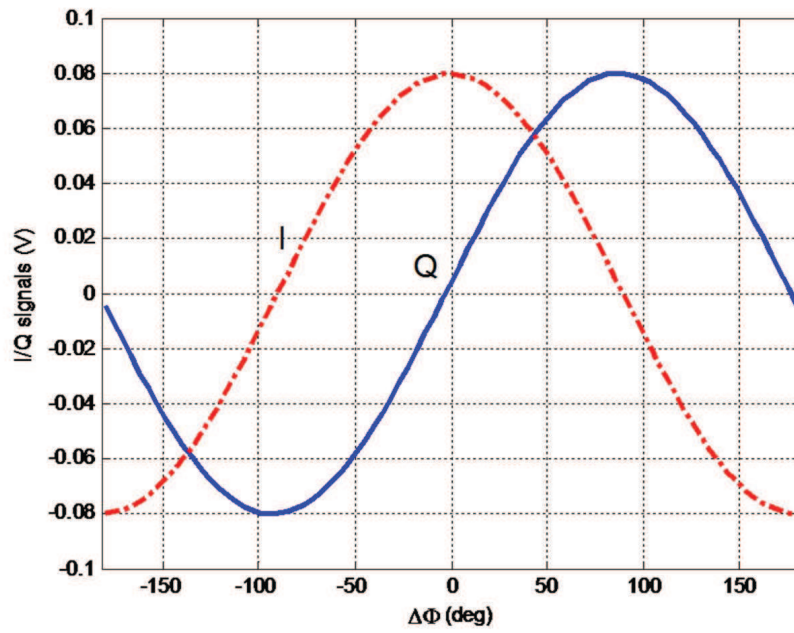
Figure 6.15: In-phase (I) and quadrature (Q) signals from the DF system
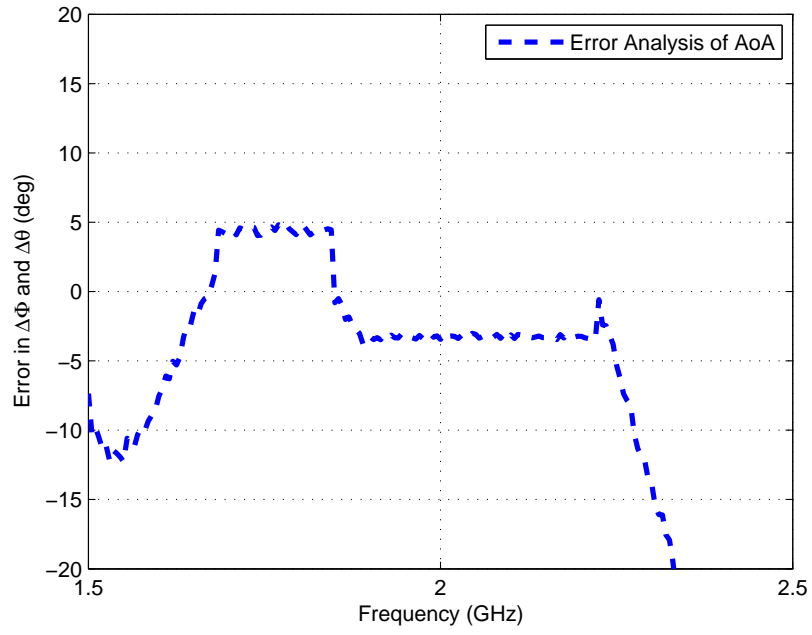
Figure 6.16: Error analysis due to the asymmetry of the SPs and power detectors
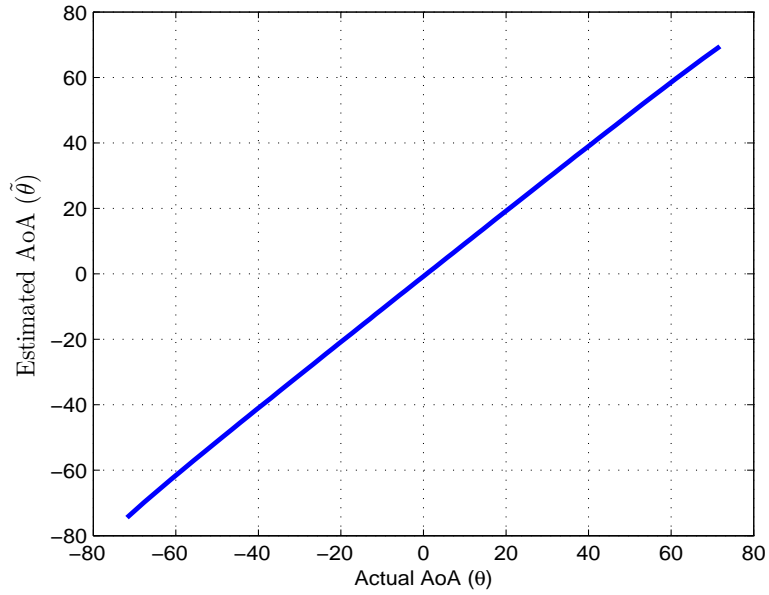
Figure 6.17: Actual (θ) vs Estimated ($\tilde{\theta}$)

Figure 6.15. represents the in-phase and quadrature components (I/Q) of the output from the difference amplifier. This result is based on the Eq. (6.20) and (6.21) within a simulation model. This result includes the asymmetry effect of each SP and assumes asymmetry for the power detectors and difference amplifies. Due to the symmetrical structure of both SP, similar results are obtained for both structures (i.e. SP-1 and SP-2). Figure 6.16. shows the error in $\Delta\theta$ and $\Delta\phi$ computed from the calculated values of the in-phase (I) and quadrature (Q) components. The maximum phase error due to the asymmetry in the SP was $\pm 5^o$, while the non-linearities of power detectors and the difference amplifier were assumed to have a phase error of $\pm 1^o$ in the desired band of operation from 1.68-2.25 GHz. The analytical expressions derived in (6.31) –(6.34) were simulated for phase compensation. The error in the final values of θ and ϕ in the full range was approximately $\pm 3^o$ after phase compensation. Figure 6.17 shows the estimated AoA (θ) based on the measured values of $\Delta\theta$ using (6.9) for the given band. The figure shows the scanning of target RF source with variation of measured phase difference $\Delta\theta$ given in terms of estimated AoA $(\tilde{\theta})$. Practically, with the current setup of SP and an array of micro-strip patch antennas, the feasible range of scanning angle is from -75° to 75° with a maximum phase error in estimated AoA $(\tilde{\theta})$ is $\pm 3^o$ in the given band of operation from 1.68-2.25 GHz.

Table 6.1: Comparison between proposed SP and others.

	Bands (GHz)	Compact Design	Area (mm²)	Use in Mobile Devices	Dual DF	Phase Error
Ref [145]	2-2.45,5.8	Yes	85×85	No	No	$\pm 5^o$
Ref [12]	24	Yes	-	No	No	-
Ref [146]	5 - 6	No	-	No	No	-
Ref [147]	27	No	-	No	No	$\pm 1^o$
Proposed System	1.68 - 2.25	Yes	65×65	Yes	Yes	$\pm 3^o$

Table 6.1 compares the proposed SP features with others that appeared in literature. It is clear that our design is more compact, supports lower frequency

bands, provides dual angle DF capability and can be easily integrated within wireless handheld terminals.

6.9 SP Circuit Integration with Reconfigurable MIMO Antenna System

The principle of an RF direction finding system utilization SP structure is completely described in section 6.4. This section will describe the integration of single SP circuit with the MIMO antenna system described in section 5.1. The whole system consists of a transmitting antenna as source and a receiving MIMO antenna system integrated with a SP circuit for AoA estimation.

6.9.1 Measurements Setup

To find the AoA from a distant source , a reconfigurable MIMO antenna system is integrated with a single SP circuit. The source used is the UWB sensing antenna described in section 5.1. Figure 6.18 shows an overview of the implemented system. The receiving antennas were separated by a distance of 41 mm. Owing to the path difference between the two receiving antennas, the propagated signal had a shift and is useful to find the AoA.

A detailed view of the measurement setup at receiving side is shown in Figure 6.19. The receiving antenna used is the two element MIMO reconfigurable antenna as discussed in section 5.1. The antenna was operating at four distinct modes covering several frequency bands. In the current scenario, we have used it in mode-1 and mode-4 at frequency bands 2020 MHz and 1690 MHz. The proposed SP circuit covered frequency ranges starting from 1.68 GHz to 2.25 GHz. The two reconfigurable antennas are connected with low noise amplifiers (LNA). The LNA used was the ZX60-33LN-S+, with wide bandwidth covering frequency bands from 50∼3000 MHz. Its gain was between 13∼14.4 dB in the 1690∼2020 MHz.
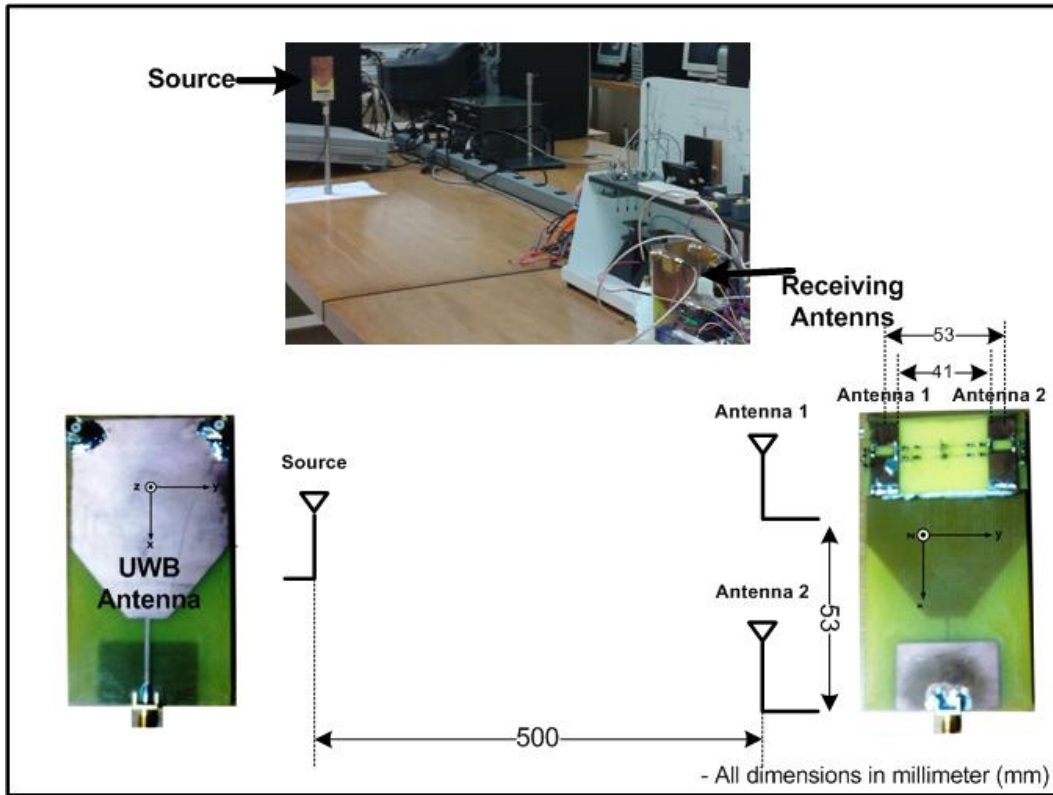
Figure 6.18: Block diagram of the DF measurement setup
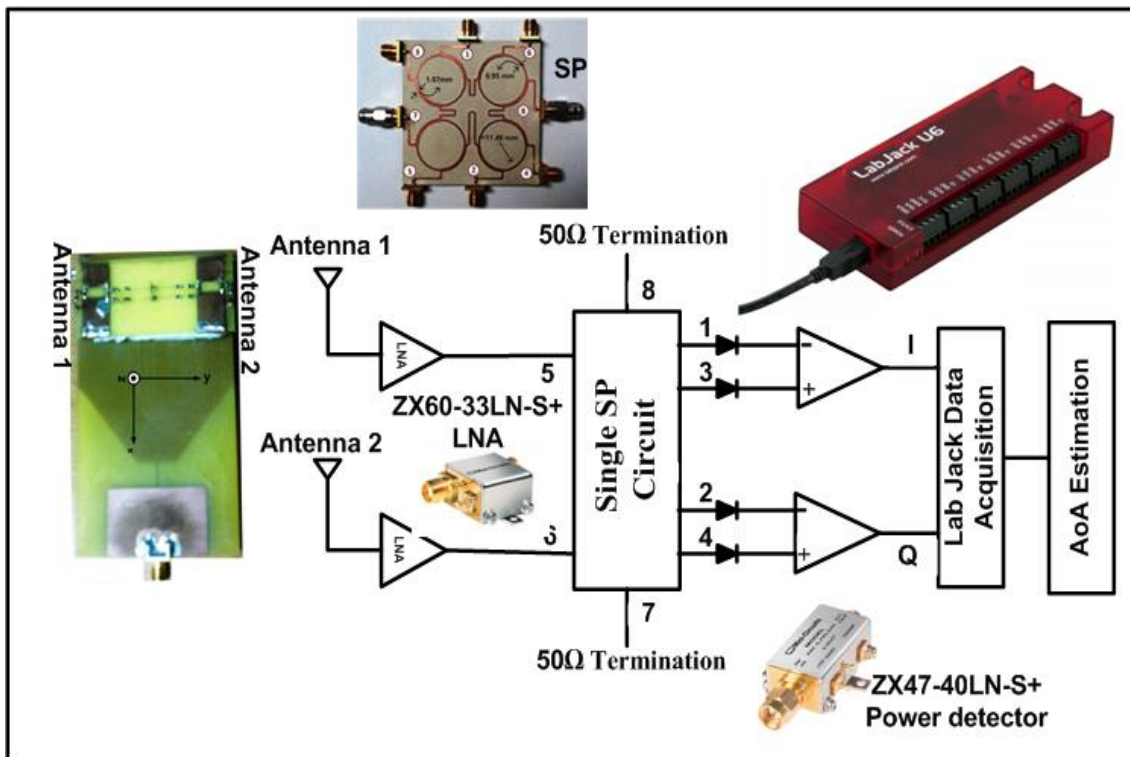
Figure 6.19: Detailed view of SP integration with reconfigurable MIMO antenna system for RF DF.

The output of the LNA was fed to the SP circuit at port-5 and port-6. Two ports of SP circuit were terminated with 50Ω load. The four output ports of the SP structure were connected with the power detectors (ZX47-40LN-S+) followed by a difference amplifier based on LM 741 IC. The output of SP is passed through a power detector to get the DC signal. The power detector operating at wide range with low noise DC output and needs a single 5V supply. The outputs of the difference amplifiers are the in-phase (I) and quadrature (Q) components. Both (I) and (Q) are DC and were acquired by a data acquisition card LabJack u6. Two channels were used for acquiring this data. The data acquired by the data acquisition system were processed in matlab for AoA estimation using Eq.(6.9).
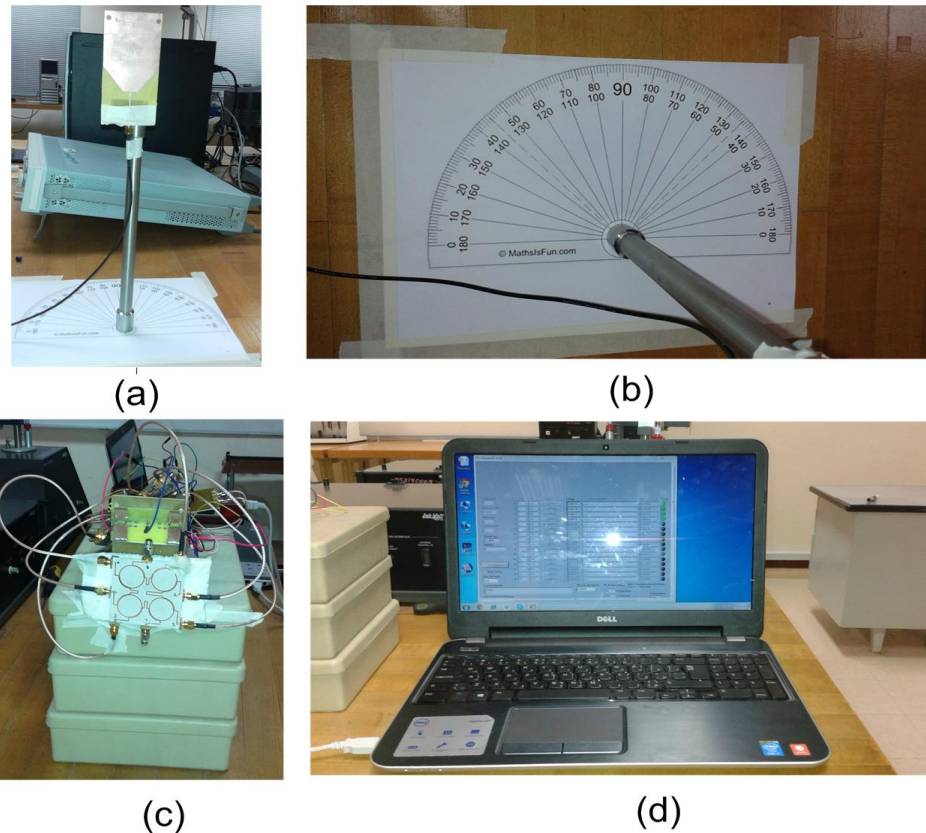
Figure 6.20: (a) RF source (2) Setup for angle adjustment (c) SP circuit integrated with two MIMO antenna system (d) LabJack interface for data acquisition

Figure 6.20 shows all the components of the measurement setup. Figure 6.20(a) shows the source while Figure 6.20(b) shows the setup used for the direction of the source. Figure 6.20(c) shows the SP circuit integrated with MIMO antenna

system while Figure 6.20(d) shows the LabJack u6 interface for data acquisition.

6.9.2   Measurements Results

In the given setup shown in Figure 6.20, a single SP circuit was used to determine the AoA in 2D. Using single SP with two element antenna setup can be used to determine the AoA in single plane. For complete 3D(i.e. ϕ and θ) DF, dual SP circuit with four antenna elements are required. Due to hardware limitation, in this work we have determined the AoA in 2D only.

A.1 Description of AoA Measurements

The ultimate objective of this part was to find the AoA of an RF distant source using the SP circuit integrated with a reconfigurable MIMO antenna system. In this experiment, AoA measurements were made under known conditions. The transmitting antenna was located with known orientation. The AoA of the incoming signal wave was known beforehand. A single antenna was positioned at known angles with respect to the receiver. The transmitting antenna was operated at single tone signal at 1690 MHz and 2020 MHz for two different measurements of AoA determination. This experiment was conducted at the Microwave Lab at KFUPM.

In this AoA experiment, transmitting and receiving antennas were placed at a distance of 500 mm. The distance was made to ensure the minimum level of power to be received for accurate AoA estimation. The orientation of the transmitting antenna was changed for azimuth angles between $\pm 80^o$. It has been found that the error was becoming drastic for angles above $\pm 60^o$. The maximum errors found in the AoA measurements for azimuth angle between $\pm 60^o$ were $\pm 16^o$ and $\pm 13^o$ for frequency bands 1690 MHz and 2020 MHz, respectively. The analytical expressions derived in (6.31) $\sim$(6.34) were utilized for phase compensation. The error introduced in the phase by SP was subtracted from the final error plots. Figures6.21 and 6.22 shows the error in the estimated AoA (θ) based on the measured values of (I) and (Q) using (6.9) for the frequency bands 1690 MHz and
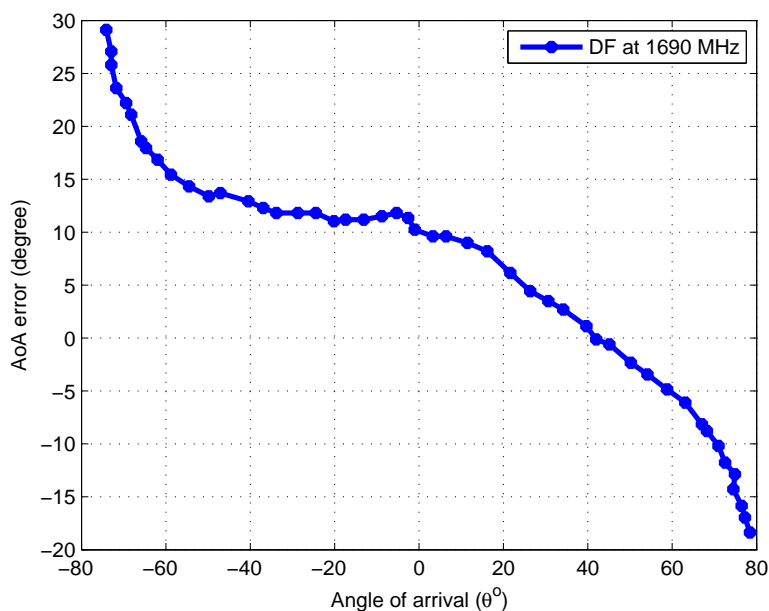
Figure 6.21: Angle of arrival at 1690 MHz

2020 MHz. The figures show the error in estimated AoA ($\tilde{\theta}$). Practically, with the current setup of SP and two elements MIMO antennas, the feasible range of scanning angle is from -60° to 60° with a maximum phase error in estimated AoA ($\tilde{\theta}$) was ±16° in the given two bands of operations.

A.2 Sources of Error in AoA Estimation

The measurement results of AoA estimation were able to estimate the direction of arrival with maximum error of ±16°. Though, the error was high but it helps in understanding the problem and its implementation. The possible sources of errors are discussed in this sections.

1. Ideally, the antenna elements are supposed to be 0.5λ apart. The accuracy of the results drops for closely spaced antenna elements. In the current scenario, the two antennas are separated by a distance 0.23λ and 0.27λ apart, for two frequency bands of 1690 MHz and 2020 MHz, respectively.

2. Although, all the circulators in the SP were designed to be symmetrical in the SP design, due to fabrication tolerances, some phase error was observed
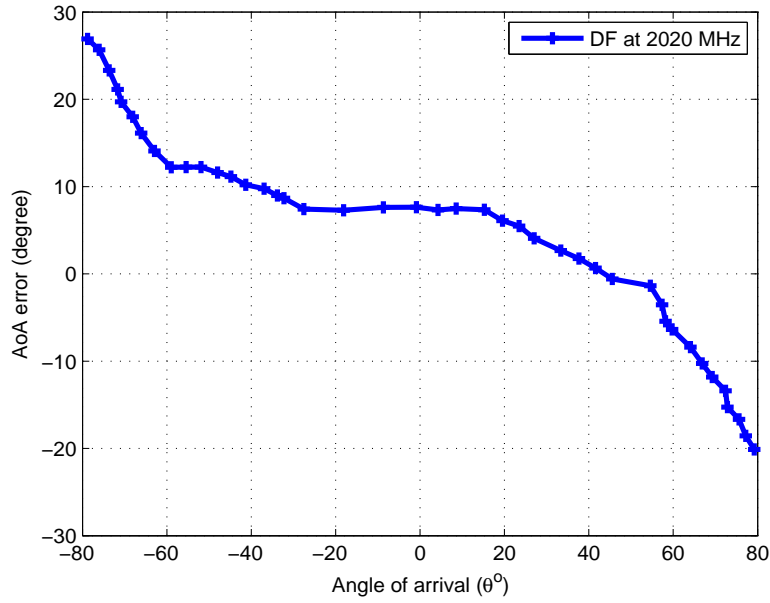
Figure 6.22: Angle of arrival at 2020 MHz

in the phases at the output of SP circuit and this contributes to the final final estimated error.

3. Asymmetry and non-linearities from the power detectors and difference amplifies contributed phase errors as well.

4. Different circuit modules were connected using wires. The slight difference in the lengths of wires might have added extra phase contributing to this high error.

6.10 Conclusions

In this chapter, a compact single and dual-angle resolution based dual-SP system is proposed. The developed system operated between 1.68-2.25 GHz and targets software defined radio and cognitive radio platforms. The unique feature of the proposed system is its ability to find the azimuth and elevation direction of an incoming RF wave simultaneously. Prototypes of the SP circuits were fabricated and tested. The proposed system is low cost, targeting lower frequency bands of practical wireless devices and highly suitable to be used in handheld DF devices.

The single SP circuit was integrated with a MIMO reconfigurable antenna system to demonstrate the complete setup for AoA determination. The max error observed using this complete system after implying an error mitigation technique was $\pm 16^o$.

<div align="center">

CHAPTER 7

CONCLUSION AND FUTURE WORK

</div>

7.1 Conclusions

The use of wireless handheld devices has increased tremendously in recent years. New features are continuously added to these devices resulting in intensive processing and high data rate requirement. Moreover, it is required to perform multitude of functions across several frequency bands and support various standards in different countries as well. Thus, the design of compact and efficient reconfigurable antennas that can be used in MIMO systems with additional capability of efficient spectrum utilization are becoming more popular within mobile phones and other wireless handheld devices. MIMO reconfigurable antenna design for CR applications has received considerable attention among the researchers over past few years.

This work presents and evaluates novel printed MIMO reconfigurable antenna systems integrated with UWB sensing antennas for CR applications. The desired frequency band of interest was 0.7∼3 GHz covering several frequency bands including 4G-LTE bands and WiFi bands. The work focused on the integration of these novel compact reconfigurable MIMO antenna systems with UWB sensing antennas along with SP circuits to provide RF DF capabilities. Among others, the

main challenges in such a design were to develop reconfigurable MIMO antenna systems with UWB sensing antennas in a confined space of 65×120 mm^2 along with its integration with SP circuits while maintaining high isolation between the antenna elements.

Five different frequency reconfigurable antenna designs were completed and analyzed for MIMO performance. Two frequency reconfigurable designs were embedded with UWB sensing antenna structure for the desired frequency band of operation. These two designs were basically completely representing the front end of CR platforms. The designs conform to 4G wireless standard for compact wireless handheld devices. Additionally, the whole antenna system was integrated with SP circuit to add the RF DF to the structure. Modeling and prototyping results were in good agreement for all designs provided. The complete integrated system with direction finding capability were aimed for frequency band between 0.7 GHz to 3 GHz. The maximum error found in the direction of RF source is $\pm 16^o$.

The research carried out in this work is very useful and of practical value as it provides viable solutions to the second generation CR standards that requires a lot of capability from the radio unit None of the known (present in literature) CR antennas had addressed this problem and were able to provide an integrated solution as needed because of the area constraints of smart phone and other compact wireless devices.

7.2   Future Works

The work presented here was based on 2-element and 4-element reconfigurable MIMO antenna system. The reconfigurability was achieved using PIN and varactor diode. The biasing circuit can be optimized. The bias voltage connections by wires should be replaced by on board battery holder with printed circuit board connection. This will minimize the wiring effects on the antenna parameters especially the radiation pattern. One of the important MIMO parameter is the channel

capacity measurement to validate the high data throughput of the antenna system. All the MIMO antenna designs presented in this work can be tested for channel capacity measurement using an SDR platform.

The work presented here utilized two MIMO antennas with a single SP circuit. This work can be extended to four element MIMO with dual-SP circuit for dual-angle AoA estimation (both in θ and ϕ planes). The SP circuit can be integrated on the same PCB with discrete components. The reconfigurable communication antennas could be optimized further to enhance the gain and efficiency in all frequency bands. Isolation enhancement methods can be applied and this effect can be analyzed especially when multi-band operation is considered. In addition, the proposed single substrate 2-element reconfigurable MIMO antenna system with sensing antenna for CR application works in sequential mode. However, the current trends lead to concurrent operation of CR platforms. A mechanism can be introduced in the current design to work in concurrent mode.

REFERENCES

[1] V. Pereira and T. Sousa, "Evolution of mobile communications: from 1g to 4g," *Department of Informatics Engineering of the University of Coimbra, Portugal*, 2004.

[2] M. S. Sharawi, "Printed mimo antenna engineering," *Artech House*, 2014.

[3] D. Piazza, N. J. Kirsch, A. Forenza, R. W. Heath, and K. R. Dandekar, "Design and evaluation of a reconfigurable antenna array for mimo systems," *IEEE Transactions on Antennas and Propagation*, vol. 56, no. 3, pp. 869–881, 2008.

[4] I.-R. R. SM.2152, "Definitions of software defined radio and cognitive radio system," 2009.

[5] F. S. P. T. Force, "Report of the spectrum efficiency working group," 2002.

[6] M. Matinmikko, M. Höyhtyä, M. Mustonen, H. Sarvanko, A. Hekkala, M. Katz, A. Mämmelä, M. Kiviranta, and A. Kautio, "Cognitive radio: An intelligent wireless communication system," *Tech. Rep VTT Technical Research Centre of Finland*, 2008.

[7] B. Sadhu and R. Harjani, *Cognitive Radio Receiver Front-Ends: RF/Analog Circuit Techniques.* Springer, 2014.

[8] R. Schmidt, "Multiple emitter location and signal parameter estimation," *IEEE Transactions on Antennas and Propagation*, vol. 34, no. 3, pp. 276–280, 1986.

[9] R. Roy and T. Kailath, "Esprit-estimation of signal parameters via rotational invariance techniques," *IEEE Transactions on Acoustics, Speech and Signal Processing*, vol. 37, no. 7, pp. 984–995, 1989.

[10] D. Peavey and T. Ogumfunmi, "The single channel interferometer using a pseudo-doppler direction finding system," in *IEEE International Conference on Acoustics, Speech, and Signal Processing*, vol. 5. IEEE, 1997, pp. 4129–4132.

[11] S. O. Tatu and T. A. Denidni, "A new beam direction finding circuit based on six port technology," in *IEEE MTT-S International Microwave Symposium Digest*. IEEE, 2005, pp. 4–pp.

[12] G. Vinci, F. Barbon, B. Laemmle, R. Weigel, and A. Koelpin, "Wide-range, dual six-port based direction-of-arrival detector," in *The 7th German Microwave Conference (GeMiC)*. IEEE, 2012, pp. 1–4.

[13] K.-C. Lin, C.-H. Wu, C.-H. Lai, and T.-G. Ma, "Forecast: Devices by operating system and user type, worldwide, 2010-2017," 2013.

[14] J.-M. P. Jennifer Bernhard, Jeff Reed, "Final report on ears workshop," *NSF, Workshop on Enhancing Access to the Radio Spectrum*, 2010.

[15] T. Aboufoul, A. Alomainy, and C. Parini, "Reconfiguring uwb monopole antenna for cognitive radio applications using gaas fet switches," *Antennas and Wireless Propagation Letters, IEEE*, vol. 11, pp. 392–394, 2012.

[16] Y. T. F. A. J. Costantine, S. Saeed, "A new reconfigurable meander line antenna," in *IEEE International Symposium Antennas and Propagation Society*. IEEE, 2013, pp. 388–389.

[17] M. Amini, H. Hassani, and S. M. A. Nezhad, "A single feed reconfigurable polarization printed monopole antenna," in *6th European Conference on Antennas and Propagation (EUCAP)*. IEEE, 2012, pp. 1–4.

[18] M. Boti, L. Dussopt, and J.-M. Laheurte, "Circularly polarised antenna with switchable polarisation sense," *Electronics Letters*, vol. 36, no. 18, pp. 1518–1519, 2000.

[19] G. M. R. Kevin Ming-Jiang Ho, "Tunable microstrip antenna with circular polarization across 1.4:1 frequency span," in *IEEE International Symposium Antennas and Propagation Society.* IEEE, 2013, pp. 394–395.

[20] S. Zhang, G. Huff, J. Feng, and J. Bernhard, "A pattern reconfigurable microstrip parasitic array," *IEEE Transactions on Antennas and Propagation*, vol. 52, no. 10, pp. 2773–2776, 2004.

[21] S.-L. Yang and K.-M. Luk, "Design of a wide-band l-probe patch antenna for pattern reconfiguration or diversity applications," , *IEEE Transactions on Antennas and Propagation*, vol. 54, no. 2, pp. 433–438, 2006.

[22] M. J. T. M. R. K. M. I. Jais, M. F. Jamlos, "2.45 ghz beam-steering textile antenna for wban application," in *IEEE International Symposium Antennas and Propagation Society*, 2013, pp. 394–395.

[23] M. Manteghi and Y. Rahmat-Samii, "Broadband characterization of the total active reflection coefficient of multiport antennas," in *IEEE International Symposium on Antennas and Propagation Society, 2003.*, vol. 3. IEEE, 2003, pp. 20–23.

[24] T. Taga, "Analysis for mean effective gain of mobile antennas in land mobile radio environments," *IEEE Transactions on Vehicular Technology*, vol. 39, no. 2, pp. 117–131, 1990.

[25] S. Blanch, J. Romeu, and I. Corbella, "Exact representation of antenna system diversity performance from input parameter description," *Electronics Letters*, vol. 39, no. 9, pp. 705–707, 2003.

[26] Z. Li, Z. Du, M. Takahashi, K. Saito, and K. Ito, "Reducing mutual coupling of mimo antennas with parasitic elements for mobile terminals," *IEEE*

Transactions on Antennas and Propagation, vol. 60, no. 2, pp. 473–481, 2012.

[27] M. Muramoto, N. Ishii, and K. Itoh, "Radiation efficiency measurement of a small antenna using the wheeler method," *Electronics and Communications in Japan (Part I: Communications)*, vol. 79, no. 6, pp. 93–100, 1996.

[28] S. C. Ko and R. D. Murch, "Compact integrated diversity antenna for wireless communications," *IEEE Transactions on Antennas and Propagation*, vol. 49, no. 6, pp. 954–960, 2001.

[29] Y. Ding, Z. Du, K. Gong, and Z. Feng, "A novel dual-band printed diversity antenna for mobile terminals," *AIEEE Transactions on ntennas and Propagation*, vol. 55, no. 7, pp. 2088–2096, 2007.

[30] P.-S. Kildal and K. Rosengren, "Correlation and capacity of mimo systems and mutual coupling, radiation efficiency, and diversity gain of their antennas: simulations and measurements in a reverberation chamber," *, IEEE Communications Magazine*, vol. 42, no. 12, pp. 104–112, 2004.

[31] B. Huyart, J.-J. Laurin, R. G. Bosisio, and D. Roscoe, "A direction-finding antenna system using an integrated six-port circuit," *IEEE Transactions onAntennas and Propagation*, vol. 43, no. 12, pp. 1508–1512, 1995.

[32] J. Mitola Iii, "Cognitive radio for flexible mobile multimedia communications," in *IEEE International Workshop on Mobile Multimedia Communication*. IEEE, 1999, pp. 3–10.

[33] M. John, M. J. Ammann, and P. McEvoy, "Uwb vivaldi antenna based on a spline geometry with frequency band-notch," in *IEEE International Symposium on Antennas and Propagation Society*. IEEE, 2008, pp. 1–4.

[34] L. Tianming, R. Yuping, and N. Zhongxia, "Analysis and design of uwb vivaldi antenna," in *International Symposium on Microwave, Antenna, Prop-*

agation and EMC Technologies for Wireless Communications. IEEE, 2007, pp. 579–581.

[35] L. Bian and X.-Q. Che, "Application of equivalent circuit method in designing the vivaldi uwb antenna," in *4th International Conference on Wireless Communications, Networking and Mobile Computing.* IEEE, 2008, pp. 1–3.

[36] Y. Che, K. Li, X. Hou, and W. Tian, "Simulation of a small sized antipodal vivaldi antenna for uwb applications," in *IEEE International Conference on Ultra-Wideband*, vol. 1. IEEE, 2010, pp. 1–3.

[37] D. Sarkar and K. V. Srivastava, "Srr-loaded antipodal vivaldi antenna for uwb applications with tunable notch function," in *International Symposium on Electromagnetic Theory(EMTS).* IEEE, 2013, pp. 466–469.

[38] J. Bai, S. Shi, and D. W. Prather, "Modified compact antipodal vivaldi antenna for 4–50-ghz uwb application," *EEE Transactions on Microwave Theory and Techniques*, vol. 59, no. 4, pp. 1051–1057, 2011.

[39] M. Hamid, P. Hall, P. Gardner, and F. Ghanem, "Frequency reconfigurable vivaldi antenna," in *Fourth European Conference on Antennas and Propagation (EuCAP).* IEEE, 2010, pp. 1–4.

[40] D. T. Le and Y. Karasawa, "A simple broadband antenna for mimo applications in cognitive radio," *IEICE transactions on communications*, vol. 95, no. 1, pp. 18–26, 2012.

[41] T. Aboufoul and A. Alomainy, "Reconfigurable notched tapered slot ultra wideband antenna for cognitive radio applications," in *IEEE International Symposium Antennas and Propagation Society (APSURSI).* IEEE, 2012, pp. 1–2.

[42] H. Sharma, M. Kumar, and G. Parmar, "Reconfigurable tapered slot antenna for wireless applications," in *6th IEEE International Conference on Industrial and Information Systems (ICIIS), 2011.* IEEE, 2011, pp. 23–26.

[43] F. Ghanem, P. Hall, and J. Kelly, "Two port frequency reconfigurable antenna for cognitive radios," *Electronics Letters*, vol. 45, no. 11, pp. 534–536, 2009.

[44] D. T. Le and Y. Karasawa, "Design of a broadband reconfigurable antenna for cognitive radio," in *IEEE International Symposium on Antennas and Propagation Society.* IEEE, 2012, pp. 1–2.

[45] M. Al-Husseini, Y. Tawk, C. Christodoulou, K. Kabalan, and A. El Hajj, "A reconfigurable cognitive radio antenna design," in *IEEE International Symposium on Antennas and Propagation Society (APSURSI).* IEEE, 2010, pp. 1–4.

[46] E. Ebrahimi and P. S. Hall, "A dual port wide-narrowband antenna for cognitive radio," in *Proceedings of the 3rd European Conference on Antennas and Propagation (EuCAP).* IEEE, 2009, pp. 809–812.

[47] T. Aboufoul, K. Ali, A. Alomainy, and C. Parini, "Combined pattern and frequency reconfiguration of single-element ultra-wideband monopole antenna for cognitive radio devices," in *7th European Conference on Antennas and Propagation (EuCAP).* IEEE, 2013, pp. 932–936.

[48] G. Jin, D. Zhang, and R. Li, "Optically controlled reconfigurable antenna for cognitive radio applications," *Electronics letters*, vol. 47, no. 17, pp. 948–950, 2011.

[49] Y. Tawk and C. Christodoulou, "A new reconfigurable antenna design for cognitive radio," *IEEE Antennas and Wireless Propagation Letters*, vol. 8, pp. 1378–1381, 2009.

[50] T. Wu, R. Li, S. Eom, K. Lim, S. Jeon, J. Laskar, and M. Tentzeris, "A multiband/scalable reconfigurable antenna for cognitive radio base stations," in *EEE International Symposium on Antennas and Propagation Society I.* IEEE, 2008, pp. 1–4.

[51] M. Jusoh, M. Jamlos, M. Kamarudin, and M. Malek, "A novel compact reconfigurable multi-band antenna," in *IEEE International RF and Microwave Conference (RFM),2011.* IEEE, 2011, pp. 377–380.

[52] M. Al-Husseini, A. El-Hajj, Y. Tawk, K. Y. Kabalan, and C. G. Christodoulou, "A simple dual-port antenna system for cognitive radio applications," in *International Conference on High Performance Computing and Simulation (HPCS).* IEEE, 2010, pp. 549–552.

[53] M. Al-Husseini, A. Ramadan, M. Zamudio, C. Christodoulou, A. El-Hajj, and K. Kabalan, "A uwb antenna combined with a reconfigurable bandpass filter for cognitive radio applications," in *IEEE-APS Topical Conference on Antennas and Propagation in Wireless Communications (APWC).* IEEE, 2011, pp. 902–904.

[54] Y. Tawk, J. Costantine, S. Hemmady, G. Balakrishnan, K. Avery, and C. G. Christodoulou, "Demonstration of a cognitive radio front end using an optically pumped reconfigurable antenna system (opras)," *IEEE Transactions on Antennas and Propagation*, vol. 60, no. 2, pp. 1075–1083, 2012.

[55] E. Erfani, J. Nourinia, C. Ghobadi, M. Niroo-Jazi, and T. A. Denidni, "Design and implementation of an integrated uwb/reconfigurable-slot antenna for cognitive radio applications," *IEEE Antennas and Wireless Propagation Letters*, vol. 11, pp. 77–80, 2012.

[56] Y. Tawk, M. Al-Husseini, S. Hemmady, A. Albrecht, G. Balakrishnan, and C. Christodoulou, "Implementation of a cognitive radio front-end using optically reconfigurable antennas," in *International Conference on Electromagnetics in Advanced Applications (ICEAA).* IEEE, 2010, pp. 294–297.

[57] T. Aboufoul, I. Shoaib, A. Alomainy, and X. Chen, "Pattern reconfigurable planar uwb antenna array for future cognitive radio portable devices," in *Antennas and Propagation Conference (LAPC), Loughborough.* IEEE, 2012, pp. 1–4.

[58] E. T. Rahardjo, F. Y. Zulkifli, and A. Widiastri, "Printed antenna design for cognitive radio application at 1.8 ghz and 2.35 ghz spectrum allocation," in *Asia-Pacific Microwave Conference Proceedings (APMC), 2011*. IEEE, 2011, pp. 1881–1884.

[59] Y. Cai, Y. J. Guo, and T. Bird, "A frequency reconfigurable printed yagi-uda dipole antenna for cognitive radio applications," *IEEE Transactions on Antennas and Propagation*, vol. 60, no. 6, pp. 2905–2912, 2012.

[60] Y. Tawk, C. Christodoulou, J. Costantine, and S. Barbin, "A frequency and radiation pattern reconfigurable antenna system with sensing capabilities for cognitive radio," in *IEEE International Symposium on Antennas and Propagation Society*. IEEE, 2012, pp. 1–2.

[61] F. Ghanem, K. Ghanem, P. Hall, and M. Hamid, "A miniature frequency reconfigurable antenna for cognitive radios," in *IEEE International Symposium Antennas and Propagation Society*. IEEE, 2011, pp. 171–174.

[62] J. R. Kelly and P. S. Hall, "Reconfigurable slot antenna for cognitive radio applications," in *IEEE International Symposium on Antennas and Propagation Society*. IEEE, 2009, pp. 1–4.

[63] H. Majid, M. Rahim, M. Hamid, and M. Ismail, "Reconfigurable wide to narrow band antenna for cognitive radio systems," in *RF and Microwave Conference (RFM), 2011 IEEE International*. IEEE, 2011, pp. 285–288.

[64] H. F. Abu Tarboush, S. Khan, R. Nilavalan, H. Al-Raweshidy, and D. Budimir, "Reconfigurable wideband patch antenna for cognitive radio," in *Antennas & Propagation Conference, 2009. LAPC 2009. Loughborough*. IEEE, 2009, pp. 141–144.

[65] H.-T. C. J.-S. K. Wen-Shan Chen, Yi-Tien Chen, "Two port frequency reconfigurable antenna for cognitive radios," *IEEE International Symposium Antennas and Propagation Society*, pp. 1–4, 2009.

[66] I. Elfergani, R. Abd-Alhameed, C. See, T. Sadeghpour, J. Noras, and S. Jones, "Small size tuneable printed f-slot antenna for mobile handset applications," *Microwave and Optical Technology Letters*, vol. 54, no. 3, pp. 794–802, 2012.

[67] N. Behdad and K. Sarabandi, "Dual-band reconfigurable antenna with a very wide tunability range," *IEEE Transactions on Antennas and Propagation*, vol. 54, no. 2, pp. 409–416, 2006.

[68] T. Korosec and P. Ritosa, "Varactor-loaded microstrip patch antenna with frequency-tuning capability and complete polarization diversity," in *IEEE EUROCON 2009.* IEEE, 2009, pp. 80–85.

[69] J. Liang and H. Y. D. Yang, "Varactor loaded tunable printed pifa," *Progress In Electromagnetics Research B*, vol. 15, pp. 113–131, 2009.

[70] H. F. AbuTarboush, R. Nilavalan, and T. Peter, "Pifa based reconfigurable multiband antenna for wireless applications," in *International Conference on Electromagnetics in Advanced Applications (ICEAA),2010.* IEEE, 2010, pp. 232–235.

[71] M. N. M. Kehn, O. Quevedo-Teruel, and E. Rajo-Iglesias, "Reconfigurable loaded planar inverted-f antenna using varactor diodes," *Antennas and Wireless Propagation Letters*, vol. 10, pp. 466–468, 2011.

[72] T. Korosec, L. Naglic, J. Tratnik, L. Pavlovic, B. Batagelj, and M. Vidmar, "Evolution of varactor-loaded frequency and polarization reconfigurable microstrip patches," in *Asia-Pacific Microwave Conference Proceedings (APMC), 2011.* IEEE, 2011, pp. 705–708.

[73] Y. Park and Y. Sung, "A reconfigurable antenna for quad-band mobile handset applications," *IEEE Transactions on Antennas and Propagation*, vol. 60, no. 6, pp. 3003–3006, 2012.

[74] G. Yang, M. R. Islam, R. A. Dougal, and M. Ali, "A reconfigurable stacked patch antenna for wireless power transfer and data telemetry in sensors," *Progress In Electromagnetics Research C*, vol. 29, pp. 67–81, 2012.

[75] Y. Li, Z. Zhang, W. Chen, Z. Feng, and M. F. Iskander, "A quadband antenna with reconfigurable feedings," *IEEE Antennas and Wireless Propagation Letters*, vol. 8, pp. 1069–1071, 2009.

[76] H. F. Abutarboush, R. Nilavalan, S. Cheung, K. M. Nasr, T. Peter, D. Budimir, and H. Al-Raweshidy, "A reconfigurable wideband and multiband antenna using dual-patch elements for compact wireless devices," *Antennas and Propagation, IEEE Transactions on*, vol. 60, no. 1, pp. 36–43, 2012.

[77] J.-H. Lim, G.-T. Back, Y.-I. Ko, C.-W. Song, and T.-Y. Yun, "A reconfigurable pifa using a switchable pin-diode and a fine-tuning varactor for uspcs/wcdma/m-wimax/wlan," *Antennas and Propagation, IEEE Transactions on*, vol. 58, no. 7, pp. 2404–2411, 2010.

[78] J.-H. Lim, Z.-J. Jin, and T.-Y. Yun, "A frequency reconfigurable pifa using a pin diode for mobile-wimax applications," in *Intelligent Radio for Future Personal Terminals (IMWS-IRFPT), 2011 IEEE MTT-S International Microwave Workshop Series on*. IEEE, 2011, pp. 1–2.

[79] T. D. Nguyen, Y. Duroc, T. P. Vuong *et al.*, "Novel reconfigurable 8-shape pifa antenna using pin diode," in *Advanced Technologies for Communications (ATC), 2011 International Conference on*. IEEE, 2011, pp. 272–275.

[80] T.-Y. Han and C.-T. Huang, "Reconfigurable monopolar patch antenna," *Electronics letters*, vol. 46, no. 3, pp. 199–200, 2010.

[81] J. Choi and S. Lim, "Frequency reconfigurable metamaterial resonant antenna," in *Microwave Conference, 2009. APMC 2009. Asia Pacific*. IEEE, 2009, pp. 798–801.

[82] H. Mirzaei and G. V. Eleftheriades, "A compact frequency-reconfigurable metamaterial-inspired antenna," *Antennas and Wireless Propagation Letters, IEEE*, vol. 10, pp. 1154–1157, 2011.

[83] R. Sorrentino, R. V. Gatti, L. Marcaccioli, and B. Mencagli, "Electronic steerable mems antennas," in *First European Conference on Antennas and Propagation, EuCAP.* IEEE, 2006, pp. 1–8.

[84] R. Valkonen, C. Luxey, J. Holopainen, C. Icheln, and P. Vainikainen, "Frequency-reconfigurable mobile terminal antenna with mems switches," in *Proceedings of the Fourth European Conference on Antennas and Propagation (EuCAP).* IEEE, 2010, pp. 1–5.

[85] H. Mirzajani, M. Nasiri, and H. B. Ghavifekr, "A new design of mems-based wideband frequency reconfigurable microstrip patch antenna," in *Mechatronics and its Applications (ISMA), 2012 8th International Symposium on.* IEEE, 2012, pp. 1–6.

[86] R.-H. Chen and J.-S. Row, "Single-fed microstrip patch antenna with switchable polarization," *Antennas and Propagation, IEEE Transactions on*, vol. 56, no. 4, pp. 922–926, 2008.

[87] N. Jin, F. Yang, and Y. Rahmat-Samii, "A novel patch antenna with switchable slot (pass): Dual-frequency operation with reversed circular polarizations," *Antennas and Propagation, IEEE Transactions on*, vol. 54, no. 3, pp. 1031–1034, 2006.

[88] Y. Chen, Y. Jiao, and F. Zhang, "Polarization reconfigurable cpw-fed square slot antenna using pin diodes," *Microwave and Optical Technology Letters*, vol. 49, no. 6, pp. 1233–1236, 2007.

[89] Y. Li, Z. Zhang, W. Chen, and Z. Feng, "Polarization reconfigurable slot antenna with a novel compact cpw-to-slotline transition for wlan application," *Antennas and Wireless Propagation Letters, IEEE*, vol. 9, pp. 252–255, 2010.

[90] G. Huff, J. Feng, S. Zhang, and J. Bernhard, "A novel radiation pattern and frequency reconfigurable single turn square spiral microstrip antenna," *Microwave and Wireless Components Letters, IEEE*, vol. 13, no. 2, pp. 57–59, 2003.

[91] E. Palantei, D. Thiel, and S. O'Keefe, "Rectangular patch with parasitic folded dipoles: A reconfigurable antenna," in *Antenna Technology: Small Antennas and Novel Metamaterials, 2008. iWAT 2008. International Workshop on*. IEEE, 2008, pp. 251–254.

[92] S. Nikolaou, G. E. Ponchak, J. Papapolymerou, and M. M. Tentzeris, "Design and development of an annular slot antenna (asa) with a reconfigurable radiation pattern," in *Microwave Conference Proceedings, 2005. APMC 2005. Asia-Pacific Conference Proceedings*, vol. 5. IEEE, 2005, pp. 3–pp.

[93] W. Kang, J. Park, and Y. Yoon, "Simple reconfigurable antenna with radiation pattern," *Electronics Letters*, vol. 44, no. 3, pp. 182–183, 2008.

[94] D. Jiawei, W. Anguo, and L. Hang, "A simple radiation pattern reconfigurable printed dipole antenna," in *Microwave, Antenna, Propagation and EMC Technologies for Wireless Communications, 2009 3rd IEEE International Symposium on*. IEEE, 2009, pp. 619–622.

[95] M. Donelli, R. Azaro, L. Fimognari, and A. Massa, "A planar electronically reconfigurable wi-fi band antenna based on a parasitic microstrip structure," *Antennas and Wireless Propagation Letters, IEEE*, vol. 6, pp. 623–626, 2007.

[96] A. Ghasemi, N. Ghahvehchian, A. Mallahzadeh, and S. Sheikholvaezin, "A reconfigurable printed monopole antenna for mimo application," in *Antennas and Propagation (EUCAP), 2012 6th European Conference on*. IEEE, 2012, pp. 1–4.

[97] A. Lackpour, P. Mookiah, M. Olivieri, and K. Dandekar, "Evaluation of the reconfigurable printed fractal tree antenna for enhanced pattern diversity

in mimo systems," in *Radio and Wireless Symposium (RWS), 2010 IEEE*. IEEE, 2010, pp. 96–99.

[98] Z. Hu, P. Hall, and P. Gardner, "Reconfigurable dipole-chassis antennas for small terminal mimo applications," *Electronics letters*, vol. 47, no. 17, pp. 953–955, 2011.

[99] C.-Y. Chiu and R. D. Murch, "Reconfigurable multi-port antennas for hand-held devices," in *IEEE International Symposium on Antennas and Propagation Society*. IEEE, 2009, pp. 1–4.

[100] Z.-J. Jin, J.-H. Lim, and T.-Y. Yun, "Frequency reconfigurable multiple-input multiple-output antenna with high isolation," *IET microwaves, antennas and propagation*, vol. 6, no. 10, pp. 1095–1101, 2012.

[101] S. C. Del Barrio, B. Yanakiev, and G. F. Pedersen, "Portable mimo-lte antennas for different hand-held device sizes," in *Antennas and Propagation Conference (LAPC), 2012 Loughborough*. IEEE, 2012, pp. 1–4.

[102] J. Lim, Z. Jin, C. Song, and T. Yun, "Simultaneous frequency and isolation reconfigurable mimo pifa using pin diodes," vol. 60, no. 12, pp. 5939—5946, December, 2012.

[103] Z. H. Hu, P. S. Hall, P. Gardner, and Y. Nechayev, "Wide tunable balanced antenna for mobile terminals and its potential for mimo applications," in *Antennas and Propagation Conference (LAPC), 2011 Loughborough*. IEEE, 2011, pp. 1–4.

[104] A. Grau, M.-J. Lee, J. Romeu, H. Jafarkhani, L. Jofre, and F. De Flaviis, "A multifunctional mems-reconfigurable pixel antenna for narrowband mimo communications," in *IEEE International Symposium on Antennas and Propagation Society*. IEEE, 2007, pp. 489–492.

[105] C.-Y. Chiu and R. D. Murch, "Reconfigurable multi-slot multi-port antennas using rf-mems switches for handheld devices," in *Microwave Conference Proceedings (APMC), 2010 Asia-Pacific*.   IEEE, 2010, pp. 999–1002.

[106] A. Grau, J. Romeu, L. Jofre, and F. De Flaviis, "A software defined mems-reconfigurable pixel-antenna for narrowband mimo systems," in *Adaptive Hardware and Systems, 2008. AHS'08. NASA/ESA Conference on*.   IEEE, 2008, pp. 141–146.

[107] M. Mowlér and B. Lindmark, "Reconfigurable mems antenna for wireless applications," in *Proceedings of the First European Conference on Antennas and Propagation (EuCAP)*.   IEEE, 2006, pp. 1–6.

[108] D. Chung, D. Anagnostou, G. Ponchak, M. Tentzeris, and J. Papapolymerou, "Light weight mimo phased arrays with beam steering capabilities using rf mems," in *Personal, Indoor and Mobile Radio Communications, 2007. PIMRC 2007. IEEE 18th International Symposium on*.   IEEE, 2007, pp. 1–3.

[109] M. Unlu, Y. Damgaci, H. S. Mopidevi, O. Kaynar, and B. A. Cetiner, "Reconfigurable, tri-band rf mems pifa antenna," in *IEEE International Symposium Antennas and Propagation Society*.   IEEE, 2011, pp. 1563–1565.

[110] P.-Y. Qin, Y. J. Guo, A. R. Weily, and C.-H. Liang, "A pattern reconfigurable u-slot antenna and its applications in mimo systems," *IEEE Transactions on Antennas and Propagation*, vol. 60, no. 2, pp. 516–528, 2012.

[111] P. Qin, A. Weily, Y. J. Guo, C. Liang, and Y. Cai, "A pattern reconfigurable u-slot patch antenna," in *IEEE International Symposium on Antennas and Propagation Society*.   IEEE, 2010, pp. 1–4.

[112] P.-Y. Qin, Y. J. Guo, and E. Dutkiewicz, "Capacity enhancement of 2× 2 mimo system using pattern reconfigurable antennas," in *Microwave Conference Proceedings (APMC), 2011 Asia-Pacific*.   IEEE, 2011, pp. 1694–1697.

[113] I. Lim and S. Lim, "Pattern reconfigurable antenna for adaptive multi-input multi-output switching applications," in *IEEE International Symposium on Antennas and Propagation Society.*   IEEE, 2012, pp. 1–2.

[114] D. Piazza, P. Mookiah, M. D'Amico, and K. R. Dandekar, "Pattern and polarization reconfigurable circular patch for mimo systems," in *Proceedings of the Third European Conference on Antennas and Propagation (EuCAP).* IEEE, 2009, pp. 1047–1051.

[115] M. Yousefbeiki and J. Perruisseau-Carrier, "Pattern-reconfigurable built-in antenna for data multiplexing with a single radio," 2013.

[116] M.-I. Lai and S.-K. Jeng, "Compact pattern reconfigurable antenna array based on l-shaped slots and pin diodes for adaptive mimo systems," in *IEEE International Symposium on Antennas and Propagation Society.*   IEEE, 2008, pp. 1–4.

[117] H. Li, J. Xiong, and S. He, "A compact planar mimo antenna system of four elements with similar radiation characteristics and isolation structure," *Antennas and Wireless Propagation Letters, IEEE*, vol. 8, pp. 1107–1110, 2009.

[118] V. A. Nguyen and P. S. Ook, "Compact switched and reconfigurable 4-ports beam antenna array for mimo applications," in *Intelligent Radio for Future Personal Terminals (IMWS-IRFPT), 2011 IEEE MTT-S International Microwave Workshop Series on.*   IEEE, 2011, pp. 1–3.

[119] M. Yousefbeiki and J. Perruisseau-Carrier, "Towards compact and frequency-tunable antenna solutions for mimo transmission with a single rf chain," *arXiv preprint arXiv:1306.4514*, 2013.

[120] D. Piazza, P. Mookiah, M. D'Amico, and K. Dandekar, "Two port reconfigurable circular patch antenna for mimo systems," 2007.

[121] Y. Xu, Z. Zeng, C. Feng, and H. Huang, "Reconfigurable antenna array for imt-advanced mimo systems," in *Communications Technology and Applications, 2009. ICCTA'09. IEEE International Conference on.* IEEE, 2009, pp. 626–628.

[122] P. Mookiah, D. Piazza, and K. R. Dandekar, "Reconfigurable spiral antenna array for pattern diversity in wideband mimo communication systems," in *IEEE International Symposium on Antennas and Propagation Society.* IEEE, 2008, pp. 1–4.

[123] H.-I. Lin and W.-J. Liao, "A beam switching array based on rotman lens for mimo technology," in *Microwave and Millimeter Wave Technology (ICMMT), 2012 International Conference on*, vol. 2. IEEE, 2012, pp. 1–4.

[124] K. K. Kishor and S. V. Hum, "A reconfigurable chassis-mode mimo antenna," in *Proceedings of the 7th European Conference on Antennas and Propagation (EuCAP).* IEEE, 2013, pp. 1992–1996.

[125] D. Pinchera and F. Schettino, "A dual-polarized parasitic patch antenna for mimo systems," in *Microwave Conference, 2009. EuMC 2009. European.* IEEE, 2009, pp. 642–644.

[126] J. S. K. Raj, J. Bonney, P. Herrero, and J. Schoebel, "A reconfigurable antenna for mimo application," in *Antennas & Propagation Conference, 2009. LAPC 2009. Loughborough.* IEEE, 2009, pp. 269–272.

[127] L. Ge and K.-M. Luk, "Frequency-reconfigurable low-profile circular monopolar patch antenna," *IEEE Transactions on Antennas and Propagation*, vol. 62, no. 7, pp. 3443–3449, 2014.

[128] J.-H. Lim, C.-W. Song, Z.-J. Jin, and T.-Y. Yun, "Frequency reconfigurable planar inverted-f antenna using switchable radiator and capacitive load,"

IET, Microwaves, Antennas and Propagation, vol. 7, no. 6, pp. 430–435, 2013.

[129] J. Cho, C. Jung, and K. Kim, "Frequency-reconfigurable two-port antenna for mobile phone operating over multiple service bands," *Electronics letters*, vol. 45, no. 20, pp. 1009–1011, 2009.

[130] H. T. Chattha, M. Nasir, Q. H. Abbasi, Y. Huang, and S. S. Alja'afreh, "Compact low profile dual port single wideband planar inverted-f mimo antenna," *Antenna and Wireless Propagation Letters*, vol. 12, pp. 1673–1675, 2013.

[131] G. Mansour, P. S. Hall, P. Gardner, and M. K. A. Rahim, "Tunable slot-loaded patch antenna for cognitive radio," in *Antennas and Propagation Conference (LAPC), 2012 Loughborough*. IEEE, 2012, pp. 1–4.

[132] Y. Tawk, J. Costantine, K. Avery, and C. Christodoulou, "Implementation of a cognitive radio front-end using rotatable controlled reconfigurable antennas," *Antennas and Propagation, IEEE Transactions on*, vol. 59, no. 5, pp. 1773–1778, 2011.

[133] M. R. Hamid, P. Gardner, P. S. Hall, and F. Ghanem, "Reconfigurable vivaldi antenna," *microwave and optical technology letters*, vol. 52, no. 4, pp. 785–787, 2010.

[134] Y. Tawk, J. Costantine, and C. Christodoulou, "A mimo cognitive radio antenna system," *IEEE Antennas and Propagation Society (APSURSI)*, 2013.

[135] ——, "Reconfigurable filtennas and mimo in cognitive radio applications," *IEEE Transactions on Antennas and Propagation*, vol. 62, no. 3, pp. 1074–1084, 2014.

[136] G. F. Engen, "The six-port reflectometer: An alternative network analyzer," *Microwave Theory and Techniques, IEEE Transactions on*, vol. 25, no. 12, pp. 1075–1080, 1977.

[137] C. A. Hoer, "A network analyzer incorporating two six-port reflectometers," *Microwave Theory and Techniques, IEEE Transactions on*, vol. 25, no. 12, pp. 1070–1074, 1977.

[138] G. F. Engen, "An improved circuit for implementing the six-port technique of microwave measurements," *Microwave Theory and Techniques, IEEE Transactions on*, vol. 25, no. 12, pp. 1080–1083, 1977.

[139] D. Woods, "Analysis and calibration theory of the general 6-port reflectometor employing four amplitude detectors," in *Proceedings of the Institution of Electrical Engineers*, vol. 126, no. 2.   IET, 1979, pp. 221–228.

[140] H. Cronson and L. Susman, "A new calibration technique for automated broadband microwave measurements," in *Microwave Conference, 1976. 6th European*.   IEEE, 1976, pp. 205–209.

[141] S. Li and R. G. Bosisio, "Calibration of multiport reflectometers by means of four open/short circuits," *Microwave Theory and Techniques, IEEE Transactions on*, vol. 30, no. 7, pp. 1085–1090, 1982.

[142] G. Riblet and E. B. Hansson, "Aspects of the calibration of a single six-port using a load and offset reflection standards," *Microwave Theory and Techniques, IEEE Transactions on*, vol. 30, no. 12, pp. 2120–2125, 1982.

[143] V. Bilik, "Six-port measurement technique: Principles, impact, applications," 1998.

[144] R. Hammerle, "Factors limiting the accuracy of doppler and adcock direction finding systems," in *Passive Direction Finding, IEE Colloquium on*.   IET, 1989, pp. 3–1.

[145] S. Tatu, K. Wu, and T. Denidni, "Direction-of-arrival estimation method based on six-port technology," *IEE Proceedings-Microwaves, Antennas and Propagation*, vol. 153, no. 3, pp. 263–269, 2006.

[146] H. Peng, Z. Yang, and T. Yang, "Design and implementation of a practical direction finding receiver," *Progress In Electromagnetics Research Letters*, vol. 32, pp. 157–167, 2012.

[147] S. O. Tatu, E. Moldovan, K. Wu, R. G. Bosisio, and T. A. Denidni, "Ka-band analog front-end for software-defined direct conversion receiver," *Microwave Theory and Techniques, IEEE Transactions on*, vol. 53, no. 9, pp. 2768–2776, 2005.

[148] T. Yakabe, F. Xiao, K. Iwamoto, F. M. Ghannouchi, K. Fujii, and H. Yabe, "Six-port based wave-correlator with application to beam direction finding," *Instrumentation and Measurement, IEEE Transactions on*, vol. 50, no. 2, pp. 377–380, 2001.

[149] H. Peng, Z. Yang, and T. Yang, "Calibration of a six-port receiver for direction finding using the artificial neural network technique," *Progress In Electromagnetics Research Letters*, vol. 27, pp. 17–24, 2011.

[150] G. Vinci, A. Koelpin, F. Barbon, and R. Weigel, "Six-port-based direction-of-arrival detection system," in *Microwave Conference Proceedings (APMC), 2010 Asia-Pacific*. IEEE, 2010, pp. 1817–1820.

[151] G. Vinci, F. Barbon, R. Weigel, and A. Koelpin, "A novel, wide angle, high resolution direction-of-arrival detector," in *Radar Conference (EuRAD), 2011 European*. IEEE, 2011, pp. 265–268.

[152] G. Vinci, B. Laemmle, F. Barbon, R. Weigel, and A. Koelpin, "A 77 ghz direction of arrival detector system with sige integrated six-port receiver," in *Radio and Wireless Symposium (RWS), 2012 IEEE*. IEEE, 2012, pp. 247–250.

[153] M. S. Sharawi, "Printed multi-band mimo antenna systems and their performance metrics," *IEEE Antennas and Propagation Magazine*, vol. 55, pp. 218–232, 2013.

[154] D. Gesbert, M. Shafi, D.-s. Shiu, P. J. Smith, and A. Naguib, "From theory to practice: an overview of mimo space-time coded wireless systems," *IEEE Journal on Selected Areas in Communications*, vol. 21, no. 3, pp. 281–302, 2003.

Vitae

- Name: Rifaqat Hussain

- Nationality: Pakistani

- Date of Birth: 1st April, 1979

- Email: *engr.rifaqat@gmail.com*

- Permenant Address: House 1152(F.F), street 95, I10/1, Islamabad, Pakistan.

- PhD (Electrical Engineering) KFUPM, Saudi Arabia, 2015

- MS (Systems Engineering) PIEAS, Islamabad, Pakistan, 2005

- BE (Electrical Engineering) UET, Peshawar, Pakistan, 2003

LIST OF PUBLICATIONS

- **Journal Publications**

1. R. Hussain and M. S. Sharawi, "A Cognitive Radio Reconfigurable MIMO and Sensing Antenna System", IEEE Antenna and Wireless Propagation Letters, October, 2014.

2. R. Hussain and M. S. Sharawi, "An Integrated Reconfigurable MIMO Antenna System with an UWB Sensing Antenna for Cognitive Radio Platforms", Accepted, IET, Microwave Antenna and Propagation Journal.

3. R. Hussain and M. S. Sharawi, "An Planar Meandered-F-Shaped 4-Element Reconfigurable MIMO Antenna System with Isolation Enhancement for Cognitive Radio Platforms", submitted to TAP communications.

4. R. Hussain and M. S. Sharawi, "Planar 4-element Frequency Agile MIMO Antenna System with Chassis Mode Reconfigurability", submitted to Microwave and Optical Technology Letters.

- **International Conferences**

1. R. Hussain and M. S. Sharawi, "A 4-Element Cognitive Radio Front-End MIMO Antenna System for Mobile Terminals", submitted to EuMW 2015.

2. R. Hussain and M. S. Sharawi, "4-Element Planar MIMO Reconfigurable Antenna System for Cognitive Radio Applications", submitted to APS 2015.

3. R. Hussain and M. S. Sharawi, "A Low Profile Compact Reconfigurable MIMO Antenna for Cognitive Radio Applications", Accepted, EuCAP, 2015.

4. R. Hussain and M. S. Sharawi, "A Reconfigurable Dual-Band MIMO Antenna System for Mobile Terminals", Loughborough Antennas and Propagation Conference (LAPC), 2014.

5. R. Hussain and M. S. Sharawi, "A Compact Reconfigurable Multi-band MIMO Antenna System", IEEE International Symposium on Antennas and Propagation, Memphis, June 2014.

6. R. Hussain and M. S. Sharawi, "A Dual Six-Port with two-Angle Resolution and Compact Size for Mobile Terminals", Radio Wireless Symposium,Newport Beach, CA, USA, 2014.

7. R. Hussain and M. S. Sharawi, "Compact Low Frequency Six-Port Design for Wireless Communication Devices", 17th IEEE Mediterranean Electrotechnical Conference, Beirut, Lebanon 2014.

8. F. Sultan, R. Hussain and S. S. Iqbal, "Design of a reduced size 7-patch antenna array with FSS based directivity enhancement", 2013 IEEE International Symposium on Phased Array Systems and Technology, Boston, USA, October 2013.

9. Amin-ud-din and R. Hussain, "Direction Finding of a Single far Field Acoustic Source using a Smart 3-D Array of Acoustic Sensors", IEEE International Conference on Emerging Technologies (ICET), November 12-13, 2007, Islamabad Pakistan.

- **Patents**

1. M. S. Sharawi and R. Hussain, "Dual-Angle Resolution Based Six Port Direction Finding System", Filed on Feb. 2013 to USPO, Patent Pending.

2. M. S. Sharawi and R. Hussain, "Compact Reconfigurable MIMO Antennas Integrated with Sensing Antennas for Cognitive Radio Applications", Filed on April 2014 to USPO, Patent Pending.

3. M. S. Sharawi and R. Hussain"A Low Profile Compact Reconfigurable MIMO and Sensing Antenna System for Cognitive Radio Applications", Filed on August 2014 to USPO, Patent Pending.

4. M. S. Sharawi and R. Hussain, "Four Element Reconfigurable Antennas for Cognitive Radio Platforms", Filed on February 2014 to USPO, Patent Pending.